INFLUENCE OF TEMPERATURE ON THE HYDRATION OF BELITE-CALCIUM SULFOALUMINATE CEMENTS

Maruša Mrak

Doctoral Dissertation
Jožef Stefan International Postgraduate School
Ljubljana, Slovenia

Supervisor: Asst. Prof. Dr. Sabina Dolenec, Slovenian National Building and Civil Engineering Institute, Ljubljana, Slovenia
Co-Supervisor: Assoc. Prof. Dr. Nina Daneu, Jožef Stefan Institute, Ljubljana, Slovenia

Evaluation Board:
Assoc. Prof. Dr. Srečo Davor Škapin, Chair, Jožef Stefan International Postgraduate School and Jožef Stefan Institute, Ljubljana, Slovenia
Prof. Dr. Barbara Lothenbach, Member, Swiss Federal Laboratories for Materials Science and Technology, Dübendorf, Switzerland
Assoc. Prof. Dr. Mirijam Vrabec, Member, Faculty of Natural Sciences and Engineering, University of Ljubljana, Ljubljana, Slovenia

MEDNARODNA PODIPLOMSKA ŠOLA JOŽEFA STEFANA
JOŽEF STEFAN INTERNATIONAL POSTGRADUATE SCHOOL

Maruša Mrak

INFLUENCE OF TEMPERATURE ON THE HYDRATION OF BELITE-CALCIUM SULFOALUMINATE CEMENTS

Doctoral Dissertation

VPLIV TEMPERATURE NA HIDRATACIJO BELITNO-KALCIJEVO SULFOALUMINATNIH CEMENTOV

Doktorska disertacija

Supervisor: Asst. Prof. Dr. Sabina Dolenec

Co-Supervisor: Assoc. Prof. Dr. Nina Daneu

Ljubljana, Slovenia, October 2023

Acknowledgments

Firstly, I would like to thank Asst. Prof. Dr. Sabina Dolenec as my supervisor during my doctoral studies. I am very grateful for her guidance, patience, and understanding, and for providing me with opportunities for excellent research collaborations. I would also like to thank my co-supervisor Assoc. Prof. Dr. Nina Daneu, for her collaboration and for sharing her knowledge on microscopy techniques. I would like to thank the members of the Evaluation Board, Assoc. Prof. Dr. Srečo Davor Škapin, Prof. Dr. Barbara Lothenbach and Assoc. Prof. Dr. Mirijam Vrabec for the time and effort they invested in the review and for evaluating the dissertation.

I would also like to express my gratitude to Prof. Dr. Barbara Lothenbach and Dr. Frank Winnefeld for the enjoyable and successful scientific visit to EMPA and for all their help and support. At the same time, I would like to thank Prof. Dr. Christian L. Lengauer for the hospitality offered at the University of Vienna.

I would like to thank Dr. Erika Švara Fabjan and Tina Radoševič for conducting FE-SEM analysis, Ana Brunčič for her help with the rheological measurements and the coworkers at the Laboratory for Cements, Mortars and Ceramics for their help with the preparation of samples. Furthermore, I would like to thank my colleagues at ZAG for all the pleasant coffee breaks.

Last, but not least, I am very grateful for all the support and encouragement received from my family and friends throughout the course of my Ph.D.

Finally, I would like to acknowledge the support provided by the Slovenian Research Agency for this research, under contract number 1000-18-1502.

Abstract

In this doctoral thesis influence of different temperatures (5 °C - 60 °C) on the hydration of belite-ye'elimite-ferrite cement was studied. Fluctuations in temperature can cause changes in the phase assemblage, kinetics of hydration and mechanical properties. Besides temperature, other factors such as the cement clinker phase composition, calcium sulfate amount and the type of secondary raw material used in the raw meal affect the cement hydration, which was also studied in this work.

Cement clinkers with different phase compositions were synthesised from various natural and secondary raw materials. The cement was prepared by adding gypsum to the cement clinker based on the M-ratios selected. The kinetics of hydration was studied by isothermal calorimetry. The microstructure and phase composition of the hydrated cements at different hydration times were investigated by XRD, TGA, SEM/EDXS, FE/SEM, NMR, and TEM. The development of compressive strength of the cements was determined and porosity was assessed by MIP, while the rheological properties of cement pastes were investigated by rotational and oscillatory measurements. A thermodynamic model was established using GEMS and compared to the experimental data.

Elevated temperatures significantly accelerate early hydration. Ye'elimite and gypsum react rapidly at higher temperatures, leading to increased early compressive strength. The hydration of belite intensifies with temperature. Higher temperatures result in less ettringite due to its increased solubility, but more monosulfate. Higher temperatures also favor siliceous hydrogarnet over strätlingite and produce more C—S—H from belite, enhancing the compressive strength. At 60 °C, C—A—S—H is detected, as higher temperatures promote greater aluminum uptake from the solution. At 5°C, a dense, uniform microstructure is observed, whereas at higher temperatures it's more varied and intermixed. Although the chemical composition of ettringite and strätlingite remains unaffected by temperature fluctuations, it's observed that iron becomes more prominent at lower temperatures in siliceous hydrogarnet and C—S—H. At a low w/c, hydration of belite is slower at late ages, as ye'elimite consumes more water. In this case, the cements cured at 60 °C showed more residual gypsum, less ettringite and C—S—H at later ages, and lower strength, indicating a lower degree of hydration. More gypsum in the cement clinker accelerates hydration. A higher M-ratio increases ettringite and decreases monosulfate and strätlingite content, leading to a higher compressive strength. More belite produces a greater amount of siliceous hydrogarnet and C—S—H and less strätlingite. Cement with red mud shows accelerated hydration, due to more mayenite and alkali sulfates, compared to cement with natural raw materials and waste concrete. The impact of secondary raw materials on the hydration processes of belite and ferrite is noticeable at 5 °C but far less so at increased temperatures, while the impact on the hydration of ye'elimite is even smaller compared to belite. A rise in temperature leads to an enhanced storage modulus because of accelerated hydration, while its development is shifted to earlier times, due to the fast structural build-up formation at higher temperatures. The amount of ye'elimite increases viscosity, while the storage modulus is lower which was possibly attributed to its weaker gel structure.

Povzetek

V doktorski disertaciji smo proučevali vpliv različnih temperatur (od 5 do 60 °C) na hidratacijo belitno-ye'elimitno-feritnega cementa. Nihanja v temperaturi lahko povzročijo spremembe v fazni sestavi, kinetiki hidratacije in mehanskih lastnostih. Poleg temperature na hidratacijo teh cementov vplivajo tudi drugi dejavniki, kot so sestava cementnega klinkerja, količina kalcijevega sulfata in vrsta sekundarnih surovin, uporabljenih v surovinski mešanici, kar je bilo prav tako proučevano v disertaciji.

Cementni klinkerji z različnimi faznimi sestavami so bili sintetizirani iz različnih naravnih in sekundarnih surovin. Cement je bil pripravljen z dodajanjem sadre cementnemu klinkerju na podlagi izbranih M-razmerij. Kinetiko hidratacije smo proučevali z izotermno kalorimetrijo. Mikrostrukturo in sestavo faz hidratiziranih cementov pri izbranih časih hidratacije smo preiskovali z XRD, TGA, SEM/EDXS, FE/SEM, NMR in TEM. Razvoj tlačnih trdnosti vzorcev je bil določen, poroznost pa je bila ocenjena z MIP. Raziskane so bile reološke lastnosti cementnih past z rotacijskimi in oscilatornimi testi. Termodinamski model je bil vzpostavljen z uporabo programa GEMS in primerjan z eksperimentalnimi podatki.

Višje temperature znatno pospešijo zgodnjo hidratacijo. Ye'elimit in sadra hitro reagirata pri višjih temperaturah, kar vodi do višje začetne tlačne trdnosti. Hidratacija belita se povečuje s temperaturo. Pri višjih temperaturah nastane manj etringita zaradi povečane topnosti, vendar več monosulfata. Pri višjih temperaturah nastane več silicijevega hidrogranata kot strätlingita in več C—S—H iz belita, kar poveča tlačno trdnost. Pri 60 °C je prisoten C—A—S—H, saj višje temperature spodbujajo večjo vgradnjo aluminija iz raztopine. Pri 5 °C opazimo gosto, enotno mikrostrukturo, medtem ko je pri višjih temperaturah bolj raznolika in prepletena. Kemijska sestava etringita in strätlingita se ne spreminja pri različnih temperaturah, v silicijevem hidrogranatu in C—S—H pa je več železa prisotnega pri nižjih temperaturah. Pri nizkem v/c je pozna hidratacija belita upočasnjena, saj ye'elimite porabi več vode. V tem primeru imajo cementi, negovani pri 60 °C, več preostale sadre, manj etringita in C—S—H v poznejših fazah, in nižjo trdnost, kar kaže na nižjo stopnjo hidratacije.

Več dodane sadre cementnemu klinkerju pospešuje hidratacijo. Pri višjih M-razmerjih nastane več etringita in manj monosulfata, kar vpliva na tlačno trdnost, saj več etringita pomeni večjo trdnost. Če je več belita v klinkerju, nastane več silicijevega hidrogranata in C—S—H in manj strätlingita. Cement iz rdečega blata kaže pospešeno hidratacijo, zaradi več mayenita in alkalijskih sulfatov v primerjavi s cementom iz naravnih surovin in z odpadnim betonom. Vpliv sekundarnih surovin na hidratacijske procese belita in ferita je bolj opazen pri 5 °C, vendar je veliko manjši pri višjih temperaturah, medtem ko je vpliv na hidratacijo ye'elimita še manjši v primerjavi z belitom.

Višje temperature vodijo do povečanega elastičnega modula zaradi pospešene hidratacije, medtem ko se le-ta razvije prej zaradi hitrega nastajanja strukture pri višjih temperaturah. Količina ye'elimita poveča viskoznost, medtem ko je elastični modul nižji, kar je pripisano njegovi šibkejši strukturi.

Contents

List of Figures

List of Tables

Abbreviations

BFS	...	Blast furnace slag
BCSA	...	Belite-calcium sulfoaluminate
BCSAF	...	Belite-calcium sulfoaluminate-ferrite
BSE	...	Backscattered electrons
BYF	...	Belite-ye'elimite-ferrite
CAC	...	Calcium aluminate cement
CDW	...	Construction and demolition waste
EDXS	...	Energy dispersive X-ray spectroscopy
FA	...	Fly ash
FE	...	Field emission
FHWM	...	Full width at half maximum
ICSD	...	Inorganic crystal structure data
LC^3	...	Limestone calcined clay cement
MIP	...	Mercury intrusion porosimetry
NMR	...	Nuclear magnetic resonance
OPC or PC	...	(Ordinary) Portland cement
PSD	...	Particle size distribution
PXRD	...	Powder X-ray diffraction
SCM	...	Supplementary cementitious material
SEM	...	Scanning electron microscopy
SRM	...	Secondary raw materials
TEM	...	Transmission electron microscopy
TGA	...	Thermogravimetric analysis
XRD	...	X-ray diffraction
XRF	...	X-ray fluorescence

Chapter 1

Introduction

1.1 Low-Carbon Cements

Concrete is recognized to be both, the most manufactured product and the most widely utilized construction material globally [1], [2]. Notably, the cement sector, a vital subset of various industries, accounts for a substantial carbon footprint, generating approximately 8 % of total emissions [1], [3]. Consequently, the use of concrete has a significant impact on the environment [2]. In 2015, the total volume of cement produced globally exceeded more than 4 billion tonnes [1], [4]. Current projections claim that by 2050, the global demand for concrete will escalate in order to satisfy global construction needs (Figure 1.1), subsequently increasing the emissions of carbon dioxide emissions from cement production [2], [5].

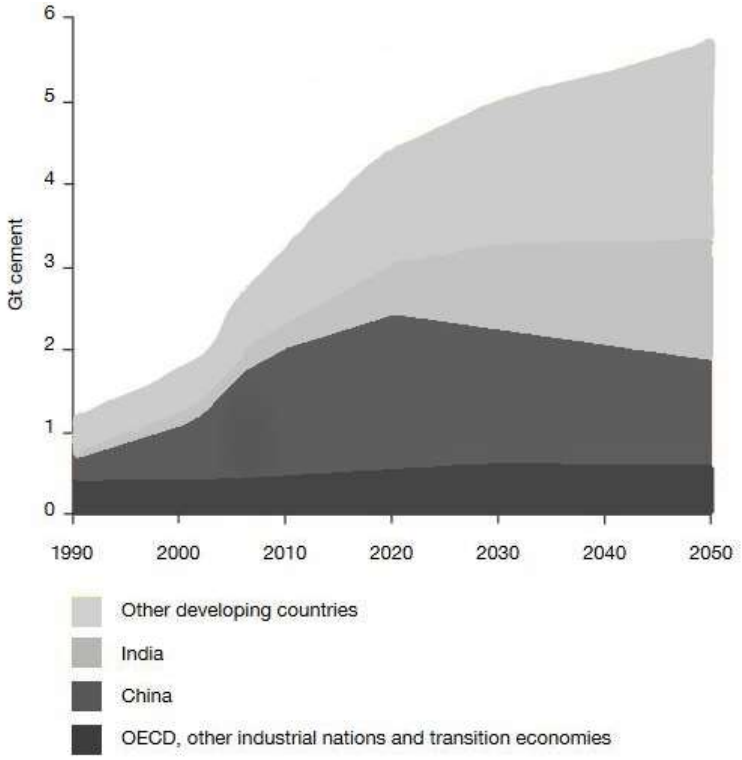

Figure 1.1: Cement production in industrialized and developing countries [6].

The production of ordinary Portland cement (OPC), the type of cement typically used worldwide, leads to the release of high amounts of carbon dioxide and requires are high energy consumption [1], [7]. In general, there are two sources of carbon dioxide: from the decomposition of limestone ($CaCO_3$) into CaO and CO_2 during the calcination process and from the combustion of fuel. Limestone is the main ingredient of Portland cement raw meal and its decomposition accounts for approximately 60 % of the overall CO_2 emitted. The rest results from the fossil combustion of fuel for energy production during clinkering in the kiln [5], [6].

It is imperative to take decisive action in order to diminish the environmental impact of construction over the coming decades. In line with this, numerous initiatives have taken place over recent decades aiming to develop concrete that is environmentally friendly [2], [5], [7], [8].

In addition to strategies employing carbon capture and storage to reduce carbon dioxide emissions [1], two main approaches have emerged. One approach is the use and replacement of a substantial proportion of clinker with supplementary cementitious materials (SCMs) such as fly ash (FA) and blast furnace slag (BFS) [2], [4]. However, considering the changes occurring in the energy sector (shift from the coal industry, increase of steel recycling) and the move towards more sustainable practices in other industries, the traditionally used SCMs may not be available in quantities sufficient to meet the demand for concrete and cement [1], [4]. Recent research has shown that clay, a material abundant worldwide, can serve as a highly reactive SCM when calcined at a high temperature (600 °C). Cements known as limestone calcined clay cement or LC^3 exhibit good performance, in addition, it is projected that the use of LC^3 could facilitate a reduction in CO_2 emissions between 15 and 30% [9]–[11].

The second approach to lowering carbon dioxide emissions is the use of alternative mineral binders. Alternative binders have the potential to reduce the environmental impact in comparison to conventional cements. Constraints related to the availability and cost of materials, however coupled with technical limitations rising from the use of alternative technologies, may prevent them from being used on a large scale in the coming decades [12], [13]. Many different alternative mineral binders have been proposed, including magnesium-based cements, hydraulic calcium silicate clinkers manufactured by hydrothermal processing, alkali-activated cements, carbonation-hardening cements, calcium sulfoaluminate cements (CSA), and belite-calcium sulfoaluminate cements (BCSA), amongst others [1], [4], [7], [14].

1.2 History and Potential of BCSA Cements

Over the past few decades, the development and use of mineral binders has shifted into a new generation of cements based on belite and ye'elimite. These cements are considered eco-friendly alternatives to traditional Portland cement, reducing CO_2 emissions by approximately 30% compared to that generated from Portland cement and consuming less energy during their production [7], [12], [14]–[16].

Researchers have found that by combining ye'elimite ($C_4A_3\overline{S}$; constituting over 50 %), the main phase of calcium sulfoaluminate (CSA) cements with belite (C_2S) - a relatively slow-reacting clinker phase found in ordinary Portland cement - it is possible to combine the advantages of both systems in a single material, known as belite-calcium sulfoaluminate (BCAS) cements (Figure 1.2) [12], [15]. The hydration of ye'elimite results in the formation of ettringite ($C_6A\overline{S}_3H_{32}$), which facilitates a high early strength (owing to the very high reactivity of ye'elimite), while the hydration of belite leads to the formation of calcium silicate hydrates (C—S—H), which contribute to the late age

strength of the cements [14], [16]. Calcum sulfoaluminate cements are primarily divided into two categories: high ye'elimite calcium sulfoaluminate cements and low ye'elimite calcium sulfoaluminate cements or belite-calcium sulfoaluminate cements [17]. The literature identifies two primary sub-groups of BCSA clinkers: iron-rich and aluminium-rich BCSA clinkers [18]. Iron-rich clinkers contain belite, ye'elimite, and at least 5 wt. % of ferrite phase. Meanwhile, aluminium-rich clinkers feature aluminium-rich minor phases like mayenite and calcium aluminate [18]–[20]. Due to the economic challenges and profitability concerns associated with the mass production of high-aluminium clinkers, such as the cost of Al-sources and sintering temperature, current research is heavily leaning towards iron-rich BCSA clinkers. These types of cements have been designated with the name "belite–calcium sulfoaluminate–ferrite" (BCSAF) cements [21] but the preferred nomenclature nowadays tends to be the more concise "belite–ye'elimite–ferrite" (BYF) cements [5], [12].

One of the main advantages of these cement clinkers is that the rotary kiln systems used in manufacturing are fundamentally the same as those used for the Portland clinker [5], [14]. Belite-calcium sulfoaluminate cements demand a lower sintering temperature within the kiln, typically ranging between 1250–1350 °C. This is considerably lower compared to ordinary Portland cement, which undergoes sintering at temperatures between 1400-1500 °C, a range where the formation of alite (C_3S), a principal clinker phase in ordinary Portland cement, occurs. Additionally, this reduction in sintering temperature leads to a reduction in NOx emissions [16]. Belite-calcium sulfoaluminate cement clinkers have a higher porosity, making them easier to grind [7], [16], [22]. They usually contain a minimum of 3% sulfur, denoted as SO_3, which is mostly found in the ye'elimite phase. Given that contemporary cement kiln systems are exceedingly efficient at SO_2 scrubbing, the vast majority of the sulfur is retained within the clinker, resulting in minimal emissions into the atmosphere [12].

Moreover, the reduction in the amount of CO_2 is also attributed to the smaller quantity of limestone (20-30 %) used in the raw meal. This means, it contains a lower amount of calcium carbonate, which transforms into calcium oxide and CO_2 during the clinker formation process. A part of the calcium carbonate is substituted by calcium sulfate [7], [12], [16].

The primary raw materials used for the production of cement clinker for belite-calcium sulfoaluminate cements include limestone, clay, and bauxite, with the addition of calcium sulfate to provide the CaO, SiO_2, Al_2O_3, and SO_3 required for phase formation [23]. Industrial by-product or waste materials, referred to as secondary raw materials (SRM), can be utilized for the production of belite-calcium sulfoaluminate cements, thus contributing to the preservation of natural raw materials [16], [24]–[26]. Examples of such materials include slag, fly ash, phosphogypsum and red mud amongst others [16], [24], [26].

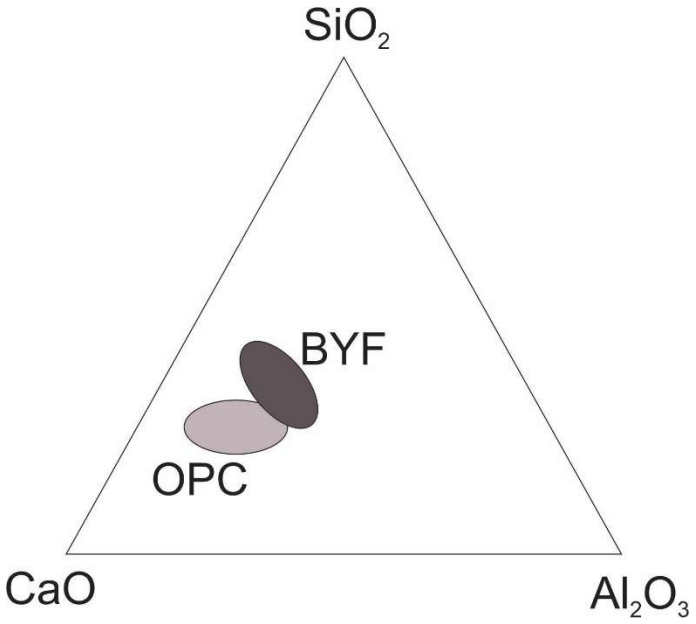

Figure 1.2: Ternary CaO-Al_2O_3-SiO_2 diagram. The diagram showing the chemical composition of OPC and BYF cement clinkers (adapted by [27], [28]).

The major phase in belite-calcium sulfoaluminate cement clinker is belite (typically about 30-50 %), while the other two main phases are ye'elimite (25-50 %), and ferrite (5-20 %) [5], [29]. The cement is formulated by mixing the finely ground clinker with calcium sulfate in the form of gypsum ($C\overline{S}H_2$), bassanite ($C\overline{S} \cdot 0.5H$) or anhydrite ($C\overline{S}$). Calcium sulfate works as a setting regulator and can be used to alter the hydration [23], [30]. The performance and properties of belite-calcium sulfoaluminate cements are influenced by several factors, including the raw materials chosen, the clinkering process, the composition of the clinker, the fineness of the cement, the kinetics of hydration and the microstructure development, amongst other things. [31].

Although calcium sulfoaluminate cements have been produced for several decades, because of their specific characteristic their use has been limited to specific applications and special cement markets. Currently, belite-calcium sulfoaluminate cements are not produced or used on a large scale in Europe. In the United States, belite-calcium sulfoaluminate cements have been used for highways and airfield pavements for more than 30 years [32]. Over the past three decades, BCSA technology has developed substantially in China, and Chinese norms have been established to govern this category of cement [6]. Nonetheless, its usage is presently confined to specialized structural and non-structural applications, largely because of its higher cost compared to ordinary Portland Cement [6], [33], [34].

1.3 Cement Chemistry Nomenclature

In cement chemistry, chemical compositions are denoted using their respective oxides. Special notations are utilized when expressing these oxides in cement nomenclature. It is noteworthy that compounds written with these notations do not, however, represent pure compounds, as they also contain various impurities. For the representation of pure compounds, comprehensive chemical formulas are used. These oxides form different minerals, which are identified as phases within the context of cement chemistry [35], [36].

The main abbreviations for these oxides are presented in Table 1.1, while the main cement clinker phases along with the hydration products, are shown in Table 1.2.

Table 1.1: Cement chemistry notation for the main oxides present in cements.

Cement chemistry notation	Chemical formula
C	CaO
S	SiO_2
A	Al_2O_3
F	Fe_2O_3
H	H_2O
$\overline{C}$	CO_2
$\overline{S}$	SO_3

Table 1.2: Cement chemistry notation for the main cement clinker phases and hydration products.

Phase	Cement chemist notation	Chemical formula
Alite	C_3S	Ca_3SiO_5
Aluminium hydroxide (gibbsite)	AH_3	$Al(OH)_3$
Anhydrite	$C\overline{S}$	$CaSO_4$
Aphtitalite	$K_3N\overline{S}_4$	$K_3Na(SO_4)_2$
Arcanite	$K\overline{S}$	K_2SO_4
Bassanite	$C\overline{S} \cdot 0.5H$	$2CaSO_4 \cdot H_2O$
Belite	C_2S	Ca_2SiO_4
Calcium aluminate decahydrate	CAH_{10}	$CaAl_2O_4 \cdot 10H_2O$
Calcium monosulfate	$C_4A\overline{S}H_{12}$	$3CaO \cdot (Al,Fe)_2O_3 \cdot CaSO_4 \cdot nH_2O$
Calcium silicate hydrate	C—S—H	$3CaO \cdot SiO_2 \cdot 4H_2O$
Dicalcium aluminate hydrate	C_2AH_8	$2CaO \cdot Al_2O_3 \cdot (8\pm n)H_2O$
Ettringite	$C_6A\overline{S}_3H_{32}$	$Ca_6Al_2(SO_4)_3(OH)_{12} \cdot 26H_2O$
Ferrite	C_4AF	$Ca_2(Al,Fe)_2O_5$
Gehlenite	C_2AS	$Ca_2Al_2SiO_7$
Gypsum	$C\overline{S}H_2$	$CaSO_4 \cdot 2H_2O$
Iron hydroxide	FH_3	$Fe(OH)_3$
Katoite	C_3AH_6	$Ca_3Al_2(OH)_{12}$
Lime	C	CaO
Magnetite	fF	Fe_3O_4
Mayenite	$C_{12}A_7$	$12CaO \cdot 7Al_2O_3$
Monocalcium aluminate	CA	$CaAl_2O_4$
Monocarbonate	$C_4A\overline{C}H_{11}$	$3CaO \cdot Al_2O_3 \cdot CaCO_3 \cdot 11H_2O$
Pentacalcium trialuminate	C_5A_3	$5CaO_3\ Al_2O_3$

Periclase	M	MgO
Perovskite	CT	$CaTiO_3$
Portlandite	CH	$Ca(OH)_2$
Siliceous hydrogarnet	$C_3(A,F)SH_4$	$C_3(A,F)SH_4$
Strätlingite	C_2ASH_8	$Ca_2Al_2SiO_7 \cdot 8H_2O$
Ternesite	$C_5S_2\overline{S}$	$Ca_5(SiO_4)_2SO_4$
Tricalcium aluminate	C_3A	$Ca_3Al_2O_6$
Water	H	H_2O
Ye'elimite	$C_4A_3\overline{S}$	$Ca_4(AlO_2)_6SO_4$

1.4 Phase Composition of BCSA Cement Clinker

Belite-calcium sulfoaluminate cement clinkers contain three main phases: belite, ye'elimite and ferrite. The presence and proportion of additional minor phases depend on the quantity and origin of the raw materials used [23], [37], [38].

1.4.1 Belite

Belite (C_2S), which is di-calcium silicate found naturally as larnite, typically constitutes 40-55 % of the mass. It is one of the main phases in ordinary Portland cement [12]. The hydration of belite usually takes place in the later stages, significantly affecting the density of the cement's microstructure [37], [39].

Belite can exist in several polymorphic forms, including α, α'_L, α'_H, β or γ-belite [15], [31]. At high temperatures, α-C_2S is stable and transitions into α'_H-C_2S at 1425 °C. This form remains stable up to a temperature of 1160 °C, at which point, it transforms into α'_L-C_2S. At a temperature of around 650 °C, α'_L-C_2S transforms into β-C_2S. Further cooling causes the transformation of β-C_2S into γ-C_2S, a modification that is stable at room temperature [36].

Belite consists of Ca^{2+} and SiO_4^{4-} ions [40]. The distribution of these ions is similar in both the alpha (α, α'_L, and α'_H) and beta (β) polymorphs, but differences occur in the gamma (γ) polymorph [40]. These differences are associated with the lower density of the γ-modification, which is also the reason for the stability of γ-C_2S at room temperature [40]. Moreover, the polymorphs of C_2S also differ in terms of the arrangement of ions within the crystal structure. The alpha modifications contain Ca^{2+} cations coordinated with eight or nine oxygens ions in an irregular spatial arrangement, while the crystal structure of β-C_2S has two Ca^{2+} cations surrounded by eight oxygen ions in an irregular spatial coordination. In contrast, the crystal structure of γ-C_2S is characterized by having two Ca^{2+} cations in a regular octahedral coordination [41]. Substitutions occasionally occur in the crystal lattice of belite; monovalent and divalent ions replace Ca^{2+} ions, while multivalent ions such as Al^{3+}, Fe^{3+}, and S^{6+} substitute Si^{4+} ions [42].

Increased reactivity can be realized through rapid quenching of the clinker, which stabilizes the high-temperature α-belite polymorph, by incorporating different ions as activators [43]. The addition of minor components such as Mg, Na, B, K, S, or Na helps stabilize the reactive α-belite polymorph [15].

1.4.2 Ye'elimite

Ye'elimite ($C_4A_3\overline{S}$) is a naturally occurring form of calcium sulfoaluminate. This phase usually constitutes 10-35 wt. % of belite-calcium sulfoaluminate cement clinkers, while it is the major phase in calcium sulfoaluminate cement clinkers. Ye'elimite forms at temperatures of approximately 1100 °C and remains stable up to approximately 1400 °C [16]. At high sintering temperatures, ye'elimite starts to decompose, leading to the evaporation of sulfur and the formation of other phases, such as $C_{12}A_7$, and CA [44].

Ye'elimite can appear in two distinct polymorphic forms: cubic and orthorhombic. The form depends on the presence of specific ions in its crystal structure [31], [45]. The properties of ye'elimite depend on the size and the distribution of ions. Substitutions are common; Ca^{2+} is replaced with Mg^{2+} and Na^{+}, while Al^{3+} is replaced with Si^{4+}, Fe^{3+}, B^{3+}, and Ti^{3+} [16], [46]. The incorporation of minor elements such as iron and boron into ye'elimite can change its reactivity, and it can further increase the reactivity of belite [12]. The incorporation of iron ions into the ye'elimite structure can stabilize the cubic form of ye'elimite over the orthorhombic form [31]. The cubic ye'elimite, which contains iron, exhibits slower consumption during hydration and consequently produces less ettringite [45]. This results in a reduced heat of hydration in comparison to the orthorhombic form of ye'elimite, which doesn't contain iron [45]. The hydration of ye'elimite plays a key role in determining the early age properties of cement, significantly contributing to high early strength [37], [39]. The presence of calcium sulfate accelerates the hydration of ye'elimite [45].

1.4.3 Ferrite

Ferrite (C_4AF) is a calcium alumino-ferrite, which naturally occurs in the form of brownmillerite [12]. The ferrite phase is an orthorhombic solid solution with the composition $Ca_2(Al_xFe_{1-x})_2O_5$ (x = 0 - 0.7), with a continuous series formed from C_2F to C_6A_2F. Each of the 2 Ca^{2+} ions are surrounded by seven oxygens, in combination with Al^{3+} and Fe^{3+} ions, which are distributed between octahedral and tetrahedral sites. Fe^{3+} ions are substituted by Mg^{2+}, while Al^{3+} ions are substituted by Si^{4+} and Ti^{4+} ions [17].

Typically, belite-calcium sulfoaluminate cement clinker contains between 5 and 20 wt. % of the ferrite phase. The incorporation of ferrite in the production of belite-calcium sulfoaluminate cements enables the utilization of industrial by-products rich in iron, as raw materials [12]. Ferrite is a slow reactive phase, much slower than ye'elimite, although plays a minimal role in enhancing the early strength of the cement. It is often termed the "flux phase" because it crystallizes from liquid melt in the kiln when it is cooled. This liquid phase is important, as it accelerates the reactions within the clinker. Furthermore, the ferrite phase can form a solid solution, accommodating various minor elements such as titanium, silicon, and magnesium in the clinker [35], [36]. In addition, up to 2.5 % of C_3A and C_5A_3 and even up to 5 % of CA can be taken in the solid solution of C_4AF [47].

1.4.4 Calcium Sulfate

Calcium sulfate can be incorporated at different stages in the cement production process: it can either be mixed with other primary raw materials during the clinker production stage or added to the clinker when the cement is being prepared [37], [39]. Calcium sulfate controls the kinetics of hydration, thereby determining factors such as the initial setting time, the development of strength, and the volumetric expansion of the cement [33], [39], [48], [49]. Anhydrite can be formed during the sintering of clinker [37]. These can result from: (a) a lack of alumina or surplus lime in the initial feed, (b) insufficient

temperature to transition $C\overline{S}/C_2AS$ to $C_2S/C_4A_3\overline{S}$, (c) inadequate residence time leading to incomplete conversion, or (d) not appropriate SO_2 and O_2 partial pressures of SO_2 and O_2 in the kiln [50]. Different sources of calcium sulfate such as anhydrite, basanite and gypsum can be added to cement clinker. Bassanite exhibits the highest dissolution rate, causing reactions to start very early and significantly shortening the initial setting time. This makes it challenging to achieve homogeneity in the samples. On the other hand, anhydrite has the slowest dissolution rate, leading to extended initial setting times. This results in a high plasticity, to accommodate the formation of ettringite [30]. Gypsum with ye'elimite stands at an intermediate level: it reacts faster than anhydrite but slower than basanite [51].

1.4.5 Minor Phases

In addition to the major components, belite-calcium sulfoaluminate cement clinkers may contain small quantities- between 0.01 wt. % and 10 wt. %, of other phases called minor phases, such as ternesite, gehlenite, mayenite, perovskite, periclase, arcanite, magnetite, and excess lime. The components mentioned can be introduced into the clinker raw meal using natural raw materials, alternative fuels, supplementary cementitious materials (SCM), or industrial by-products and waste [52]. These materials are present in lesser amounts but may still influence the properties and behavior of the cement to a varying degree [31].

1.5 Hydration of BCSA Cements

The hydration of belite-calcium sulfoaluminate cements is characterized by three main features:

1. The dissolution of crystalline anhydrous phases such as belite, ye'elimite and ferrite.
2. The formation of crystalline phases such as ettringite, strätlingite and monosulfate, accompanied by the development of amorphous phases including gibbsite and calcium silicate hydrate and the amorphous part of other crystalline AFm phases (aluminate ferrite mono; such as calcium monosulfate, strätlingite).
3. The consumption of free water [15], [38], [53].

1.5.1 Hydration of Ye'elimite

Firstly, at early age of hydration, ettringite ($C_6A\overline{S}_3H_{32}$) or Aft phase (aluminate ferrite tri) is formed from ye'elimite which reacts with calcium sulfate (gypsum, basanite or anhydrite) and water [15], [29], [49]. This reaction also gives amorphous or poorly crystalline aluminium hydroxide (AH_3) as a product [15], [20], [23], [30], [49], [54], according to Eq. (1.1):

$$C_4A_3\overline{S} + 2\,C\overline{S}H_x + (38-2x)\,H \rightarrow C_6A\overline{S}_3H_{32} + 2\,AH_3\ (x = 0,0.5,2) \tag{1.1}$$

This reaction is significantly influenced by the water to cement ratio as well as the quantities of ye'elimite and calcium sulfate in the cement. This process tends to consume a substantial portion of the initial water volume, with the resulting hydrates rapidly filling the initial porosity. Typically concluding within 1 to 2 days, although sometimes

as early as 6 hours; this reaction provides the mixture high early mechanical strength [55].

Ettringite formation occurs when the molar ratio of calcium sulfate to ye'elimite, referred to as the "M-value", is less than 2 (M < 2), and continues until the all available calcium sulfate is exhausted [45], [56]–[58]. On the other hand, if this M-value exceeds 2 (M > 2), a residual quantity of calcium sulfate remains even after the hydration process has been completed [48], [56]. Calcium sulfoaluminate cements, which are generally characterized by rapid setting and hardening, typically exhibit an M-value below 1.5, whereas in the case of expansive cements, the M-value usually ranges between 1.5 and 2.5 [34], [56], [59].

If there is sufficient water still available when the source of the calcium sulfate is depleted, calcium monosulfate or usually denoted just monosulfate ($C_4A\overline{S}H_{12}$) begins to precipitate, again together with aluminum hydroxide [20], [34], [45], [57], [60], according to Eq. (1.2):

$$C_4A_3\overline{S} + 18\,H \rightarrow C_4A\overline{S}H_{12} + 2\,AH_3 \tag{1.2}$$

1.5.2 Hydration of Belite

The hydration reactivity of belite is slow and leads to later strength development [37]. The hydration of belite consumes the aluminium hydroxide that has already precipitated, leading to the formation of strätlingite (C_2ASH_8) [20], [55], [57], according to Eq. (1.3):

$$C_2S + AH_3 + 5\,H \rightarrow C_2ASH_8 \tag{1.3}$$

If aluminum hydroxide is no longer present, calcium silicate hydrates (C–S–H) and portlandite (CH) precipitate [20], [23], [31], [57], as delineated in Eq. (1.4):

$$C_2S + nH \rightarrow C-S-H + mCH \tag{1.4}$$

1.5.3 Hydration of Ferrite

The reactivity of ferrite throughout hydration in these kinds of cements is notably slower compared to that of ye'elimite and remains somewhat unclear and complex due to the formation of solid solutions between iron- and aluminium-containing hydrates which could stabilize the iron-rich AFt [61] and iron-rich AFm [62].

Following the depletion of gypsum, the hydration of ferrite can contribute to a higher amount of monosulfate, according to Eq. (1.5). The portlandite that has precipitated will engage in later reactions, like combining with aluminium hydroxide to produce AFm phases.

$$2\,C_4AF + C_6A\overline{S}_3H_{32} + 12\,H \rightarrow 3\,C_4A\overline{S}H_{12} + 2\,FH_3 + 2\,CH \tag{1.5}$$

Siliceous hydrogarnet containing iron ($C_3(A,F)SH_4$) may form through the hydration of ferrite [20], facilitated by the presence of strätlingite, as described in Eq. (1.6):

$$C_4AF + C_2ASH_8 + 3\,H \rightarrow 2\,C_3(A,F)SH_4 + AH_3 \tag{1.6}$$

1.6 The Influence of Temperature on the Cement Hydration

The hydration of belite-calcium sulfoaluminate cements is considerably complex, largely owing to the many variations in the composition of the cement clinker. Current research investigating the impact of various parameters on the hydration of belite-calcium sulfoaluminate cements is relatively limited, and their findings are incomparable to studies on ordinary Portland or calcium sulfoaluminate cements, both of which have been studied more extensively. Furthermore, in addition to the effect of temperature, the hydration of these cements is significantly influenced by various other parameters, including the quantity and reactivity of the calcium sulfate added, the fineness of the cement particles, the water-to-cement ratio, and the presence of minor phases, amongst other things [20].

Temperature is a crucial factor affecting the development of hydration products and the kinetics of the hydration process. Cements are subjected to various temperatures, both due to diverse climate conditions and because of the hydration heat produced during the setting time of concrete. These variations in temperature significantly influence the kinetics of hydration, altering the composition of the pore solution and affecting the precipitation, as well as the morphology and stability of the hydrates formed [63].

The influence of temperature on the hydration of Portland cement and blended Portland cements [63]–[71] has been thoroughtly investigated, while some tudies have also been performed on calcium sulfoaluminate cements [39], [72]–[74]. Studies in the literarature examining the effect of temperature on the hydration of belite-calcium sulfoaluminate cements are, however, scarce. It is important to assess the sensitivity of cements to temperature in order to verify if a particular cement can perform reliably across a diverse range of environmental conditions.

1.6.1 The Influence of Temperature on Portland Cement and Blended Portland Cements

Investigations concerning the effect of temperature on the hydration kinetics of Portland cement and blended Portland cements have revealed that cement pastes exhibit accelerated hydration at higher temperatures, which contributes to early strength gain [65], [68], [69], [71], [75], [76]. Conversely, a decrease in temperature lowers the hydration rate [70]. Higher temperatures also contribute to significant changes in the stability of the hydrated phases [63], [65]. When subjected to elevated temperatures, hydrates like ettringite and monocarbonate show lower stability and calcium monosulfate starts to form instead of ettringite. This is primarily attributed to the increased solubility of ettringite in such conditions, making it less stable compared to other compounds like calcium monosulfate and siliceous hydrogarnet [65], [77], [78]. Lower temperatures promote the development of a denser and more homogeneous matrix, a result of the slow yet persistent hydration process. Furthermore, at low temperatures, the porosity within the C—S—H gel is increased, accompanied by a decrease in its density [63], [67], [79], [80]. In contrast, at elevated temperatures, uneven distribution of the hydration products has been observed, together with coarser porosity [65], [69]. A noticeable decrease in the amount of ettringite and the formation of significantly shorter needles of ettringite is also apparent at higher temperatures [65].

Also the crystallinity of aluminium hydroxide is significantly affected by temperature. At room temperature or below, aluminium hydroxide precipitates in a nanocrystalline

amorphous form. At temperatures exceeding 60 °C, however, its less soluble form, gibbsite, precipitates [78].

1.6.2 The Influence of Temperature on Calcium Sulfoaluminate Cement

Studies investigating the effect of temperature on the hydration kinetics of calcium sulfoaluminate cements (high ye'elimite calcium sulfoaluminate cements) have indicated as with Portland cement, elevated temperatures accelerate hydration [39], [72], [74]. Compressive strength during the early ages is found to increase with elevated temperatures [72]. Some researchers have reported a decrease in compressive strength at later ages at higher temperatures [72], [74]. Additionally, the porosity of calcium sulfoaluminate cement tends to decrease at lower temperatures, resulting in a less heterogeneous microstructure [74], [81], as has previously been shown in Portland cements. Although different curing temperatures do not alter the types of hydrates formed, they do affect the quantities of these hydrates [72]. The hydration rate of ettringite formation noticeably accelerates at higher temperatures [39]. It has been shown in ye'elimite-rich calcium sulfoaluminate cements that ettringite remains stable up to about 90 °C in the absence of monocarbonate. This stability can have a positive effect on the compressive strength of cement pastes [73], [82].

1.6.3 The Influence of Temperature on Belite-Calcium Sulfoaluminate Cement

In contrast to Portland cement and ye'elimite-rich calcium sulfoaluminate cement, limited research exist concerning the effect of temperature on the hydration of belite-rich calcium sulfoaluminate cements. The heat of hydration has been studied by isothermal calorimetry at 5 °C, 23 °C and 38 °C [23] and the results were comparable to those seen in ordinary Portland and blended Portland cements. Increasing the temperature to 38 °C led to rapid strength development compared to 23 °C., whereas at 5 °C the hydration was considerably slower [23]. Another study investigated the impact of temperature on the hydration of belite-ye'elimite cement containing only a very small amount of Fe in the system[83]. The hydration degree of belite increased at both 5°C and 60°C, leading to the formation of C—S—H. Strätlingite amount was found to be lower at elevated temperatures. At 60°C, siliceous hydrogarnet was identified in small amounts, which was attributed to the low amount of Fe present in the system [83].

1.7 Research Aims and Hypothesis

Given that cement is one of the most important building materials understanding its hydration is crucial. It is further important to study hydration at both higher and lower temperatures, as temperature can alter both (i) the kinetics of hydration and (ii) the composition of the hydration products. This is significant, since it is possible to use cement both during summer (or hot conditions) and winter (or cold conditions), while the hydration heat produced when concrete is setting also results in a change of temperature. The results of the research will thus help understand the effect of hydration of belite-calcium sulfoaluminate cement on the final physico-mechanical properties and durability, which will contribute to the use of such materials in practice. In particular, it is important to acquire data on temperature dependence that influences the changes and stability of a particular hydration product and that could lead to the deterioration of

mechanical properties and consequently the potential collapse of an object. Furthermore, the effect of clinker composition and microstructure on the hydration process, hydration products, and mechanical properties of cements has not been reported in full. The hydration kinetics and chemistry are not well understood and sometimes contradictory, such as the hydration of the ferrite phase or the formation of different hydration products, not only at low and elevated temperatures, but also at room temperature. The physical and mechanical properties of cement reflected on the macro-level are directly related to its microstructure and nanostructure, so it is therefore essential to understand the structure at different levels.

The main aim of the dissertation is to study the hydration processes of belite-calcium sulfoaluminate cements of various compositions at different temperatures, with the specific objectives as follows:

1) To determine how different temperatures affect the kinetics and course of the hydration process of belite-calcium sulfoaluminate cements.

2) To investigate the influence of temperature on the formation of hydration products, changes in their composition and morphology and on the conversion and stability of phase assemblage.

3) To determine the effect of temperature on the physico-mechanical properties of belite-calcium sulfoaluminate cements.

4) To investigate the influence of different amounts of calcium sulfate on the hydration process and precipitation of hydrates of belite-calcium sulfoaluminate cements.

5) To study the hydration of belite-calcium sulfoaluminate cements made from clinkers with different phase compositions.

6) To study the hydration of belite-calcium sulfoaluminate cements made from different raw materials at various temperatures.

The main working hypotheses are as follows:

- Temperature significantly affects the course of hydration processes and the composition of hydration products.

- The properties of cement depend on the reaction kinetics and hydration of the clinker phases, both of which are temperature-dependent.

- The hydration temperature will affect the long-term stability and phase conversions and consequently the physico-mechanical properties of the cement in its solidified state.

- The initial phase composition of the cement clinker (i.e., the proportions of ye'elimite, belite and ferrite) significantly affects the hydration, as well as resulting composition of the hydration products.

- The introduction of different raw materials into the cement clinker mixture will change the hydration kinetics and the hydrate assemblage.

- The amount of calcium sulfate determines the phase assemblage precipitated and affects the physico-mechanical properties of the cement.

1.8 Layout of the Thesis

The thesis is organized into 8 distinct chapters, with the contents presented as follows:

- Chapter 1 includes the introduction, where the scientific background is presented alongside the state of art. The main aims, hypothesis, approach, and the layout of the thesis are described.

The subsequent chapters (from 2 to 7) present the principal findings of this research. Chapters 2, 3 and 4 are original papers that have already been accepted and published in international scientific journals are included in the Science Citation Index and referenced in the Web of Science with an Impact Factor. Chapters 5, 6 and 7 are written in a format suitable for submission to peer-reviewed journals, some of these have already been submitted, while others are currently at a stage of preparation.

- Chapter 2 is a paper published in the international peer-reviewed journal Ceramics International entitled: '*Phase development and hydration kinetics of belite-calcium sulfoaluminate cements at different curing temperatures'*. The paper reports results on the hydration of belite-calcium sulfoaluminate cement at ambient and elevated temperatures, using a variety of experimental techniques.

- Chapter 3 is a paper published in the international peer-reviewed journal Minerals entitled: '*Quantitative in situ X-ray diffraction analysis of early hydration of belite-calcium sulfoaluminate cement at various defined temperatures'*. The paper provides the results from a study investigating the influence of temperature on the early hydration (first 24 hours) of belite-calcium sulfoaluminate cement.

- Chapter 4 is a paper published in the international peer-reviewed journal Materials and Structures entitled: '*The influence of calcium sulfate content on the hydration of belite-calcium sulfoaluminate cements with different clinker phase compositions'*. The paper discusses how different amounts of calcium sulfate control the phase assemblage and physico-mechanical properties of belite-calcium sulfoaluminate cement.

- Chapter 5 is a paper submitted to the international peer-reviewed journal Construction and Building Materials entitled: '*Experimental study and thermodynamic modelling of the temperature effect on the hydration of belite-ye'elimite-ferrite cements'*. The paper presents the results of a study investigating the influence of low, ambient and elevated temperatures on the hydration of belite-calcium sulfoaluminate cement through experimental work and thermodynamic modelling.

- Chapter 6 is a paper currently being prepared with the working title: '*Influence of different secondary raw materials on the physico-mechanical properties and hydration evolution of belite-ye'elimite-ferrite cement at different curing temperatures'*. The paper provides the results of a study investigating how

incorporation of various secondary raw materials into cement clinker raw meal affects the hydrate phase assemblage and hydration kinetics when exposed to different curing temperatures.

- Chapter 7 presents the results of a research study yet to be published, with a working title: '*Rheological properties of belite-calcium sulfoaluminate cement at defined temperatures'.* The paper presents the results regarding the rheological behavior of belite-calcium sulfoaluminate cement pastes in a fresh state at defined temperatures.

Chapter 8 summarizes the main findings of the doctoral dissertation.

Chapter 2

Phase Development and Hydration Kinetics of Belite-Calcium Sulfoaluminate Cements at Different Curing Temperatures

This chapter is based on the published paper: M. Borštnar, N. Daneu, S. Dolenec, "Phase development and hydration kinetics of belite-calcium sulfoaluminate cements at different curing temperatures," *Ceramics international*, vol. 46, iss. 18, pp. 29421-29428, 2020 [84].

Belite-calcium sulfoaluminate cement has gained attention in the cement industry for its potential environmental benefits over traditional ordinary Portland cement [12], [15]. Owing to the reduced sintering temperature and a lower decarbonation of limestone, the manufacturing process for belite-calcium sulfoaluminate cement is more eco-friendly than conventional cements[7], [16], [22]. The hydration of belite-calcium sulfoaluminate cements is highly influenced by variations in temperature, which originate from varying environmental conditions and heat produced during cement hydration [69], [75]. These differences in temperature do not only impact the hydration kinetics but also the types of hydrates that form.

The study deals with the effect of temperature on the hydration of belite-calcium sulfoaluminate cement using various experimental techniques. Molar ratio of calcium sulfate to ye'elimite (M-value) of 4.3 was used, while phase composition was 65 wt. % belite, 20 wt. % ye'elimite and 10 wt. % ferrite. Three curing temperatures, 20 °C, 40 °C and 60 °C, were selected. The investigation focused on analyzing the composition and microstructure of hydration products at different hydration times (specifically at 1, 7, 28, and 90 days of hydration). Various experimental techniques were employed for this research to determine the hydrate assemblage that formed during hydration, including differential thermal analysis and thermogravimetric analysis, X-ray powder diffraction and Rietveld refinement. These results were further analysed using field emission scanning electron microscopy to provide a comprehensive view of the microstructure forming. The hydration kinetics were studied using isothermal calorimetry, and the development of compressive strength of the cement pastes was determined.

The results revealed faster hydration and higher early compressive strength at higher temperatures. The hydration product formed were ettringite, aluminium hydroxide and C—S—H, while their amounts were more similar at 20 and 40 °C, than at 60 °C. Cements cured at 60 °C contained a lower amount of ettringite, together with more unreacted gypsum and a lower compressive strength at later ages, indicating a lower degree of

hydration at higher temperatures. Furthermore, elevated temperatures led to the formation of smaller ettringite crystals, due to the accelerated hydration of ye'elimite and altered the presence of other hydration products, including a notable decrease in belite hydration and C—S—H formation at 60 °C.

This chapter addresses the thesis objectives 1, 2 and 3.

The contribution of the doctoral candidate was writing the first draft of the manuscript and conducting the experiment detailed in the manuscript, including preparation of the materials (cement clinker and cement) and performing the majority of the experiments (differential thermal analysis and thermogravimetric analysis, X-ray powder diffraction, Rietveld refinement, isothermal calorimetry, compressive strength measurements).

Ceramics International 46 (2020) 29421–29428

Contents lists available at ScienceDirect

Ceramics International

journal homepage: www.elsevier.com/locate/ceramint

Phase development and hydration kinetics of belite-calcium sulfoaluminate cements at different curing temperatures

Maruša Borštnar[a,b,*], Nina Daneu[c], Sabina Dolenec[a]

[a] Slovenian National Building and Civil Engineering Institute, Dimičeva ulica 12, 1000, Ljubljana, Slovenia
[b] Jožef Stefan International Postgraduate School, Jamova cesta 39, 1000, Ljubljana, Slovenia
[c] Jožef Stefan Institute, Jamova cesta 39, 1000, Ljubljana, Slovenia

ARTICLE INFO

Keywords:
Hydration
Cement
Temperature
Belite
Calcium sulfoaluminate

ABSTRACT

The influence of different curing temperatures on the hydration of belite-calcium sulfoaluminate cement was investigated at 20, 40 and 60 °C. The hydration kinetics and the hydrated phase assemblages were studied by isothermal calorimetry, X-ray powder diffraction, differential thermal analysis and thermogravimetric analysis, as well as field emission scanning electron microscopy. The compressive strength development of the cement pastes was also determined. Results showed that, at early ages, hydration was faster and early compressive strength was higher at elevated temperatures than at ambient temperature. On the other hand, at late ages in cement pastes cured at 60 °C, the amount of ettringite decreased, leading to lower compressive strength, indicating that the degree of hydration was lower at higher temperatures. Moreover, at elevated temperatures prismatic ettringite crystals became smaller due to faster hydration. Other hydration products present were aluminium hydroxide, which is formed together with ettringite from the hydration of calcium sulfoaluminate and gypsum, and C–S–H which precipitates as a main hydration product of belite. Belite hydrated in a lesser amount, especially at 60 °C, when the lowest amount of C–S–H was observed.

1. Introduction

Belite-calcium sulfoaluminate cements are a new generation of low energy and low-CO_2 cements, and are considered an alternative to conventional Portland cement, reducing CO_2 emissions by up to 30% as they require less limestone due to the substitution in part by calcium sulfate [1–4]. Furthermore, these cements demand a lower firing temperature in the kiln (typically around 1250 °C) and thus also emit a lower amount of NOx [4]. In addition, belite-calcium sulfoaluminate cement clinkers are more easily ground in comparison to Portland cement clinker due to their higher porosity [3–5]. The main phases present in BCSA cements are belite (Ca_2SiO_4 or C_2S in cement notation), calcium sulfoaluminate ($Ca_4(AlO_2)_6SO_3$ or $C_4A_3\bar{S}$) and ferrite ($Ca_2(Al,Fe)_2O_5$ or C_4AF), followed by calcium sulfate ($CaSO_4$ or $C\bar{S}$) [6] in a form of anhydride, gypsum or bassanite [7–11]. The amount of calcium sulfate controls the setting of calcium sulfoaluminate in cement paste and can modify the kinetics of the hydration process [7,8]. Depending on the amount and source of the raw materials or sintering conditions belite-calcium sulfoaluminate cements can also contain other minor phases such as gehlenite ($Ca_2Al_2SiO_7$ or C_2AS), mayenite ($12CaO{\cdot}7Al_2O_3$ or $C_{12}A_7$), perovskite ($CaTiO_3$ or CT), periclase (MgO or M), arcanite (K_2SO_4 or $K\bar{S}$), magnetite (Fe_3O_4 or fF) and excess of lime (CaO or C) [12–15].

The hydration of belite-calcium sulfoaluminate cements is a complex process mainly due to the different minor phases in addition to main phases [12–14]. The hydration of calcium sulfoaluminate leads to the formation of ettringite ($Ca_6Al_2(SO_4)_3(OH)_{12}{\cdot}26H_2O$ or $C_6\bar{S}_3H_{32}$) and aluminium hydroxide ($Al(OH)_3$ or AH_3), which contribute to the early strength of the cement [1,10]. When the source of sulfate is consumed, calcium monosulfate is formed ($Ca_4Al_2(OH)_{12}{\cdot}SO_4{\cdot}6H_2O$ or $C_4A\bar{S}H_{12}$) [1,5,10]. Furthermore, the hydration of the belite leads to the formation of calcium silicate hydrates ($3CaO{\cdot}SiO_2{\cdot}4H_2O$ or C–S–H) and portlandite ($Ca(OH)_2$ or CH), which contributes to the late age strength of the cement [12,15,16]. Also, other phases such as strätlingite ($Ca_2Al_2SiO_7{\cdot}8H_2O$ or C_2ASH_8) and katoite ($Ca_3Al_2(OH)_{12}$ or C_3AH_6) can precipitate [16–18].

One of the main parameters influencing the hydration of cements is temperature. As a result of different environmental conditions and also heat which is produced during the hydration, cement materials are exposed and affected by different temperatures [19,20]. While studies mainly deal with the hydration of ordinary Portland cement, blended cements and calcium sulfoaluminate cements, the studies on the

* Corresponding author. Slovenian National Building and Civil Engineering Institute, Dimičeva ulica 12, 1000, Ljubljana, Slovenia.
E-mail address: marusa.borstnar@zag.si (M. Borštnar).

https://doi.org/10.1016/j.ceramint.2020.05.029
Received 9 February 2020; Received in revised form 6 April 2020; Accepted 2 May 2020
Available online 05 May 2020

Table 1
Chemical composition of raw materials (in wt. %).

	Limestone	Flysch	Bottom ash	Calcined bauxite	Titanogypsum	Mill scale
SiO_2	4.76	32.02	59.75	5.88	0.13	0.64
Al_2O_3	0.86	7.74	18.73	87.69	1.16	0.34
Fe_2O_3	0.51	3.49	10.03	1.89	0.04	97.96
CaO	51.51	28.83	5.63	0.06	32.62	0.82
MgO	0.90	1.69	2.20	0.52	0.04	0.29
SO_3	0.09	0.07	0.15	0.17	45.39	0.09
Na_2O	0.61	0.54	1.01	0.08	0.06	0.67
K_2O	0.14	1.23	1.60	0.39	0.01	0.02
TiO_2	0.04	0.38	0.53	3.71	0.62	0.01
LOI 950 °C	41.41	24.65	1.20	0.15	21.35	0.00

kinetics of hydration processes and formation of hydration products of belite-calcium sulfoaluminate cement cured at different temperatures are rare.

Studies on ordinary Portland cement and blended cements at increased temperatures showed that an increase of curing temperature leads to an increase of the hydration rate and consequently to an increased early strength development [19–25]. However, at elevated temperatures the compressive strength decrease at a later period of hydration, and furthermore it is lower at high temperatures in comparison to cement pastes hydrated at lower temperatures [20,21,24,26–28]. At elevated temperatures there is only a short time for the diffusion of dissolved ions and for hydration products to precipitate rapidly, resulting in a heterogeneous distribution of hydration products and increased coarse porosity, and therefore a decreased compressive strength [19–21,23–27,29,30]. At elevated temperatures C–S–H density is increased [27] and its polymerization is increased [21,31,32]. Lothenbach et al. [25] observed a decrease in the amount of ettringite and shorter ettringite needles at higher temperatures. On the other hand, at a later age at lower temperatures the hydration rate is decreased, compressive strength is increased and coarse porosity decreased [24–26,29,30] due to the longer diffusion of dissolved ions and the slower precipitation of hydration products, which lead to a more homogenous distribution of hydration products [25,26,29]. At lower temperatures C–S–H has a higher gel porosity and is less polymerized [32].

Recent studies that deal with the hydration of calcium sulfoaluminate cement at elevated temperatures revealed that at temperatures around 90 °C ettringite is unstable, loses water and decomposes to metaettringite, which can influence the mechanical properties of the cement paste [33,34]. With the further addition of water to metaettringite, ettringite forms again. Metaettringite decomposes to monosulfate under steaming conditions and causes the delayed formation of ettringite [33,34]. Jeong et al. [33] indicated that the compressive strength of samples cured at 90 °C was at 1 day of hydration lower than at 30 and 60 °C due to the decomposition of ettringite. Another study on calcium sulfoaluminate cement [11], where hydration was studied in the first 24 h, showed that at higher temperatures the hydration of calcium sulfoaluminate and gypsum was faster, resulting in the rapid formation of ettringite and a higher hydration rate. Also, there was no precipitation of katoite, which would probably cause a regression of compressive strength. Furthermore, increasing the temperature also results in fewer but larger pores [11].

As concerns the effect of temperature on the belite-calcium sulfoaluminate cements, until now only the heat of hydration at different temperatures (5, 23 and 38 °C) was studied with isothermal calorimetry [12]. The results were similar to those on ordinary Portland cement and blended Portland cements, indicating that with increasing the temperature to 38 °C, strength development is more rapid than at ambient temperature. At lower temperatures (5 °C) the hydration reaction is significantly slower [12].

The aim of this study was to investigate the effects of different curing temperatures on the hydration of belite – calcium sulfoaluminate cement. The composition of hydration products and microstructure at 1, 7, 28 and 90 days of hydration was studied using differential thermal analysis and thermogravimetric analysis, X – ray powder diffraction and Rietveld refinement, as well as field emission scanning electron microscopy. Furthermore, hydration kinetics was studied with isothermal calorimetry and the compressive strength development of the cement pastes was determined.

2. Experimental

2.1. Materials

The cement clinker with the targeted phase composition 65 wt% belite (C_2S), 20 wt% calcium sulfoaluminate ($C_4A_3\bar{S}$) and 10 wt% ferrite (C_4AF) was synthesized for the study [35]. The clinkers were prepared of the following raw materials: limestone, flysch (sequence of sedimentary rock layers of calcareous breccia, calcareous sandstones and marls), bottom ash from a coal thermal power plant, white titanogypsum, calcined bauxite and mill scale. Chemical composition of raw materials is given in (Table 1). The materials were proportioned by a modified Bogue method [12] (Table 2).

All the raw materials were ground to pass a 200 μm mesh sieve before making batch compositions. After homogenization, 200 g of raw meal was ground for 3 h in 200 mL of isopropanol using a ball mill (CAPCO Test Equipment Ball Mill Model 9VS) and then dried at 40 °C for 24 h. Pressed pellets of 15 g of the raw meal with the diameter 30 mm and height 13 mm were prepared using a HPM 25/5 press at 10.6 kN and subjected to heating to 1250 °C with a heating rate of 10 °C/min in a Protherm furnace PLF 160/9. The holding time at the final temperature was 60 min. Finally, cooling was natural in a closed furnace. The heating and cooling were carried out under oxidizing conditions.

The synthesized clinker was ground below 0.125 mm in a vibratory disc mill (SIEBTECHNIK Labor Scheibenschwingmühle TS. 250) and blended with 20.3 wt % of white titanogypsum. The amount of gypsum needed was calculated according to Chen & Juenger [12]. The cement made was ground to a Blaine fineness of 497 m^2/kg using a ball mill (CAPCO Test Equipment Ball Mill Model 9VS).

Table 2
Amount of raw materials used in a raw meal (in wt. %).

	Limestone	Flysch	Bottom ash	Calcined bauxite	Titanogypsum	Mill scale
Amount (wt. %)	57.9	23.6	9.0	5.3	4.0	0.2

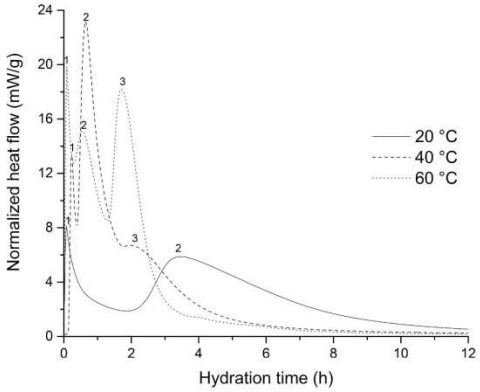

Fig. 1. Hydration heat flow for cement samples cured at 20, 40 and 60 C°.

Cement pastes were prepared using a water to cement/ratio of 0.4. Specimens were mixed by hand for 3 min and cast into prismatic moulds, 10 × 10 × 25 mm in size, demoulded after 24 h and cured in sealed plastic containers at 20, 40 and 60 °C until testing.

The hydration of the cement pastes was stopped by solvent exchange with isopropanol at 1, 7, 28 and 90 days. A part of the crushed cement paste from the interior (pieces close to the upper surface were discarded) was submerged in 100 mL of isopropanol for 15 min, filtered with a Buchner filter and rinsed twice with isopropanol. Samples were dried in a ventilated oven at 40 °C for 8 min [36].

2.2. Methods

The hydration kinetics of the cement was assessed by isothermal conduction calorimetry using an eight-channel TAM Air 8 calorimeter (TA Instruments). 4 g of the cement with a water/cement ratio of 0.4 was mixed in situ with an admix ampoule for 3 min. The heat evolution was evaluated for 7 days at 20, 40 and 60 °C on two replicate measurements per sample at a particular temperature.

The compressive strength of the cement pastes was measured on the prepared 10 × 10 × 25 mm prisms, cured at 20, 40 and 60 °C. The samples were demoulded after 24 h. The compressive strength was determined on four replicas per curing temperature at 1, 7, 28 and 90 days using ToniNORM, Toni Technic by Zwick testing machine with a loading rate of 0.05 kN/s.

X-ray powder diffraction was performed to determine the phase composition of the cement pastes with the hydration stopped at 1, 7, 28 and 90 days using a PANalytical Empyrean X-ray diffractometer equipped with CuKα radiation with λ = 1.54 Å. 5 g of the samples were ground in an agate mortar to a particle size below 0.063 mm. The ground powder was manually back-loaded into a circular sample holder (diameter 16 mm) to mitigate the preferred orientation effect for X-ray diffraction data collection. The samples were scanned at 45 kV and a current of 40 mA, over the 2θ range from 4° to 70°, at a scan rate of 0.026° 2θ/min and step time 172 s. The obtained X-ray diffraction patterns were analysed using X'Pert High Score Plus diffraction software v. 4.8 from PANalytical, using PAN ICSD v. 3.4 powder diffraction files. All Rietveld refinements were preformed using the PANalytical X'Pert High Score Plus diffraction software, using the structures for the phases from ICDD PDF 4 + 2016 RDB powder diffraction files and publication references. The powder diffraction file (PDF) codes for the identified phases used for Rietveld refinements were: β-C_2S (01-086-0398), γ-C_2S (01-086-0391), $C_4A_3\bar{S}$-orthorhombic (04-011-1786), $C_4A_3\bar{S}$-cubic (04–009 – 7268), C_4AF (01-071-0667) and $C\bar{S}H_2$ (00-33-0311), and $C_6\bar{S}_3H_{32}$ (00-041-1451). The amorphous phase was not considered.

Thermogravimetric (DTA/TG) measurements of the cement pastes with stopped hydration at 1, 7, 28 and 90 days of hydration were carried out using a Netzsch STA 409 instrument in the temperature range from 30 to 1000 °C, at a heating rate of 10 °C/min, under nitrogen flow at a rate of 20 mL/min. The samples were ground to a particle size below 0.063 mm with an initial mass of approx. 15 mg and placed in Al_2O_3 crucibles. Measurements were performed on two replicas per curing temperature at 1, 7, 28 and 90 days. Results were analysed using the Netzsch Proteus Thermal Analysis software.

Freshly fractured surfaces of cement pastes with hydration stopped at 1, 7, 28 and 90 days were examined using a Field Emission Scanning Electron Microscope (FE/SEM) JEOL JSM-7600F equipped with an Energy Dispersive X-ray spectrometer (EDXS). All FE/SEM images were recorded at an accelerating voltage of 5 kV, a working distance of 15 mm and probe current 0.7 nA using backscattered electrons (BSE). Specimens were coated with a thin layer of platinum using Precision Etching Coating System (PECS Model682, Gatan, USA) to enhance electrical conductivity.

3. Results and discussion

3.1. Isothermal calorimetry

The results of the isothermal calorimetry are shown in Fig. 1. The first initial exothermic peak (labelled 1) was within the first 10–15 min for all samples, and is related to the wetting of the system and rapid dissolution of cement clinker phases, and an initial formation of hydration products [9–11,37,38]. The difference between the samples with different curing temperatures was evident, thus, the heat released during the initial period increased at elevated temperature.

The induction period following the initial peak was at ambient temperature with respect to the samples cured at a higher temperature much longer. Namely, while the induction period for the sample at 20 °C lasted for 3 h, for samples cured at an elevated temperature (40, 60 °C) is shortened to about 10 min. During the induction period, the clinker phases and gypsum slowly dissolute and ettringite slowly precipitates [9,37,38].

The acceleration period, when another exothermic (2) peak occurs, was exhibited around the 3rd hour of the hydration time for the samples cured at ambient temperature (20 °C), which however was shifted to an earlier time as the temperature was elevated. Accelerated hydration at elevated temperatures and therefore a faster dissolution of the anhydrous phases and precipitation of the hydrated phases was observed in Portland cement [23] and blended cements [11,23,39]. The acceleration period for the samples cured at 40 °C and 60 °C occurred after 75 min and 30 min, respectively. The acceleration peak could be attributed to the hydration reaction of calcium sulfoaluminate with gypsum and the formation of ettringite, as well as aluminium hydroxide [10,11].

Furthermore, as can be seen from the results, samples cured at 40 °C and 60 °C displayed another exothermic peak (labelled 3), which can be assigned to the further dissolution of gypsum and calcium sulfoaluminate, and the formation of ettringite and aluminium hydroxide [10]. However, at 40 °C, this peak was significantly smaller and rather represents a shoulder in comparison to 60 °C. Moreover, the difference was also observed in time periods as the corresponding times to these events were 2 h 15 min for a sample cured at 40 °C and 1 h 45 min for a sample cured at 60 °C.

The hydration rate slowed down earlier at elevated temperatures, after 5 h for samples cured at 40 and 60 °C, while for a sample cured at 20 °C after 12 h, meaning the initial reaction was faster at higher temperatures.

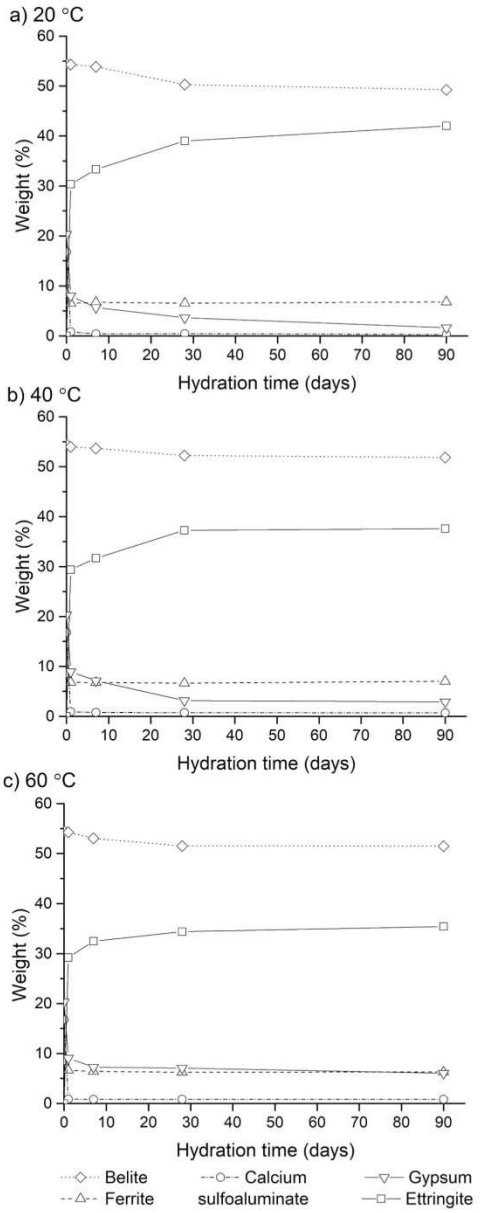

Fig. 2. Amounts of anhydrous phases and hydration products remained at different hydration times by Rietveld analysis at 20 °C, 40 °C and 60 °C.

3.2. X-ray powder diffraction

Fig. 2 shows the time-dependent evolution of the phases in the samples cured at different temperatures as calculated from the X−ray powder diffraction patterns using the Rietveld refinement. X−ray powder diffraction patterns of cement pastes cured at 20, 40 and 60 °C at 1, 7, 28 and 90 days of hydration are shown in Fig. 3.

The crystalline phases present in the cement pastes were belite, ferrite, calcium sulfoaluminate and gypsum as unhydrated relicts of the cement, while ettringite formed as a hydration product. Fig. 2 shows that the amount of calcium sulfoaluminate and belite clinker phases, as well as gypsum, decreased with time at all curing temperatures indicating the formation of hydration products. On the other hand, there was no notable difference in the amount of the ferrite phase with time or elevated temperature as ferrite reacts slower and is a less reactive phase in comparison to other clinker phases [40,41]. Most of the calcium sulfoaluminate has already reacted in the first 24 h of hydration with only less than 1 wt % remaining in the samples (Fig. 2a). Moreover, a significantly higher amount of non-reacted gypsum at 28 and 90 days of hydration was observed for the cement cured at 60 °C, which could be due to a lower degree of hydration at elevated temperatures (Fig. 2b and c). The amount of gypsum decreased continuously up to 28 days of hydration, after 28 days its amount was almost constant. Surplus gypsum was present in the cement pastes at all temperatures due to the high molar ratio of calcium sulfate to calcium sulfoaluminate beyond 4 [42]. Belite reacted only in lower amounts even at 90 days of hydration due to the high consumption of water by calcium sulfoaluminate and the consequently insufficient amount for belite to hydrate [43].

The hydrated phase identified in the samples, at ambient and elevated temperatures, was ettringite. The results indicated that the amount of ettringite increased with time as more hydrates precipitate from the hydration of the anhydrous phases. During the 28 days of hydration the amount of ettringite increased significantly at all temperatures. However, it is evident that at 40 and 60 °C the increase of the amount of ettringite after 28 days of hydration was almost negligible in comparison to 20 °C when the amount of ettringite still increased, suggesting a higher degree of hydration. Moreover, the amount of ettringite at 28 and 90 days of hydration was noticeably lower at 60 °C (Fig. 2c) than at 20 °C and 40 °C.

3.3. Differential thermal analysis/Thermogravimetric analysis

The results of the differential thermal analysis plotted in Fig. 4 are in agreement with the X-ray powder diffraction results, but also revealed the presence of some additional phases. The data indicated the presence of ettringite, C–S–H, aluminium hydroxide and gypsum.

The first and largest endothermic peak around 120 °C was attributed to ettringite and C–S–H [9,16,44]. Ettringite is formed with the hydration of calcium sulfoaluminate with calcium sulfate source [1,10], whereas C–S–H is formed with the hydration of belite [12,15,16]. As these two peaks overlap it is difficult to quantify the amount of the ettringite and C–S–H present in the samples. However, an increasing weight loss in this area with time (from 11.7% at 1 day to 15.8% at 90 days, 11.6%–14.2% and 12.6%–14.1% for 20, 40 and 60 °C, respectively) was observed, indicating the rising amount of ettringite and C–S–H.

A peak at 150 °C corresponds to the decomposition of gypsum. The differential thermal analysis and thermogravimetric analysis indicated that the amount of gypsum slightly decreased after 1–90 days (from the average 1.4% at 1 day to 1.1% at 90 days), since it is consumed in the hydration process (Fig. 4a and b).

An endothermic peak at 250 °C could be assigned to aluminium hydroxide [9,16,44], which was not detectable with X−ray powder diffraction due to its amorphous character [42,45]. The amount of aluminium hydroxide, that precipitates from the reaction of calcium

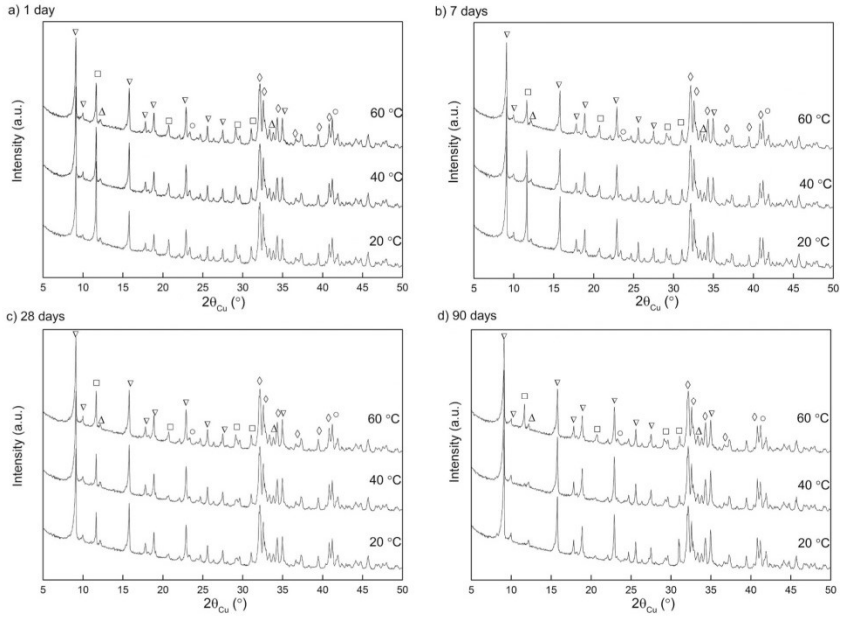

Fig. 3. X−ray powder diffraction patterns of cement pastes cured at 20, 40 and 60 °C. ∇ − ettringite, □ − gypsum, ○ − calcium sulfoaluminate, ◊ − belite, Δ − ferrite.

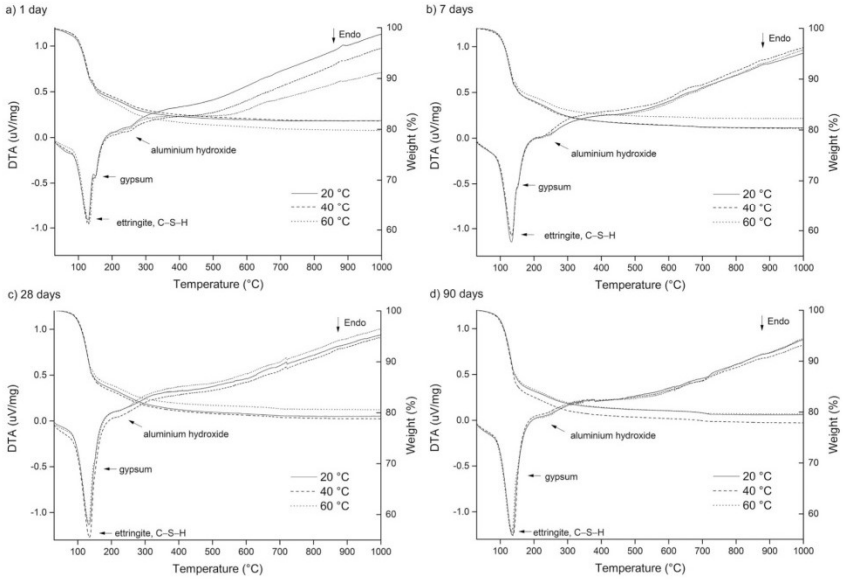

Fig. 4. Results of differential thermal and thermogravimetric analysis of cement pastes at different curing temperatures.

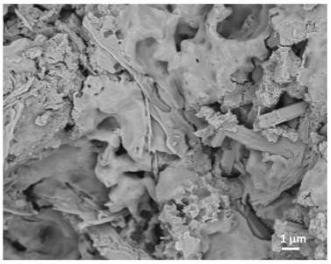

Fig. 5. FE/SEM microphotographs of cement paste at ambient temperature at 1 day of hydration where due to slow hydration at early age anhydrous gel-like clinker is observed.

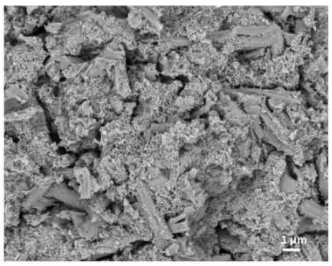

Fig. 6. FE/SEM microphotographs of cement paste cured at 40 °C at 28 days of hydration. Lower amount of clinker is present due to the formation of ettringite ad C–S–H.

sulfoaluminate with gypsum and water, together with ettringite [1,10], did not change significantly with time or elevated temperatures (Fig. 4c and d).

3.4. Field emission scanning electron microscopy

The influence of temperature on the development of the microstructure and the development of different phases was furthermore studied using a field emission scanning electron microscope. The analyses revealed the presence of clinker relicts and non-reacted gypsum in addition to the hydration products ettringite and C–S–H.

In general, the amount of clinker relicts decreased with time at all curing temperatures, due to the formation of hydration products, which is in accordance with the X-ray powder diffraction and thermal analysis. At 1-day of hydration in the samples cured at 20 °C gel-like clinker grains (Fig. 5) were observed, due to the slower hydration at an early age with respect to higher temperatures where anhydrous gel-like clinker was not observed due to accelerated hydration. Over 28 days the amount of clinker decreased slowly, whereas at 28 and 90 days of hydration its amount was significantly lower at all curing temperatures (Fig. 6). Similarly, the amount of gypsum decreased with time as well as the amount of clinker.

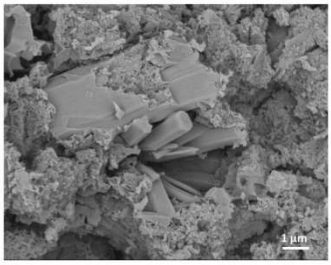

Fig. 8. FE/SEM microphotographs of cement paste cured at 60 °C at 7 days of hydration with smaller and less abundant ettringite crystals.

Ettringite as one of the hydration products was present in all the samples, but its amount at 28 days of hydration was the most prominent at 20 and 40 °C in comparison to 60 °C when its amount was the lowest. The amount of ettringite increased with time as the hydration continued. Up to 28 days of hydration the amount of newly precipitated ettringite increased quickly at all curing temperatures, while at 28 and 90 days the amount of ettringite did not change significantly, which support the X-ray diffraction results. The length of ettringite crystals in the samples at 20 °C after 1 day of hydration was on average up to 7 µm and 2 µm wide (Fig. 7) and it increased with time. With higher temperatures the size of the ettringite continued to become smaller, thus at 60 °C is on average 3 µm long and 1 µm wide (Fig. 8). These observations were also indicated by Lothenbach et al. [25], due to the faster formation of ettringite at elevated temperatures. Furthermore, the results showed that the size of the ettringite was the smallest at 1 day of hydration and increased with time. Ettringite crystals are prismatic with a hexagonal cross-section (Fig. 8) that became better developed with time.

In addition, by using the field emission scanning electron microscopy C–S–H was identified. This phase precipitated from the hydration of the belite phase and mainly covered the surface of the clinker relics and gypsum, whereas ettringite crystals were covered to a lesser extent (Figs. 7 and 8). The amount of C–S–H increased with time. However, at 1 and 7 days of hydration a lower amount of C–S–H was present,

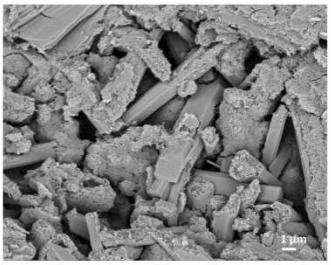

Fig. 7. FE/SEM microphotographs of cement paste showing long prismatic ettringite crystals in samples cured at 20 °C temperature at 7 days of hydration.

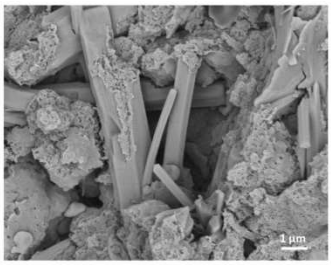

Fig. 9. FE/SEM microphotographs of flake-like C–S–H in cement paste cured at 20 °C at 1 day of hydration.

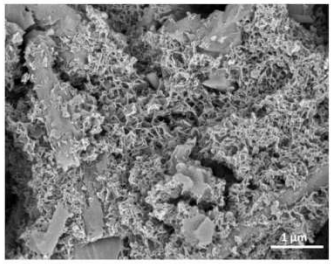

Fig. 10. FE/SEM microphotographs of honeycomb-like C–S–H in cement paste cured at 60 °C at 28 day of hydration.

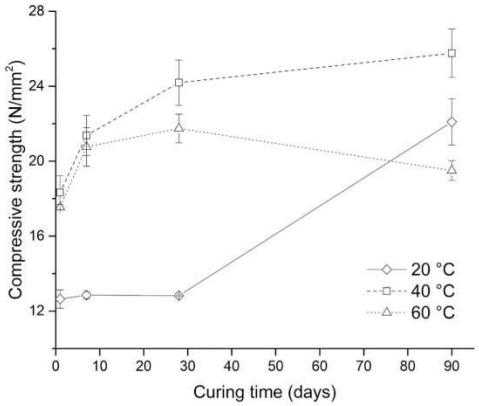

Fig. 11. Compressive strength development of cement pastes cured at different temperatures.

whereas after 28 days it increased significantly and continuously up to 90 days of hydration at all curing temperatures. Its amount decreased with elevated temperatures, especially at 60 °C after 28 and 90 days of hydration. These observations are also in agreement with the previous literature data, which indicated that due to accelerated hydration at higher temperatures hydration dissolved ions do not have enough time to dissolve before the formation of new hydration products, which lead to denser and more polymerized C–S–H and higher porosity, and therefore a decrease in compressive strength [19,20,25]. The results are in accordance with the X-ray powder diffraction, therefore the amount of unhydrated belite is higher in the samples cured at elevated temperatures, where the amount of C–S–H, which precipitated with the hydration of belite, is lower. The results showed that C–S–H is flake-like (Fig. 9) but became more honeycomb-like (Fig. 10) at higher temperatures and later ages. This is the most evident in samples cured at 60 °C after 28 and 90 days of hydration, where it can also be observed that the fibres became longer and thicker as observed by Zhang et al. [46].

3.5. Compressive strength

The effect of different temperatures on the compressive strength evolution of the cement pastes can be seen in Fig. 11.

At the early ages of the hydration, the compressive strength gain was significantly lower at 20 °C with respect to elevated temperatures. For instance, the 1-day compressive strength of the sample cured at 20 °C was much lower (1.6 N/mm^2) with respect to the other two samples where no evident difference was observed (18.3 N/mm^2 and 17.5 N/mm^2 for samples cured at 40 °C and 60 °C, respectively). The results showed that temperature mainly affected early age strength development, while at the 90 days of hydration the compressive strength values for samples cured at 20 °C were close to the samples cured at elevated temperature. These findings were also reported in other studies [19,20,23], where due to accelerated hydration reactions compressive strength increased with higher curing temperature. These results are also in accordance with the results obtained by isothermal calorimetry, where it can be seen that hydration is accelerated at elevated temperatures. Furthermore at 1-day of hydration in the samples cured at 20 °C, an anhydrous gel-like clinker was observed, due to the slower hydration at an early age, which is confirmed with the compressive strength results. The results also support the X-ray powder diffraction data since the amount of ettringite increased with time as well as compressive strength.

As seen from Fig. 11, the compressive strength of cement cured at 20 °C did not change significantly until 28 days, when it increased sharply due to the hydration of the belite phase and the formation of C–S–H. After 7 days of hydration the two samples hydrated at 40 and 60 °C show similar compressive strength development. While compressive strength at 40 °C increased steadily with time, the strength evolution after 28 days for samples cured at 60 °C decreased. Namely, at 90 days of hydration, the compressive strength of cement cured at 60 °C was the lowest (19.5 N/mm^2) in comparison to 20 and 40 °C (22.1 N/mm^2 and 25.2 N/mm^2 for samples cured at 20 °C and 40 °C, respectively). In accordance, while the lowest compressive strength at 90 days of hydration and also the lowest amount of ettringite was indicated for samples cured at 60 °C. According to previous studies this may be due to higher porosity due to denser C–S–H and heterogeneous distribution of hydration products in cement paste [19,21], or to the decomposition of ettringite to metaettringite [33].

4. Conclusions

The influence of temperature on the hydration kinetics, formation of phase assemblage, microstructure and compressive strength of belite-calcium sulfoaluminate cement was studied at 20, 40 and 60 °C.

At higher temperatures, cement reacted earlier and released more heat during hydration in comparison to ambient temperature. Also, the compressive strength results showed that early strength was significantly higher at elevated temperatures than at ambient temperature. Furthermore, at 90 days of hydration, the compressive strength at 60 °C decreased and was the lowest, which corresponds to the higher amount of non-reacted gypsum and lower amount of precipitated ettringite at 90 days of hydration and suggests that at a higher temperature the degree of hydration was lower. On the other hand, due to the faster hydration of calcium sulfoaluminate at elevated temperatures the size of the prismatic ettringite crystals was smaller at higher temperatures. Besides ettringite, aluminium hydroxide was also formed with the hydration of calcium sulfoaluminate and gypsum with water. The hydration of belite yielded C–S–H, which covered the surface of other phases. The amount of C–S–H decreased at higher temperatures due to a lower degree of reaction at elevated temperatures. Furthermore, the shape of C–S–H changed from flake-like to honeycomb-like with an increase in temperature and time.

Declaration of competing interest

The authors declare that they have no known competing financial interests or personal relationships that could have appeared to influence the work reported in this paper.

Acknowledgments

The research is performed within the Young researcher programme and is financially supported by the Slovenian Research Agency, contract number 1000-18-1502.

References

[1] A.J.M. Cuberos, Á.G. De la Torre, G. Álvarez-Pinazo, M.C. Martín-Sedeño, K. Schollbach, H. Pöllmann, M.A.G. Aranda, Active iron-rich belite sulfoaluminate cements: clinkering and hydration, Environ. Sci. Technol. 44 (2010) 6855–6862, https://doi.org/10.1021/es101785n.
[2] E. Gartner, T. Sui, Alternative cement clinkers, Cement Concr. Res. 114 (2018) 27–39, https://doi.org/10.1016/j.cemconres.2017.02.002.
[3] E. Gartner, Industrially interesting approaches to "low-CO2" cements, Cement Concr. Res. 34 (2004) 1489–1498, https://doi.org/10.1016/j.cemconres.2004.01.021.
[4] K. Quillin, Performance of belite–sulfoaluminate cements, Cement Concr. Res. 31 (2001) 1341–1349, https://doi.org/10.1016/S0008-8846(01)00543-9.
[5] G.S. Li, G. Walenta, E. Gartner, Formation and hydration of low CO2 cements based on belite, calcium sulfoaluminate and calcium aluminoferrite, Proceedings of the 12th ICCC, Canada, Montreal, 2007, pp. 9–12.
[6] F. Winnefeld, B. Lothenbach, Phase equilibria in the system Ca4Al6O12SO4 – Ca2SiO4 – CaSO4 – H2O referring to the hydration of calcium sulfoaluminate cements, RILEM Tech. Lett. 1 (2016) 10–16, https://doi.org/10.21809/rilemtechlett.v1.5.
[7] M. García-Maté, A.G. De la Torre, L. León-Reina, E.R. Losilla, M.A.G. Aranda, I. Santacruz, Effect of calcium sulfate source on the hydration of calcium sulfoaluminate eco-cement, Cement Concr. Compos. 55 (2015) 53–61, https://doi.org/10.1016/j.cemconcomp.2014.08.003.
[8] M.C.G. Juenger, F. Winnefeld, J.L. Provis, J.H. Ideker, Advances in alternative cementitious binders, Cement Concr. Res. 41 (2011) 1232–1243, https://doi.org/10.1016/j.cemconres.2010.11.012.
[9] F. Winnefeld, S. Barlag, Calorimetric and thermogravimetric study on the influence of calcium sulfate on the hydration of ye'elimite, J. Therm. Anal. Calorim. 101 (2010) 949–957, https://doi.org/10.1007/s10973-009-0582-6.
[10] F. Winnefeld, B. Lothenbach, Hydration of calcium sulfoaluminate cements — experimental findings and thermodynamic modelling, Cement Concr. Res. 40 (2010) 1239–1247, https://doi.org/10.1016/j.cemconres.2009.08.014.
[11] L. Zhang, F.P. Glasser, Hydration of calcium sulfoaluminate cement at less than 24 h, Adv. Cement Res. 14 (2002) 15, https://doi.org/10.1680/adcr.2002.14.4.141.
[12] I.A. Chen, M.C.G. Juenger, Synthesis and hydration of calcium sulfoaluminate-belite cements with varied phase compositions, J. Mater. Sci. 46 (2011) 2568–2577, https://doi.org/10.1007/s10853-010-5109-9.
[13] F.P. Glasser, L. Zhang, High-performance cement matrices based on calcium sulfoaluminate–belite compositions, Cement Concr. Res. 31 (2001) 1881–1886, https://doi.org/10.1016/S0008-8846(01)00649-4.
[14] J. Majling, S. Sahu, M. Vlna, D.M. Roy, Relationship between raw mixture and mineralogical composition of sulphoaluminate belite clinkers in the system CaO-SiO2-Al203-Fe203.SO3, Cement Concr. Res. 23 (1993) 1351–1356, https://doi.org/10.1016/0008-8846(93)90072-H.
[15] F. Bullerjahn, D. Schmitt, M. Ben Haha, Effect of raw mix design and of clinkering process on the formation and mineralogical composition of (ternesite) belite calcium sulphoaluminate ferrite clinker, Cement Concr. Res. 59 (2014) 87–95, https://doi.org/10.1016/j.cemconres.2014.02.004.
[16] G. Álvarez-Pinazo, I. Santacruz, M.A.G. Aranda, Á.G. De la Torre, Hydration of belite–ye'elimite–ferrite cements with different calcium sulfate sources, Adv. Cement Res. 28 (2016) 529–543, https://doi.org/10.1680/jadcr.16.00030.
[17] B. Lothenbach, B. Albert, M. Vincent, G. Ellis, Hydration of Belite-Ye'elimite-Ferrite cements: thermodynamic modeling, 14th International Conference on the Chemistry of Cement, Beijing, China, 2015, p. 12.
[18] Y. Jeong, C.W. Hargis, S.-C. Chun, J. Moon, The effect of water and gypsum content on strätlingite formation in calcium sulfoaluminate-belite cement pastes, Construct. Build. Mater. 166 (2018) 712–722, https://doi.org/10.1016/j.conbuildmat.2018.01.153.
[19] F. Deschner, B. Lothenbach, F. Winnefeld, J. Neubauer, Effect of temperature on the hydration of Portland cement blended with siliceous fly ash, Cement Concr. Res. 52 (2013) 169–181, https://doi.org/10.1016/j.cemconres.2013.07.006.
[20] I. Elkhadiri, F. Puertas, The effect of curing temperature on sulphate-resistant cement hydration and strength, Construct. Build. Mater. 22 (2008) 1331–1341, https://doi.org/10.1016/j.conbuildmat.2007.04.014.
[21] I. Elkhadiri, M. Palacios, F. Puertas, Effect of curing temperature on cement hydration, Ceramics 53 (2009) 65–75.
[22] W. Ma, D. Sample, I.R. Martin, P.W. Brown, Calorimetric Study of Cement Blends Containing Fly Ash, Silica Fume, and Slag at Elevated Temperatures, (1994), p. 7.
[23] J.I. Escalante-Garcia, J.H. Sharp, The effect of temperature on the early hydration of Portland cement and blended cements, Adv. Cement Res. 12 (2000) 121–130, https://doi.org/10.1680/adcr.2000.12.3.121.
[24] J.I. Escalante-García, J.H. Sharp, Effect of temperature on the hydration of the main clinker phases in portland cements: part i, neat cements, Cement Concr. Res. 28 (1998) 1245–1257, https://doi.org/10.1016/S0008-8846(98)00115-X.
[25] B. Lothenbach, F. Winnefeld, C. Alder, E. Wieland, P. Lunk, Effect of temperature on the pore solution, microstructure and hydration products of Portland cement pastes, Cement Concr. Res. 37 (2007) 483–491, https://doi.org/10.1016/j.cemconres.2006.11.016.
[26] K.O. Kjellsen, R.J. Detwiler, O.E. Gjørv, Development of microstructures in plain cement pastes hydrated at different temperatures, Cement Concr. Res. 21 (1991) 179–189, https://doi.org/10.1016/0008-8846(91)90044-I.
[27] B. Lothenbach, T. Matschei, G. Möschner, F.P. Glasser, Thermodynamic modelling of the effect of temperature on the hydration and porosity of Portland cement, Cement Concr. Res. 38 (2008) 1–18, https://doi.org/10.1016/j.cemconres.2007.08.017.
[28] Y. Maltais, J. Marchand, Influence of curing temperature on cement hydration and mechanical strength development of fly ash mortars, Cement Concr. Res. 27 (1997) 1009–1020, https://doi.org/10.1016/S0008-8846(97)00098-7.
[29] K.O. Kjellsen, R.J. Detwiler, O.E. Gjørv, Backscattered electron imaging of cement pastes hydrated at different temperatures, Cement Concr. Res. 20 (1990) 308–311, https://doi.org/10.1016/0008-8846(90)90085-C.
[30] K. De Weerdt, M. Ben Haha, G. Le Saout, K.O. Kjellsen, H. Justnes, B. Lothenbach, The effect of temperature on the hydration of composite cements containing limestone powder and fly ash, Mater. Struct. 45 (2012) 1101–1114, https://doi.org/10.1617/s11527-011-9819-5.
[31] T.T.H. Bach, C.C.D. Coumes, I. Pochard, C. Mercier, B. Revel, A. Nonat, Influence of temperature on the hydration products of low pH cements, Cement Concr. Res. 42 (2012) 805–817, https://doi.org/10.1016/j.cemconres.2012.03.009.
[32] A. Bentur, R.L. Berger, J.H. Kung, N.B. Milestone, J.F. Young, Structural properties of calcium silicate pastes: II, effect of curing temperature, J. Am. Ceram. Soc. 62 (1979) 362–366, https://doi.org/10.1111/j.1151-2916.1979.tb19079.x.
[33] Y. Jeong, C.W. Hargis, H. Kang, S.-C. Chun, J. Moon, The effect of elevated curing temperatures on high ye'elimite calcium sulfoaluminate cement mortars, Materials 12 (2019) 1072, https://doi.org/10.3390/ma12071072.
[34] J. Kaufmann, F. Winnefeld, B. Lothenbach, Stability of ettringite in CSA cement at elevated temperatures, Adv. Cement Res. 28 (2016) 251–261, https://doi.org/10.1680/jadcr.15.00029.
[35] L. Žibret, A. Ipavec, S. Kramar, Microstructure of belite sulfoaluminate clinker and its influence on clinker reactivity, International Workshop on Calcium Sulfoaluminate Cements, Murten, Switzerland, 2018, p. 1.
[36] R. Snellings, J. Chwast, Ö. Cizer, N. Belie, Y. Dhandapani, P. Durdziński, J. Elsen, J. Haufe, D. Hooton, C. Patapy, M. Santhanam, K. Scrivener, D. Snoeck, L. Steger, S. Tongbo, A. Vollpracht, F. Winnefeld, B. Lothenbach, RILEM TC-238 SCM Recommendation on Hydration Stoppage by Solvent Exchange for the Study of Hydrate Assemblages, Materials and Structures, (2018), p. 51, https://doi.org/10.1617/s11527-018-1298-5.
[37] Y. Shen, X. Li, X. Chen, W. Zhang, D. Yang, Synthesis and calorimetric study of hydration behavior of sulfate-rich belite sulfoaluminate cements with different phase compositions, J. Therm. Anal. Calorim. 133 (2018) 1281–1289, https://doi.org/10.1007/s10973-018-7251-6.
[38] A. Rungchet, C.S. Poon, P. Chindaprasirt, K. Pimraksa, Synthesis of low-temperature calcium sulfoaluminate-belite cements from industrial wastes and their hydration: comparative studies between lignite fly ash and bottom ash, Cement Concr. Compos. 83 (2017) 10–19, https://doi.org/10.1016/j.cemconcomp.2017.06.013.
[39] I.G. Richardson, C.R. Wilding, M.J. Dickson, The hydration of blastfurnace slag cements, Adv. Cement Res. 2 (1989) 147–157, https://doi.org/10.1680/adcr.1989.2.8.147.
[40] W. Kurdowski, Cement and Concrete Chemistry, Springer, New York, 2014 Dordrecht.
[41] N.B. Winter, Understanding Cement: an Introduction to Cement Production, Cement Hydration and Deleterious Processes in Concrete, Microanalysis Consultants, 2012.
[42] F. Winnefeld, L.H.J. Martin, C.J. Müller, B. Lothenbach, Using gypsum to control hydration kinetics of CSA cements, Construct. Build. Mater. 155 (2017) 154–163, https://doi.org/10.1016/j.conbuildmat.2017.07.217.
[43] H. Beltagui, G. Jen, M. Whittaker, M.S. Imbabi, The influence of variable gypsum and water content on the strength and hydration of a belite-calcium sulphoaluminate cement, Adv. Appl. Ceram. 116 (2017) 199–206, https://doi.org/10.1080/17436753.2017.1289722.
[44] K. Scrivener, R. Snellings, B. Lothenbach (Eds.), A Practical Guide to Microstructural Analysis of Cementitious Materials, first ed., CRC Press, 2018, , https://doi.org/10.1201/b19074.
[45] M. Ben Haha, F. Winnefeld, A. Pisch, Advances in understanding ye'elimite-rich cements, Cement Concr. Res. 123 (2019) 105778, https://doi.org/10.1016/j.cemconres.2019.105778.
[46] Z. Zhang, G.W. Scherer, A. Bauer, Morphology of cementitious material during early hydration, Cement Concr. Res. 107 (2018) 85–100, https://doi.org/10.1016/j.cemconres.2018.02.004.

Chapter 3

Quantitative in Situ X-ray Diffraction Analysis of Early Hydration of Belite-Calcium Sulfoaluminate Cement at Various Defined Temperatures

This chapter is based on the published paper: M. Borštnar, C. L. Lengauer, S. Dolenec, "Quantitative in situ X-ray diffraction analysis of early hydration of belite-calcium sulfoaluminate cement at various defined temperatures," *Minerals*, vol. 11, no. 3, pp. 1-21, 2021 [85].

The early reactions of hydration are crucial, as they determine the initial and final mechanical properties of concrete and their durability [39]. Additionally, a significant amount of the heat generated during cement hydration occurs within the first 24 hours [86]. The hydration is influenced by a variety of parameters, including amongst others, the temperature and calcium sulfate source available, which affect the amount and type of the phases precipitated during hydration [30], [86], [86]. Utilizing in-situ X-ray powder diffraction analysis and Rietveld refinement allows us to determine the quantitative phase composition of cement samples during the initial stages of hydration [87], [88].

This study assesses how temperature affects the phase composition of belite-calcium sulfoaluminate cement pastes in the initial 24 hours of hydration. The phase composition of cement clinker was 65 wt. % belite, 20 wt. % ye'elimite and 10 wt. % ferrite. Cement pastes with differing calcium sulfate to ye'elimite molar ratios, namely M = 1 and M = 2.5 were compared. In-situ X-ray powder diffraction measurements and quantitative Rietveld analysis were employed to investigate the formation of hydrates in order to understand how the quantity of calcium sulfate influenced the formation of hydration assemblage. The experiments were conducted at temperatures of 25 °C, 40 °C and 60 °C.

At 24 hours, the degree of hydration was highest at ambient temperatures, but at elevated temperatures was accelerated in the first hours, particularly when increasing from 25 °C to 40 °C, as opposed to from 40 °C to 60 °C. The quantity of ettringite that precipitated was controlled by the amount of calcium sulfate added to the cement clinker, with the amount increasing at a higher molar ratio. Additionally, the results indicated that variations in temperature impacted the full width at half maximum of ettringite peaks, detected as a reduction in the crystallite size of ettringite at higher temperatures caused by faster precipitation. At elevated temperatures, higher d-values of the ettringite peaks were observed when a calcium sulfate to ye'elimite molar ratio of 1 was employed, implying a greater release of ions from the cement clinker, which

facilitated an increase in the incorporation of ions into the ettringite structure. These differences were not shown when a 2.5 molar ratio was used, as amount of clinker in this mixture was lower, the availability of substitute ions for incorporation into the ettringite structure was reduced.

This chapter addresses the thesis objectives 1, 2 and 4.

The contribution of the doctoral candidate was writing the first draft of the manuscript and conducting the experiment detailed in the manuscript, including preparation of the materials (cement clinker and cement) and performing the experimental part (X-ray powder diffraction and Rietveld refinement).

minerals

MDPI

Article

Quantitative in Situ X-ray Diffraction Analysis of Early Hydration of Belite-Calcium Sulfoaluminate Cement at Various Defined Temperatures

Maruša Borštnar [1,2,*], Christian L. Lengauer [3] and Sabina Dolenec [1]

[1] Slovenian National Building and Civil Engineering Institute, Dimičeva ulica 12, 1000 Ljubljana, Slovenia; sabina.dolenec@zag.si
[2] Jožef Stefan International Postgraduate School, Jamova cesta 39, 1000 Ljubljana, Slovenia
[3] Department of Mineralogy and Crystallography, University of Vienna, UZA 2, Althanstraße 14, 1090 Vienna, Austria; christian.lengauer@univie.ac.at
* Correspondence: marusa.borstnar@zag.si

Abstract: The influence of temperature on the early hydration of belite-calcium sulfoaluminate cements with two different calcium sulfate to calcium sulfoaluminate molar ratios was investigated. The phase composition and phase assemblage development of cements prepared using molar ratios of 1 and 2.5 were studied at 25, 40 and 60 °C by in situ X-ray powder diffraction. The Rietveld refinement method was used for quantification. The degree of hydration after 24 h was highest at ambient temperatures, but early hydration was significantly accelerated at elevated temperatures. These differences were more noticeable when we increased the temperature from 25 °C to 40 °C, than it was increased from 40 °C to 60 °C. The amount of calcium sulfate added controls the amount of the precipitated ettringite, namely, the amount of ettringite increased in the cement with a higher molar ratio. The results showed that temperature also affects full width at half maximum of ettringite peaks, which indicates a decrease in crystallite size of ettringite at elevated temperatures due to faster precipitation of ettringite. When using a calcium sulfate to calcium sulfoaluminate molar ratio of 1, higher d-values of ettringite peaks were observed at elevated temperatures, suggesting that more ions were released from the cement clinker at elevated temperatures, allowing a higher ion uptake in the ettringite structure. At a molar ratio of 2.5, less clinker is available in the cement, therefore these differences were not observed.

Keywords: in situ X-ray diffraction; hydration; temperature; cement; Rietveld analysis

Citation: Borštnar, M.; Lengauer, C.L.; Dolenec, S. Quantitative in Situ X-ray Diffraction Analysis of Early Hydration of Belite-Calcium Sulfoaluminate Cement at Various Defined Temperatures. *Minerals* **2021**, *11*, 297. https://doi.org/10.3390/min11030297

Academic Editor: Thomas N. Kerestedjian
Received: 4 February 2021
Accepted: 9 March 2021
Published: 11 March 2021

1. Introduction

The trend towards sustainability and lowering the carbon footprint has led to the development and production of new mineral binders. Within this context, iron-rich belite-calcium sulfoaluminate, also known as sulfobelite cements [1–3] or belite-ye'elimite-ferrite [4–6] cements, represent a low carbon and low energy alternative to ordinary Portland cement. Up to 35 % less CO_2 is released during the production of belite-calcium sulfoaluminate cements compared to ordinary Portland cement. Furthermore, belite-calcium sulfoaluminate clinkers demand lower clinkering temperatures (1250–1350 °C in comparison to around 1450 °C) and are easier to grind [7–9]. One of the advances is also the replacement of a part of raw materials with industrial by-products and waste [1,5,10–12].

Belite-calcium sulfoaluminate cement clinkers are usually described to contain around 40–75 wt. % belite, 15–35 wt. % calcium sulfoaluminate, and 5–25 wt. % ferrite [7,13]. They are typically prepared by adding varying amounts of calcium sulfate in order to achieve the optimal compressive strength, setting time and volume stability [14–

16]. The hydration of these cements depends on several factors, including the composition of the cement clinker, polymorphism of the clinker phases present, the presence of minor phases, and the water-to-binder ratio, amongst others [4,9,17–21]. One of the major factors affecting hydration is temperature, which influences hydration kinetics, phase assemblage, and the rheological and mechanical properties of cement [18,22–24]. Different weather conditions, and the amount of heat released during the hydration process, may therefore have a significant impact on cementitious materials [25,26].

One of the main and important phases of belite-calcium sulfoaluminate cements, which reacts at an early age, is calcium sulfoaluminate ($C_4A_3\bar{S}$; hereafter cement notation was used throughout the paper: C = CaO, S = SiO_2, A = Al_2O_3, F = Fe_2O_3, $\bar{S}$ = SO_3, N = N_2O, K = K_2O, T = TiO_2, H = H_2O), the synthetic analogue of the sodalite-type mineral ye'elimite, $Ca_4Al_6(SO_4)O_{12}$. Calcium sulfoaluminate causes rapid strength development and controls the evolution of early cement performance, setting, and hardening [5,18,27–29]. The hydration of calcium sulfoaluminate, and the formation of hydration products, strongly depend on the type and amount of calcium sulfate (anhydrite $C\bar{S}$, gypsum $C\bar{S}H_2$ or bassanite $C\bar{S}H_{0.5}$) added [14,18,27]. When the molar ratio of calcium sulfate to calcium sulfoaluminate is below 2 (M-value < 2), and until the added calcium sulfate is depleted, the main crystalline hydration product formed is ettringite-type $C_6A\bar{S}_3H_{32}$, which precipitates together with amorphous aluminum hydroxide (AH_3) according to the reaction shown in Equation (1) [14,20,27,30]:

$$C_4A_3\bar{S} + 2C\bar{S}H_x + (38 - 2x)H \rightarrow C_6A\bar{S}_3H_{32} + 2\ AH_3\ (x = 0, 0.5, 2), \quad (1)$$

In case the molar ratio of calcium sulfate to calcium sulfoaluminate exceeds the value of 2 (M-value > 2), besides ettringite, surplus calcium sulfate is also present [14,15].

In the absence of calcium sulfate, or when the calcium sulfate source is depleted, the main hydration products formed are monosulfate ($C_4A\bar{S}H_{12}$) and aluminum hydroxide [14,27,28,30], according to Equation (2).

$$C_4A_3\bar{S} + 18H \rightarrow C_4A\bar{S}H_{12} + 2AH_3, \quad (2)$$

The M-value is also used to designate the type of calcium sulfoaluminate cement, where M < 1.5 classifies cements with rapid hardening and high strength, an M value between 1.5 and 2.5 defines expansive cements, and M > 2.5 refers to self-stressing cements [15,31].

At an advanced hydration age, belite (C_2S), the synthetic analogue of another important clinker phase, the mineral larnite (Ca_2SiO_4), starts to react. This primarily contributes to the late compressive strength of the cement [16,18]. Belite, together with aluminum hydroxide and the addition of water, may yield either strätlingite-type C_2ASH_8 [30], according to Equation (3), or amorphous calcium silicate hydrate (C–S–H) and portlandite-type CH after the depletion of aluminum hydroxide [30], according to reaction Equation (4).

$$C_2S + AH_3 + 5H \rightarrow C_2ASH_8, \quad (3)$$

$$C_2S + nH \rightarrow C\text{–}S\text{–}H + mCH, \quad (4)$$

Furthermore, katoite-type C_3ASH_4 can precipitate in the reaction of strätlingite with portlandite [30], according to Equation (5):

$$C_2ASH_8 + CH \rightarrow C_3ASH_4, \quad (5)$$

Early hydration is an important period, which determines the fresh properties of concrete and also its final mechanical properties and durability [18,32]. Moreover, most of the hydration heat of cement, as determined by isothermal calorimetry, evolves within the first 24 h of hydration [1]. The most prominent method to study phase composition

/

and the development of phase assemblage in the hardening paste is powder X-ray diffraction (PXRD) [29,32,33]. Through in situ analysis of PXRD patterns by Rietveld refinement [34], the quantitative phase composition of the cement samples during early hydration reactions could be determined [12,33].

The early hydration reactions of belite-calcium sulfoaluminate cement pastes, with different amounts and sources of added calcium sulfate, have already been studied by in situ PXRD, but only at ambient temperatures [1,12]. The early reactions in these cement pastes at ambient temperatures were also investigated by Bullerjahn et al. [5], who focused their study on the effect of boron during early hydration. Studies of the early age hydration of calcium sulfoaluminate at ambient temperature were evaluated by Zajac et al. [28] and Jansen et al. [27] At elevated temperatures (55 and 85 °C), the hydration in the first 24 h was studied only on calcium sulfoaluminate cements, however, just a qualitative phase analysis was performed. Despite the fact that the literature provides some studies of early hydration reactions, a detailed study of early age hydration phases of belite-calcium sulfoaluminate cements at different temperatures has not been presented to date.

The aim of the present study was to characterize the influence of different temperatures on the phase composition of belite-calcium sulfoaluminate cement pastes during the first 24 h of hydration, while comparing pastes of different calcium sulfate to calcium sulfoaluminate molar ratios. To determine the hydration phase assemblage and investigate the influence of the amount of calcium sulfate source on the formation of hydration products, in situ PXRD measurements and quantitative analysis using the Rietveld method were performed on cements with M-values of 1 and 2.5 at 25, 40 and 60 °C.

2. Materials and Methods

The targeted phase composition of the cement clinker used for the study was 65.0 wt. % belite (C_2S), 20.0 wt. % calcium sulfoaluminate ($C_4A_3\bar{S}$) and 10.0 wt. % ferrite (C_4AF) [35]. In order to obtain the targeted phase composition, the raw materials (calculated to Total = 95 wt. %) were proportioned using an adapted Bogue method [22]. The Bogue calculation is only used to determine the phase composition of the main phases, while the minor phases are neglected [36]. The clinker was synthesized from the following raw materials: limestone (57.9 wt. %), flysch (sedimentary rock sequence consisting of layers of calcareous breccia, calcareous sandstones and marls; 23.6 wt. %), bottom ash from a coal thermal power plant (9.0 wt. %), calcined bauxite (5.3 wt. %), white titanogypsum (4.0 wt. %) and mill scale (0.2 wt. %). The chemical composition of the raw meal used has been described by Dolenec et al. [37], while the chemical composition of the raw materials and the proportions were presented in the study by Borštnar et al. [24] The phase composition of the clinker, obtained by Rietveld refinement, is given in Table 1, where the amount of calcium sulfoaluminate is the sum of the orthorhombic and cubic polymorph, and the amount of belite is the sum of β-belite and γ-belite.

Table 1. Calculated targeted and observed phase composition of the synthesized cement clinker as obtained by Rietveld refinement in wt. %.

	Σ Belite	Σ Calcium Sulfoaluminate	Ferrite	Mayenite	Periclase	Gehlenite	Arcanite	Aphthitalite
Targeted phase composition (wt. %)	65.0	20.0	10.0	-	-	-	-	-
Observed phase composition (wt. %)	65.7	17.7	11.6	2.5	1.1	0.4	0.4	0.6

Raw materials were first ground and sieved through a 200 μm mesh and then homogenized. Each 200 g batch of proportioned raw materials was dispersed in 200 mL of

isopropanol, mixed for 3 h in a ball mill (Capco Ball Mill 9VS, Capco Test Equipment, Ipswich, IP1 5AP, UK), and then dried in a 40 °C oven for 24 h; 15 g of the raw meal was subsequently pressed into pellets 30 mm wide and 13 mm high using an HPM 25/5 press at 10.6 kN. The pellets were placed in a Protherm PLF 160/9 (Protherm Furnaces, Ankara, Turkey) furnace and fired to 1250 °C at a heating rate of 10 °C/min. Following this, they were held at the final temperature for 60 min and then cooled in the closed furnace for 20 h. The entire process was performed under oxidizing conditions.

Before blending the synthesized clinker with white titanogypsum (ground < 0.125 mm), the clinker was first hand-crushed using an agate mortar and ground to less than 0.125 mm using a vibratory disc mill (Siebtechnik TS. 250, Siebtechnik GmbH, Mülheim an der Ruhr, Germany). Two cements were prepared with different proportions of white titanogypsum, based on the M-value, which designates the molar ratio of calcium sulfate ($CaSO_4$) to calcium sulfoaluminate [14]. The cements were prepared by blending a ground cement clinker with 5.6 and 12.9 wt. % titanogypsum, which is equivalent to M = 1 and 2.5, respectively. These M-values were chosen to compare the influence of the amount of calcium sulfate on the formation of hydration products. At M = 1, the reactions defined in Equation (1) or (2) occur, whereas at M = 2.5 only the Equation (1) reaction takes place and surplus gypsum remains present in the system [14]. Next, 200 g of cement was ground for 5 h using the Capco ball mill. The Blaine specific surface area of the cements, determined according to standard test method EN 196-6 [38], was 5200 cm^2/g and 5990 cm^2/g for M =1 and M= 2.5, respectively. The particle size distributions of the two cements, which are shown in Figure 1, were determined using a laser particle analyzer (Sync Microtrac MRB, dry operation, Microtrac MRB, Haan, Germany). The phase compositions of the unhydrated cements, as determined by the Rietveld method, are listed in Table 2.

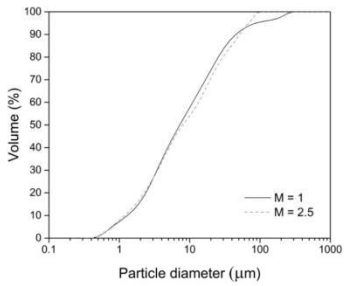

Figure 1. Particle size distributions of prepared cement mixtures with two molar ratios (M).

Table 2. Phase composition of unhydrated cements with M = 1 and M = 2.5 in wt. % determined with Rietveld method.

	M = 1	M = 2.5
Calcium sulfoaluminate-orthorhombic	8.0	6.8
Calcium sulfoaluminate-cubic	10.7	10.3
Σ Calcium sulfoaluminate	18.7	17.1
Belite-beta	58.0	53.4
Belite-gamma	5.1	5.3
Σ Belite	63.1	58.7
Ferrite	9.1	8.5

Periclase	0.9	0.8
Mayenite	1.4	1.1
Gehlenite	0.4	0.6
Arcanite	0.1	0.1
Aphthitalite	0.5	0.4
Gypsum	5.7	12.8

In situ PXRD measurements were performed to study the phase formation of the cement pastes during the early age hydration process within the first 24 h.

The prepared cements were mixed with deionized water in a water to cement ratio of 0.6 and manually stirred for 1 min. The mixture was then immediately cast in the sample holder (14 mm diameter, 1 mm depth). Measurements were performed at 25, 40 and 60 °C, at a relative humidity of 95 ± 2 %, using an Anton Paar XRK900 (Anton Paar GmbH, Graz, Austria) reactor chamber without internal Be-shielding and an automated z-alignment stage. The temperature-specific maximum relative humidity was established by continuous flow (20 mL/min) of water saturated gas (N_2) combined by heating the XRK900 chamber together with an external heating/cooling device for avoiding vapor condensation.

PXRD patterns of the cement pastes were obtained using a Bruker D8-Advance theta-theta goniometer (Bruker, Massachusetts, ZDA), equipped with a LynxEye position-sensitive detector. CuKa radiation was used at 40 kV and 40 mA, using a primary Ni-filter, an automatic divergence slit (l = 12 mm), and 2.3° primary and secondary soller slits. Measurements were performed from 5 to 75 °2θ, at increments of 0.02 °2θ/min, with an overall counting time of 20 min per scan. Under these conditions, 69 X-ray diffraction patterns per sample were collected in repetition mode during the first 24 h of hydration.

The obtained PXRD patterns of cement pastes at different temperatures were analyzed using X'Pert High Score Plus diffraction software v. 4.9 from PANalytical (Malvern Panalytical, Malvern, Worcestershire, United Kingdom), using PAN ICSD v. 3.4 powder diffraction data database. For qualitative phase analyses the entries of ICDD PDF 4+ 2020 RDB powder diffraction files were used. The initial crystal structural models used for the Rietveld refinements of the cementitious phases [39] were taken from Cuesta et al. [40,41] for orthorhombic and cubic calcium sulfoaluminate, for the other identified phases entries of the ICSD (Inorganic Crystal Structure Data) were applied, as listed in Table 3. First, the overall zero error and phase scale factors were refined and the background was fitted to a cosine Chebyshev function of 10 polynomial terms. Furthermore, the cell parameters and phase-specific Lorentzian functions (CS_L parameters) allowing for peak shape broadening were included in the refinement. For the determination of X-ray amorphous content, corundum (Al_2O_3, NIST SRM 676a) was used as an external standard.

In order to determine the degree of hydration of clinker phases, the obtained phase composition of cement clinker was normalized to paste content, taking into account the amount of water added at time 0.0 h of hydration (w/c = 0.6). The degree of hydration of selected phases (calcium sulfoaluminate and gypsum) was calculated by comparing the amount of individual anhydrous phase remaining in the cement paste to the amount of the normalized anhydrous phase in cement. To this end, also all the graphs are showing direct results of Rietveld refinement. Moreover, on the graphs β-C_2S and γ-C_2S is given as Σ belite and calcium sulfoaluminate-orthorhombic and -cubic as Σ calcium sulfoaluminate.

Table 3. Phase designations and ICSD entries used for the Rietveld refinement.

Phase	Cement Notation	ICSD	References
Calcium sulfoaluminate-orthorhombic	$C_4A_3\overline{S}$	237892	[40]
Calcium sulfoaluminate-cubic	$C_4A_3\overline{S}$	194482	[41]
Belite-beta	β-C_2S	81096	[42]
Belite-gamma	γ-C_2S	81095	[42]
Ferrite	C_4AF	98836	[43]
Gypsum	$C\overline{S}H_2$	409581	[44]
Periclase	M	9863	[45]
Mayenite	$C_{12}A_7$	261586	[46]
Gehlenite	C_2AS	158171	[47]
Arcanite	$K_2\overline{S}$	79777	[48]
Aphthitalite	$K_3N\overline{S}_2$	26818	[49]
Ettringite	$C_6\overline{S}_3H_{32}$	155395	[50]

In order to assess differences in the composition of ettringite, and the influence of temperature on its composition and structure, d-values and full widths at half maximum were studied. Ettringite was selected because it is the main hydrated phase in the early hydration of belite calcium sulfoaluminate cements. The strongest lines of powder diffraction pattern of ettringite with reference pattern 00-041-1451 [29,50] are at d-values of 9.720 Å and 5.610 Å, corresponding to Miller indices (hkl) of 100 and 110, respectively. The d-value, or interplanar spacing between atoms in the crystal, and full widths at half maximum (FHWM) of the (100) and (110) peaks of ettringite were collected and plotted at 20 min and every 100 min from the start of the hydration up to 24 h.

3. Results

3.1. Cement Hydration at 25 °C

Results of in situ X-ray diffraction analysis of the cement pastes at 25 °C with a molar ratio of calcium sulfate to calcium sulfoaluminate 1 and 2.5 are shown in Figure 2. Figure 3 plots the degrees of hydration for calcium sulfoaluminate and gypsum, i.e., the main constituents reacting during the first 24 h, as well as the increasing ettringite content as their main hydration product. Figure 4 shows the evolution of the X-ray diffraction patterns at selected hydration times of the two investigated mixtures at 25, 40 and 60 °C.

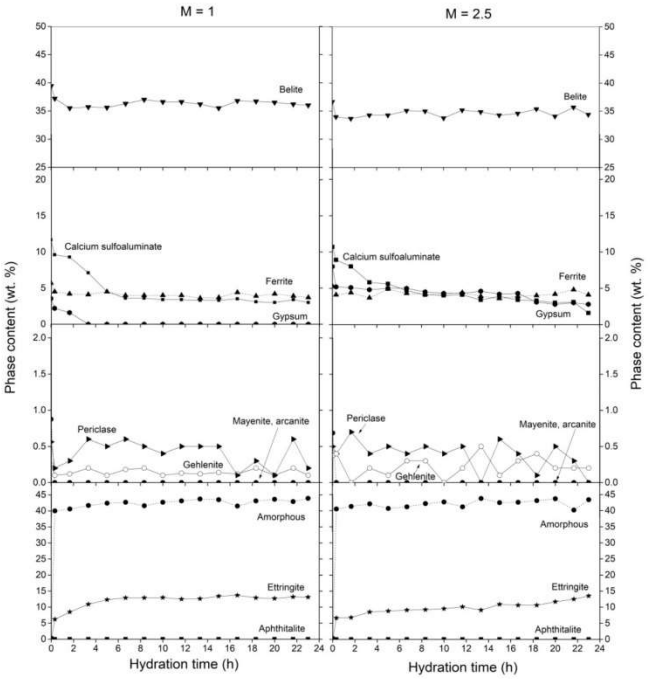

Figure 2. Phase content in the cement pastes with M = 1 and M = 2.5 cured at 25 °C during the first 24 h of hydration.

The clinker phases identified in the cement paste with a molar ratio of 1 (M = 1) were belite, calcium sulfoaluminate, ferrite, gypsum, gehlenite, and periclase. The only provable crystalline hydrate in the cement pastes was ettringite. In addition, amorphous content was present. As seen from Figure 2, the early age hydration started immediately after adding the defined amount of water to the unhydrated cement. Within the first 5 h of hydration, therefore, calcium sulfoaluminate and gypsum were proportionally dissolved with a high degree of hydration (Figure 3). Within the first 5 h the amount of calcium sulfoaluminate decreased rapidly from 11.7 wt. % to 4.6 wt. %, indicating that 61.5 % of the calcium sulfoaluminate reacted in 5 h. After that, it decreased only slightly, to 3.0 wt. %, and reached its final degree of hydration at 74.3 % (Figure 3), which indicates the amount of calcium sulfoaluminate which reacted in the first 24 h of hydration. The gypsum was completely depleted after 3 h. When the gypsum was consumed, the rate of dissolution of calcium sulfoaluminate slowed, remaining at almost the same level, as did the formation rate of ettringite. Simultaneously, the ettringite content increased during the first 5 h to 12.3 wt. %, while later on it increased slightly, to 13.1 wt. %. With ongoing hydration between 5 and 24 h, both the formation of ettringite and dissolution of calcium sulfoaluminate were much reduced, with only small changes in their amounts being observed. The amount of belite and ferrite did not significantly change within the first 24 h of the hydration process. Additionally, the minor clinker phase gehlenite was consumed after 20 min of hydration. The periclase content stayed almost constant throughout the

hydration. Mayenite, arcanite and aphthitalite, which were all present in the unhydrated cement, were not detected. Amorphous content increased with the hydration time from 40.0 wt. % to 43.8 wt. %.

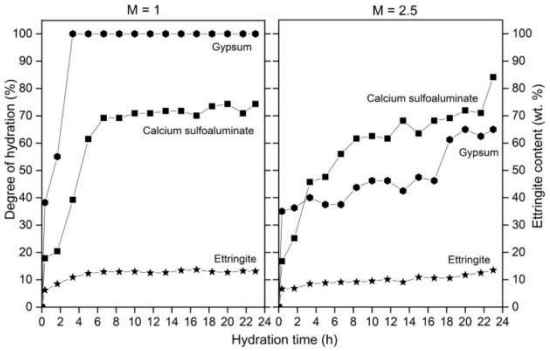

Figure 3. Degree of hydration of calcium sulfoaluminate and gypsum with ettringite content during the first 24 h of hydration of the M = 1 and M = 2.5 samples at 25 °C.

For the cement paste with a molar ratio of 2.5 (M = 2.5) the detected phases were belite, calcium sulfoaluminate, ferrite, gypsum, gehlenite, periclase and ettringite, in addition to amorphous content. At 25 °C, gypsum was measurable during 24 h of hydration. The results indicate a steady dissolution of calcium sulfoaluminate and gypsum, accompanied by the precipitation of ettringite as the major crystalline product. Over the first 3.3 h of the hydration, calcium sulfoaluminate rapidly diminished, from 10.7 wt. % to 5.7 wt. %. This was followed by a slow but continuous decline, until it reached a final value of 1.6 wt. % after 24 h, corresponding to the degree of hydration of calcium sulfoaluminate of 84.1 % (Figure 3). Accordingly, most of the gypsum reacted in the first 3.3 h of hydration from 8 wt. % to 4.7 wt. % and then only slowly decreased to 2.8 wt. % at 24 h. The degree of hydration of gypsum at 24 h was 65.0 %. The ettringite content constantly increased during hydration, increasing significantly to 8.6 wt. % in the first 3.3 h, then steadily increasing up to 13.5 wt. % at 24 h of hydration. Belite was observed in approximately the same amounts throughout the hydration, and the amounts of ferrite, periclase and gehlenite also did not significantly change in the first 24 h of hydration. Mayenite, arcanite and aphthitalite peaks, which were present in the unhydrated cement, were not observed. Furthermore, the amorphous content increased from 40.5 wt. % to 43.3 wt. % during hydration.

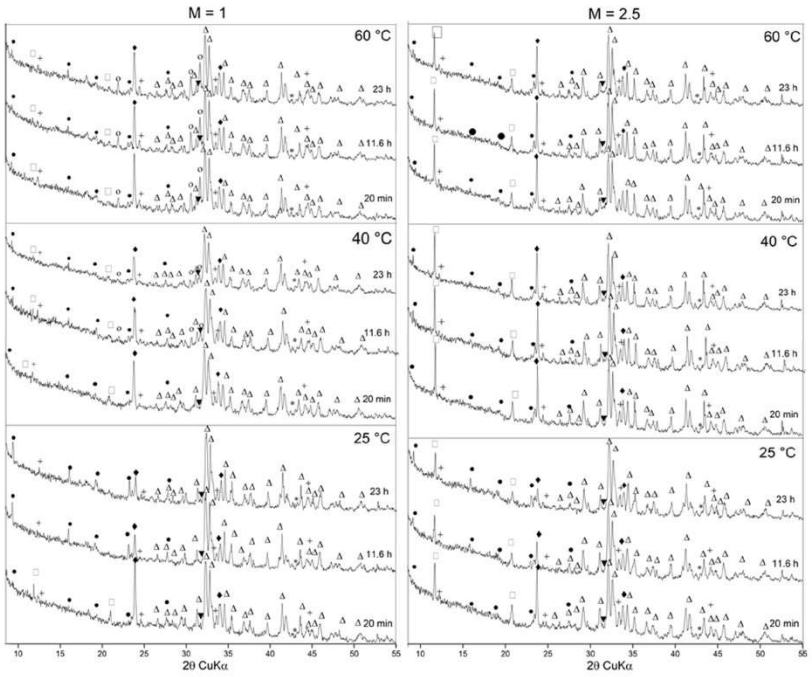

Figure 4. In situ X-ray powder diffraction patterns of the M = 1 and M = 2.5 samples at 25, 40 and 60 °C after 20 min, 11.6 and 23 h in a selected 2θ CuKα range. Δ = belite, ♦ = calcium sulfoaluminate, + = ferrite, □ = gypsum, * = periclase, ▼ = gehlenite, ○ = aphthitalite, ● = ettringite.

3.2. Cement Hydration at 40 °C

Results of in situ X-ray diffraction analysis of the cement pastes with molar ratios of 1 and 2.5 at 40 °C are shown in Figures 5 and 6. The evolution of the X-ray diffraction patterns at selected hydration times is given in Figure 4.

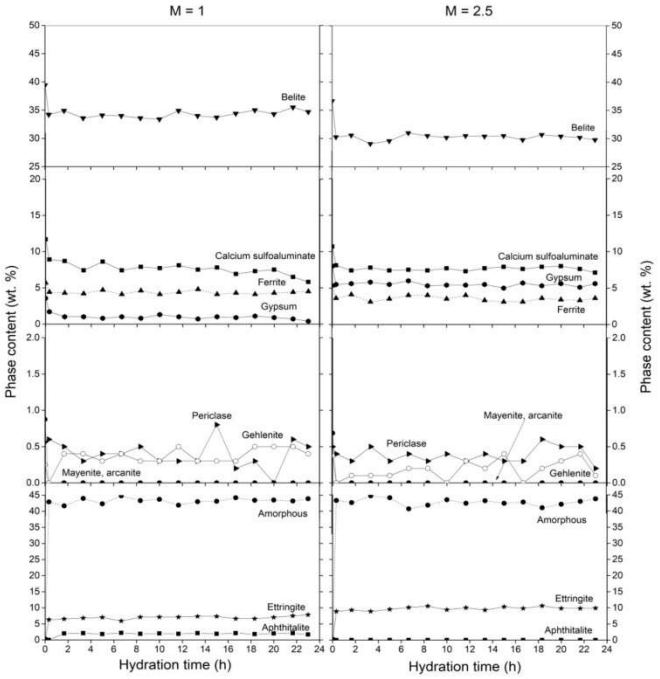

Figure 5. Phase content in the cement pastes with M = 1 and M = 2.5 cured at 40 °C during the first 24 h of hydration.

At a molar ratio of 1, the following phases were identified: belite, calcium sulfoaluminate, ferrite, gypsum, aphthitalite, gehlenite, periclase, and ettringite, as the only hydrated phase. In addition, amorphous content was present. After mixing with water the amount of calcium sulfoaluminate and gypsum declined sharply within the first 1.6 h, i.e., from 11.7 wt. % to 8.7 wt. % and from 3.6 wt. % to 1 wt. %, respectively. Accordingly, 36.7% of calcium sulfoaluminate and 71.9% of gypsum reacted during the first 1.6 h of hydration (Figure 6). Between 1.6 and 24 h, their amount declined slower, with gypsum remaining present in the amount of 0.4 wt. % after 24 h of hydration. After 24 h, the degree of hydration of calcium sulfoaluminate was 50.4% (5.8 wt. %). The results show that the main and only hydrate phase formed was ettringite, which increased to 6.5 wt. % within the first 1.6 h and reached a final value of 7.8 wt. % after 24 h of hydration. The contents of belite and ferrite exhibited no change over 24 h, which also held for the periclase and gehlenite content. Mayenite, arcanite and aphthitalite were clearly depleted in the first 20 min of hydration, while aphtitalite again appeared at 1.6 h with an amount of 1.6 wt. %, which then remained constant up to 24 h of hydration. Amorphous content was almost constant during hydration, with values between 42.0 and 43.0 wt. %.

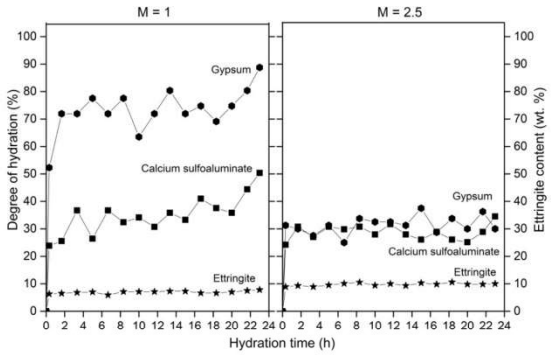

Figure 6. Degree of hydration of calcium sulfoaluminate and gypsum with ettringite content during the first 24 h hydration of the M = 1 and M = 2.5 samples at 40 °C.

Phase composition analysis of the mixture with a molar ratio of 2.5 (M = 2.5) at 40 °C showed that the phases present were belite, calcium sulfoaluminate, ferrite, gypsum, gehlenite and periclase. The only hydrate identified in the cement pastes was ettringite. Amorphous content was also present. The amounts of calcium sulfoaluminate and gypsum diminished in the first 20 min of hydration, in concert with the formation of ettringite. 2.5 wt. % of gypsum was consumed in the first 20 min, with calcium sulfoaluminate decreasing from 10.7 wt. % to 8.1 wt. %, but subsequently their amounts decreased slower. After 24 h the degree of hydration of calcium sulfoaluminate and gypsum was approximately 34.5% and 30.0%, respectively (Figure 6). Ettringite precipitated to the amount of 8.9 wt. % within the first 20 min of hydration, after which time it increased only slightly to 9.9 wt. %. The results showed no change in the amount of belite and ferrite. The quantities of periclase and gehlenite did not change significantly after 20 min of hydration. No mayenite, arcanite, and aphthitalite were detected. The amorphous content did not significantly change and it was around 43 wt. %.

3.3. Cement Hydration at 60 °C

Results of in situ X-ray diffraction analysis of the cement pastes at 60 °C with molar ratios of 1 and 2.5 are shown in Figures 7 and 8. The evolution of the X-ray diffraction patterns at selected hydration times is given in Figure 4.

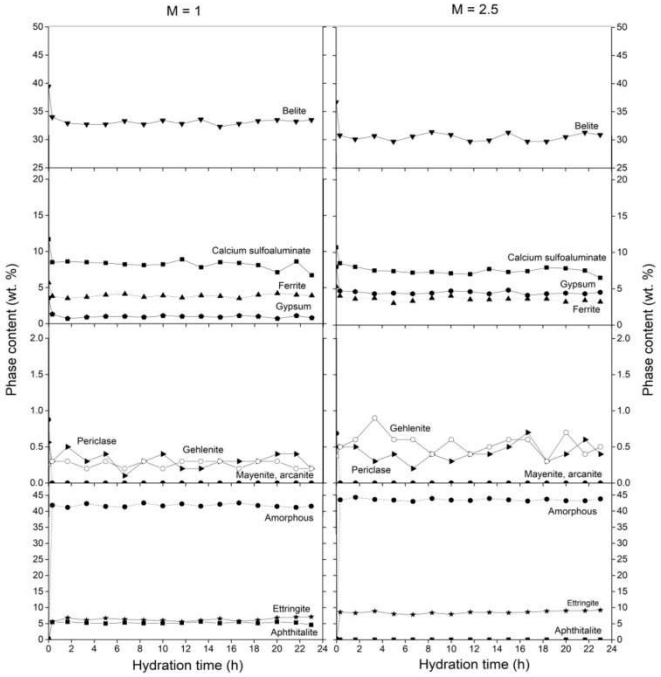

Figure 7. Phase content of clinker phases and hydrates in the cement pastes with M = 1 and M = 2.5 cured at 60 °C during first 24 h of hydration.

The phases observed in the cement paste with a molar ratio calcium sulfate to calcium sulfoaluminate of 1 included belite, calcium sulfoaluminate, ferrite, gypsum, aphthitalite, gehlenite, and periclase as clinker phases, ettringite as a hydrated phase and amorphous content (Figure 7). The results show that hydration started directly after mixing the cement with water, by exhibiting a high degree of hydration of calcium sulfoaluminate and gypsum within the first 20 min. This caused the formation of ettringite, the only hydrate phase detected (Figure 8). After 20 min the amount of calcium sulfoaluminate decreased slightly, from 11.7 wt. % to 8.5 wt. %, when it converged to an almost constant value with a slow decrease with time. The results show that 27.3 wt. % of the calcium sulfoaluminate reacted in 20 min. Furthermore, at 60 °C all of the gypsum was dissolved to 1.3 wt. % within 20 min of the start of the reaction and reached a final degree of reaction after 23 h at 77.5 %. At the same time, ettringite rapidly increased to 5.6 wt. %, and then continuously increased to a maximum of 7.1 wt. % after 24 h. The belite and ferrite content did not significantly change at an early age. Periclase and gehlenite content remained almost constant throughout the hydration. Mayenite and arcanite were not detected after the hydration proceeded. Aphthitalite content increased from 0.5 wt. % to 4.6 wt. % in the first 20 min and stayed constant up to 24 h. Around 42 wt. % amorphous content was present during the hydration.

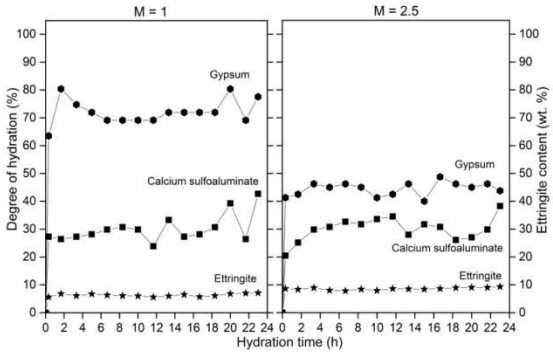

Figure 8. Degree of hydration of calcium sulfoaluminate and gypsum with ettringite content during first 24 h of hydration of the M = 1 and M = 2.5 samples at 60 °C.

At a molar ratio of 2.5, the following phases were identified: belite, calcium sulfoaluminate, ferrite, gypsum, gehlenite, periclase, and ettringite, in addition to amorphous content. Most of the calcium sulfoaluminate and gypsum were dissolved in the first 20 min of hydration, with the calcium sulfoaluminate content reducing from 10.7 wt. % to 8.5 wt. %, and the gypsum decreasing from 8.0 wt. % to 4.7 wt. %. The degree of hydration of calcium sulfoaluminate was 38.2% at 24 h, while the degree of hydration of gypsum was 43.8% (Figure 8). 8.6 wt. % of ettringite precipitated in 20 min hours, consecutively its content did not change significantly. After 24 h, 9.2 wt. % of ettringite was measured. The clinker phases belite, ferrite, periclase, and gehlenite did not show any significant change after 20 min of hydration, while mayenite, arcanite, and aphthitalite were not detected. The amorphous content was almost constant during hydration, maintaining levels of around 43.5 wt. %.

3.4. Ettringite during Cement Hydration

Figure 9 plots the full width at half maximum (FWHM) of (100) and (110) peaks of ettringite, while Figure 10 shows the d-values of (100) and (110) peaks of ettringite, both as a function of time.

The results of the mixture with a molar ratio of 1 at 25 °C showed that the FWHMs of (100) and (110) peaks of ettringite increased up to 10 h of hydration. After 13.3 h, however, the values decreased then remained almost constant up to 24 h of hydration. At 40 °C, the FWHM was roughly constant up to 10 h, at which point it showed a slight increase and then stayed constant up to 24 h. At 60 °C, an increase in the FWHM was observed up to 10 h of hydration, followed by a decrease. The results show that FWHMs values were the lowest at a temperature of 25 °C.

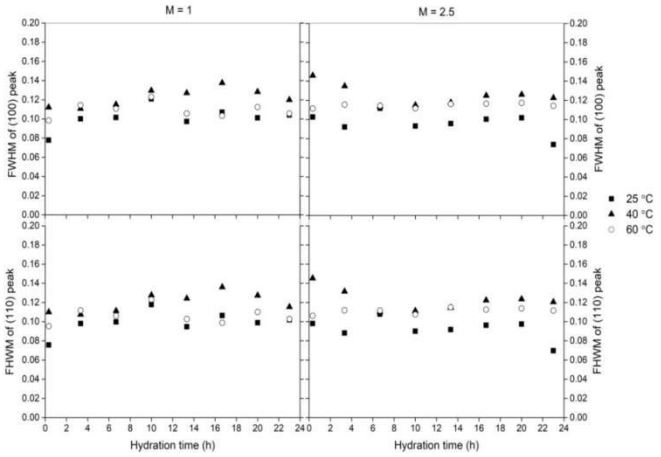

Figure 9. Full width at half maximum (FWHM) of (100) and (110) peaks of ettringite during first 24 h of hydration.

At a molar ratio of 2.5 at 25 °C, results showed that FWHMs of (100) and (110) peaks of ettringite were roughly constant until 6.6 h, after which point they increased significantly until 10 h but then started to decrease. Between 10 and 22 h of hydration the FWHM was almost constant, until 23 h, when it significantly decreased. At 40 °C FWHMs of (100) and (110) peaks of ettringite were the highest at 20 min of hydration. The values then decreased until 6.6 h, after which time the values did not significantly change up to 24 h of hydration. At 60 °C, the FWHMs of (100) and (110) peaks of ettringite were roughly constant throughout the entire hydration period. The results show that FWHMs were the lowest at 25 °C.

The d-values of (100) and (110) peaks of ettringite at a molar ratio of 1 (M = 1) were almost constant at 25 °C, with slightly lower values at 20 min of hydration. At 40 °C, the d-values of (100) and (110) peak of ettringite did not change significantly in the first 24 h of hydration. At 60 °C, the d-values of (100) and (110) peaks of ettringite remained constant up to 20 h of hydration, at which point the values decreased. D-values were lowest at ambient temperatures, and highest at 40 °C.

The results of the mixture with a molar ratio of 2.5 (M = 2.5) show that at 25, 40 and 60 °C the d-values of (100) and (110) peaks of ettringite did not change significantly with time and temperature.

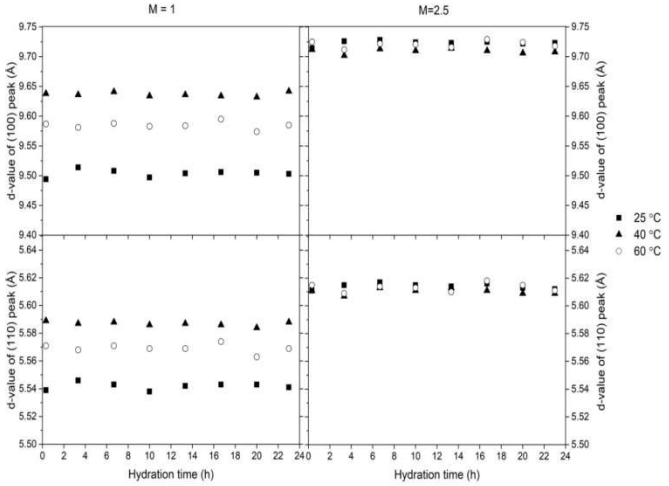

Figure 10. D-values of (100) and (110) peaks of ettringite during first 24 h of hydration.

4. Discussion

During the first 24 h, belite calcium sulfoaluminate cement pastes with different molar ratio of calcium sulfate to calcium sulfoaluminate mainly consisted of belite and calcium sulfoaluminate with ferrite and gypsum. At an early age the calcium sulfoaluminate reacted with gypsum and water to form ettringite, according to Equation (1).

At 25, 40 and 60 °C, the main and only detected hydrate phase formed in both cement pastes (calcium sulfate to calcium sulfoaluminate molar ratios of 1 and 2.5) was ettringite. The results show that the hydration started immediately after adding the defined amount of water to the unhydrated cement with the dissolution of calcium sulfoaluminate and gypsum and the formation of ettringite. Aluminum hydroxide, which, according to Equation (1), precipitates with ettringite, was not detected by PXRD in either mixture, which relates to its amorphous character at an early age [5,15,51]. The amorphous content in the mixtures was attributed mainly to the residual water, and to a lesser extent to noncrystalline phases [39,52], in this case aluminum hydroxide, which is formed at an earlier stage. C-S-H precipitates later, with the hydration of belite [7,18]. Amorphous content increased at ambient temperatures with hydration time for both molar ratios; however, at elevated temperatures, it remained constant during hydration. This is due to the slower formation of ettringite at an ambient temperature, and consequently aluminum hydroxide formed with it, leading to a continuous increase in amorphous content. At elevated temperatures, ettringite precipitated very fast at the beginning of the hydration and only slowly increased after, therefore the amount of amorphous content did not change significantly. Furthermore, monosulfate, which was predicted according to Equation (2), was not detected during the first 24 h of hydration, which was due to poor crystallinity or small crystalline size [15,20,30], and which would have contributed to the amorphous content measured [53]. The amount of belite did not change significantly in the first 24 h of hydration, because belite exhibits low reactivity at early ages and reacts at a later hydration time [54]. Due to its low and slow solubility, ferrite content did not decrease with hydration time [55]. Moreover, the minor phase mayenite, which is known to rapidly dissolve and increases the aluminum and calcium ion concentration [56], accordingly was depleted within the first 20 min of hydration. Mayenite can accel-

erate early hydration by reacting with water and gypsum and therefore accelerate the formation of ettringite [56]. Due to their low reactivity, periclase and gehlenite are considered inert in these types of cements [57], therefore their amounts did not change during hydration. After the start of hydration, the minor clinker phase arcanite was not detected in the cement pastes, because it is a rapid soluble alkali sulfate phase [36,58] that was already depleted. Aphthitalite, however, which is also a rapid soluble phase [36], was depleted after 20 min of hydration at 25 °C. On the other hand, during hydration at 40 °C and 60 °C, it precipitated in M = 1 sample. At 40 °C it precipitated after 1.6 h, while at 60 °C it was detected already at 20 min of hydration. Moreover, a much higher amount of aphthitalite precipitated at 60 °C compared to at 40 °C, indicating that with increasing temperature above ambient, the formation of aphthitalite is increased due to a higher release of alkalis from the clinker phases. Apart from alkali sulfates present in the clinkers, the alkalis, which are incorporated in the main clinker phases, mainly in calcium sulfoaluminate [37], could be released through the dissolution of these phases [37,59] as well, reacting with sulfate from the gypsum, and form the alkali sulfate phase aphthitalite. Namely, another alkali sulfate phase thenardite (Na_2SO_4) was found forming in calcium sulfoaluminate cements at high alkalinity, explained as a product of excess alkalis initially reacting with anhydrite, which retards calcium sulfoaluminate hydration and ettringite formation [60]. This mechanism could also explain the lower amount of precipitated ettringite in samples at M = 1 in comparison to M = 2.5 at 40 and 60 °C. Furthermore, aphthitalite was detected only at a lower molar ratio of M = 1, probably due to a higher proportion of clinker and a consequently larger amount of alkalis introduced into the hydrating system in addition to lower gypsum content. Moreover, aphthitalite was present only at the two elevated temperatures, as crystallization is highly temperature-dependent [61].

At ambient temperatures, more calcium sulfoaluminate reacted in the cement pastes with a higher molar ratio of calcium sulfate to calcium sulfoaluminate, indicating that calcium sulfate accelerates the dissolution of calcium sulfoaluminate [14]. However, at elevated temperatures, less calcium sulfoaluminate was consumed in the samples with a higher molar ratio of calcium sulfate to calcium sulfoaluminate. Furthermore, at a molar ratio of M = 1, gypsum had a higher degree of reaction, meaning a higher amount of gypsum was dissolved in comparison to samples with a molar ratio of 2.5. Moreover, the results showed that, at ambient temperatures, the hydration of calcium sulfoaluminate is more rapid in a mixture with higher calcium sulfate content, which is also in accordance with data from the literature [6,55]. The rate of hydration could also influence the fact that cement with M = 2.5 had a slightly higher specific surface area in comparison cement with M =1, which could also enhance the reactivity of cement [10]. Nevertheless, both cements have similar particle size distribution (Figure 1). In addition, at all temperatures, the amount of ettringite precipitated after 24 h was higher in the mixtures with a greater amount of calcium sulfate. It has already been reported that more ettringite is formed when the addition of gypsum is higher [9]. However, the ettringite precipitation rate at a lower molar ratio was slower at the beginning, in comparison to higher molar ratios, where the precipitation rate was very fast and more constant over the first 24 h of hydration.

Comparing the results at different temperatures, it can be seen that hydration was accelerated at elevated temperatures in comparison to ambient temperatures, for both molar ratios of calcium sulfate to calcium sulfoaluminate of 1 and 2.5. At 25 °C most of the calcium sulfoaluminate and gypsum reacted in the first 3 h of hydration, while at 40 and 60 °C these reactions occurred in the first 1.6 h and 20 min, respectively. This is in line with the previous study investigating hydration of belite-calcium sulfoaluminate cements [24], where isothermal calorimetry results showed the main exothermic peak of cement paste cured at 20 °C right after 3 h of hydration and after 75 and 30 min at 40 and 60 °C, respectively. Accelerated hydration at an elevated temperature has also been observed by other researchers, not only in calcium sulfoaluminate cements, but also in

Portland cement, calcium aluminate cements and blended cements [18,62–64]. On the other hand, the degree of hydration was much lower at elevated temperatures in comparison to ambient temperature, with less calcium sulfoaluminate and gypsum consumed and, consequently, a lower precipitation of ettringite. A decrease in the amount of ettringite at elevated temperatures was also observed by Lothenbach et al. [65], due to less time for the diffusion of dissolved ions and precipitation of hydration products [65–67]. However, the degree of reaction of calcium sulfoaluminate was comparable at 40 °C and 60 °C, and the amount of ettringite was also almost the same. Only at 25 °C in the cement paste with a molar ratio of calcium sulfate to calcium sulfoaluminate of 1 gypsum was completely depleted after 3 h of hydration.

According to Scherrer's Equation [68], which can be used for the determination of the particle sizes, the FWHM is inversely proportional to crystallite size [68], meaning the broader the peak (i.e, the higher the FWHM), the smaller the crystallite size. The FWHMs of (100) and (110) peak of ettringite at a molar ratio of calcium sulfate to calcium sulfoaluminate of 1 were lowest at 25 °C, indicating that crystallite size decreased at elevated temperatures in comparison to ambient temperature due to faster formation of ettringite at increased temperatures, which was already indicated in previous literature data by microscopical observations [24,65]. Crystallite sizes were, however, higher at 40 °C compared to 60 °C. Differences in the FWHMs between the molar ratio of calcium sulfate to calcium sulfoaluminate 1 and 2.5 were not significant, indicating crystallite sizes did not vary with a different gypsum amount.

The structure of ettringite is open and flexible, and thus allows other atoms to be incorporated into the structure [69], resulting in variable d-values. Ettringite has the capability to substitute Ca^{2+}, Al^{3+}, SO_4^{2-} sites with other anions or cations, such as Sr^{2+}, Ba^{2+}, or Pb^{2+} for the Ca^{2+} site, Cr^{3+}, Si^{4+}, or Fe^{3+} for the Al^{3+} site, and CO_3^{2-}, Cl^-, or OH^- for the SO_4^{2-} site and also other ions [70,71], which have different ionic radii and can cause a change in the d-spacings of the ettringite, e.g., larger ionic radii of the substitute ions increase the cell parameters [72]. The d-spacings of (100) and (110) peaks of ettringite at a molar ratio of calcium sulfate to calcium sulfoaluminate of 1 and 2.5 at each temperature during hydration only slightly changed. There was, however, a significant difference when comparing values at 25, 40 and 60 °C at a molar ratio of calcium sulfate to calcium sulfoaluminate of 1, for which the results showed that d-spacings are lowest at 25 °C, and increased at an elevated temperature. D-values were, however, higher at 40 °C compared to 60 °C. It is therefore evident that the d-spacing changes with temperature, suggesting the incorporation of ions with larger ion radii or a higher ion intake for ettringite at elevated temperatures, as more ions are released from the main clinker phases. However, at a molar ratio of calcium sulfate to calcium sulfoaluminate of 2.5 these differences in temperature were almost negligible, probably due to the lower clinker proportion at this molar ratio, and less potential substitution ions available to incorporate into the ettringite structure. On the other hand, comparing the results at different molar ratios of calcium sulfate to calcium sulfoaluminate, it is evident that the d-values of (100) and (110) peaks of ettringite were greater when the molar ratio was 2.5.

5. Conclusions

The influence of different temperatures on the phase composition of belite-calcium sulfoaluminate cement pastes with M-values of 1 and 2.5 during the first 24 h of hydration was studied at 25, 40 and 60 °C.

The amount of gypsum and calcium sulfoaluminate decreased with time at all curing temperatures, due to the formation of ettringite. More calcium sulfoaluminate and gypsum were consumed, and, consequently, the amount of ettringite was higher in the samples cured at 25 °C in comparison to those cured at elevated temperatures at both molar ratios (M = 1 and 2.5). Increasing the temperature from 40 °C to 60 °C also affects the formation of ettringite and the hydration degree of clinker phases; however not that significantly as in comparison to ambient temperature. At ambient temperatures less

calcium sulfoaluminate reacted in the samples with a lower calcium sulfate to calcium sulfoaluminate molar ratio, while at elevated temperatures the degree of hydration of calcium sulfoaluminate was higher at a lower calcium sulfate to calcium sulfoaluminate molar ratio. Moreover, at 25 °C, in the samples with a calcium sulfate to calcium sulfoaluminate molar ratio of 1, the gypsum was completely consumed by the reaction with calcium sulfoaluminate to form ettringite, while it remained present in all other mixtures.

Furthermore, hydration was accelerated at elevated temperatures in comparison to an ambient temperature, as a higher degree of hydration of calcium sulfoaluminate was observed at the beginning of the hydration, and more ettringite was formed.

Full width at half maximum of ettringite peaks increased at elevated temperatures at a molar ratio of calcium sulfate to calcium sulfoaluminate 1 and 2.5, indicating a decrease in crystallite size at elevated temperatures, due to a higher degree of hydration and faster precipitation of ettringite. However, different gypsum amounts (M-value) did not affect crystallite sizes of ettringite.

At a molar ratio of calcium sulfate to calcium sulfoaluminate 1, the d-values of ettringite peaks increased at elevated temperatures, suggesting a higher ion uptake in the ettringite structure as more ions were released from the cement clinker. At a molar ratio of 2.5, however, there is no significant difference in the d-values, due to a higher addition of gypsum, the cement mixture contains less clinker is in and consequently less substitute ions are available to incorporate into the ettringite.

Author Contributions: Conceptualization, S.D., C.L.L. and M.B.; methodology, S.D., C.L.L. and M.B.; analysis, C.L.L. and M.B.; writing—original draft preparation, M.B.; writing—review and editing, M.B., S.D., C.L.L.; funding acquisition, M.B., S.D., C.L.L. All authors have read and agreed to the published version of the manuscript.

Funding: The research is performed within the Young researcher program (contract number 1000-18-1502) and bilateral project SI-AT Effect of clinkering process on the mineralogy of belite-sulfoaluminate cement clinker (BI-AT/18-19-014), both supported by the Slovenian Research Agency and the Austrian Agency for International Cooperation in Education and Research (OeAD) from grant SI-16-2018.

Acknowledgments: The Metrology Institute of the Republic of Slovenia is acknowledged for the use of XRF.

Conflicts of Interest: The authors declare no conflict of interest.

References

1. Álvarez-Pinazo, G.; Cuesta, A.; García-Maté, M.; Santacruz, I.; Losilla, E.R.; Sanfélix, S.G.; Fauth, F.; Aranda, M.A.G.; De la Torre, A.G. In-Situ Early-Age Hydration Study of Sulfobelite Cements by Synchrotron Powder Diffraction. *Cem. Conc. Res.* **2014**, *56*, 12–19, doi:10.1016/j.cemconres.2013.10.009.
2. Senff, L.; Castela, A.; Hajjaji, W.; Hotza, D.; Labrincha, J.A. Formulations of Sulfobelite Cement through Design of Experiments. *Constr. Build. Mater.* **2011**, *25*, 3410–3416, doi:10.1016/j.conbuildmat.2011.03.032.
3. Álvarez-Pinazo, G.; Santacruz, I.; León-Reina, L.; Aranda, M.A.G.; De la Torre, A.G. Hydration Reactions and Mechanical Strength Developments of Iron-Rich Sulfobelite Eco-Cements. *Ind. Eng. Chem. Res.* **2013**, *52*, 16606–16614, doi:10.1021/ie402484e.
4. Álvarez-Pinazo, G.; Santacruz, I.; Aranda, M.A.G.; De la Torre, Á.G. Hydration of Belite–Ye'elimite–Ferrite Cements with Different Calcium Sulfate Sources. *Adv. Cem. Res.* **2016**, *28*, 529–543, doi:10.1680/jadcr.16.00030.
5. Bullerjahn, F.; Zajac, M.; Skocek, J.; Ben Haha, M. The Role of Boron during the Early Hydration of Belite Ye'elimite Ferrite Cements. *Constr. Build. Mater.* **2019**, *215*, 252–263, doi:10.1016/j.conbuildmat.2019.04.176.
6. Morin, V.; Termkhajornkit, P.; Huet, B.; Pham, G. Impact of Quantity of Anhydrite, Water to Binder Ratio, Fineness on Kinetics and Phase Assemblage of Belite-Ye'elimite-Ferrite Cement. *Cem. Concr. Res.* **2017**, *99*, 8–17, doi:10.1016/j.cemconres.2017.04.014.
7. Bullerjahn, F.; Schmitt, D.; Ben Haha, M. Effect of Raw Mix Design and of Clinkering Process on the Formation and Mineralogical Composition of (Ternesite) Belite Calcium Sulphoaluminate Ferrite Clinker. *Cem. Concr. Res.* **2014**, *59*, 87–95, doi:10.1016/j.cemconres.2014.02.004.
8. Cuberos, A.J.M.; De la Torre, Á.G.; Álvarez-Pinazo, G.; Martín-Sedeño, M.C.; Schollbach, K.; Pöllmann, H.; Aranda, M.A.G. Active Iron-Rich Belite Sulfoaluminate Cements: Clinkering and Hydration. *Environ. Sci. Technol.* **2010**, *44*, 6855–6862, doi:10.1021/es101785n.
9. Jeong, Y.; Hargis, C.W.; Chun, S.-C.; Moon, J. The Effect of Water and Gypsum Content on Strätlingite Formation in Calcium Sulfoaluminate-Belite Cement Pastes. *Constr. Build. Mater.* **2018**, *166*, 712–722, doi:10.1016/j.conbuildmat.2018.01.153.

10. Rossetto, C.M.; Ichikawa, R.U.; Martinez, L.G.; Carezzato, G.L.; Carvalho, A.M.G.; Turrillas, X. In Situ Hydration of Sulfoaluminate Cement Mixtures Monitored by Synchrotron X-Ray Diffraction. *MSF* **2018**, *930*, 153–157, doi:10.4028/www.scientific.net/MSF.930.153.
11. Liao, Y.; Wei, X.; Li, G. Early Hydration of Calcium Sulfoaluminate Cement through Electrical Resistivity Measurement and Microstructure Investigations. *Constr. Build. Mater.* **2011**, *25*, 1572–1579, doi:10.1016/j.conbuildmat.2010.09.042.
12. Martín-Sedeño, M.C.; Cuberos, A.J.M.; De la Torre, Á.G.; Álvarez-Pinazo, G.; Ordónez, L.M.; Gateshki, M.; Aranda, M.A.G. Aluminum-Rich Belite Sulfoaluminate Cements: Clinkering and Early Age Hydration. *Cem. Concr. Res.* **2010**, *40*, 359–369, doi:10.1016/j.cemconres.2009.11.003.
13. Morin, V.; Walenta, G.; Gartner, E.; Termkhajornkit, P.; Baco, I.; Casabonne, J.M. Hydration of a Belite-Calcium Sulfoaluminate-Ferrite cement: Aether™. In Proceedings of the 13th International Congress on the Chemistry of Cement, Madrid, Spain, 3–8 July 2011.
14. Winnefeld, F.; Martin, L.H.J.; Müller, C.J.; Lothenbach, B. Using Gypsum to Control Hydration Kinetics of CSA Cements. *Constr. Build. Mater.* **2017**, *155*, 154–163, doi:10.1016/j.conbuildmat.2017.07.217.
15. Winnefeld, F.; Barlag, S. Calorimetric and Thermogravimetric Study on the Influence of Calcium Sulfate on the Hydration of Ye'elimite. *J. Therm. Anal. Calorim.* **2010**, *101*, 949–957, doi:10.1007/s10973-009-0582-6.
16. Glasser, F.P.; Zhang, L. High-Performance Cement Matrices Based on Calcium Sulfoaluminate–Belite Compositions. *Cem. Concr. Res.* **2001**, *31*, 1881–1886, doi:10.1016/S0008-8846(01)00649-4.
17. Sahu, S.; Havlica, J.; Tomkova, V.; Majling, J. Hydration Behaviour of Sulphoaluminate Belite Cement in the Presence of Various Calcium Sulphates. *Thermochim. Acta* **1991**, *175*, 45–52, doi:10.1016/0040-6031(91)80244-D.
18. Zhang, L.; Glasser, F.P. Hydration of Calcium Sulfoaluminate Cement at Less than 24 h. *Adv. Cem. Res.* **2002**, *14*, 15, doi:10.1680/adcr.2002.14.4.141.
19. García-Maté, M.; De la Torre, A.G.; León-Reina, L.; Losilla, E.R.; Aranda, M.A.G.; Santacruz, I. Effect of Calcium Sulfate Source on the Hydration of Calcium Sulfoaluminate Eco-Cement. *Cem. Concr. Compos.* **2015**, *55*, 53–61, doi:10.1016/j.cemconcomp.2014.08.003.
20. Zajac, M.; Skocek, J.; Bullerjahn, F.; Ben Haha, M. Effect of Retarders on the Early Hydration of Calcium-Sulpho-Aluminate (CSA) Type Cements. *Cem. Concr. Res.* **2016**, *84*, 62–75, doi:10.1016/j.cemconres.2016.02.014.
21. Beltagui, H.; Jen, G.; Whittaker, M.; Imbabi, M.S. The Influence of Variable Gypsum and Water Content on the Strength and Hydration of a Belite-Calcium Sulphoaluminate Cement. *Adv. Appl. Ceram.* **2017**, *116*, 199–206, doi:10.1080/17436753.2017.1289722.
22. Chen, I.A.; Juenger, M.C.G. Synthesis and Hydration of Calcium Sulfoaluminate-Belite Cements with Varied Phase Compositions. *J. Mater. Sci.* **2011**, *46*, 2568–2577, doi:10.1007/s10853-010-5109-9.
23. Kaufmann, J.; Winnefeld, F.; Lothenbach, B. Stability of Ettringite in CSA Cement at Elevated Temperatures. *Adv. Cem. Res.* **2016**, *28*, 251–261, doi:10.1680/jadcr.15.00029.
24. Borštnar, M.; Daneu, N.; Dolenec, S. Phase Development and Hydration Kinetics of Belite-Calcium Sulfoaluminate Cements at Different Curing Temperatures. *Ceram. Int.* **2020**, *46*, 29421–29428, doi:10.1016/j.ceramint.2020.05.029.
25. Jakob, C.; Jansen, D.; Ukrainczyk, N.; Koenders, E.; Pott, U.; Stephan, D.; Neubauer, J. Relating Ettringite Formation and Rheological Changes during the Initial Cement Hydration: A Comparative Study Applying XRD Analysis, Rheological Measurements and Modeling. *Materials* **2019**, *12*, 2957, doi:10.3390/ma12182957.
26. Hesse, C.; Goetz-Neunhoeffer, F.; Neubauer, J.; Braeu, M.; Gaeberlein, P. Quantitative in Situ X-Ray Diffraction Analysis of Early Hydration of Portland Cement at Defined Temperatures. *Powder Diffr.* **2009**, *24*, 112–115, doi:10.1154/1.3120603.
27. Jansen, D.; Spies, A.; Neubauer, J.; Ectors, D.; Goetz-Neunhoeffer, F. Studies on the Early Hydration of Two Modifications of Ye'elimite with Gypsum. *Cem. Conc. Res.* **2017**, *91*, 106–116, doi:10.1016/j.cemconres.2016.11.009.
28. Zajac, M.; Skocek, J.; Bullerjahn, F.; Lothenbach, B.; Scrivener, K.; Ben Haha, M. Early Hydration of Ye'elimite: Insights from Thermodynamic Modelling. *Cem. Conc. Res.* **2019**, *120*, 152–163, doi:10.1016/j.cemconres.2019.03.024.
29. Merlini, M.; Artioli, G.; Meneghini, C.; Cerulli, T.; Bravo, A.; Cella, F. The Early Hydration and the Set of Portland Cements: In Situ X-Ray Powder Diffraction Studies. *Powder Diffr.* **2007**, *22*, 201–208, doi:10.1154/1.2754713.
30. Gastaldi, D.; Paul, G.; Marchese, L.; Irico, S.; Boccaleri, E.; Mutke, S.; Buzzi, L.; Canonico, F. Hydration Products in Sulfoaluminate Cements: Evaluation of Amorphous Phases by XRD/Solid-State NMR. *Cem. Conc. Res.* **2016**, *90*, 162–173, doi:10.1016/j.cemconres.2016.05.014.
31. Jeong, Y.; Hargis, C.W.; Kang, H.; Chun, S.-C.; Moon, J. The Effect of Elevated Curing Temperatures on High Ye'elimite Calcium Sulfoaluminate Cement Mortars. *Materials* **2019**, *12*, 1072, doi:10.3390/ma12071072.
32. Valentini, L.; Dalconi, M.C.; Favero, M.; Artioli, G.; Ferrari, G. In-Situ XRD Measurement and Quantitative Analysis of Hydrating Cement: Implications for Sulfate Incorporation in C-S-H. *J. Am. Ceram. Soc.* **2015**, *98*, 1259–1264, doi:10.1111/jace.13401.
33. Hesse, C.; Goetz-Neunhoeffer, F.; Neubauer, J. A New Approach in Quantitative In-Situ XRD of Cement Pastes: Correlation of Heat Flow Curves with Early Hydration Reactions. *Cem. Conc. Res.* **2011**, *41*, 123–128, doi:10.1016/j.cemconres.2010.09.014.
34. Rietveld, H.M. A Profile Refinement Method for Nuclear and Magnetic Structures. *J. Appl. Crystallogr.* **1969**, *2*, 65–71, doi:10.1107/S0021889869006558.
35. Žibret, L.; Ipavec, A.; Kramar, S. Microstructure of Belite Sulfoaluminate Clinker and Its Influence on Clinker Reactivity. In Proceedings of the International Workshop on Calcium Sulfoaluminate Cements, Murten, Switzerland, 4 June 2018; Volume 2018, p. 1.

36. Taylor, H.F.W. *Cement Chemistry*, 2nd ed.; T. Telford: London, UK, 1997; ISBN 978-0-7277-2592-9.
37. Dolenec, S.; Šter, K.; Borštnar, M.; Nagode, K.; Ipavec, A.; Žibret, L. Effect of the Cooling Regime on the Mineralogy and Reactivity of Belite-Sulfoaluminate Clinkers. *Minerals* **2020**, *10*, 910, doi:10.3390/min10100910.
38. NSAI. *EN 196-6:2018. Methods of Testing Cement-Part 6: Determination of Fineness*; NSAI: Dublin, Ireland, 2010.
39. Snellings, R. X-ray powder diffraction applied to cement. In *A Practical Guide to Microstructural Analysis of Cementitious Materials*; CRC Press: Florida, FL, USA, 2016; pp. 126–195.
40. Cuesta, A.; De la Torre, A.G.; Losilla, E.R.; Peterson, V.K.; Rejmak, P.; Ayuela, A.; Frontera, C.; Aranda, M.A.G. Structure, Atomistic Simulations, and Phase Transition of Stoichiometric Yeelimite. *Chem. Mater.* **2013**, *25*, 1680–1687, doi:10.1021/cm400129z.
41. Cuesta, A.; De la Torre, Á.G.; Losilla, E.R.; Santacruz, I.; Aranda, M.A.G. Pseudocubic Crystal Structure and Phase Transition in Doped Ye'elimite. *Cryst. Growth Des.* **2014**, *14*, 5158–5163, doi:10.1021/cg501290q.
42. Mumme, W.G.; Hill, R.J.; Bushnell-Wye, G.; Segnit, E.R. Rietveld Crystal Structure Refinements, Crystal Chemistry and Calculated Powder Diffraction Data for the Polymorphs of Dicalcium Silicate and Related Phases. *Miner. Geochem.* **1995**, *1*, 35–68.
43. Redhammer, G.J.; Tippelt, G.; Roth, G.; Amthauer, G. Structural Variations in the Brownmillerite Series $Ca_2(Fe_{2-x}Al_x)O_5$: Single-Crystal X-Ray Diffraction at 25 °C and High-Temperature X-Ray Powder Diffraction (25 °C ≤ T ≤ 1000 °C). *Am. Mineral.* **2004**, *89*, 405–420, doi:10.2138/am-2004-2-322.
44. Boeyens, J.; Ichharam, V. Redetermination of the Crystal Structure of Calcium Sulphate Dihydrate, $CaSO_4{\cdot}2H_2O$. Zeitschrift für Kristallographie. *New Cryst. Struct.* **2002**, *217*, 9–10.
45. Sasaki, S.; Fujino, K.; Takéuchi, Y. X-Ray Determination of Electron-Density Distributions in Oxides, MgO, MnO, CoO, and NiO, and Atomic Scattering Factors of Their Constituent Atoms. *Proc. Jpn. Acad. Ser. B* **1979**, *55*, 43–48, doi:10.2183/pjab.55.43.
46. Sakakura, T.; Tanaka, K.; Takenaka, Y.; Matsuishi, S.; Hosono, H.; Kishimoto, S. Determination of the Local Structure of a Cage with an Oxygen Ion in $Ca_{12}Al_{14}O_{33}$. *Acta Cryst.* **2011**, *67*, 193–204, doi:10.1107/S0108768111005179.
47. Gemmi, M.; Merlini, M.; Cruciani, G.; Artioli, G. Non-Ideality and Defectivity of the Akermanite-Gehlenite Solid Solution: An X-Ray Diffraction and TEM Study. *Am. Mineral.* **2007**, *92*, 1685–1694, doi:10.2138/am.2007.2380.
48. Ojima, K.; Nishihata, Y.; Sawada, A. Structure of Potassium Sulfate at Temperatures from 296 K down to 15 K. *Acta Cryst. B* **1995**, *51*, 287–293, doi:10.1107/S0108768194013327.
49. Okada, K.; Ossaka, J. Structures of Potassium Sodium Sulphate and Tripotassium Sodium Disulphate. *Acta Cryst. B* **1980**, *36*, 919–921, doi:10.1107/S0567740880004852.
50. Goetz-Neunhoeffer, F.; Neubauer, J. Refined Ettringite ($Ca_6Al_2(SO_4)_3(OH)_{12}{\cdot}26H_2O$) Structure for Quantitative X-Ray Diffraction Analysis. *Powder Diffr.* **2006**, *21*, 4–11, doi:10.1154/1.2146207.
51. Champenois, J.-B.; Dhoury, M.; Cau Dit Coumes, C.; Mercier, C.; Revel, B.; Le Bescop, P.; Damidot, D. Influence of Sodium Borate on the Early Age Hydration of Calcium Sulfoaluminate Cement. *Cem. Conc. Res.* **2015**, *70*, 83–93, doi:10.1016/j.cemconres.2014.12.010.
52. Cuesta, A.; Zea-Garcia, J.D.; Londono-Zuluaga, D.; De la Torre, A.G.; Santacruz, I.; Vallcorba, O.; Dapiaggi, M.; Sanfélix, S.G.; Aranda, M.A.G. Multiscale Understanding of Tricalcium Silicate Hydration Reactions. *Sci. Rep.* **2018**, *8*, 8544, doi:10.1038/s41598-018-26943-y.
53. Scrivener, K.L.; Füllmann, T.; Gallucci, E.; Walenta, G.; Bermejo, E. Quantitative Study of Portland Cement Hydration by X-Ray Diffraction/Rietveld Analysis and Independent Methods. *Cem. Conc. Res.* **2004**, *34*, 1541–1547, doi:10.1016/j.cemconres.2004.04.014.
54. Cuberos, A.J.M.; De la Torre, Á.G.; Martín-Sedeño, M.C.; Moreno-Real, L.; Merlini, M.; Ordónez, L.M.; Aranda, M.A.G. Phase Development in Conventional and Active Belite Cement Pastes by Rietveld Analysis and Chemical Constraints. *Cem. Conc. Res.* **2009**, *39*, 833–842, doi:10.1016/j.cemconres.2009.06.017.
55. Zajac, M.; Skocek, J.; Stabler, C.; Bullerjahn, F.; Ben Haha, M. Hydration and Performance Evolution of Belite-Ye'elimite-Ferrite Cement. *Adv. Cem. Res.* **2019**, *31*, 124–137, doi:10.1680/jadcr.18.00110.
56. Bullerjahn, F.; Zajac, M.; Ben Haha, M.; Scrivener, K.L. Factors Influencing the Hydration Kinetics of Ye'elimite; Effect of Mayenite. *Cem. Conc. Res.* **2019**, *116*, 113–119, doi:10.1016/j.cemconres.2018.10.026.
57. Jeong, Y.; Hargis, C.; Chun, S.; Moon, J. Effect of Calcium Carbonate Fineness on Calcium Sulfoaluminate-Belite Cement. *Materials* **2017**, *10*, 900, doi:10.3390/ma10080900.
58. Halaweh, M. Effect of Alkalis and Sulfates on Portland Cement Systems. Ph.D. Thesis, University of South Florida, Florida, FL, USA, 2006.
59. Ye, H.; Radli, A. Effect of Alkalis on Cementitious Materials: Understanding the Relationship between Composition, Structure, and Volume Change Mechanism. *J. Adv. Concr. Technol.* **2017**, *15*, 14.
60. Tambara, L.U.D.; Cheriaf, M.; Rocha, J.C.; Palomo, A.; Fernández-Jiménez, A. Effect of Alkalis Content on Calcium Sulfoaluminate (CSA) Cement Hydration. *Cem. Concr. Res.* **2020**, *128*, 105953, doi:10.1016/j.cemconres.2019.105953.
61. López-Acevedo, V.; Viedma, C.; Gonzalez, V.; La Iglesia, A. Salt Crystallization in Porous Construction Materials. II. Mass Transport and Crystallization Processes. *J. Cryst. Growth* **1997**, *182*, 103–110, doi:10.1016/S0022-0248(97)00341-2.
62. Escalante-Garcia, J.I.; Sharp, J.H. The Effect of Temperature on the Early Hydration of Portland Cement and Blended Cements. *Adv. Cem. Res.* **2000**, *12*, 121–130, doi:10.1680/adcr.2000.12.3.121.
63. Richardson, I.G.; Wilding, C.R.; Dickson, M.J. The Hydration of Blastfurnace Slag Cements. *Adv. Cem. Res.* **1989**, *2*, 147–157, doi:10.1680/adcr.1989.2.8.147.

64. Goergens, J.; Manninger, T.; Goetz-Neunhoeffer, F. In-Situ XRD Study of the Temperature-Dependent Early Hydration of Calcium Aluminate Cement in a Mix with Calcite. *Cem. Concr. Res.* **2020**, *136*, 106160, doi:10.1016/j.cemconres.2020.106160.
65. Lothenbach, B.; Winnefeld, F.; Alder, C.; Wieland, E.; Lunk, P. Effect of Temperature on the Pore Solution, Microstructure and Hydration Products of Portland Cement Pastes. *Cem. Conc. Res.* **2007**, *37*, 483–491, doi:10.1016/j.cemconres.2006.11.016.
66. Kjellsen, K.O.; Detwiler, R.J.; Gjørv, O.E. Development of Microstructures in Plain Cement Pastes Hydrated at Different Temperatures. *Cem. Conc. Res.* **1991**, *21*, 179–189, doi:10.1016/0008-8846(91)90044-I.
67. Kjellsen, K.O.; Detwiler, R.J.; Gjørv, O.E. Backscattered Electron Imaging of Cement Pastes Hydrated at Different Temperatures. *Cem. Conc. Res.* **1990**, *20*, 308–311, doi:10.1016/0008-8846(90)90085-C.
68. Thomas, S.; Thomas, R.; Zachariah, A. *Microscopy Methods in Nanomaterials Characterization*; Elsevier: Amsterdam, The Netherlands, 2017.
69. Clark, S.M.; Colas, B.; Kunz, M.; Speziale, S.; Monteiro, P.J.M. Effect of Pressure on the Crystal Structure of Ettringite. *Cem. Conc. Res.* **2008**, *38*, 19–26.
70. Chen, Q.Y.; Tyrer, M.; Hills, C.D.; Yang, X.M.; Carey, P. Immobilisation of Heavy Metal in Cement-Based Solidification/Stabilisation: A Review. *Waste Manag.* **2009**, *29*, 390–403, doi:10.1016/j.wasman.2008.01.019.
71. Chen, B.; Kuznik, F.; Horgnies, M.; Johannes, K.; Morin, V.; Gengembre, E. Physicochemical Properties of Ettringite/Meta-Ettringite for Thermal Energy Storage: Review. *Sol. Energy Mater. Sol. Cells* **2019**, *193*, 320–334, doi:10.1016/j.solmat.2018.12.013.
72. Suyolcu, Y.E.; Wang, Y.; Baiutti, F.; Al-Temimy, A.; Gregori, G.; Cristiani, G.; Sigle, W.; Maier, J.; van Aken, P.A.; Logvenov, G. Dopant Size Effects on Novel Functionalities: High-Temperature Interfacial Superconductivity. *Sci. Rep.* **2017**, *7*, doi:10.1038/s41598-017-00539-4.
.

Chapter 4

The Influence of Calcium Sulfate Content on the Hydration of Belite-Calcium Sulfoaluminate Cements with Different Clinker Phase Compositions

This chapter is based on the published paper: M. Mrak, F. Winnefeld, B. Lothenbach, S. Dolenec, "The influence of calcium sulfate content on the hydration of belite-calcium sulfoaluminate cements with different clinker phase compositions," *Materials and Structures,* vol. 45, no. 6, pp. 17, 2021 [89].

Belite-calcium sulfoaluminate cement clinkers primarily consist of belite, calcium sulfoaluminate and ferrite [20], [33]. Belite-calcium sulfoaluminate cements are then prepared by mixing the clinker with a source of calcium sulfate, such as gypsum, anhydrite, and/or basanite [23], [30]. Calcium sulfate acts as a setting regulator, and its incorporation is essential to attain the compressive strength desired and to ensure dimensional stability [56], [59]. Moreover, the specific type and quantity of calcium sulfate used can influence the hydration and the amount of water needed for complete hydration to occur [20], [48], [56].

The study examines how the addition of varying amounts of calcium sulfate to the cement clinker influences the hydration of two different belite-calcium sulfoaluminate cements with different phase compositions. Calcium sulfate to ye'elimite molar ratios (M value) of 1, 1.5, and 2 were used, while the phase compositions were 65 wt. % belite, 20 wt. % ye'elimite and 10 wt. % ferrite for the CBCSA-B mixture and 50 wt. % belite, 35 wt. % ye'elimite and 10 wt. % ferrite for the CBCSA-Y mixture. X-ray powder diffraction with Rietveld refinement and thermogravimetric analysis were utilized to assess the phase compositions at 1, 7, 28, and 150 days of hydration. The heat of hydration was determined using isothermal calorimetry and the compressive strength of the mortars was determined. The evolution of hydrates was also predicted using the geochemical modelling code GEMS. Porosity was calculated and correlated to the compressive strength.

The results showed that increasing the gypsum content, significantly influenced the hydration kinetics and phase composition of the cement mixes during hydration. Cements react slower when more gypsum is added (as indicated by higher M-values). The gypsum

content controls the amounts of ettringite and monosulfate formed: as the M-ratio increases, more ettringite forms, while less monosulfate is observed. This led to a decrease in the amount of pore solution, as the more water-rich ettringite formed and furthermore, the dissolution kinetics of belite and ferrite decreased. Compared to belite-rich mixture, a higher compressive strength was observed in the ye'elimite-rich mixture, due to greater ettringite content filling the space. Conversely, a higher belite content in the clinker resulted in greater amounts of C–S–H (at the expense of strätlingite) and a reduction in compressive strength. This is because (a) the reaction degree of belite is lower than that of ye'elimite and (b) more C–S–H and strätlingite precipitated than the space-filling ettringite, compared to ye'elimite-rich mixture. The thermodynamic model is consistent with the experimental data collected. A direct correlation was observed between the compressive strength and the amount of bound water determined from thermogravimetric analyses, while there was an inverse correlation with porosity calculated through thermodynamic modelling.

This chapter addresses the thesis objectives 4 and 5.

The contribution of the doctoral candidate was writing the first draft of the manuscript and conducting the experiment detailed in the manuscript, including preparation of the materials (cement clinker and cement) and performing the experimental part (thermogravimetric analysis, X-ray powder diffraction, Rietveld refinement, isothermal calorimetry, compressive strength measurements) and by performing thermodynamic modelling.

Materials and Structures (2021)54:212
https://doi.org/10.1617/s11527-021-01811-w

ORIGINAL ARTICLE

The influence of calcium sulfate content on the hydration of belite-calcium sulfoaluminate cements with different clinker phase compositions

Maruša Mrak · Frank Winnefeld · Barbara Lothenbach · Sabina Dolenec

Received: 4 September 2021 / Accepted: 22 October 2021

Abstract The influence of different amounts of gypsum on the hydration of a belite-rich and a ye'elimite-rich belite-calcium sulfoaluminate clinker (BCSA) was investigated. The hydration kinetics, phase assemblages and compressive strength development of cements prepared using ye'elimite/ calcium sulfate molar ratios of 1, 1.5 and 2 were studied. Besides ettringite and monosulfate, aluminium hydroxide, strätlingite, C−S−H, iron-containing siliceous hydrogarnet and hydrotalcite were present as hydration products. Increasing the amount of gypsum increased the ratio of ettringite to monosulfate formed in the cement paste, lowered the amount of pore solution, delayed the dissolution of belite and ferrite, decreased the formation of strätlingite and, in the case of the ye'elimite-rich BCSA, led to an increase in compressive strength. Increased amounts of belite in the clinker led to the formation of higher quantities of C–S–H, at the expense of strätlingite and a lower compressive strength, as belite has a lower degree of reaction than ye'elimite and due to the formation of more C–S–H and strätlingite compared to the more space-filling ettringite. The thermodynamic model established for BCSA cement hydration agrees well with the experimental data. Compressive strength directly correlated with bound water from thermogravimetric analyses and inversely correlated with the porosity calculated from thermodynamic modelling.

Keywords Belite-calcium sulfoaluminate cement · Gypsum · Hydration · Thermodynamic modelling

1 Introduction

Cement manufacturing is one of the most important industries. After water, the most used material in the world is concrete, which is mainly based on Portland cement, aggregates and water. During the production of Portland cement high emissions of CO_2 are released

Supplementary Information The online version contains supplementary material available at https://doi.org/10.1617/s11527-021-01811-w.

M. Mrak · S. Dolenec (✉)
Slovenian National Building and Civil Engineering Institute, Dimičeva ulica 12, 1000 Ljubljana, Slovenia
e-mail: sabina.dolenec@zag.si

M. Mrak
Jožef Stefan International Postgraduate School, Jamova cesta 39, 1000 Ljubljana, Slovenia

F. Winnefeld · B. Lothenbach
Empa, Swiss Laboratories for Materials Science and Technology, Überlandstrasse 129, 8600 Dübendorf, Switzerland

B. Lothenbach
Department of Structural Engineering, Norwegian University of Science and Technology (NTNU), Trondheim, Norway

Published online: 05 November 2021

into the atmosphere, and a high amount of energy is consumed [1, 2]. To reduce the environmental impact related to cement production, alternative binders, such as belite-calcium sulfoaluminate (BCSA) cements, have been developed. BCSA cements are considered low CO_2 and eco-friendly building materials, not only reducing emissions by up to 30% compared to Portland cement, but also lowering energy consumption [3–5]. Furthermore, substantial amounts of industrial wastes can be used to prepare BCSA cements, allowing natural raw materials to be preserved. As indicated by their name, belite-calcium sulfoaluminate cement clinkers contain belite (Ca_2SiO_4 or C_2S) and calcium sulfoaluminate ($Ca_4(AlO_2)_6SO_3$ or $C_4A_3\overline{S}$) as the main phases, together with ferrite ($Ca_2(Al,Fe)_2O_5$ or C_4AF) and other minor phases [6, 7].

Belite-calcium sulfoaluminate cements are prepared by blending the clinker with a calcium sulfate source in the form of gypsum ($C\overline{S}H_2$), anhydrite ($CaSO_4$ or $C\overline{S}$) and/ or bassanite ($C\overline{S}H_{0.5}$) [8–12]. Calcium sulfate works as a set regulator, an its addition is used to achieve optimum compressive strength and dimensional stability [12–16]. Furthermore, the type and amount of calcium sulfate can also modify the hydration processes and the water required to achieve full hydration [6, 10, 11, 15, 17, 18].

During early hydration, ye'elimite rapidly reacts with calcium sulfate and water, which leads to the formation of ettringite ($C_6A\overline{S}_3H_{32}$) as the main crystalline hydration product and amorphous or poorly crystalline aluminium hydroxide (AH_3) [3, 6, 8, 10, 19, 20], according to Eq. 1:

$$C_4A_3\overline{S} + 2C\overline{S}H_x + (38-2x)H \rightarrow C_6A\overline{S}_3H_{32} + 2AH_3 \quad (x = 0, 0.5, 2) \quad (1)$$

Ettringite precipitates when the molar ratio of calcium sulfate to ye'elimite (M-value) is below 2 ($M < 2$), until the added calcium sulfate is depleted [11, 15, 21, 22]. If the molar ratio of calcium sulfate to ye'elimite (the so-called "M-value") is more than 2 ($M > 2$) a surplus of calcium sulfate is still present after hydration has been completed [15, 16]. An M-value below 1.5 is typical for CSA cements with rapid setting and hardening properties, while values between 1.5 and 2.5 are used for expansive cements [16, 23, 24].

Once the calcium sulfate source has been consumed and sufficient water is still available, monosulfate ($C_4A\overline{S}H_{12}$) precipitates, again together with aluminium hydroxide [6, 11, 15, 21, 25, 26], according to Eq. 2:

$$C_4A_3\overline{S} + 18H \rightarrow C_4A\overline{S}H_{12} + 2AH_3 \quad (2)$$

Furthermore, the hydration of belite in the presence of aluminium hydroxide, which has already precipitated, leads to the formation of strätlingite (C_2ASH_8) [6, 21, 27], according to Eq. 3:

$$C_2S + AH_3 + 5H \rightarrow C_2ASH_8 \quad (3)$$

In the absence of aluminium hydroxide, calcium silicate hydrates (C–S–H), and portlandite (CH) precipitates [6, 8, 21, 28], according to Eq. 4:

$$C_2S + nH \rightarrow C-S-H + mCH \quad (4)$$

Iron-containing siliceous hydrogarnet can be formed by the hydration of ferrite [6] in the presence of strätlingite, according to Eq. 5:

$$C_2ASH_8 + C_4AF + 5H \rightarrow 2\,C_3(A,F)SH_4 + AH_3 \quad (5)$$

After depletion of gypsum, ferrite hydration may also lead to an increase of monosulfate and to a decrease of gypsum according to Eq. 6.; the portlandite formed will participate in further reactions e.g. with aluminium hydroxide to form AFm phases, and iron hydroxide may be incorporated in iron-containing siliceous hydrogarnet.

$$C_4AF + C_6A\overline{S}_3H_{32} + 12\,H \rightarrow 3\,C_4A\overline{S}H_{12} + 2\,FH_3 + 2\,CH \quad (6)$$

While the influence of the source and amount of calcium sulfate on hydration has been widely studied in ye'elimite-rich calcium sulfoaluminate cements [10, 14–16, 29–31], only a limited number of studies have focused on belite-calcium sulfoaluminate cements, in which belite is the most abundant phase in the system. Chen & Juenger [8] investigated clinkers with a differing content of belite and ye'elimite with calcium sulfate added to a varying degree, although belite was the predominant phase (60 wt.%) in only one clinker sample. Even though, isothermal calorimetry was the only method used to investigate the hydration of these cements, the study revealed that the phase composition of clinker and the

amount of calcium sulfate significantly affects the hydration kinetics; no data on phase composition and compressive strength is however available. Sulfate-rich belite-calcium sulfoaluminate cements with different phase compositions were studied by Shen et al. [17], showing the significant effect of phase composition on compressive strength and hydrate assemblage. The influence of different anhydrite contents on compressive strength, hydration kinetics and phase assemblage in a belite-calcium sulfoaluminate cement was studied by Morin et al. [27]. No systematic influence of anhydrite quantity on compressive strength was found by the authors, while increasing the quantity of anhydrite retarded the dissolution of the α'-dicalcium silicate and ferrite phase present in the clinker. These results were confirmed by Zajac et al. [32], who observed that gypsum accelerated early hydration, while retarding late hydration. Furthermore the authors presented a micromechanical model to predict compressive strength.

Nevertheless, the data available regarding the impact of the quantities of calcium sulfate and belite/ye'elimite ratio of cement on the hydration kinetics and strength development of belite-calcium sulfoaluminate cements remains rather limited. In order to tackle the current research gaps, and improve understanding of the hydration processes of belite-calcium sulfoaluminate cements, a more systematic study is needed i.e. it is necessary to assess the influence of different amounts of gypsum and belite/ye'elimite ratio of cement on the hydration of different belite-ye'elimite-ferrite systems, where hydration kinetics and the formation of hydration products are linked to the development of compressive strength and porosity.

The aim of this study is therefore to investigate the effect of the amount of calcium sulfate on the hydration of synthesized belite-calcium sulfoaluminate clinkers with two different phase compositions, using *M*-values of 1, 1.5 and 2. The phase assemblages at 1, 7, 28 and 150 days of hydration are studied by X-ray powder diffraction with Rietveld refinement and thermogravimetric analysis. Furthermore, hydration kinetics is investigated by isothermal calorimetry, and the compressive strength evolution is determined using mortar samples. In addition, a thermodynamic model is established applying the geochemical modelling code GEMS together with the cement-specific database CEMDATA18 in order to predict the evolution of the hydrate phases and to link compressive strength based on the calculated porosities.

2 Materials and methods

2.1 Materials

Six cements were prepared and investigated using either a belite-rich (CBCSA-B) or a ye'elimite-rich belite-calcium sulfoaluminate clinker (CBCSA-Y), and three different quantities of gypsum (M = 1, 1.5 and 2).

The targeted phase composition for the synthesized belite-rich clinker CBCSA-B was 65 wt.% belite (C_2S), 20 wt.% ye'elimite ($C_4A_3\overline{S}$) and 10 wt.% ferrite (C_4AF), compared to 50 wt.% belite (C_2S), 35 wt.% ye'elimite ($C_4A_3\overline{S}$) and 10 wt.% ferrite (C_4AF) for the ye'elimite-rich CBCSA-Y. The investigated belite and calcium sulfoaluminate contents were chosen with respect to the compositions of BYF clinkers suggested by Morin et al. [33] (BCSA-B has maximum and BCSA-Y minimum belite content regarding their suggestion). Both clinkers were produced by firing appropriate mixtures of limestone, fly ash, bottom ash, calcined bauxite, titanogypsum and mill scale in a Protherm furnace PLF 160/9 at 1250 °C at a heating rate of 10 K/min, with a holding time of 60 min at the final temperature followed by slow cooling in the closed furnace. The synthesis of cement clinkers is described in detail in Borštnar et al. [34]. Natural gypsum was used as the source of calcium sulfate.

X-ray fluorescence analyses of the clinkers and gypsum were conducted according to EN 196-2 (Table 1), while phase compositions were derived from quantitative X-ray diffraction (Table 2). The actual phase compositions of the clinkers are close to the targeted ones. Besides ye'elimite, belite and ferrite, around 5 wt. % of minor phases (mayenite, periclase, gehlenite, γ-dicalcium silicate, perovskite, aphthitalite, arcanite) are present.

The synthesized clinkers were first ground below 0.125 mm in a vibratory disc mill (SIEBTECHNIK Labor Scheibenschwingmühle TS. 250) and afterwards using a ball mill (CAPCO Test Equipment Ball Mill Model 9VS). The Blaine specific surface areas of the cement clinkers, determined according to EN

Table 1 Chemical analyses of the BCSA clinkers and gypsum, wt. % (WD-XRF, fused beads)

	CBCSA-B	CBCSA-Y	Gypsum
CaO	55.17	51.23	33.87
SiO_2	22.21	16.90	0.32
Al_2O_3	12.15	19.55	0.05
Fe_2O_3	3.62	3.66	0.04
MgO	1.53	1.28	0.39
K_2O	0.68	0.52	< 0.04
Na_2O	0.29	0.23	< 0.06
TiO_2	0.674	1.068	< 0.016
P_2O_5	0.092	0.091	0.006
Cr_2O_3	0.083	0.078	0.002
MnO	0.060	0.047	0.003
SO_3	2.93	4.88	44.25
L.O.I. [1]	0.31	0.24	21.02
Total	99.77	99.76	99.95

[1]Loss on ignition

196-6, were 4740 cm^2/g (specific density 3.18 g/cm^3) for the CBCSA-B cement clinker and 4250 cm^2/g (specific density 3.07 g/cm^3) for the CBCSA-Y. The gypsum was sieved to below 0.063 mm prior to use. The particle size distributions of the clinker and gypsum were determined using a laser particle analyzer (Malvern Mastersizer X). The powders were dispersed in isopropanol by ultrasound. The results are shown in Fig. 1. As expected from the Blaine values, the CBCSA-B clinker shows a slightly finer particle size distribution than clinker CBCSA-Y. The particle size distribution of the gypsum is broader than the distributions of the CBCSA clinkers.

The cement mixtures BCSA-B and BCSA-Y were prepared by blending the clinkers with different amounts of gypsum in order to achieve calcium sulfate to ye'elimite molar ratios (*M*-values) of 1, 1.5 and 2 (see Table 3) in order to cover a wide range of *M*-values (rapid setting/hardening—expansive cements). Batches of 200 g were mixed in a Turbula powder blender mixer (WAB-group) for 2 h prior to use.

2.2 Preparation of samples for hydration experiments

The hydration experiments were carried out at 20 °C, using a water to cement ratio of 0.50. Cement pastes were mixed manually for 3 min using a spatula, filled into 15 ml polyethylene vials and cured sealed at 20 °C. Hydration was stopped by solvent exchange using isopropanol and diethyl ether [35] at 1, 7, 28 and 150 days. The crushed samples were submerged in isopropanol for 15 min, filtered using a Büchner funnel, rinsed first with isopropanol and then twice with diethyl ether and finally dried for 8 min at 40 °C [36]. Afterwards, the dry pastes were ground by hand to a particle size of below 0.063 mm using an agate

Table 2 Phase compositions of the BCSA clinkers and gypsum, determined by X-ray powder diffraction and Rietveld refinement, wt. %

	CBCSA-B	CBCSA-Y	Gypsum
β-Dicalcium silicate (belite)	60.6	50.9	–
γ-Dicalcium silicate	6.9	0.8	–
Ye'elimite orthorhombic	6.9	17.4	–
Ye'elimite cubic	9.3	14.9	–
Ferrite	11.9	10.4	–
Mayenite	2.4	3.2	–
Periclase	1.2	1.0	–
Gehlenite	0.6	–	–
Perovskite	–	1.0	–
Aphthitalite	0.5	0.2	–
Arcanite	0.5	0.2	–
Gypsum	–	–	96.7
Anhydrite	–	–	3.3

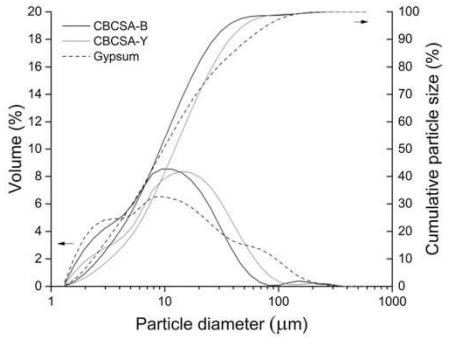

Fig. 1 Particle size distributions of cement clinkers CBCSA-B, CBCSA-Y, and gypsum

mortar and investigated by X-ray powder diffraction and thermogravimetric analyses.

2.3 X-ray powder diffraction

X-ray powder diffraction was performed using a PANalytical X'Pert Pro X-ray powder diffractometer equipped with a CuKα X-ray tube, a Johannson Ge(111) incident beam monochromator and an X'Celerator detector. Samples were back-loaded into a circular sample holder (diameter 27 mm) in order to reduce preferred orientation effects. Samples were measured at 45 kV at a current of 40 mA in a 2θ range of 5–75° with a step size of 0.017°2θ, using a 1° divergence slit and a 15 mm mask. The Rietveld refinements were performed using the PANalytical X'Pert High Score Plus V. 4.9 software and the crystal structures suggested by Snellings [37], with the exception of the structures of orthorhombic and cubic ye'elimite, which were taken from Cuesta et al. [38, 39]. To quantify the total amorphous and poorly crystalline phases, the G-factor method [40–42] was used, with CaF_2 (Sigma Aldrich) as an external standard. The results were normalized to 100 g of dry binder, taking into account the amount of bound water derived from the thermogravimetric analysis, which was determined from the weight loss at 550 °C [43].

2.4 Thermogravimetric analyses

Thermogravimetric (TGA) analyses of the hydrated samples were carried out using a Mettler Toledo TGA/SDTA 851^e in the temperature range 30 to 980 °C at a heating rate of 20 K per minute under a nitrogen atmosphere. About 60 mg of the samples were placed in 150 µl alumina crucibles.

2.5 Isothermal calorimetry

Isothermal conduction calorimetry was performed to determine the hydration heat flow and cumulative heat of cement pastes using a TAM Air (TA instruments). 4 g of the prepared cement and 2 g of deionized water (at a water to cement ratio of 0.5) were mixed manually for 3 min using a spatula, filled into a glass ampoule, capped and then placed directly into the calorimeter. All measurements were carried out at 20 °C and recorded for 168 h. The first 30 min of hydration could not be observed due to the external mixing procedure.

2.6 Compressive strength

For compressive strength measurements, mortars were prepared with quartz sand (CEN-Standard Sand EN 196-1-Normensand with grain sizes between 0.1 and 2 mm), using a cement/sand ratio of 25/75 by mass and a cement to water ratio of 0.50. Mortars were mixed according to EN 196-1, cast in 25 mm × 25 mm × 25 mm moulds, demoulded after 24 h and then cured at 20 °C and 95 ± 2% relative humidity until

Table 3 Mix design (g/100 g cement) of the analysed cements

	BCSA-B			BCSA-Y		
	$M = 1$	$M = 1.5$	$M = 2$	$M = 1$	$M = 1.5$	$M = 2$
CBCSA-B	95.5	93.3	91.3	–	–	–
CBCSA-Y	–	–	–	91.3	87.5	83.9
Gypsum	4.5	6.7	8.7	8.7	12.5	16.1

testing. Compressive strength was determined at 1, 7, 28 and 150 days on six prism halves per measurement age using an LFM 50 testing machine (Walter + Bai) at a loading rate of 0.2 MPa/s.

2.7 Thermodynamic modelling

To predict the type and amount of hydrates formed during hydration of the anhydrous binders, thermodynamic modelling was carried out using the geochemical software GEMS [44, 45] coupled with the cement-specific CEMDATA 18 thermodynamic database [46].

As a first step the phase volumes during hydration of the BCSA clinkers blended with 0–30 wt.% of gypsum were calculated. The phase compositions of the clinkers and the gypsum, as determined by X-ray powder diffraction, were used as inputs. A reaction degree of 100% was assumed for ye'elimite and mayenite, and of 50% for belite, ferrite and periclase, in agreement with the average long-term dissolution degrees reported in the literature e.g. by [14, 27, 32]. All the sulfate phases (anhydrite, gypsum, arcanite, aphthitalite) were allowed to fully react. Gehlenite, γ-belite and perovskite were considered as inert phases [15].

Furthermore, the phase changes with ongoing hydration were modelled. Here, the reaction degrees of the clinker phases depending on the hydration time obtained from X-ray powder diffraction were used and fitted with a sigmoidal non-linear equation (Eq. 7):

$$\mathrm{DoR} = \frac{a-d}{1+\left(\frac{t}{C}\right)^{b}} + d \tag{7}$$

where DoR is the reaction degree, t is the hydration time in days, a is the minimum reaction degree (set to 0), B is the maximum steepness, c is the inflection point and d is the maximum reaction degree (set to 100) [47, 48].

All thermodynamic calculations were conducted at 20 °C under oxidizing conditions. A water to cement ratio of 0.50 was applied, which corresponds to the value used in the experiments. For the C–S–H, the CSHQ model from Kulik [49] was used.

Based on the thermodynamic calculations of the phase assemblage as a function over time it is possible to calculate the porosities of the samples (Eq. 8):

$$P = \frac{V_{\mathrm{unhydratedcement},\,t=0} + V_{\mathrm{hydrates},\,t=0} + V_{\mathrm{poresolution},\,t=0} - V_{\mathrm{hydrates},\,t} - V_{\mathrm{unhydratedcement},\,t}}{V_{\mathrm{unhydratedcement},\,t=0} + V_{\mathrm{hydrates},\,t=0} + V_{\mathrm{poresolution},\,t=0}} \times 100 \tag{8}$$

where P is the porosity in %, V is the volume in cm^3, $t = 0$ is the time at the beginning of hydration and t is time [50].

3 Results and discussion

3.1 Thermodynamic modelling of the effect of gypsum on the hydrate assemblage

Figure 2a depicts the calculated long-term hydrate assemblages of the belite-rich BCSA-B clinker blended with different amounts of gypsum varying between 0 and 30 wt. %. Without gypsum, or when the gypsum content is low (< 3 wt%), it is calculated that monosulfate, strätlingite, katoite (C_3AH_6), siliceous hydrogarnet ($C_3(A,F)S_{0.84}H_{4.32}$), C–S–H and hydrotalcite are calculated to be present. Above 4.5 wt.% gypsum ettringite starts to form, and its amount increases along with an increase in gypsum, at the expense of monosulfate. The formation of the compared to monosulfate more water-rich ettringite results also in a lower amount of pore solution. C–S–H is more abundant than strätlingite. The latter phase becomes destabilized when higher contents of gypsum (above approximately 26 wt.%) are used. Aluminium hydroxide is not calculated to be present when the gypsum content is above 2 wt.%, as the aluminium hydroxide released by the hydration of ye'elimite is used for the formation of strätlingite, according to Eq. 3. The reaction of ferrite and belite is expected to result in some siliceous hydrogarnet containing both iron and aluminium.

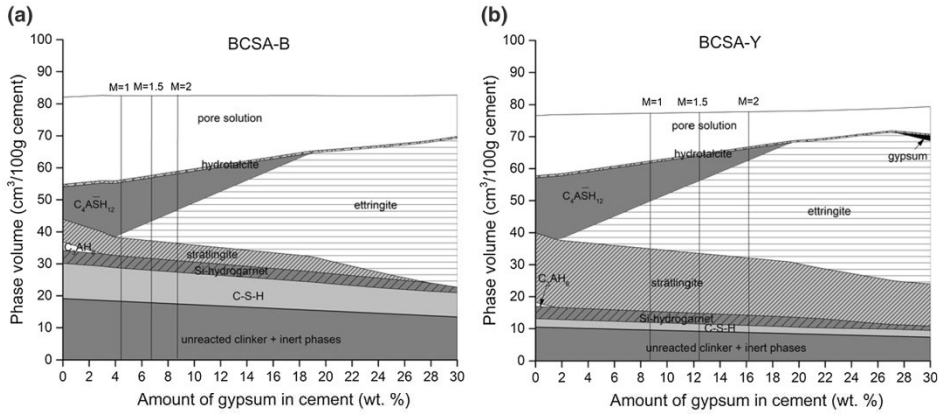

Fig. 2 Calculated hydrate assemblages in cm3 per 100 g unhydrated binder for **a** the belite-rich BCSA-B and **b** the ye'elimite-rich BCSA-Y cements, as a function of the amount of gypsum. The lines indicate the samples studied experimentally at M = 1, 1.5 and 2

Figure 2b shows the calculated hydrate assemblages of the ye'elimite-rich BCSA-Y clinker blended with gypsum. As this clinker contains less belite and more ye'elimite than the BCSA-B, an equivalent M-ratio corresponds to a higher content of gypsum and thus to more ettringite and strätlingite. The formation of ettringite is calculated already at gypsum contents of 2 wt.% and above, while aluminium hydroxide is calculated to be absent over the entire range of gypsum additions. Due to the presence of less belite and more ye'elimite in this blend, less C–S–H, but more strätlingite, is expected to form. Again, the formation of more ettringite in the presence of more gypsum lowers the amount of the pore solution, and this effect is more pronounced in the ye'elimite-rich BCSA-Y system compared to in the BCSA-B.

3.2 Hydrate assemblage

The XRD patterns of the investigated systems BCSA-B and BCSA-Y with M-values of 1, 1.5 and 2 at 150 days of hydration are presented in Fig. 3. Patterns related to the samples at other ages are provided in Fig. S1 in the Electronic Supplementary Material (ESM). Normalized quantitative X-ray powder diffraction data of cements BCSA-B and BCSA-Y with calcium sulfate to ye'elimite molar ratios of 1.5 are shown in Fig. 4. Phase quantifications of the

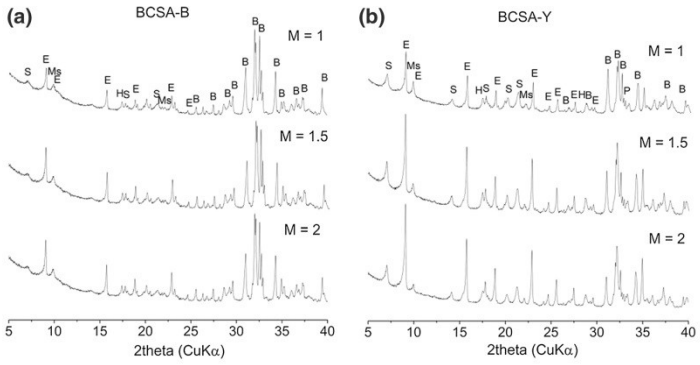

Fig. 3 X-ray diffraction patterns of **a** BCSA-B and **b** BCSA-Y at M = 1, 1.5 and 2 at 150 days of hydration. B = belite, P = perovskite, E = ettringite, Ms = monosulfate, S = strätlingite, H = siliceous hydrogarnet

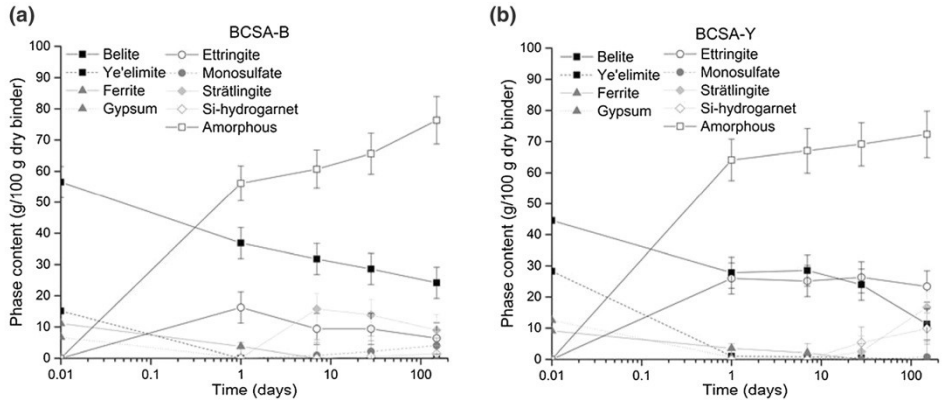

Fig. 4 X-ray powder diffraction quantification of the phase development in hydrating **a** BCSA-B and **b** BCSA-Y cement at $M = 1.5$

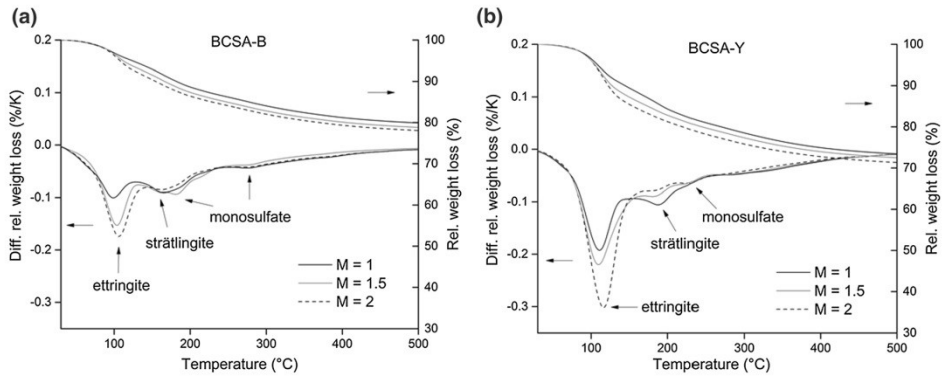

Fig. 5 Thermogravimetric analysis of cement pastes **a** BCSA-B and **b** BCSA-Y with the addition of different amounts of calcium sulfate at 150 days of hydration

samples with other molar ratios are provided in Fig. S2 in the ESM. Figure 5 plots the results of the thermogravimetric analyses of cements BCSA-B and BCSA-Y with M-values of 1, 1.5 and 2 at 150 days of hydration. TGA data of the samples at other curing times are available in Fig. S3 in the ESM.

The results of the BCSA-B cement mixtures (Figs. 3a and 4a) reveal that ye'elimite, as the early reacting phase, and gypsum have already dissolved within the first 24 h of hydration and are therefore not detected anymore at any of the calcium sulfate to ye'elimite molar ratios (see also Figs. S1–S3 in the ESM). The hydration of ye'elimite in the presence of gypsum leads to the formation of ettringite, according to Eq. 1, until the gypsum is depleted. These results are consistent with the TGA analyses, where the main weight loss measured at 120 °C can be assigned to ettringite [6, 16, 51] (see Fig. 5a and Fig. S3 in the ESM). After 7 days of hydration, the amount of ettringite decreases and the amount of monosulfate continues to increase with time due to the ongoing hydration of the ferrite phase (see Eq. 6), providing additional aluminium ions [51, 52]. As expected, more ettringite is present at higher M-values, while the

amount of monosulfate is lower, indicating that gypsum is controlling the ratio of precipitated ettringite to monosulfate, creating a shift from ettringite to monosulfate as the amount of gypsum decreases (Figs. 3a, 4a and 5a and Figs. S1–S3 in the ESM [6, 8, 14, 16, 31]). Belite dissolves as the hydration time increases, but is still present at 150 days of hydration, underlining the low reaction of belite in such aluminium-rich systems. The reaction degree of belite in the BCSA-B mixtures is rather independent of the calcium sulfate to ye'elimite molar ratio, reaching a value of approximately 60% at 150 days, similar to the data provided by Jeong et al.[14], Morin et al.[27] and Zajac et al. [32]. As sufficient water is available for hydration in these mixtures (see Fig. 2), the hydration of belite does not appear to be limited by a lack of water.

Ferrite is depleted after 7 days of hydration. At increasing M-values, however, more unreacted ferrite remained at 1 day, indicating that calcium sulfate delays the reaction of ferrite. This is consistent with the work of Morin et al. [27], which showed that the kinetics of the dissolution of ferrite is slower when higher amounts of calcium sulfate are added.. The authors speculated that an increasing lack of space due to precipitation of higher amounts of ettringite from previous ye'elimite hydration might be the reason for this delay.

Strätlingite is in BCSA-B identified from day 1 onwards at M = 1 and after 7 days of hydration at M = 1.5 and 2 (see Figs. S1–S3 in the ESM), as a result of the hydration of belite with aluminium hydroxide [21, 27]. Aluminium hydroxide is not detected by X-ray powder diffraction as a result of its poor crystallinity, but it is visible in the TGA data (Fig. S3a), identifiable as a weight loss at around 250–280 °C [6, 16, 53]. The amount of strätlingite slightly decreases at higher M-ratios (at M = 1.5 and M = 2), since the presence of more sulfate available for the formation of ettringite results in less aluminium available for the formation of strätlingite [14], confirming the findings of Jeong et al. [14] and Hargis et al. [54]. Moreover, after 28 days the reaction of ferrite, together with Ca from belite, C–S–H, or strätlingite, leads to the formation of siliceous hydrogarnet containing iron [6, 33], according to Eq. 5. The presence of C–S–H is not confirmed by TGA due to its main hydration peak overlapping with that of ettringite [32].

In the BCSA-Y cement mixtures, gypsum and ye'elimite have not yet been consumed after 1 day of hydration (see Fig. 4b and Figs. S1, S2 in the ESM), while in the BCSA-B mixtures they are already fully dissolved at that time. In the BCSA-Y systems, the gypsum is fully dissolved after 7 days at M = 1 and after 28 days at M = 1.5, while it is still present after 150 days of hydration at M = 2. At a high M-value more ettringite precipitates, which consumes more water and could slow down the hydration at later ages. This is far more evident at M = 2, where etringite is the only hydration crystalline hydration product detected after 150 days. Ye'elimite dissolves more slowly than in the BCSA-B. A few percent are still present after 1 day of hydration, and small amounts persist until 150 days. As the M-value increases, the ye'elimite is consumed slightly faster.

Regarding the hydrate assemblage, the main difference between cements BCSA-Y and BCSA-B is the presence of more ettringite and less monosulfate in the BCSA-Y cement, which is in accordance with the thermodynamic modelling and TGA analysis and also observed by Chen & Juenger [9]. However, the amount of ettringite significantly decreases with hydration time only at M = 1, where monosulfate precipitated, while at M = 1.5 and M = 2 monosulfate is hardly identified, confirming that the amount of monosulfate decreases with an increasing amount of calcium sulfate addition. At M = 2, ettringite is the only crystalline hydration product identified in large amounts, which, according to data from the literature causes a dense microstructure due to its high molar volume, thus hindering the dissolution of belite and the formation of other hydration products [8, 13, 14]. A slower dissolution of belite is therefore observed in the BCSA-Y cement as the addition of calcium sulfate is increased (see Fig. 4b and Fig. S2 in the ESM). At M = 2 the amount of belite decreases only slightly between 1 and 150 days of hydration, confirming its hydration is delayed at such a high sulfate addition [27], as stated before, due to the high water consumption of ettringite, as the only crystalline hydration product identified, which slows down the hydration.

The amount of unreacted ferrite phase increases with an increasing M-value, which is consistent with the results of the BCSA-B cement. According to TGA some aluminium hydroxide is present, however not detected by XRD. At higher M-values (i.e. M = 2) more aluminium hydroxide is observed in BCSA-Y

compared to BCSA-B. This is the result of a higher amount of reacted ye'elimite in the presence of gypsum, more precipitated ettringite and therefore more aluminium ions present [16] and also due to a lower degree of hydration of belite to strätlingite, which consumes aluminium hydroxide.

The amount of strätlingite decreases with an increasing M-value, again due to less aluminium available, as already observed in the BCSA-B cement. At $M = 1$ strätlingite is identified after 7 days, at $M = 1.5$ after 28 days, while at $M = 2$ it could not clearly be identified after 150 days. Compared to the BCSA-B mixture, significantly less strätlingite is formed in the BCSA-Y mixture, which corresponds to the lower belite content of the ye'elimite-rich BCSA. Siliceous hydrogarnet is formed at $M = 1$ and $M = 1.5$ with the reaction of belite and ferrite after 28 days, when belite and ferrite have been consumed significantly. Its amount increases between 28 and 150 days. At $M = 2$, siliceous hydrogarnet is not detected due to the low reaction degrees of belite and ferrite. In general, there is good agreement between the experimental data and the modelled phase assemblages. As predicted by thermodynamic modelling, the formation of ettringite, monosulfate, strätlingite and siliceous hydrogarnet as the main hydration products is also observed experimentally. Increasing the gypsum content led to the formation of more ettringite and less monosulfate, in agreement with previous observations [14].

3.3 Thermodynamic modelling of phase development with time

Figure 6 shows changes in the phase contents of the BCSA-B and BCSA-Y cements with ongoing hydration when the *M*-value is 1.5. Graphs for the cements with M-values of 1 and 2 can be found in the ESM (Fig. S4).

The modelled hydrate assemblages in both systems (BCSA-B, BCSA-Y) are similar; ettringite, aluminium hydroxide, monosulfate, strätlingite, C–S–H, katoite and hydrotalcite are calculated. As hydration time increases, first the dissolution of ye'elimite and gypsum takes place, resulting in the precipitation of ettringite. Once the gypsum is consumed, the amount of ettringite decreases (especially in the BCSA-B), and monosulfate is formed. At higher *M*-values the gypsum is consumed later, and more ettringite but less monosulfate is formed. In general, higher amounts of ettringite and lower amounts of monosulfate are formed in the BCSA-Y compared to the BCSA-B. In the ye'elimite-rich BCSA-Y cement no monosulfate is predicted when $M = 2$, as sufficient calcium sulfate is provided to make ettringite from the aluminium ions provided by ye'elimite and ferrite, which are not used to make strätlingite. Along with ettringite and monosulfate aluminium hydroxide is also formed, which is however consumed by the reaction with belite to form strätlingite. It is present only in small amounts in BCSA-B, while in BCSA-Y significantly higher

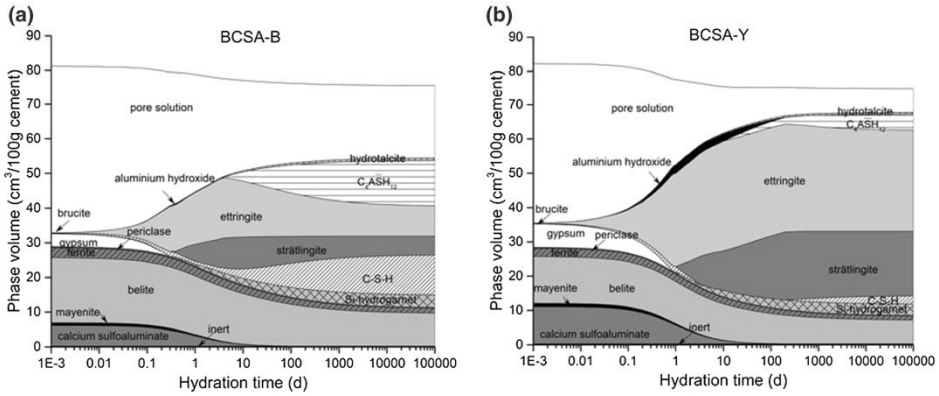

Fig. 6 Thermodynamic modelling of the phase assemblages depending on hydration time at $M = 1.5$ for **a** the BCSA-B cement and **b** the BCSA-Y cement

amounts of aluminium hydroxide precipitate. A small amount of siliceous hydrogarnet containing iron yields from the hydration of the belite and ferrite phases. The amount of C–S–H increases over time, while at the same time more belite also reacts. As expected, more strätlingite and C–S–H are formed in the belite-rich BCSA-B than in the ye'elimite-rich BCSA-Y. Traces of hydrotalcite are also calculated in all mixtures.

In general, there is good agreement between the experimental data and the modelled phase assemblages. As also observed by the experimental data, the calculations predict the formation of ettringite, aluminium hydroxide, monosulfate, strätlingite and siliceous hydrogarnet as the main hydration products. The observed increase and then later decrease in the quantities of ettringite, experimentally observed especially in the BCSA-B systems, is well represented in the calculations. C–S–H, which is calculated to be present in trace amounts in BCSA-Y and in higher amounts in BCSA-B, could not be identified experimentally by XRD due to its poor crystallinity and due to overlapping peaks in TGA. Siliceous hydrogarnet seems to be over-estimated, which could be attributed to its slow formation at room temperature [2]. Hydrotalcite could not be identified in the experiments due to its low quantities and/ or crystallinity. Strätlingite, when it is present in only low amounts such as in the ye'elimite-rich BCSA-Y at $M = 2$, is hard to identify due to the same reasons.

3.4 Isothermal calorimetry

The heat flow and cumulative heat data obtained by isothermal calorimetry are shown in Fig. 7. The initial peak, which is attributed to the wetting of the system, fast dissolution of clinker phases and early hydration reactions [8, 12, 16–18, 20] cannot be assessed due to the external mixing method and is thus not displayed and discussed.

All mixtures show a short induction period after the initial peak, which lasts for about 2 hours. Namely, this period is attributed to the slow dissolution of clinker phases and the slow formation of ettringite [12, 16, 17].

Following this, the main hydration peak, which is attributed to the dissolution of ye'elimite and gypsum and the precipitation of ettringite together with aluminium hydroxide [8, 9, 12, 18, 20], occurs after approximately 3.2 hours in both cement mixtures BCSA-B and BCSA-Y [14], regardless of the amount of gypsum added.

A further, third heat maximum occurs, which is related to ongoing hydration after depletion of sulfate and the precipitation of monosulfate and/or the secondary formation of ettringite [9, 12, 15, 16]. Its intensity increases with decreasing amounts of added gypsum, and its maximum is shifted to an earlier time. This indicates that, as more calcium sulfate is added, more ettringite precipitates according to Eq. 1, thus leaving less ye'elimite for the reaction according to Eq. 2 [8, 14, 55]. In the BCSA-B cement the third maximum occurs after 4, 5.5 and 6.5 hours at $M = 1$, $M = 1.5$ and $M = 2$, respectively. In the BCSA-Y cement this peak appears later, after 6, 8.5 and 10 h at $M = 1$, $M = 1.5$, and $M = 2$, respectively, which is due to the higher ye'elimite content in the BCSA-Y clinker compared to in the BCSA-B and therefore, as X-ray powder diffraction results showed, more ettringite and less monosulfate are formed.

Furthermore, another visible peak occurs in the BCSA-B cement mixtures, which is also shifted to an earlier time with a decreasing amount of added gypsum and occurs at 24 and 32 for $M = 1$, and $M = 1.5$. This peak appears at $M = 2$ very late, only after 50 hours. This could be explained by the reaction of belite to yield strätlingite, while increasing gypsum delays the formation of strätlingite [14, 54], as confirmed by X-ray powder diffraction (see Fig. 3 and Fig. S1 in the ESM). In the BCSA-Y system this additional peak probably related to belite hydration is hardly visible due to the lower quantities and the slower reaction of belite compared to the BCSA-B system.

The BCSA-Y cement mixtures show higher initial cumulative heat and also higher values after 7 days of hydration compared to the BCSA-B cement mixtures, indicating that the hydration of ye'elimite creates more heat than the hydration of belite (see Fig. 7c, d). In both BCSA-B and BCSA-Y the cumulative heat at all three M-ratios is rather similar.

3.5 Compressive strength

Results showing the compressive strength of the cement mixtures BCSA-B and BCSA-Y with differing amounts of gypsum are shown in Fig. 8.

All cements show rapid strength development at early ages due to the fast hydration of ye'elimite with gypsum and, consequently, the precipitation of a high

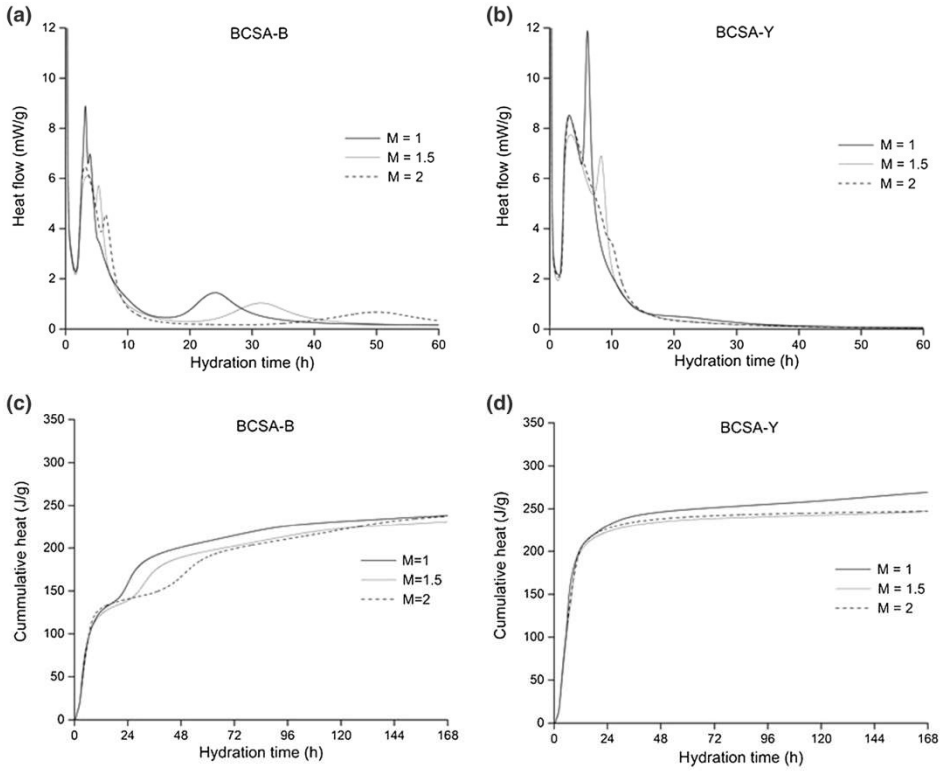

Fig. 7 Hydration heat flow of the **a** BCSA-B and **b** BCSA-Y cements and development of the cumulative heat of hydration in the **c** BCSA-B and **d** BCSA-Y cements blended with different amounts of gypsum

amount of ettringite [2, 14]. This is in accordance with the results of X-ray diffraction and thermogravimetry, which reveal that gypsum has already been consumed within the first 24 h of hydration in the BCSA-B cements, while in the BCSA-Y a small amount remains unreacted.

All cement mixtures BCSA-B show a gradual increase in compressive strength up to 150 days, with very fast compressive strength development between 1 and 7 days (Fig. 8a). Beyond 7 days of hydration, the compressive strength increases slowly. At late ages (150 days) compressive strength is lowest when $M = 2$ (24.9 MPa), followed by when $M = 1$ (27.5 MPa), with the highest compressive strength developed when $M = 1.5$ (30.3 MPa).

The compressive strength evolution of the BCSA-Y cement mixtures (Fig. 8b) shows a similar trend as to the BCSA-B cement mixtures, however at $M = 1$ and $M = 1.5$ only a slight strength gain between 1 and 7 days is observed in BCSA-B. After 7 days of hydration, the compressive strengths increase with an increasing amount of gypsum, as was also observed by Beltagui et al. [31], reaching final values of 39.6 MPa, 45.7 MPa, and 48.3 MPa at 150 days for $M = 1, M = 1.5$ and $M = 2$, respectively. This effect is due to a higher amount of precipitated ettringite with increasing M-values, as confirmed by X-ray powder diffraction (see Fig. 3). Moreover, the compressive strength of the sample with $M = 1$ is much lower with respect to the other two samples with M-values of 1.5

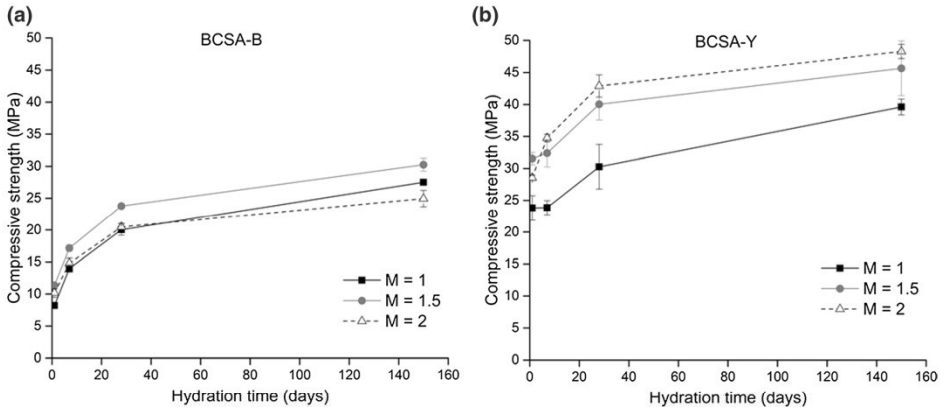

Fig. 8 Compressive strength development of the **a** BCSA-B and **b** BCSA-Y cements with differing amounts of gypsum

and 2, most likely due to much less ettringite formed at a low *M*-value.

The results show that the BCSA-Y cement mixtures have significantly higher compressive strengths than the BCSA-B cements at all hydration times, especially at an early age. This is due to the higher ye'elimite content and a higher amount of precipitated ettringite, as determined by X-ray powder diffraction and thermogravimetric analysis (Fig. 3), which has also been reported elsewhere [2, 8]. These results are in accordance with isothermal calorimetry, where it can be seen that the cumulative heat flow is higher in BCSA-Y than in BCSA-B, especially at early ages.

Figure 9a plots the compressive strength versus bound water, as determined by thermogravimetric analyses, for both cement systems. Compressive strength increases as the bound water content increases, and a linear correlation is evidenced for all data points. The amount of bound water is related to the volume of hydration products, which itself is related to porosity and thus to compressive strength.

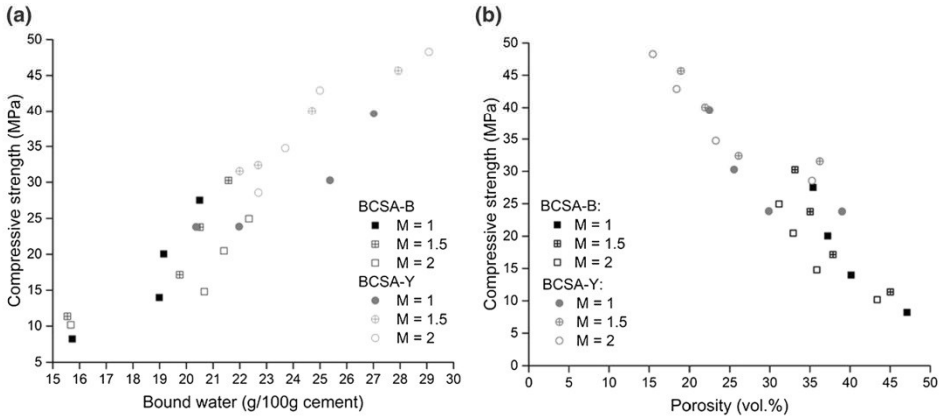

Fig. 9 **a** Bound water, as determined by TGA compared to measured compressive strength; **b** Calculated porosity compared to measured compressive strength

In Fig. 9b compressive strength is plotted against the calculated porosities as derived from thermodynamic modelling. With decreasing porosity, the compressive strength increases. Again, all data points show a linear correlation between porosity and compressive strength. This indicates that, regardless of the phase compositions of the cements (i.e. different ye'elimite/belite and ye'elimite/gypsum ratios), compressive strength is mainly governed by the volume of hydrates formed and porosity.

4 Conclusions

In this study, the effect of various amounts of gypsum (calcium sulfate to ye'elimite molar ratios i.e. *M*-values of 1, 1.5 and 2) on the hydration mechanism of belite-rich and ye'elimite-rich belite-calcium sulfoaluminate cement clinkers was investigated by means of experimental methods and thermodynamic modelling.

In all systems investigated, the main hydration products at an early age are ettringite in addition to amorphous aluminium hydroxide, which precipitated due to the rapid hydration of ye'elimite in the presence of gypsum. After consumption of gypsum monosulfate forms, while the amount of ettringite decreases due to the supply of additional aluminium ions from dissolution of the ferrite phase. At later hydration times belite dissolves significantly, and siliceous hydrogarnet, strätlingite and C–S–H are formed.

The addition of gypsum plays an important role in the kinetics and phase assemblage formed during hydration. The cements react earlier and release more heat during the hydration when less gypsum is added (lower *M*-values). The amount of gypsum controls the quantities of ettringite and monosulfate precipitated, with an increasing amount of ettringite and a decreasing amount of monosulfate at higher *M*-ratios. With increasing amounts of the water-rich ettringite formed at increasing *M*-ratios, the water demand needed for full hydration increases and thus late hydration will slow down if the water/cement ratio applied is too low. Increasing the addition of gypsum decreases the dissolution kinetics of belite and ferrite. More strätlingite is formed at lower *M*-ratios due to less ettringite formed and therefore more aluminium is available for the formation of strätlingite. In the ye'elimite-rich clinker increasing the amount of gypsum increases compressive strength, as higher quantities of the space-filling ettringite are formed. In the belite-rich systems the differences were not as significant.

A higher amount of belite, and correspondingly less ye'elimite in the clinker, leads to higher amounts of C–S–H at the expense of strätlingite. The cements with a higher belite content yielded significantly lower compressive strengths than the cements with lower belite contents as (i) the hydration degree of belite is significantly lower than the one of ye'elimite and (ii) ettringite is more space-filling than strätlingite and C–S–H [27].

The established thermodynamic hydration model shows good agreement compared to the experimental data and is able to predict the hydration of belite-ye'elimite-ferrite cements. Compressive strength is directly correlated with bound water, as determined by thermogravimetric analysis, and inversely correlated to calculated porosity derived from thermodynamic modelling.

Funding The research is performed within the Young researcher programme and is financially supported by the Slovenian Research Agency, contract number 1000-18-1502.

Declarations

Conflict of interest The authors declare that they have no conflict of interest.

References

1. Gartner E (2004) Industrially interesting approaches to "low-CO2" cements. Cem Concr Res 34:1489–1498. https://doi.org/10.1016/j.cemconres.2004.01.021
2. Lothenbach B, Albert B, Vincent M, Ellis G (2015) Hydration of Belite-Ye'elimite-Ferrite cements:

thermodynamic modeling. In: 14th International conference on the chemistry of cement, Beijing, China, p. 12
3. Cuberos AJM, De la Torre ÁG, Álvarez-Pinazo G, Martín-Sedeño MC, Schollbach K, Pöllmann H, Aranda MAG (2010) Active iron-rich belite sulfoaluminate cements: clinkering and hydration. Environ Sci Technol 44:6855–6862. https://doi.org/10.1021/es101785n
4. Gartner E, Sui T (2018) Alternative cement clinkers. Cem Concr Res 114:27–39. https://doi.org/10.1016/j.cemconres.2017.02.002
5. Quillin K (2001) Performance of belite–sulfoaluminate cements. Cem Concr Res 31:1341–1349. https://doi.org/10.1016/S0008-8846(01)00543-9
6. Álvarez-Pinazo G, Santacruz I, Aranda MAG, De la Torre ÁG (2016) Hydration of belite–ye'elimite–ferrite cements with different calcium sulfate sources. Adv Cem Res 28:529–543. https://doi.org/10.1680/jadcr.16.00030
7. Juenger MCG, Winnefeld F, Provis JL, Ideker JH (2011) Advances in alternative cementitious binders. Cem Concr Res 41:1232–1243. https://doi.org/10.1016/j.cemconres.2010.11.012
8. Chen IA, Juenger MCG (2011) Synthesis and hydration of calcium sulfoaluminate-belite cements with varied phase compositions. J Mater Sci 46:2568–2577. https://doi.org/10.1007/s10853-010-5109-9
9. Chen IA, Juenger MCG (2012) Incorporation of coal combustion residuals into calcium sulfoaluminate-belite cement clinkers. Cem Concr Compos 34:893–902. https://doi.org/10.1016/j.cemconcomp.2012.04.006
10. García-Maté M, De la Torre AG, León-Reina L, Losilla ER, Aranda MAG, Santacruz I (2015) Effect of calcium sulfate source on the hydration of calcium sulfoaluminate eco-cement. Cem Concr Compos 55:53–61. https://doi.org/10.1016/j.cemconcomp.2014.08.003
11. Jansen D, Spies A, Neubauer J, Ectors D, Goetz-Neunhoeffer F (2017) Studies on the early hydration of two modifications of ye'elimite with gypsum. Cem Concr Res 91:106–116. https://doi.org/10.1016/j.cemconres.2016.11.009
12. Rungchet A, Poon CS, Chindaprasirt P, Pimraksa K (2017) Synthesis of low-temperature calcium sulfoaluminate-belite cements from industrial wastes and their hydration: comparative studies between lignite fly ash and bottom ash. Cem Concr Compos 83:10–19. https://doi.org/10.1016/j.cemconcomp.2017.06.013
13. Glasser FP, Zhang L (2001) High-performance cement matrices based on calcium sulfoaluminate–belite compositions. Cem Concr Res 31:1881–1886. https://doi.org/10.1016/S0008-8846(01)00649-4
14. Jeong Y, Hargis CW, Chun S-C, Moon J (2018) The effect of water and gypsum content on strätlingite formation in calcium sulfoaluminate-belite cement pastes. Constr Build Mater 166:712–722. https://doi.org/10.1016/j.conbuildmat.2018.01.153
15. Winnefeld F, Martin LHJ, Müller CJ, Lothenbach B (2017) Using gypsum to control hydration kinetics of CSA cements. Constr Build Mater 155:154–163. https://doi.org/10.1016/j.conbuildmat.2017.07.217
16. Winnefeld F, Barlag S (2010) Calorimetric and thermogravimetric study on the influence of calcium sulfate on the hydration of ye'elimite. J Therm Anal Calorim 101:949–957. https://doi.org/10.1007/s10973-009-0582-6
17. Shen Y, Li X, Chen X, Zhang W, Yang D (2018) Synthesis and calorimetric study of hydration behavior of sulfate-rich belite sulfoaluminate cements with different phase compositions. J Therm Anal Calorim 133:1281–1289. https://doi.org/10.1007/s10973-018-7251-6
18. Zhang L, Glasser FP (2002) Hydration of calcium sulfoaluminate cement at less than 24 h. Adv Cem Res 14:15. https://doi.org/10.1680/adcr.2002.14.4.141
19. Telesca A, Marroccoli M, Pace ML, Tomasulo M, Valenti GL, Monteiro PJM (2014) A hydration study of various calcium sulfoaluminate cements. Cem Concr Compos 53:224–232. https://doi.org/10.1016/j.cemconcomp.2014.07.002
20. Winnefeld F, Lothenbach B (2010) Hydration of calcium sulfoaluminate cements—experimental findings and thermodynamic modelling. Cem Concr Res 40:1239–1247. https://doi.org/10.1016/j.cemconres.2009.08.014
21. Gastaldi D, Paul G, Marchese L, Irico S, Boccaleri E, Mutke S, Buzzi L, Canonico F (2016) Hydration products in sulfoaluminate cements: Evaluation of amorphous phases by XRD/solid-state NMR. Cem Concr Res 90:162–173. https://doi.org/10.1016/j.cemconres.2016.05.014
22. Zajac M, Skocek J, Bullerjahn F, Ben Haha M (2016) Effect of retarders on the early hydration of calcium-sulpho-aluminate (CSA) type cements. Cem Concr Res 84:62–75. https://doi.org/10.1016/j.cemconres.2016.02.014
23. Jeong Y, Hargis CW, Kang H, Chun S-C, Moon J (2019) The effect of elevated curing temperatures on high ye'elimite calcium sulfoaluminate cement mortars. Materials 12:1072. https://doi.org/10.3390/ma12071072
24. Zhang L, Su M, Wang Y (1999) Development of the use of sulfo- and ferroaluminate cements in China. Adv Cem Res 11:15–21. https://doi.org/10.1680/adcr.1999.11.1.15
25. Li GS, Walenta G, Gartner E (2007) Formation and hydration of low CO2 cements based on belite, calcium sulfoaluminate and calcium aluminoferrite. In: Proceedings of the 12th ICCC, Montreal, Canada, pp. 9–12
26. Zajac M, Skocek J, Bullerjahn F, Lothenbach B, Scrivener K, Ben Haha M (2019) Early hydration of ye'elimite: insights from thermodynamic modelling. Cem Concr Res 120:152–163. https://doi.org/10.1016/j.cemconres.2019.03.024
27. Morin V, Termkhajornkit P, Huet B, Pham G (2017) Impact of quantity of anhydrite, water to binder ratio, fineness on kinetics and phase assemblage of belite-ye'elimite-ferrite cement. Cem Concr Res 99:8–17. https://doi.org/10.1016/j.cemconres.2017.04.014
28. Bullerjahn F, Schmitt D, Ben Haha M (2014) Effect of raw mix design and of clinkering process on the formation and mineralogical composition of (ternesite) belite calcium sulphoaluminate ferrite clinker. Cem Concr Res 59:87–95. https://doi.org/10.1016/j.cemconres.2014.02.004
29. Telesca A, Marroccoli M, Winnefeld F (2019) Synthesis and characterisation of calcium sulfoaluminate cements produced by different chemical gypsums. Adv Cem Res 31:113–123. https://doi.org/10.1680/jadcr.18.00122
30. Zhang J, Guan X, Wang X, Ma X, Li Z, Xu Z, Jin B (2020) Microstructure and properties of sulfoaluminate cement-based grouting materials: effect of calcium sulfate variety.

Adv Mater Sci Eng 2020:1–8. https://doi.org/10.1155/2020/7564108
31. Beltagui H, Jen G, Whittaker M, Imbabi MS (2017) The influence of variable gypsum and water content on the strength and hydration of a belite-calcium sulphoaluminate cement. Adv Appl Ceram 116:199–206. https://doi.org/10.1080/17436753.2017.1289722
32. Zajac M, Skocek J, Stabler C, Bullerjahn F, Ben Haha M (2019) Hydration and performance evolution of belite-ye'elimite-ferrite cement. Adv Cem Res 31:124–137. https://doi.org/10.1680/jadcr.18.00110
33. Gartner E, Walenta G, Morin V, Termkhajornkit P, Baco I, Casabonne JM (2011) Hydration of a belite-calciumsulfoaluminate-ferrite cement: aetherTM
34. Borštnar M, Daneu N, Dolenec S (2020) Phase development and hydration kinetics of belite-calcium sulfoaluminate cements at different curing temperatures. Ceram Int 46:29421–29428. https://doi.org/10.1016/j.ceramint.2020.05.029
35. Snellings R, Chwast J, Cizer Ö, De Belie N, Dhandapani Y, Durdzinski P, Elsen J, Haufe J, Hooton D, Patapy C, Santhanam M, Scrivener K, Snoeck D, Steger L, Tongbo S, Vollpracht A, Winnefeld F, Lothenbach B (2018) Report of TC 238-SCM: hydration stoppage methods for phase assemblage studies of blended cements—results of a round robin test. Mater Struct 51:111. https://doi.org/10.1617/s11527-018-1237-5
36. Snellings R, Chwast J, Cizer Ö, Belie N, Dhandapani Y, Durdziński P, Elsen J, Haufe J, Hooton D, Patapy C, Santhanam M, Scrivener K, Snoeck D, Steger L, Tongbo S, Vollpracht A, Winnefeld F, Lothenbach B (2018) RILEM TC-238 SCM recommendation on hydration stoppage by solvent exchange for the study of hydrate assemblages. Mater Struct. https://doi.org/10.1617/s11527-018-1298-5
37. Snellings R (2016) X-ray powder diffraction applied to cement. In: A practical guide to microstructural analysis of cementitious materials, First, CRC Press, pp. 126–195. Doi: https://doi.org/10.1201/b19074-4
38. Cuesta A, De la Torre ÁG, Losilla ER, Santacruz I, Aranda MAG (2014) Pseudocubic crystal structure and phase transition in doped ye'elimite. Cryst Growth Des 14:5158–5163. https://doi.org/10.1021/cg501290q
39. Cuesta A, De la Torre AG, Losilla ER, Peterson VK, Rejmak P, Ayuela A, Frontera C, Aranda MAG (2013) Structure, atomistic simulations, and phase transition of stoichiometric yeelimite. Chem Mater 25:1680–1687. https://doi.org/10.1021/cm400129z
40. Jansen D, Goetz-Neunhoeffer F, Stabler C, Neubauer J (2011) A remastered external standard method applied to the quantification of early OPC hydration. Cem Concr Res 41:602–608. https://doi.org/10.1016/j.cemconres.2011.03.004
41. Jansen D, Stabler Ch, Goetz-Neunhoeffer F, Dittrich S, Neubauer J (2011) Does ordinary portland cement contain amorphous phase? A quantitative study using an external standard method. Powder Diffr 26:31–38. https://doi.org/10.1154/1.3549186
42. O'Connor BH, Raven MD (1988) Application of the rietveld refinement procedure in assaying powdered mixtures. Powder Diffr 3:2–6. https://doi.org/10.1017/S0885715600013026
43. Lothenbach B, Durdzinski P, De Weerdt K (2016) Thermogravimetric analysis. In: A practical guide to microstructural analysis of cementitious materials, First, CRC Press, https://www.taylorfrancis.com/chapters/thermogravimetric-analysis-barbara-lothenbach-pawe%C5%82-durdzi%C5%84ski-klaartje-de-weerdt/e/https://doi.org/10.1201/b19074-5 (accessed February 19, 2021)
44. Wagner T, Kulik DA, Hingerl FF, Dmytrieva SV (2012) GEM-Selektor geochemical modeling package: TSolMod library and data interface for multicomponent phase models. Contrib Can Mineral 50:1173–1195. https://doi.org/10.3749/canmin.50.5.1173
45. Kulik DA, Wagner T, Dmytrieva SV, Kosakowski G, Hingerl FF, Chudnenko KV, Berner U (2013) GEM-Selektor geochemical modeling package: revised algorithm and GEMS3K numerical kernel for coupled simulation codes. Comput Geosci 17:1–24. https://doi.org/10.1007/s10596-012-9310-6
46. Lothenbach B, Kulik DA, Matschei T, Balonis M, Baquerizo L, Dilnesa B, Miron GD, Myers RJ (2019) Cemdata18: a chemical thermodynamic database for hydrated Portland cements and alkali-activated materials. Cem Concr Res 115:472–506. https://doi.org/10.1016/j.cemconres.2018.04.018
47. Kulik DA, Winnefeld F, Kulik A, Miron GD, Lothenbach B (2021) CemGEMS—an easy-to-use web application for thermodynamic modeling of cementitious materials. RILEM Tech Lett 6:36–52. https://doi.org/10.21809/rilemtechlett.2021.140
48. Chitvoranund N, Winnefeld F, Hargis CW, Sinthupinyo S, Lothenbach B (2017) Synthesis and hydration of alite-calcium sulfoaluminate cement. Adv Cem Res 29:101–111. https://doi.org/10.1680/jadcr.16.00071
49. Kulik DA (2011) Improving the structural consistency of C–S–H solid solution thermodynamic models. Cem Concr Res 41:477–495. https://doi.org/10.1016/j.cemconres.2011.01.012
50. Lothenbach B, Matschei T, Möschner G, Glasser FP (2008) Thermodynamic modelling of the effect of temperature on the hydration and porosity of Portland cement. Cem Concr Res 38:1–18. https://doi.org/10.1016/j.cemconres.2007.08.017
51. Meller N, Hall C, Jupe AC, Colston SL, Jacques SDM, Barnes P, Phipps J (2004) The paste hydration of brownmillerite with and without gypsum: a time resolved synchrotron diffraction study at 30, 70, 100 and 150 °C. J Mater Chem 14:428–435. https://doi.org/10.1039/B313215C
52. Möschner G, Lothenbach B, Winnefeld F, Ulrich A, Figi R, Kretzschmar R (2009) Solid solution between Al-ettringite and Fe-ettringite (Ca6[Al1−xFex(OH)6]2(SO4)3·26H2O). Cem Concr Res 39:482–489. https://doi.org/10.1016/j.cemconres.2009.03.001
53. Scrivener K, Snellings R, Lothenbach B (2016) A practical guide to microstructural analysis of cementitious materials. CRC Press, Boca Raton
54. Hargis CW, Lothenbach B, Müller CJ, Winnefeld F (2019) Further insights into calcium sulfoaluminate cement expansion. Adv Cem Res 31:160–177. https://doi.org/10.1680/jadcr.18.00124

55. Jeong Y, Hargis C, Chun S, Moon J (2017) Effect of calcium carbonate fineness on calcium sulfoaluminate-belite Cement. Materials 10:900. https://doi.org/10.3390/ma10080900

Electronic Supplementary Material for:

The influence of calcium sulfate content on the hydration of belite-calcium sulfoaluminate cements with different clinker phase compositions

Maruša Mrak[1, 2], Frank Winnefeld[3], Barbara Lothenbach[3,4], Sabina Dolenec[1,*]

[1] Slovenian National Building and Civil Engineering Institute, Dimičeva ulica 12, 1000 Ljubljana, Slovenia

[2] Jožef Stefan International Postgraduate School, Jamova cesta 39, 1000 Ljubljana, Slovenia

[3] Empa, Swiss Laboratories for Materials Science and Technology, Überlandstrasse 129, 8600 Dübendorf, Switzerland

[4] Norwegian University of Science and Technology (NTNU), Department

[*] Corresponding author. Tel.: +386 40 693 125. E-mail address: sabina.dolenec@zag.si

In the following Figures S1–S4, the data reported in this study are summarized, as they are already discussed in detail in the paper.

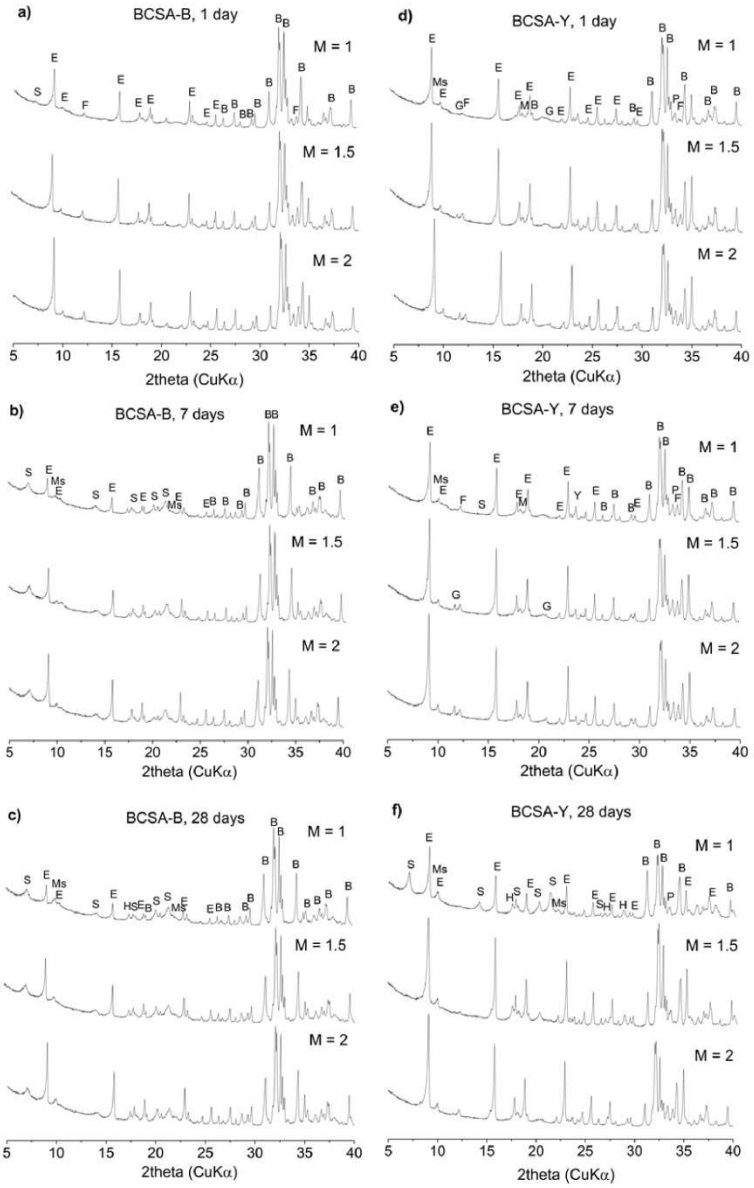
a)
BCSA-B, 1 day
M = 1
M = 1.5
M = 2
2theta (CuKα)
d)
BCSA-Y, 1 day
M = 1
M = 1.5
M = 2
2theta (CuKα)
b)
BCSA-B, 7 days
M = 1
M = 1.5
M = 2
2theta (CuKα)
e)
BCSA-Y, 7 days
M = 1
M = 1.5
M = 2
2theta (CuKα)
c)
BCSA-B, 28 days
M = 1
M = 1.5
M = 2
2theta (CuKα)
f)
BCSA-Y, 28 days
M = 1
M = 1.5
M = 2
2theta (CuKα)

Fig. S1 X-ray diffraction patterns of BCSA-B at a) 1 day, b) 7 days and c) 28 days f hydration and BCSA-Y at d) 1 day, e) 7 days and f) 28 days of hydration. B = belite, Y = ye'elimite, F = ferrite, M = mayenite, P = perovskite, E = ettringite, Ms = monosulfate, S = strätlingite, H = siliceous hydrogarnet.

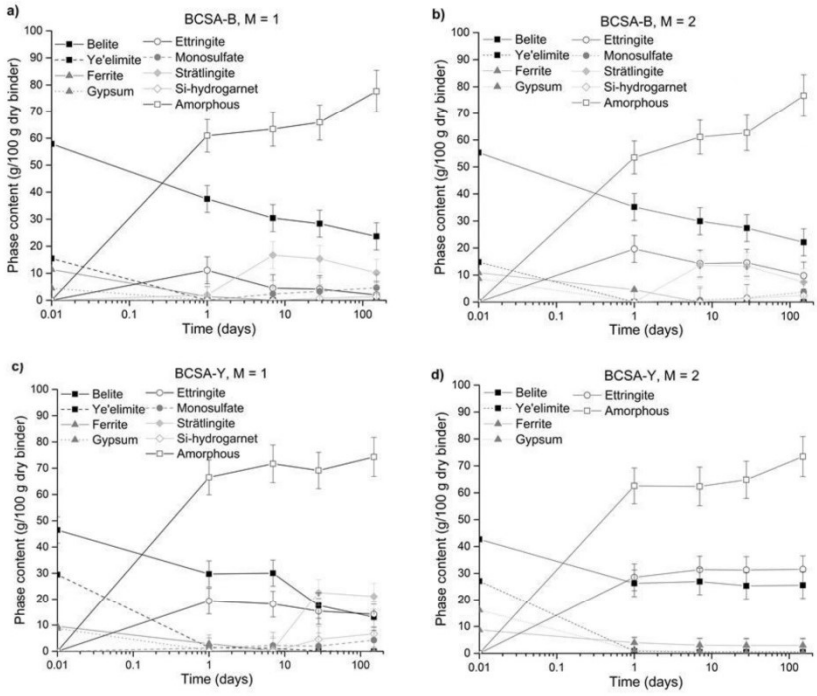

Fig. S2 X-ray powder diffraction quantification of the phase development in hydrating BCSA-B at a) M = 1 and b) M = 2 and BCSA-Y cement at c) M = 1 and d) M = 2.

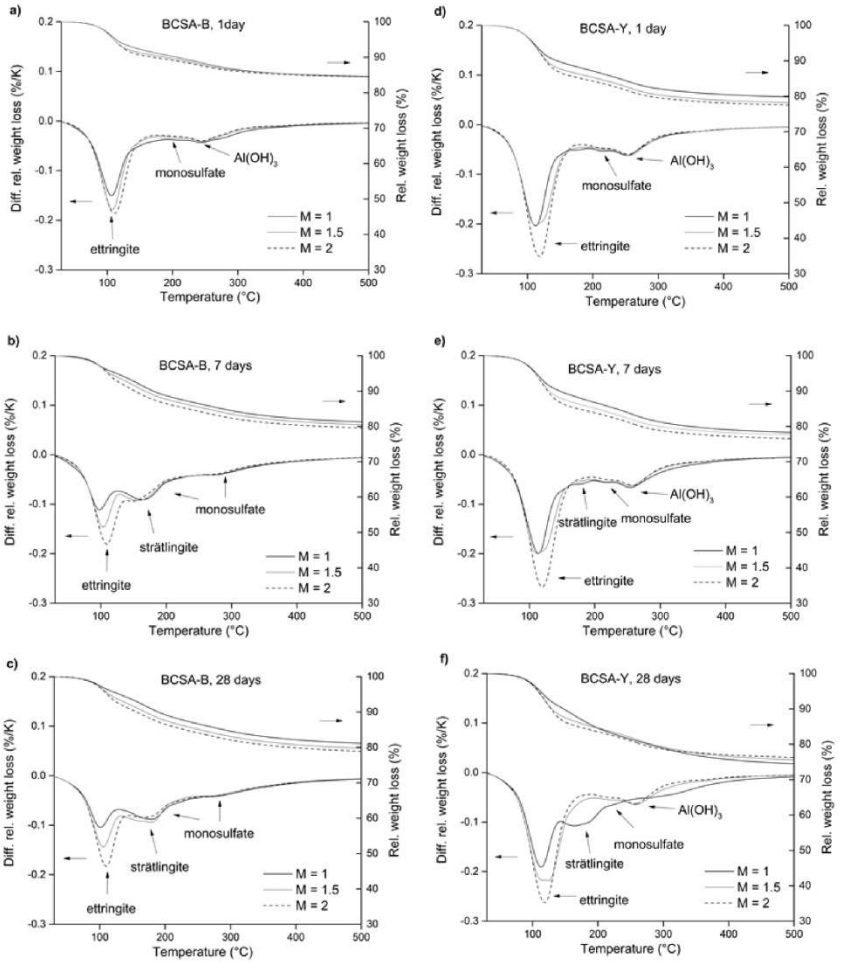

Fig. S3 Thermogravimetric analysis of cement paste BCSA-B at a) 1, b) 7 and c) 28 days of hydration and cement paste BCSA-Y at d) 1, e) 7 and f) 28 days of hydration.

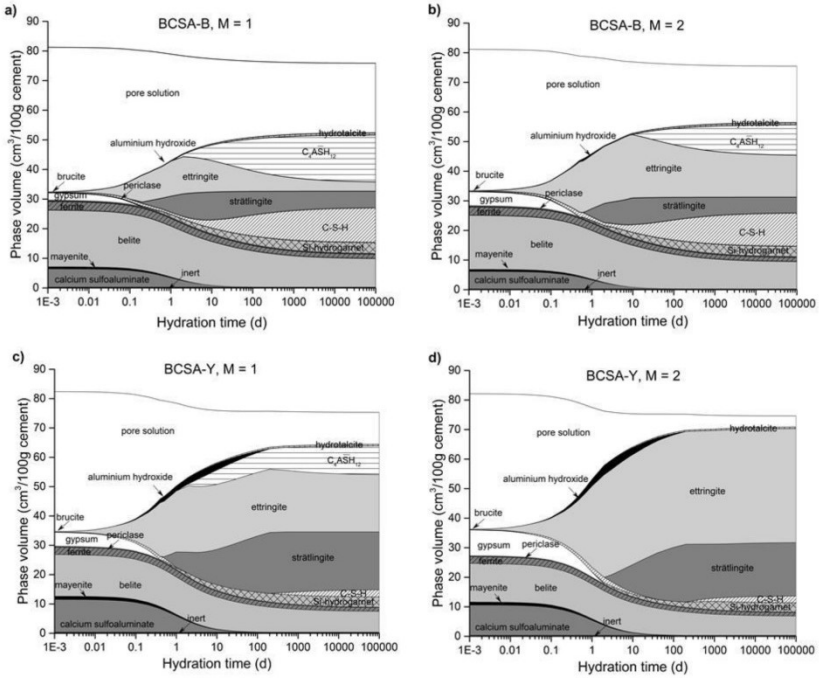

Fig. S4 Thermodynamic modelling of the phase assemblages depending on hydration time at M = 1 of a) BCSA-B cement and b) BCSA-Y cement and at M = 2 of c) BCSA-B cement and d) BCSA-Y cement.

Chapter 5

Experimental Study and Thermodynamic Modelling of the Temperature Effect on the Hydration of Belite-Ye'elimite-Ferrite Cements

This chapter is based on a paper submitted to the peer-reviewed journal, Construction and Building Materials, by M. Mrak, F. Winnefeld, B. Lothenbach, and S. Dolenec, entitled, "Experimental study and thermodynamic modelling of the temperature effect on the hydration of belite-ye'elimite-ferrite cements.,"

This chapter addresses thesis objectives 1, 2, 3 and 5.

5.1 Introduction

The hydration of cements is a temperature-sensitive process, which is influenced not only by variation in temperature caused by the external environment but also by the heat produced during an exothermic reaction between cement and water [63], [65]–[67], [69]. The influence of temperature on the hydration of cements is complex, yet is it an important factor in understanding the behavior and properties of cementitious materials [90]. A literature review concerning the influence of temperature on the hydration of different cements is discussed in detail in Chapter 1.

Previous research shown in Chapter 2 [84] focused on the hydration of belite-ye'elimite-ferrite cements, yet only at ambient and elevated temperatures, while lower temperatures (e.g. 5 °C) were not investigated. Furthermore, a low water-to-cement ratio and a very high calcium sulfate to ye'elimite molar ratio were implemented in that study resulting in insufficient water for complete hydration. As shown in Chapter 3 [85], early hydration reactions up to 1 day at 25, 40 and 60 °C were studied through in situ X-ray diffraction analysis.

While there has been significant research on belite-ye'elimite-ferrite cement at ambient temperature, there are still some gaps in understanding the behavior of belite-ye'elimite-ferrite cement at different temperatures, particularly at low temperatures and with respect to the effects on its mechanical properties and microstructure. This study examines the effects of low, ambient, and increased curing temperatures on the phase development, microstructure and hydration kinetics of belite-ye'elimite-ferrite cements. Systematical and detailed microstructural and EDXS analyses were performed at

different temperatures, which was not previously investigated, in order to improve understanding of the development of hydration products at different temperatures. In addition, thermodynamic calculations of belite-ye'elimite-ferrite systems at different temperatures have not been previously made available in the open literature. These results will therefore provide valuable insights into the behavior of belite-ye'elimite-ferrite cements in different curing environments, thus expanding our understanding of the hydration mechanisms of belite-ye'elimite-ferrite cements.

The hydration of two belite-ye'elimite-ferrite cements at temperatures between 5°C and 60°C was investigated using both experimental data and thermodynamic modelling. The hydration kinetics was studied using isothermal calorimetry, and the compressive strength of the mortars was determined. The hydrate assemblages of two different cements varying in terms of their phase composition were investigated by X-ray powder diffraction, thermogravimetric analysis, and energy-disperse X-ray microanalysis. The microstructure was assessed using scanning electron microscopy. Based on the experimental data a thermodynamic model was established that can be used to calculate the stable hydrate assemblage depending on temperature and dissolution kinetics.

5.2 Materials and Methods

5.2.1 Materials

Two belite-ye'elimite-ferrite cement clinkers with different targeted phase compositions were synthesized. The targeted phase composition was 65 wt. % belite (C_2S), 20 wt. % ye'elimite ($C_4A_3\overline{S}$) and 10 wt. % ferrite (C_4AF) for clinker CBCSA-B, and 50 wt. % belite (C_2S), 35 wt. % ye'elimite ($C_4A_3\overline{S}$) and 10 wt. % ferrite (C_4AF) for clinker CBCSA-Y.

The synthesis of the clinkers has been described in detail in a previous paper Borštnar et al. [84]. The chemical compositions of the clinkers, determined by X-ray fluorescence according to EN 196-2 and the mineralogical compositions derived from quantitative X-ray diffraction have also been reported previously by Mrak et al. [89]. The phase compositions are shown in Table 5.1 below. The Blaine specific surface areas of the cement clinkers were 4740 cm^2/g (specific density 3.18 g $/cm^3$) for cement clinker CBCSA-B and 4250 cm^2/g (specific density 3.07 g /cm3) for CBCSA-Y [89].

Table 5.1: Phase compositions of the cement clinkers (in wt. %) as determined by X-ray powder diffraction and Rietveld refinement. Data reproduced from [89].

	CBCSA-B	CBCSA-Y
β -Dicalcium silicate (belite)	60.6	50.9
γ -Dicalcium silicate	6.9	0.8
Ye'elimite orthorhombic	6.9	17.4
Ye'elimite cubic	9.3	14.9
∑ Ye'elimite	16.2	32.3
Ferrite	11.9	10.4
Mayenite	2.3	3.2
Periclase	1.1	1.0
Gehlenite	0.4	-
Perovskite	-	1.0
Aphthitalite	0.3	0.2
Arcanite	0.3	0.2

The cement mixtures BCSA-B and BCSA-Y were prepared by blending the ground clinkers with 6.7 wt. % and 12.5 wt. % natural gypsum (composed of 96.7 wt. % gypsum and 3.3 wt. % anhydrite and ground below 0.063 mm), respectively, resulting in an M-value (calcium sulfate to ye'elimite molar ratio) of 1.5 in both cements [89]. The particle size distributions of both the clinkers and the gypsum have been previously presented in Mrak et al. [89].

Prior to use, the raw materials were stored for 24 hours at either 5 °C, 20 °C, 40 °C or 60 °C. The cement pastes were prepared using a water-to-cement ratio of 0.5. Following the addition of the appropriate amount of water, the pastes were mixed manually for 3 minutes using a spatula and filled into 15 ml polyethylene vials, which were then tightly sealed and cured at the respective temperatures.

At pre-determined time intervals, i.e. 1, 7, 28 and 150 days, the hydration of the cement pastes was stopped by solvent exchange using isopropanol and diethyl ether. Following the protocol described by Snellings et al. [91], the crushed samples were immersed in isopropanol for 15 min, filtered with a Büchner funnel, then rinsed once with isopropanol and twice with diethyl ether before being dried for 8 minutes at 40 °C to evaporate any remaining solvent. The dry pastes were investigated using scanning electron microscopy. For X-ray powder diffraction and thermogravimetric analysis, pastes were ground by hand to a particle size of below 0.063 mm using an agate mortar prior to analysis. It should be noted that the results from the hydration experiments on cement mixtures BCSA-B and BCSA-Y at 20 °C, as presented in the latter part of this work have been reported previously [89].

5.2.2 Methods

Isothermal conduction calorimetry was performed at 5 °C, 20 °C, 40 °C and 60 °C, using a Thermometric TAM Air (TA instruments). 4 g of the prepared cement was manually mixed with 2 g of deionized water (corresponding to a water-to-cement ratio of 0.5), for 3 minutes using a spatula. The mixture was transferred into a glass ampoule, which was then capped and placed directly into the calorimeter before being measured for 168 hours. It was not possible to oberve the early heat of hydration (up to approximately 30 minutes) due to the external mixing procedure.

X−ray powder diffraction was conducted using a PANalytical X'Pert Pro X-ray powder diffractometer equipped with $CuK_{\alpha 1}$ radiation (Johannson Ge (111) incident beam monochromator) and an X'Celerator detector at a voltage of 45 kV and a current of 40 mA. Samples were prepared by back-loading the powder into a circular sample holder with a diameter of 27 mm in order to minimize the preferred orientation effects. Samples were measured in a 2θ range of 5-75° with a step size of 0.017 °2 θ, using a 1° divergence slit and a 15 mm mask. Rietveld refinement was performed using PANalytical X'Pert High Score Plus diffraction software (version 4.9). Crystal structures suggested by Snellings [92] were used, while the structures for orthorhombic and cubic ye'elimite were taken from Cuesta et al. [46], [93]. The G-factor method [94]–[96] was used for the quantification of amorphous content and poorly crystalline phases with CaF_2 (Sigma Aldrich) used as the external standard. The results were normalized to 100 g of dry binder, including the amount of bound water determined from thermogravimetric analysis.

Thermogravimetric (TGA) analysis was carried out using a Mettler Toledo TGA/SDTA 851e instrument. Measurements were carried out over the temperature range between 30 and 980 °C, employing a heating rate of 20 K/min under a nitrogen atmosphere. Approximately 50 mg of the samples were placed in 150 µl alumina

crucibles. Chemically bound water was calculated from the weight loss up to 550 °C and normalized to 100 g of the dry binder [97].

Polished cross-sections of selected cement pastes (cured for either 150 days at 5 °C, 20 °C, 40 °C or 60 °C and 1, 7, 28 and 150 days at 20 °C), impregnated with epoxy resin and carbon coated, were examined by scanning electron microscopy (JEOL JSM-IT500) under high vacuum in backscattered electron mode (BSE). Imaging was performed with a backscattered electron detector at an accelerating voltage of 15 kV, while energy-dispersive X-ray microanalyses (EDXS) were performed to identify the hydrates and their chemical composition. Over 100 points were analyzed per sample (matrix of hydrated cement pastes). Graphs displaying the various atomic ratios of different elements (Al/Ca, S/Ca, Si/Ca and Ca/Si) were utilized to illustrate trends in the composition of the hydration products.

Mortars were prepared using quartz sand (CEN-Standard Sand EN 196-1 - Normensand with grain sizes between 0.1 and 2 mm), with a cement-to-sand ratio of 25/75 by mass and a water-to-cement ratio of 0.5. The mortars were mixed according to EN 196-1, cast in 25 mm x 25 mm x 25 mm moulds and then cured at 5 °C, 20 °C, 40 °C and 60 °C and a relative humidity of 95 ± 2 %. After 24 hours, the samples were demoulded., The compressive strength of the samples was determined after 1, 7, 28 and 150 days using an LFM 50 (Walter + Bai) testing machine with a loading rate of 0.2 MPa/s. Three cubes were tested for each measurement age.

Geochemical modelling was carried out to predict the type and amount of hydration products at various temperatures. The geochemical software GEMS [98] coupled with the cement-specific Cemdata18 database [78] were used for this purpose. All thermodynamic calculations were done under oxidizing conditions. The CSHQ model from Kulik [99] was used for C—S—H as detailed in [78]; this model accounts for the uptake of Na and K in C—S—H but neglects Al-binding by C—S—H. Firstly, the changes in phase volumes that occurred with ongoing hydration were calculated at the respective temperatures (5, 20, 40 and 60 °C). The dissolution degree of the clinker phases at different hydration times, as obtained by X-ray powder diffraction, was fitted using the following empirical non-linear equation (Eq. 5.1):

$$DoR = \frac{A - D}{1 + \left(\frac{t}{C}\right)} + D \tag{5.1}$$

where DoR represents the reaction degree, t the hydration time in days, A the minimum reaction degree (set to 0), B the maximum steepness of the curve, C the inflection point and D the maximum reaction degree (set to 100) [100], [101]. Secondly, changes in the phase volumes that occurred during hydration of the BCSA-B and BCSA-Y clinkers were modelled across the temperature range of 0 to 85 °C. The phase compositions of the clinkers and the gypsum, as determined by X-ray powder diffraction, were utilized as input data. For ye'elimite, ferrite, periclase and mayenite, a reaction degree of 100 % was considered. For belite, a temperature-dependent reaction degree was used, which was inter- and extrapolated from a linear fit of the dissolution degrees as obtained by X-ray powder diffraction at 5 °C, 20 °C, 40 °C and 60 °C after 150 days. Anhydrite, gypsum, arcanite and aphthitalite were all assumed to fully react, while γ-dicalcium silicate, gehlenite and perovskite were considered to be inert [56]. A water-to-cement ratio of 0.5 was applied in the calculations, corresponding to the value used in the experiments. According to the results of thermodynamic modelling, the porosities of the samples were calculated according to the equation (Eq. 5.2):

$$P = \frac{V_{unhydrated\ cement,\ t=0} + V_{hydrates,\ t=0} + V_{pore\ solution,t=0} - V_{hydrates,t} - V_{unhydrated\ cement,t}}{V_{unhydrated\ cement,t=0} + V_{hydrates,t=0} + V_{pore\ solution,t=0}} \text{x100} \quad (5.2)$$

where P is the porosity (%), V the volume (cm^3), t = 0 the time at the beginning of hydration and t is the time [45].

5.3 Results and Discussion

5.3.1 Isothermal Calorimetry

The influence of temperature on the hydration heat flow is shown in Figures 5.1a (BCSA-B) and 5.1b (BCSABCSA-Y). The initial peak, which can be attributed to the wetting and first hydration reactions [23], [39], [102], [103], cannot be assessed due to the external mixing procedure.

The induction period, which occurs during the slow dissolution of the clinker phases, and the subsequent slow formation of hydrates [48], [74], [102], [103], is prolonged at lower temperatures. At 5 °C in particular, the induction period is very long, lasting approximately 11 hours in BCSA-B and 15 hours in BCSA-Y. A prolonged induction period at lower temperatures has also been observed by other authors [81], [104]. At 20 °C, the induction period stops at approximately 1.6 hours in BCSA-B and 1.5 hours in BCSA-Y. Conversely, the samples cured at elevated temperatures have very short induction periods, lasting around 20 minutes in both cement at both 40 °C and 60 °C.

The maximum heat flow released during hydration increases as temperature increases. At higher temperatures, the reactions are faster and thus show significantly higher rates of heat release, indicating that increasing the curing temperature accelerates the kinetics of hydration [74], [82], [105]–[107]. At 5 °C, the reaction is very slow, leading to a significantly lower rate of heat flow compared to at ambient and elevated temperatures.

At 5 °C, only one very broad peak is seen in BCSA-B, starting after around 11 hours of hydration, which can – as also for all other samples – be attributed to the dissolution of ye'elimite and gypsum and the early precipitation of ettringite and aluminium hydroxide [39], [49], [74], [102], [108]. A small additional maximum occurs after 27.5 hours, which can be attributed to the precipitation of monosulfate and/or ettringite [56], [102], [108]. At 20 °C, the first heat evolution peak occurs after 3.5 hours of hydration, followed by a second peak after 5.2 hours. At 40 °C the first peak occurs after 0.8 hours and the second after 1.5 hours, while at 60 °C they occur even earlier - after 0.6 and 1.2 hours, respectively.

In BCSA-Y, the first peak occurs between 15 and 37.5 hours of hydration at 5 °C, with no clear maximum, while a second maximum is visible after 40 hours. At all other temperatures, the first peaks occur at a similar time as in BCSA-B. The second peaks, however, occur later than in BCSA-B, appearing after 8.2, 2.7 and 1.4 hours at 20 °C, 40 °C and 60 °C, respectively. This is related to the fact that in BCSA-Y more ettringite forms than monosulfate due to the higher content of ye'elimite in clinker BCSA-Y compared to BCSA-B (see Table 5.1). As indicated, the reactions occur earlier at elevated temperatures. In contrast to BCSA-Y, however, it can be seen in the case of BCSA-B that raising the temperature from 40 °C to 60 °C does not significantly change the heat release.

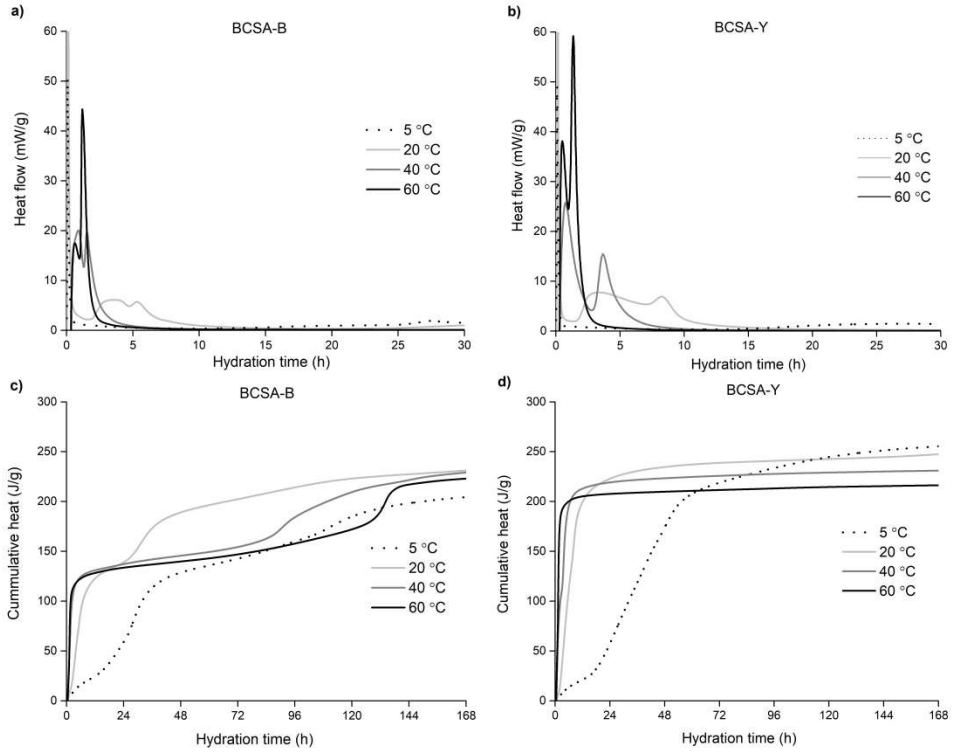

Figure 5.1: Hydration heat flow (a, b) and development of the cumulative heat of hydration (c, d) at different curing temperatures in the BCSA-B and BCSA-Y cements. Both the heat flow and cumulative heat are normalized to the weight of the cement. Data at 20 °C were taken from [89].

The development of cumulative heat is displayed in Figures 5.1c and 5.1d. The results show that after 7 days of hydration (Table 5.2), the cumulative heat in BCSA-B cement mixture decreases as the temperature increases from 20 to 60 °C. After 7 days, the cumulative heat at 5 °C is lower than it is at the other temperatures, indicating a very slow and long-term hydration. However, on the one hand, at 40 and 60 °C the very early heat of hydration might not be entirely captured as we had to discard the first 30 minutes of the heat flow due to the external mixing procedure. As in Portland cement, however, a higher degree of hydration is often reached after long hydration times at low temperatures than at higher temperatures, where fast hydration causes the formation of dense shells of hydrates around the clinker grains [65]. When the temperature is low, dissolution is slow, allowing time for the ions to distribute around the matrix and precipitate in the pore space.

Table 5.2: Cumulative heat of hydration after 7 days of hydration at 5 °C, 20 °C, 40 °C and 60 °C. The cumulative heat is normalized to the weight of the cement.

Cumulative heat (J/g)	BCSA-B	BCSA-Y
5 °C	204.49	255.38
20 °C	231.01	247.43
40°C	229.04	230.91
60 °C	222.91	216.22

In the BCSA-Y cement, the cumulative heat after 7 days decreases when the temperature is increased from 5 to 60 °C. In both cement mixtures, the long-term reaction slows down more quickly when the temperature is increased, an effect also observed by Chitvoranund [105].

5.3.2 Dissolution of Clinker Phases and Gypsum

Figures 5.2 to 5.5 plot the XRD patterns of BCSA-B and BCSA-Y at the various curing temperatures after 1, 7, 28 and 150 days of hydration. The amount of main anhydrous phases (belite, ye'elimite, ferrite and gypsum) at different curing temperatures are plotted in figures 5.6 and 5.7 for BCSA-B and BCSA-Y, respectively.

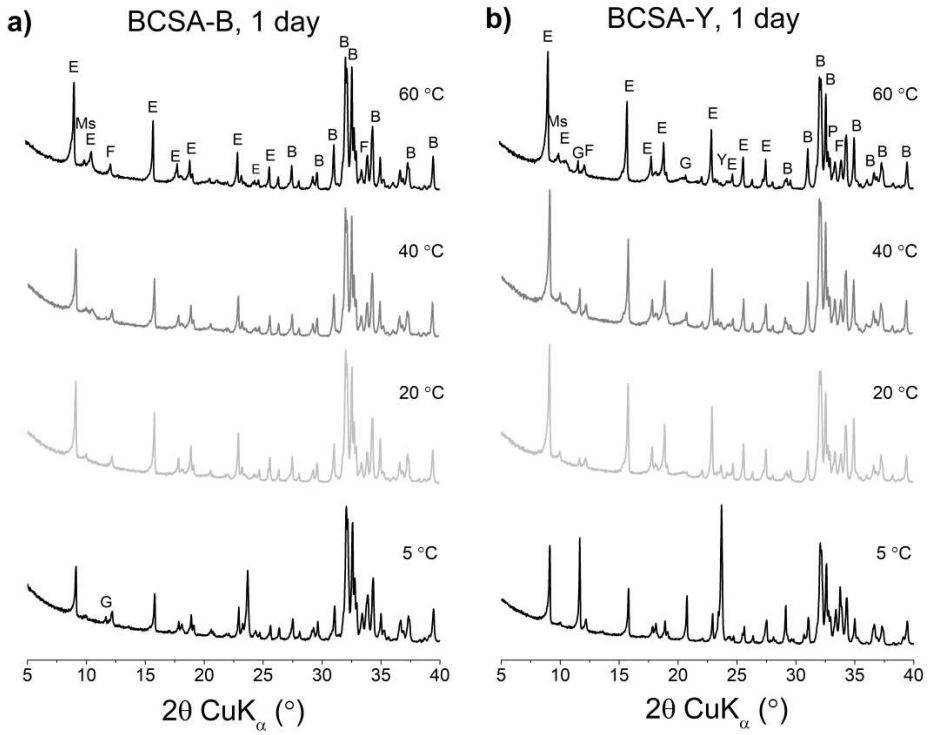

Figure 5.2: X-ray diffraction patterns of BCSA-B (a) and BCSA-Y (b) at 1 day of hydration at different curing temperatures. B = belite, E = ettringite, F = ferrite, G = gypsum, Ms = monosulfate, P = perovskite, and Y = ye'elimite. The data for 20 °C was taken from [89].

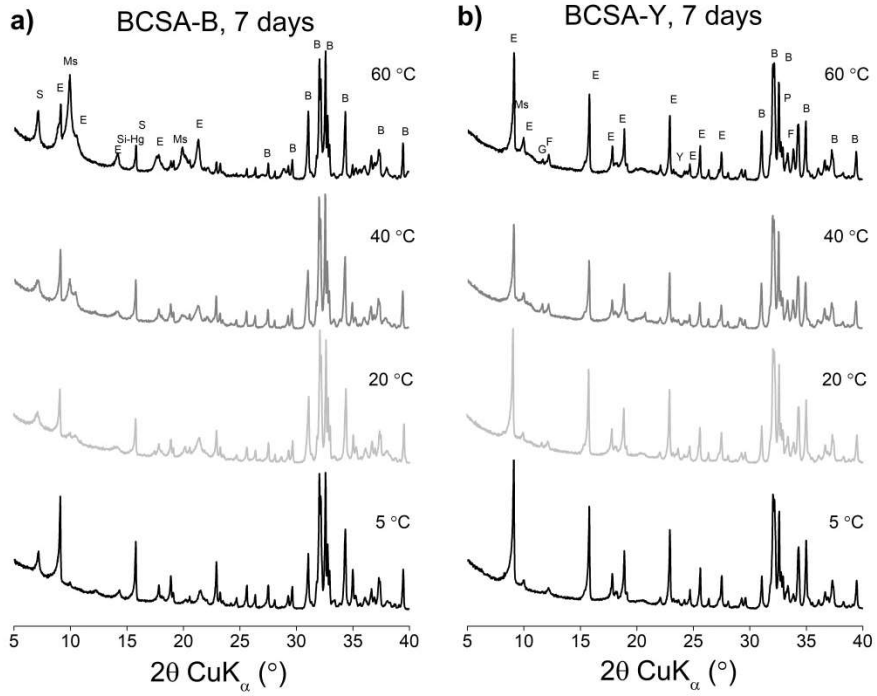

Figure 5.3: X-ray diffraction patterns of the cement mixtures BCSA-B (a) and BCSA-Y (b) at 7 days of hydration at different curing temperatures. B = belite, E = ettringite, F = ferrite, G = gypsum, Ms = monosulfate, P = perovskite, S = strätlingite, and Si-Hg = siliceous hydrogarnet. The data for 20 °C was taken from [89].

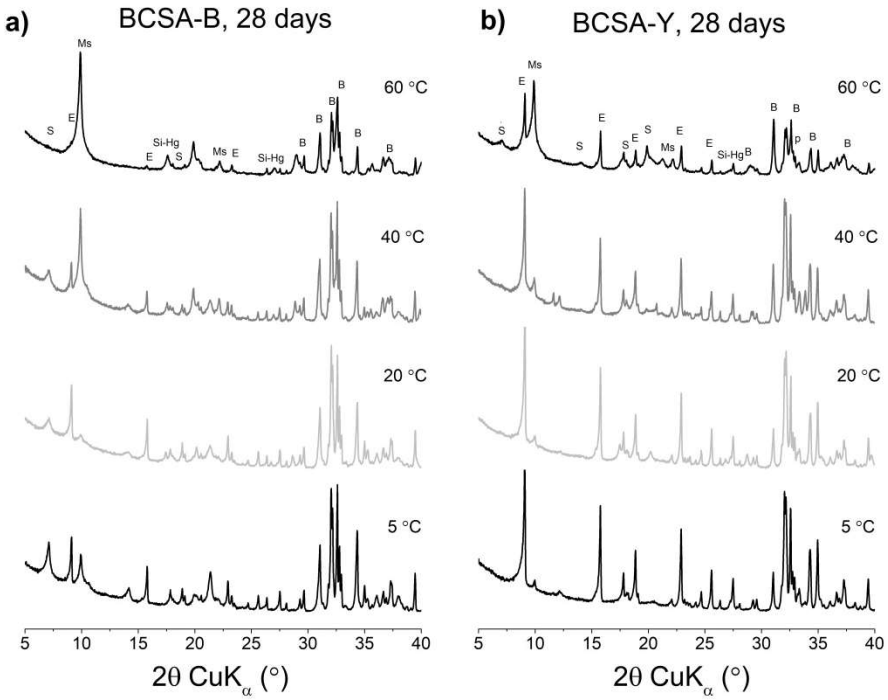

Figure 5.4: X-ray diffraction patterns of the cement mixtures BCSA-B (a) and BCSA-Y (b) at 28 days of hydration at different curing temperatures. B = belite, E = ettringite, Ms = monosulfate, P = perovskite, S = strätlingite, and Si-Hg = siliceous hydrogarnet. The data for 20 °C was taken from [89].

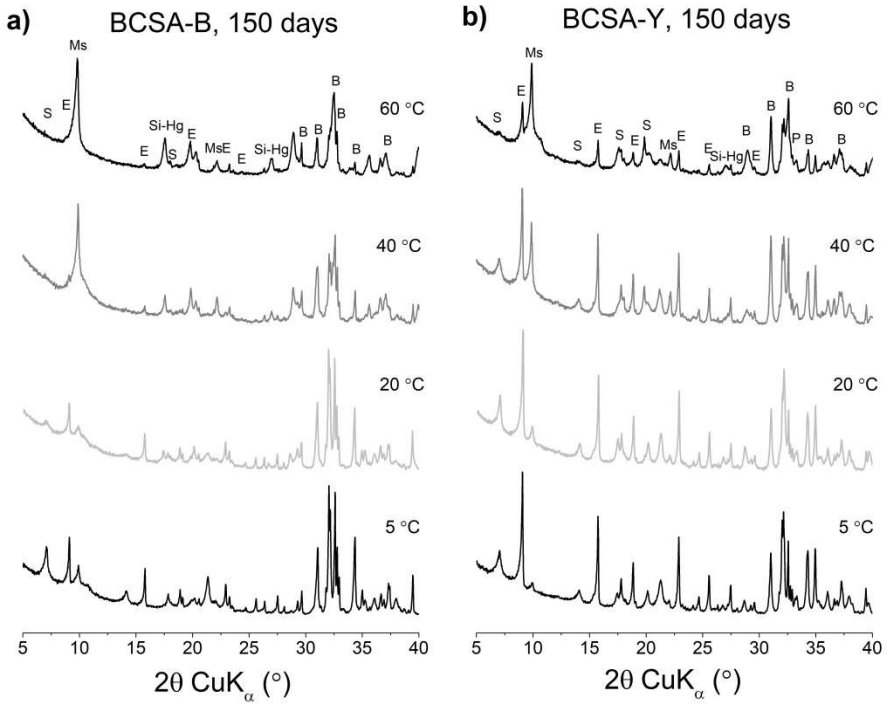

Figure 5.5: X-ray diffraction patterns of BCSA-B (a) and BCSA-Y (b) at different curing temperatures at 150 days of hydration. B = belite, E = ettringite, Ms = monosulfate, P = perovskite, S = strätlingite, and Si-Hg = siliceous hydrogarnet. The data for 20 °C was taken from[89].

As the temperature increases, dissolution of the anhydrous clinker phases becomes accelerated, as has been observed previously, both in Portland cements [63], [66], [104] and ye'elimite-based cements [39], [70], [79]. Ye'elimite reacts very rapidly, and at both ambient and elevated temperatures it becomes almost completely consumed during the first day of hydration.

At 5 °C, the consumption of ye'elimite and gypsum at early ages is significantly slowed compared to that at other temperatures. At 1 day, the reaction degree of ye'elimite is around 60 % and 55 % in BCSA-B and BCSA-Y, respectively (Figures 5.6 and 5.7). In BCSA-B, the gypsum is almost fully reacted after 1 day, whereas in BCSA-Y only approximately 60 % has reacted over the same period of time, as the amount of added gypsum in BCSA-Y is almost double that of in BCSA-B (Figure 5.7). TGA results confirm the presence of gypsum at 1 day of hydration at a curing temperature of 5 °C (Figure 5.10). The results indirectly confirm those obtained from X-ray powder diffraction, which show that, at 1 day, the degree of hydration of the clinker phases is lowest at 5 °C, as a lower quantity of bound water is identified compared to at the other temperatures.

The reaction kinetics of belite is slower than ye'elimite and gets faster with higher temperatures. In the first 24 hours, belite reacts to a certain extent at all curing temperatures. After 1 day, the hydration degree of BCSA-B reaches around 35 % at 5 °C, 20 °C and 40 °C, and almost 50 % at 60 °C. In BCSA-B, the hydration of belite increases substantially beyond 7 days of hydration and is promoted at elevated temperatures. At150 days, nearly 90 % of belite is hydrated at 60 °C, compared to a hydration degree of approximately 50 % at 5 °C. Belite has been reported to show a similar degree of

hydration at 5 °C and 60 °C after 180 days [105] although only a small reaction was observed until 90 days. In BCSA-Y, the hydration degree of belite after 1 day is around 40 % at all temperatures. At 60 °C, the hydration of belite significantly increases between 7 and 28 days of hydration, while at lower temperatures this increase takes place after 28 days. At 150 days, the hydration degree of belite is around 80 % at 60 °C and approximately 60 % at 5 °C, indicating that temperature significantly affects the kinetics of hydration.

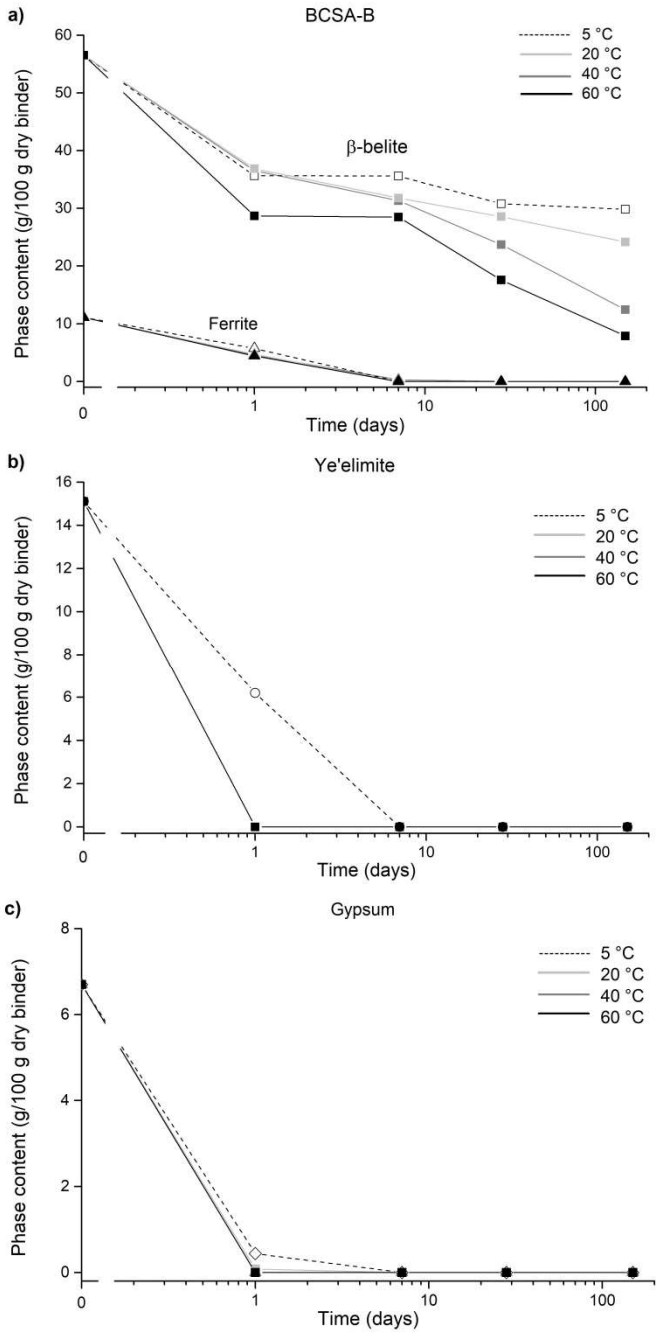

Figure 5.6: Amounts of β-belite and ferrite (a), ye'elimite (b) and gypsum (c) in the BCSA-B cement mixture obtained by quantitative X-ray diffraction. The estimated relative errors are ±5 %. The data at 20 °C was taken from [89].

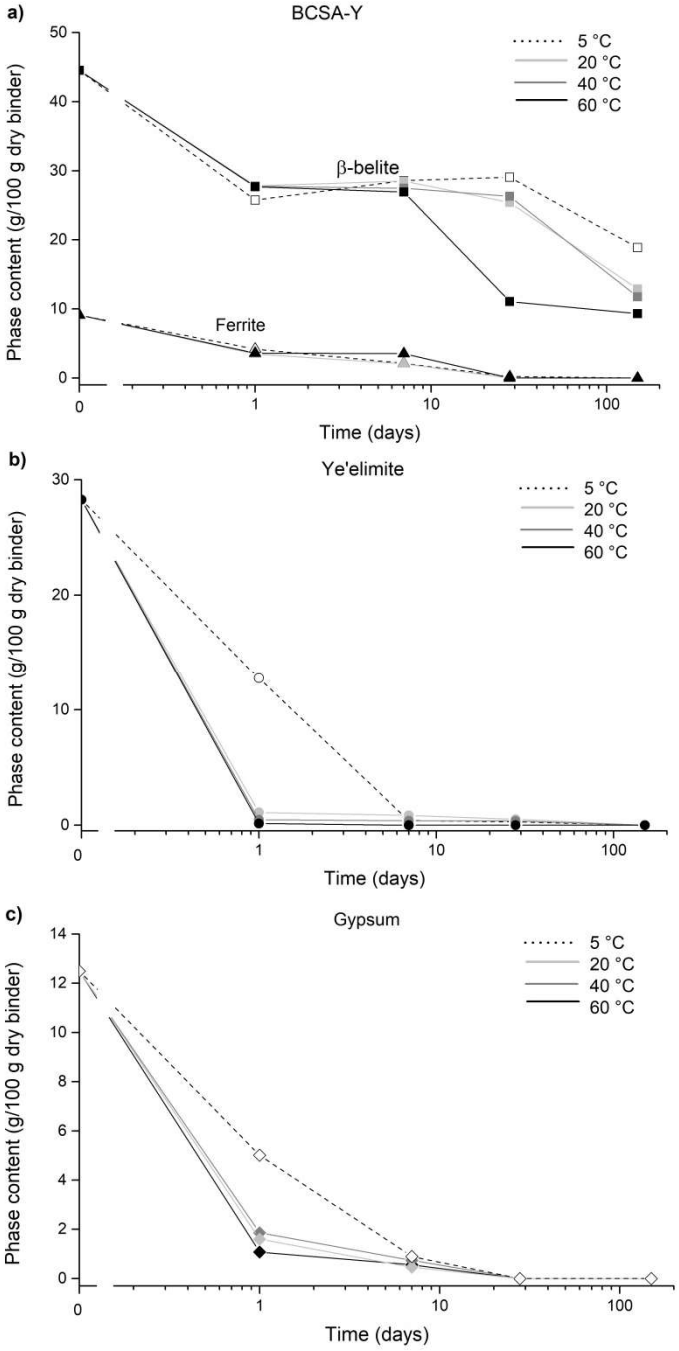

Figure 5.7: Amounts of β-belite and ferrite (a), ye'elimite (b) and gypsum (c) in the BCSA-Y cement mixture obtained by quantitative X-ray diffraction. The estimated relative errors are ±5 %. Data at 20 °C was taken from [89].

In the BCSA-B cement mixture, unreacted ferrite is only present at 1 day of hydration; after 7 days it is not detected at all, suggesting it has already dissolved. In line with previous findings [106], [107], the hydration degree of ferrite at 1 day does not change significantly with temperature, reaching around 60 % at 20 °C, 40 °C and 60 °C, and a somewhat lower value (50 %) at 5 °C. Ferrite is consumed more slowly in BCSA-Y than it is in BCSA-B, meaning it is still detected at 7 days of hydration. At 5 °C, the

hydration degree is approximately 54 % after 1 day, while at the increased temperature it is slightly higher (60 %).

5.3.3 Development of the Hydration Products

XRD results reveal the presence of ettringite, monosulfate, strätlingite and siliceous hydrogarnet as crystalline hydration products in the hydrated samples (Figures 5.8 and 5.9). Aluminium hydroxide, which also forms upon the hydration of ye'elimite-based cements, is generally X-ray amorphous but can be identified by thermogravimetric analyses, especially at early ages (see Figures 5.10, 5.11 and 5.12). C—S—H, a further potential hydration product, is difficult to detect, but can potentially be identified by a very broad signal in both XRD and TGA, and more clearly by using SEM/BSE with EDXS. In general, it can be observed in both BCSA-B and BCSA-Y that the type of hydration products does not change when the curing temperature is altered, but they do vary with respect to the amounts [65], [72], [81].

As mentioned above, the early hydration of ye'elimite in the presence of gypsum is slower at 5 °C than it is at elevated temperatures, which directly results in a lower amount of precipitated ettringite after 1 day of hydration in comparison to at increased temperatures. With ongoing hydration, however, i.e. between 7 and 150 days, less ettringite and slightly more monosulfate were formed when the temperature was increased, in agreement with previous studies [63], [65], [72], [74], [81], [106], [107], [109]. Ettringite together with aluminium hydroxide precipitate with the hydration of ye'elimite and gypsum, according to Eq. 1.1, while monosulfate forms following the depletion of sulfate, according to Eq. 1.2 [15], [20], [22], [23], [30], [49], [54], [110].

As the temperature increases, the solubility of ettringite is higher, which promotes the formation of monosulfate and leads to an increased sulfate concentration in the pore solution [65], [73], [81], [109]. At 5 °C, the hydration of ye'elimite only generates low initial amounts of ettringite; later, especially after 7 days, far more is formed, while only a small amount of monosulfate is formed in comparison to at higher temperatures [81]. Furthermore, the amount of ettringite decreases over time, at the expense of monosulfate. The results of TGA analyses are in agreement with those from X-ray powder diffraction, confirming that, in the long-term, less ettringite is generated at higher temperatures [81]. In both BCSA-B and BCSA-Y, the main weight loss measured at 120 °C, which is assigned to the decomposition of ettringite [20], [48], [81], [111], decreases with hydration time, as can be seen in Figures 5.10 to 5.13. At higher temperatures, the ettringite content decreases from 7 days onwards in both mixtures. Furthermore, as expected, the results indicate that far more ettringite is present in BCSA-Y than in BCSA-B, due to the greater presence of ye'elimite, which will subsequently lead to a higher compressive strength in the BCSA-Y cement.

Potentially, C—S—H, with a broad weight loss area between 50 and 250 °C [97] could also be present, but this is difficult to clearly assess given the intense weight loss caused by the decomposition of ettringite. Aluminium hydroxide also forms during the first day of hydration, due to the hydration of ye'elimite, but this seems to already be largely consumed after 1 day in BCSA-B, and after 28 days in BCSA-Y, due to its reaction with belite to form strätlingite, as defined in Eq. 1.3 [20], [55], [57].

Aluminium hydroxide loses its bound water and exhibits an endothermic peak at around 250-280 °C [20], [48], [81], [111], but this was not identified by X-ray diffraction due to its amorphous nature [44], [56]. TGA shows that, at elevated temperatures, more aluminium hydroxide forms initially, indicating that the formation of aluminium hydroxide is promoted at high temperatures, as has been reported previously [72], [74],

[81]. More aluminium hydroxide is observed in BCSA-Y than in BCSA-B, due to the lower belite content of the former.

In BCSA-B, strätlingite is identified after 7 days of hydration, while in BCSA-Y it is not identified until 150 days at 5 °C and after 28 days at ambient and elevated temperatures. This is due to the fact that less belite is present in BCSA-Y and because belite hydration is slower at low temperatures. Part of the strätlingite might be amorphous or poorly crystalline, however, and thus be difficult to detect by XRD. At higher temperatures, the amount of strätlingite significantly decreases - after 28 days in BCSA-B and after 150 days in BCSA-Y - coinciding with the formation of siliceous hydrogarnet, which precipitates due to the hydration of ferrite [20], as defined in Eq. 1.6.

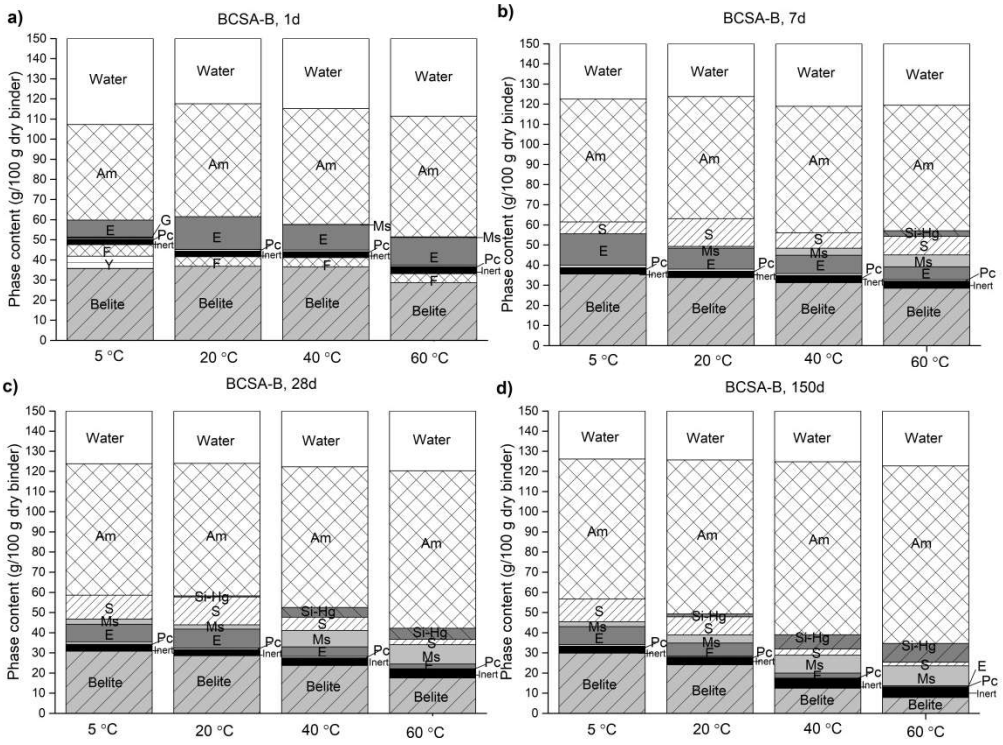

Figure 5.8: Comparison of the phase assemblages of cement mixture BCSA-B at different temperatures as determined by quantitative X-ray diffraction. Am = amorphous, E = ettringite, F = ferrite, G = gypsum, Ms = monosulfate, Pc = periclase, S = strätlingite, Si-Hg = siliceous hydrogarnet, Y = ye'elimite. The data for 20 °C was taken from [89].

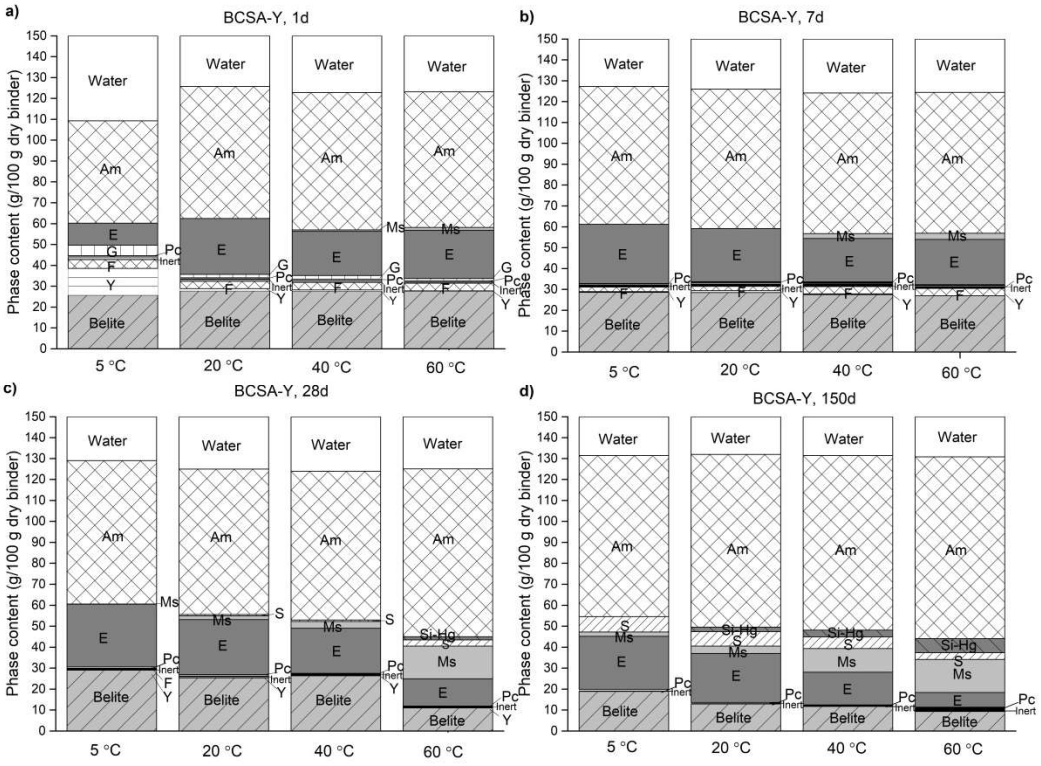

Figure 5.9: Comparison of the phase assemblages of cement mixture BCSA-Y at different temperatures as determined by quantitative X-ray diffraction. Am = amorphous, E = ettringite, F = ferrite, G = gypsum, Ms = monosulfate, Pc = periclase, S = strätlingite, Si-Hg = siliceous hydrogarnet, Y = ye'elimite. The data for 20 °C was taken from [89].

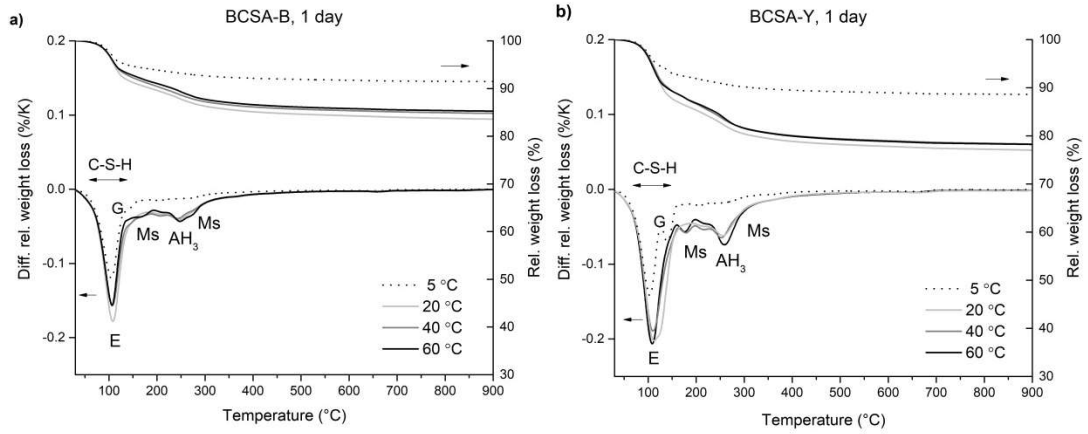

Figure 5.10: Thermogravimetric analyses of cement pastes BCSA-B (a) and BCSA-Y (b) at 1 day of hydration at different curing temperatures. AH_3 = aluminium hydroxide, C—S—H = calcium silicate hydrate, E = ettringite, G = gypsum, and Ms = monosulfate. The data for 20 °C was taken from [89].

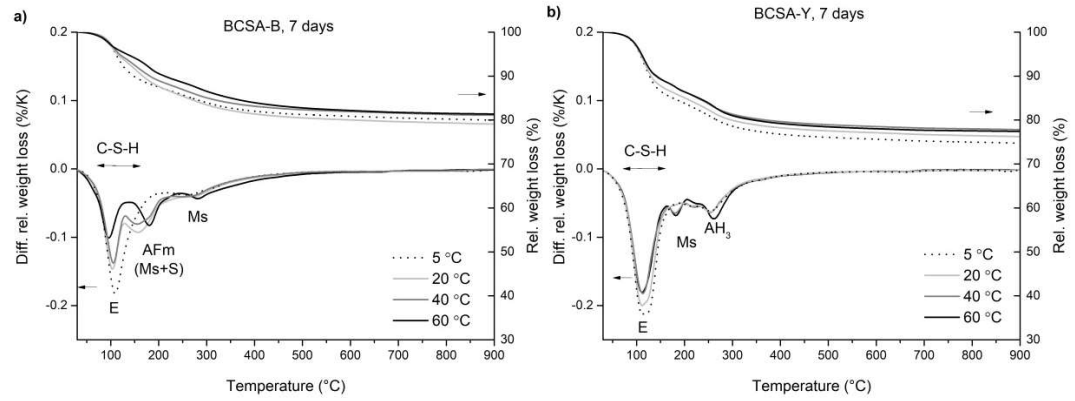

Figure 5.11: Thermogravimetric analyses of cement pastes BCSA-B (a) and BCSA-Y (b) at 7 days of hydration at different curing temperatures. AH_3 = aluminium hydroxide, C—S—H = calcium silicate hydrate, E = ettringite, G = gypsum, Ms = monosulfate and S = strätlingite. The data for 20 °C was taken from [86].

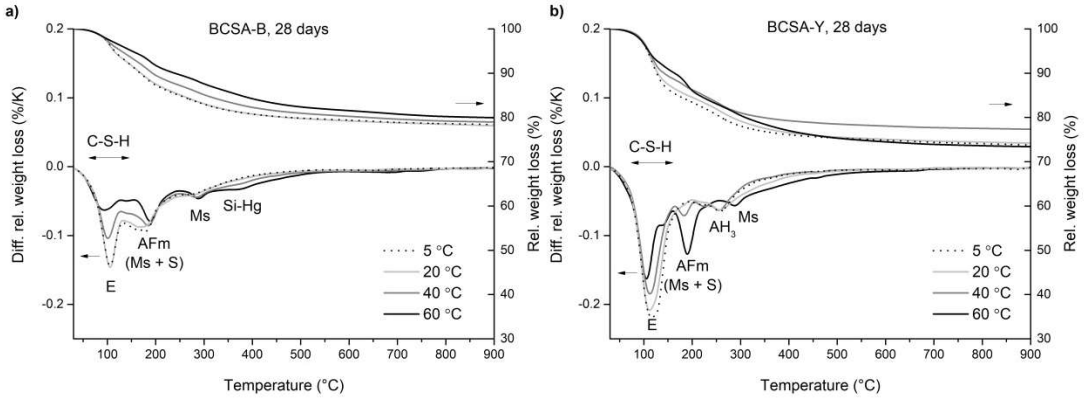

Figure 5.12: Thermogravimetric analyses of cement pastes BCSA-B (a) and BCSA-Y (b) at 28 days of hydration at different curing temperatures. AH_3 = aluminium hydroxide, C—S—H = calcium silicate hydrate, E = ettringite, G = gypsum, Ms = monosulfate, S = strätlingite, and Si-Hg = siliceous hydrogarnet. The data for 20 °C was taken from [86].

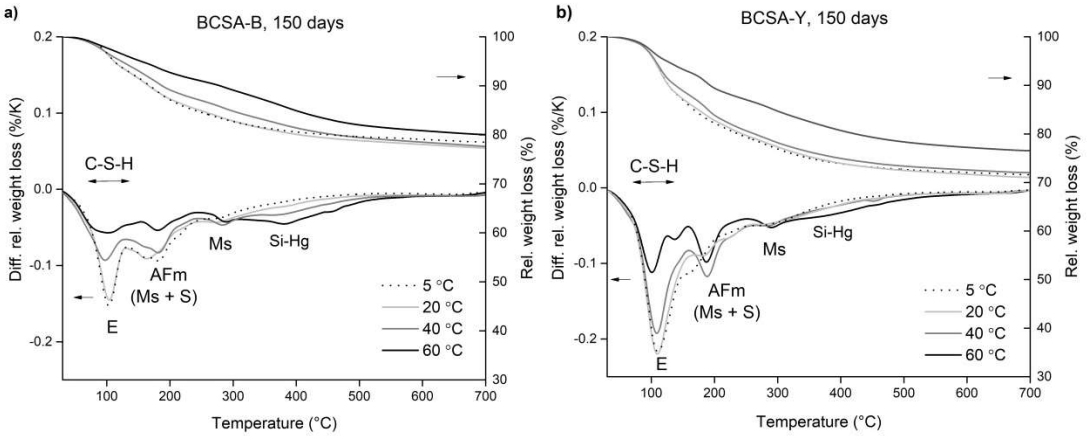

Figure 5.13: Thermogravimetric analyses of cement pastes BCSA-B (a) and BCSA-Y (b) at 150 days of hydration at different curing temperatures. C—S—H = calcium silicate hydrate, E = ettringite, G = gypsum, Ms = monosulfate, S = strätlingite, and Si-Hg = siliceous hydrogarnet. The data for 20 °C was taken from [89].

Higher amounts of siliceous hydrogarnet are observed at elevated temperatures, especially at 60 °C, which was also confirmed by the TGA data. When more belite hydrates, siliceous hydrogarnet and possibly also C—S—H form on the expenses of strätlingite as suggested by the modelling (see section 5.3.5). This increased amount of siliceous hydrogarnet at elevated temperatures is in agreement with other observations in both Portland and calcium sulfoaluminate cements [49], [63], [72]. In a recent study by Chitvoranund et al. [83] small amounts of siliceous hydrogarnet were observed in a belite-ye'elimite system, but only at 60 °C, as there was not a significant amount of ferrite present in the cement clinker. The precipitation of siliceous hydrogarnet is favoured at increased temperatures due to kinetic reasons [72], [112], a certain amount is also detected in this study at both 20 °C and 40 °C, observed after 28 days of hydration in BCSA-B and after 150 days in BCSA-Y.

The bound water contents as derived from TGA are shown in Figure 5.14, where the different amounts of ettringite are primarily reflected in the amounts of bound water. Thus, bound water content is higher in the ye'elimite-rich cement compared to the belite-rich cement, where more ettringite has formed in this cement. Although the amount of bound water after 1 day of hydration is significantly lower at 5 °C than it is at higher temperatures, both BCSA-B and BCSA-Y reach comparable bound water contents after 150 days with the exception of 60 °C, in agreement with the observed amounts of ettringite.

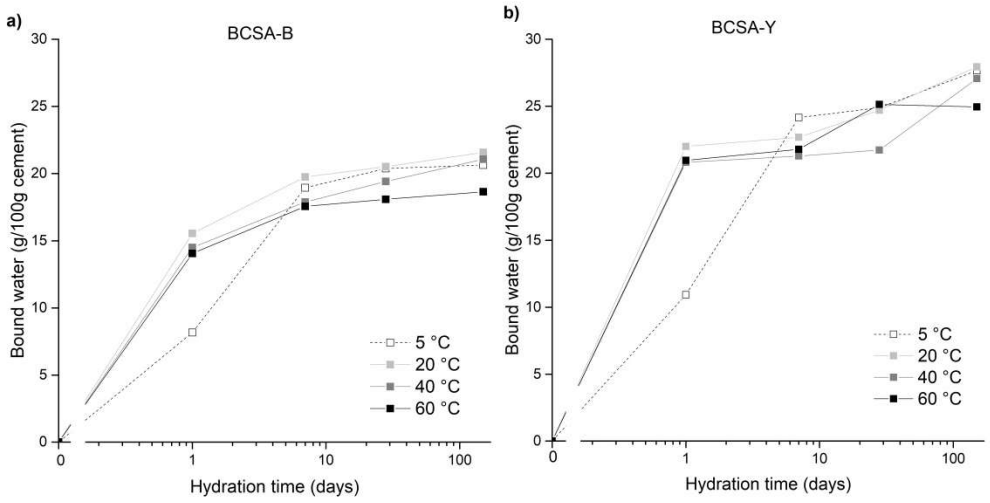

Figure 5.14: Bound water, as determined by thermogravimetric analyses up to 150 days of hydration (normalized to anhydrous cement) at different temperatures and plotted against curing time. The data for 20 °C was taken from [89].

5.3.4 Microstructural Characterization of the Hydrate Phases

Figures 5.15-5.18 show SEM/BSE images of polished sections of the BCSA-B and BCSA-Y cement at 150 days of hydration at different temperatures. All samples have a dense matrix with low porosity. At elevated temperatures (40 and 60 °C), the microstructure is less dense and the hydration products are more heterogeneously distributed in comparison to samples cured at lower temperatures, where individual hydration products are harder to detect. Previous studies on Portland cements and calcium sulfoaluminate cements have shown that the heterogeneity of cement pastes is increased at higher temperatures as a result of the faster hydration [65], [72], [113]. Grains of anhydrous clinker are present at 5 °C, as shown in Figure 5.15. At elevated temperatures (Figures 5.16-5.18), smaller and less anhydrous grains are present in comparison to at 5 °C, confirming a higher degree of hydration as observed by XRD. Similar findings have been reported previously [72]. EDXS analysis reveals that the matrix consists of ettringite, AFm phases (monosulfate, strätlingite, hydrogarnet) and C−S−H. Ettringite is far more prominent in the BCSA-Y mixture than it is in BCSA-B. The amount of ettringite is also lower at elevated temperatures, in agreement with both the XRD and TGA observations and the thermodynamic modelling. It is difficult to differentiate between monosulfate and strätlingite in the BSE images; monosulfate usually appears as platelets, while strätlingite is formed of elongated shapes. C−S−H is finely distributed in the interstitial free space between ettringite and monosulfate and, in contrast to Portland cement, does not form around the calcium silicate clinker phases (in this case only belite) [105].

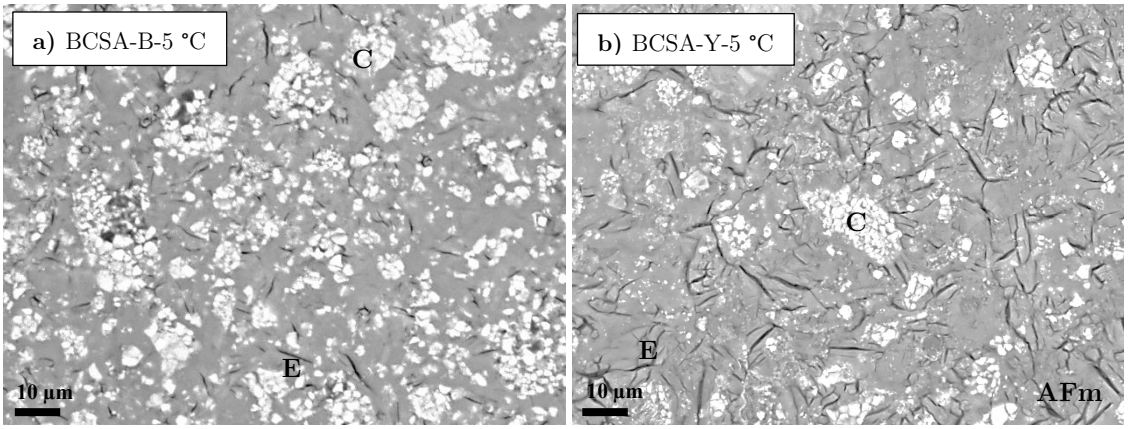

Figure 5.15: SEM/BSE images of the BCSA-B (a) and BCSA-Y (b) cements cured at 5 °C at 150 days of hydration, showing the residual clinker phases and hydration products that precipitated. C = unhydrated clinker, E = ettringite, AFm = monosulfate and/or strätlingite.

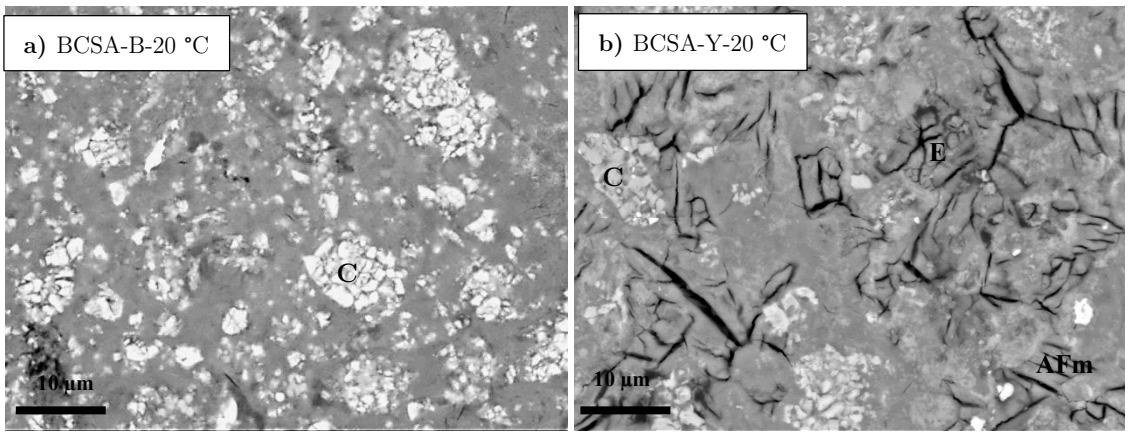

Figure 5.16: SEM/BSE images of BCSA-B (a) and BCSA-Y (b) cements cured at 20 °C at 150 days of hydration, showing the residual clinker phases and hydration products that precipitated. C = unhydrated clinker, AFm = monosulfate and/or strätlingite.

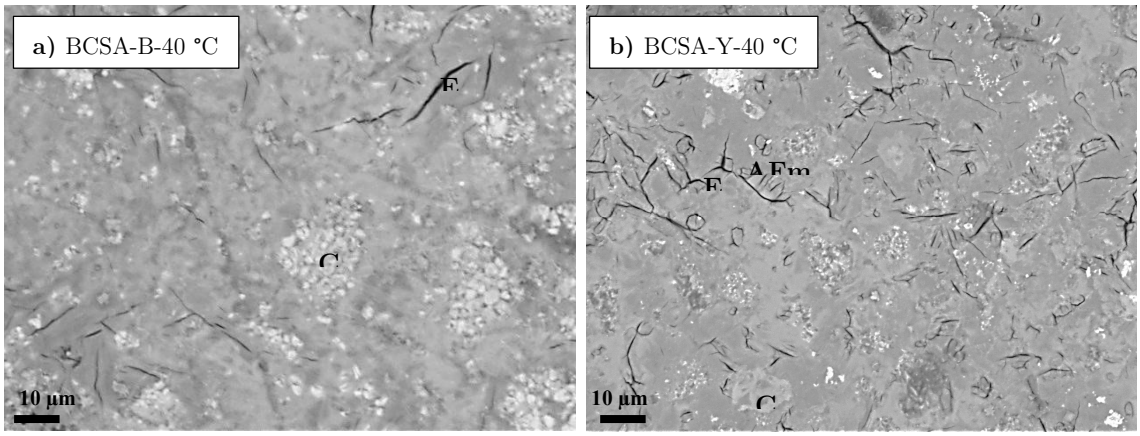

Figure 5.17: SEM/BSE images of BCSA-B (a) and BCSA-Y (b) cements cured at 40 °C at 150 days of hydration, showing the residual clinker phases and hydration products that precipitated. C = unhydrated clinker, E = ettringite, AFm = monosulfate and/or strätlingite.

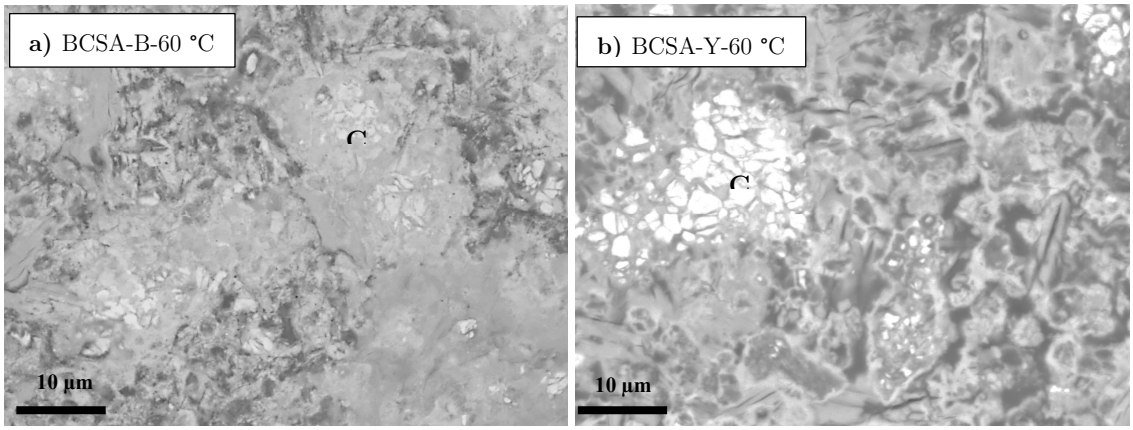

Figure 5.18: SEM/BSE images of BCSA-B (a) and BCSA-Y (b) cements cured at 60 °C at 150 days of hydration, showing the residual clinker phases and hydration products that precipitated. C = unhydrated clinker.

The results of EDXS analyses are shown as atomic ratio plots (Figures 5.19 and 5.20), due to the small size of the hydrate phases, and the interaction volume of electrons with a sample, which causes X-rays to consist of mixed signals of different phases [114].

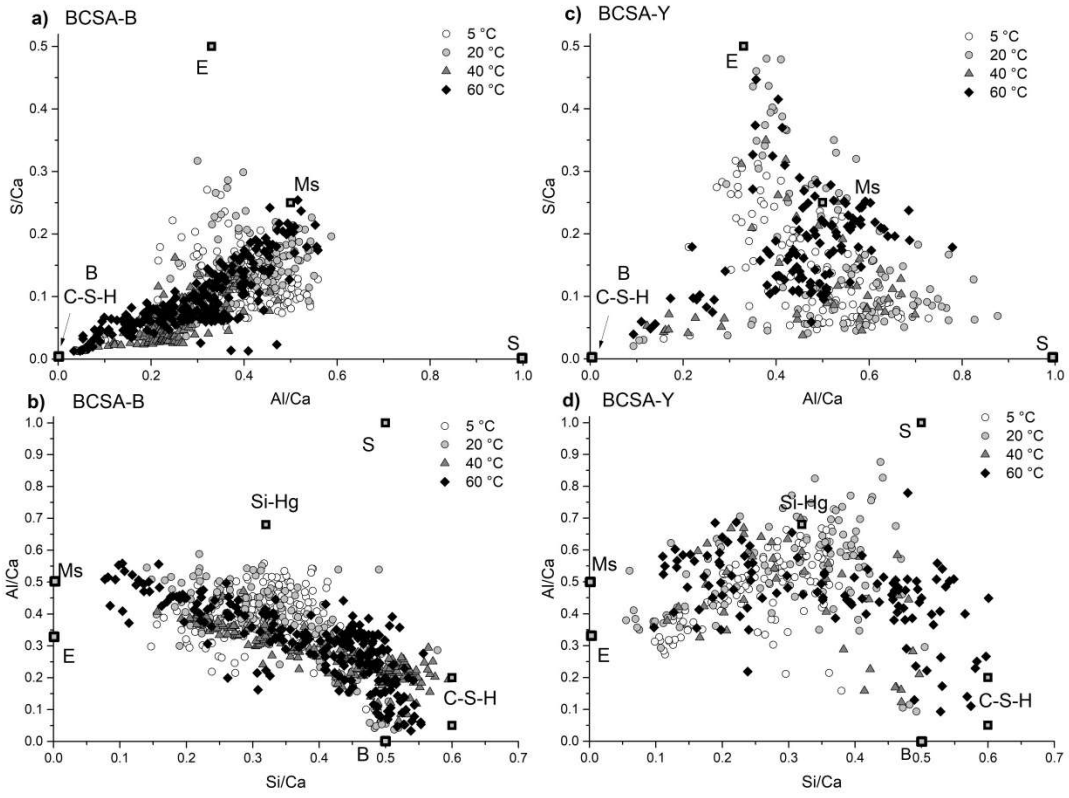

Figure 5.19: EDXS analyses of the BCSA-B (a and b) and BCSA-Y pastes (c and d) at 150 days of hydration at different curing temperatures. Grey squares = pure phases: B = belite, C—S—H = calcium silicate hydrate, E = ettringite, Ms = monosulfate, S = strätlingite and Si-Hg = siliceous hydrogarnet.

The results show that the phase composition of the hydrate assemblage changes with temperature, as well as with the compositions of the cement clinker (Figure 5.19). At 5 °C, EDXS analyses indicate the presence of ettringite and monosulfate in BCSA-B at 150 days, as the EDXS points are located in the area between the composition of these phases. Furthermore, some strätlingite and C−S−H are detected. This is in agreement with the XRD and TGA results, which indicate the formation of ettringite, monosulfate and strätlingite. It is not, however, possible to clearly identify C—S—H with either of those two methods. Similarly, both ettringite and monosulfate are observed at 20 °C, yet it can be seen that more data points are located towards monosulfate rather than ettringite compared to 5 °C. Data points between ettringite and strätlingite confirm the formation of strätlingite. Some data points also occcur between monosulfate and C−S−H. At 40 and 60 °C only a small number of data points are located towards ettringite, while the main share is directed towards monosulfate and C−S−H. In addition, it can be seen that less or almost no strätlingite is present, as only a few points are close to this phase - this also corresponds with the XRD and TGA results.

In contrast to the BCSA-B cement, in BCSA-Y significantly more data points are directed towards a composition of ettringite. Monosulfate is also indicated, and more data points related to this phase are present at elevated temperatures. The trend towards strätlingite at elevated temperatures is more pronounced in BCSA-Y than it is in BCSA-B. A low C−S−H content may also occur in BCSA-Y, as data points in the area near the composition of C−S−H are visible. According to EDXS, siliceous hydrogarnet could be present in both cements.

Figure 5.20 plots the graphs of different atomic ratios of samples cured at 20 °C at 1, 7, 28 and 150 days of hydration. In BCSA-B, EDXS analyses confirm the presence of ettringite as the main hydration product at 1 day of hydration, as was also detected by X-ray powder diffraction. At 7 days of hydration, a small number of data points are located towards monosulfate, whilst the majority of data points are located towards strätlingite. After 28 and 150 days of hydration, in addition to the presence of strätlingite, a much more visible trend is evident between the compositions of monosulfate and C−S−H.

In BCSA-Y, the data points at 1 day are far more dispersed, probably due to the presence of unreacted ye'elimite and gypsum. At all hydration times, the data points are primarily directed towards ettringite. A trend towards strätlingite is observed at 150 days. A small amount of C—S—H seems to be indicated at all hydration times, as a few points are also close to this phase.

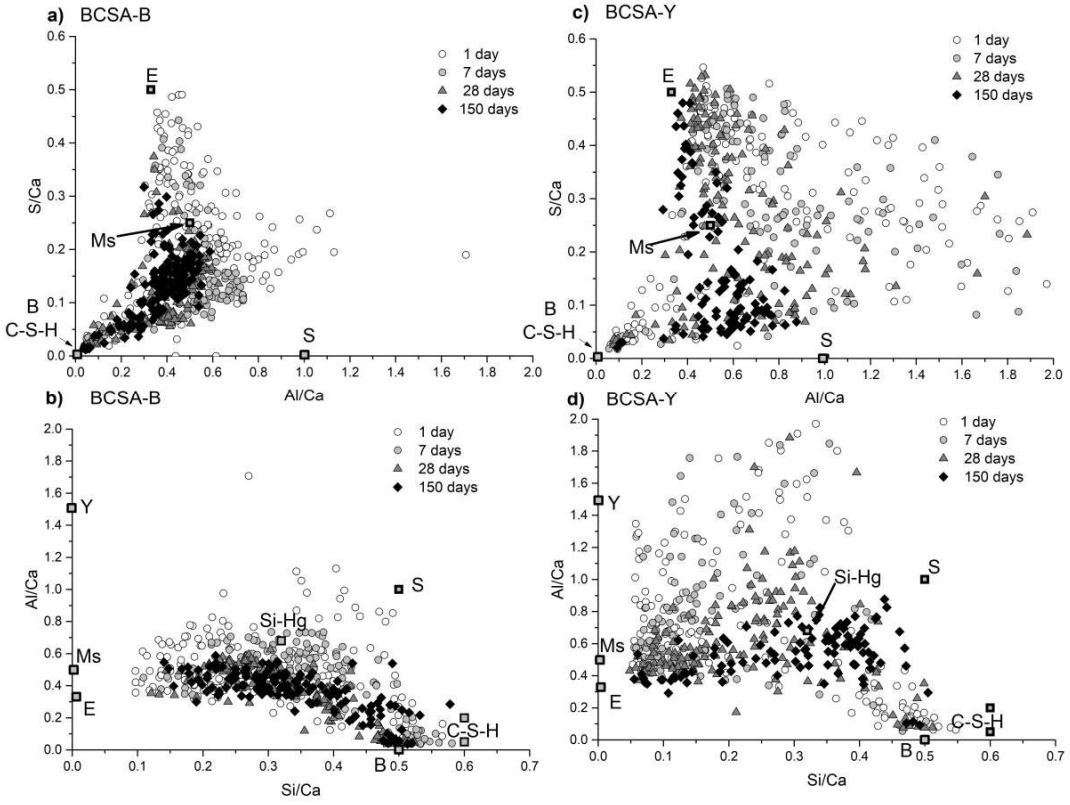

Figure 5.20: EDXS analyses of the BCSA-B (a and b) and BCSA-Y pastes (b and c) at 20 °C at different curing times. Grey squares = pure phases: B = belite, C—S—H = calcium silicate hydrate, E = ettringite, Ms = monosulfate, S = strätlingite, Si-Hg = siliceous hydrogarnet and Y = ye'elimite.

5.3.5 Thermodynamic Modelling of Phase Development with Time and Temperature

Figures 5.21 and 5.22 show the modelled hydrate assemblages of the BCSA-B and BCSA-Y cements with ongoing hydration at 5 °C, 20 °C, 40 °C and 60 °C. In both the systems investigated (BCSA-B and BCSA-Y), the stable hydrate phases calculated at all temperatures are ettringite, monosulfate, strätlingite, C–S–H, siliceous hydrogarnet, and hydrotalcite. Aluminum hydroxide is only formed in the BCSA-Y cement at 20 °C, 40 °C and 60 °C, and traces of portlandite and brucite are present in the early ages - something that was not observed experimentally. The occurrence of these phases may also be an artifact of the different reaction degrees fitted for ye'elimite and belite. In general, differences in the amount of hydrate phases between various temperatures are predicted based on the faster kinetics seen at higher temperatures and are in agreement with the experimental data. Ettringite is the main hydration product predicted at early ages, resulting from the fast hydration of ye'elimite and gypsum. When gypsum is depleted, monosulfate forms, at the expense of ettringite. As the temperature increases, a higher amount of monosulfate is predicted, whilst the amount of ettringite is reduced. Significantly more ettringite and less monosulfate are calculated in BCSA-Y compared to in BCSA-B. Furthermore, the higher amount of ettringite in BCSA-Y results in a lower amount of pore solution, as ettringite consumes more water. The modelling indicates the presence of strätlingite, C—S—H and siliceous hydrogarnet in both cements, which is in

agreement with the XRD, TGA and EDXS data. More strätlingite is predicted by thermodynamic modeling than was determined experimentally, suggesting that strätlingite is also present in an X-ray amorphous form, as has also been reported elsewhere [105]. The models predict a higher quantity of C—S—H at elevated temperatures, as more belite reacts.

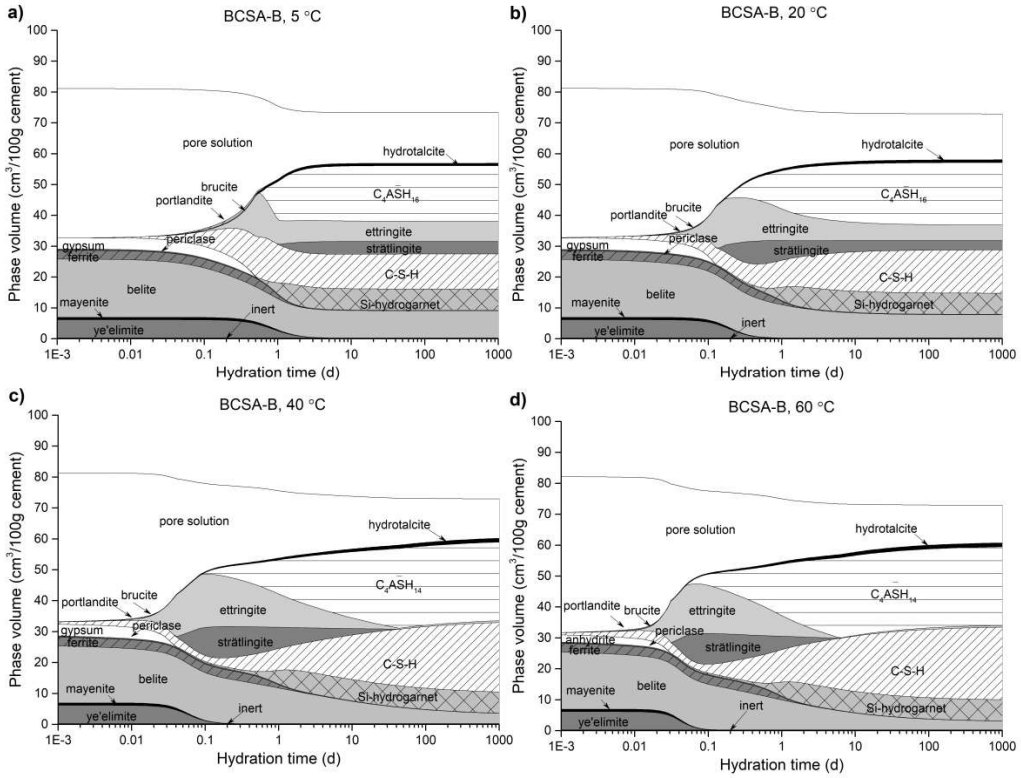

Figure 5.21: Thermodynamic models of the phase assemblages in the BCSA-B cement as a function of hydration time at curing temperatures 5 °C (a), 20 °C (b), 40 °C (c) and 60 °C (d).

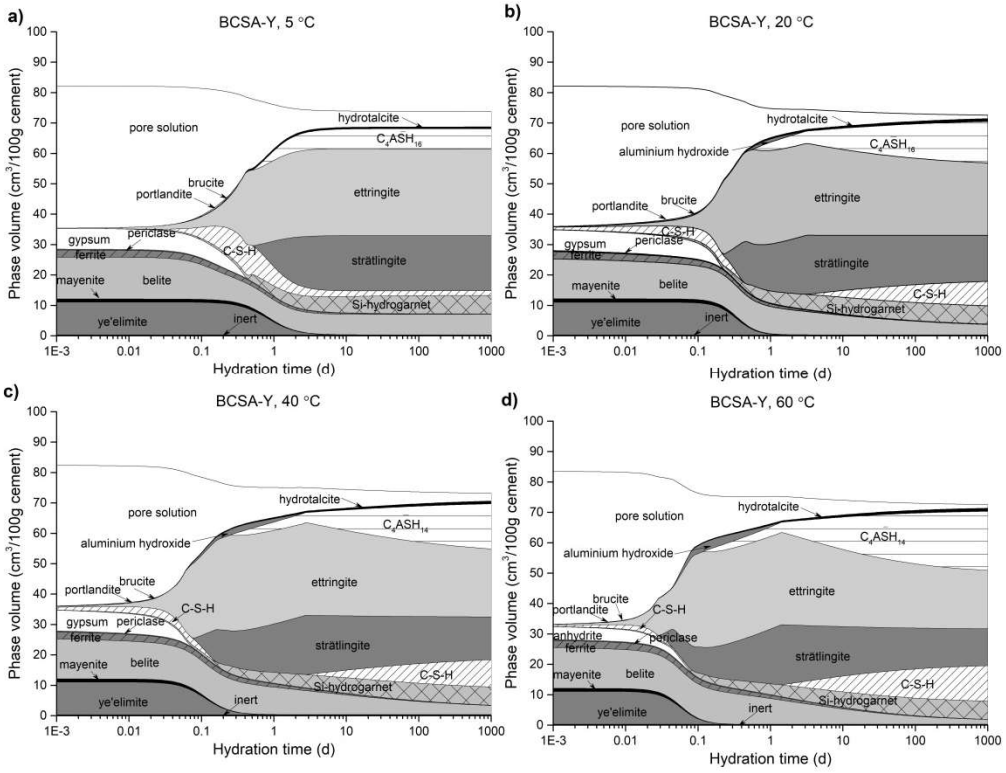

Figure 5.22: Thermodynamic models of the phase assemblages in the BCSA-Y cement as a function of hydration time at 5 °C (a), 20 °C (b), 40 °C (c) and 60 °C (d).

5.3.6 Compressive Strength

Results of the compressive strength measurements on the BCSA-B and BCSA-Y cements cured at different temperatures are shown in Figure 5.23.

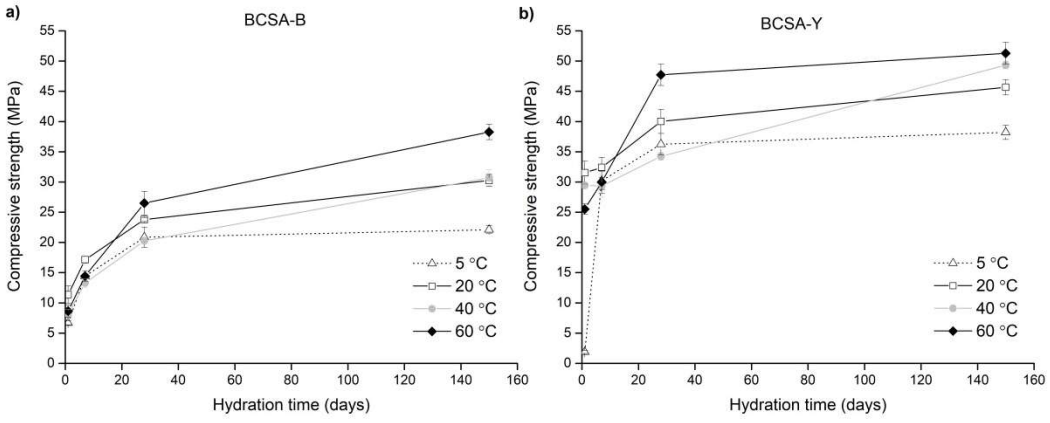

Figure 5.23: Development of compressive strength in the BCSA-B (a) and BCSA-Y (b) cement at different curing temperatures. The data for 20 °C was taken from [89].

Both cements exhibit rapid early strength development at 20 °C, 40 °C and 60 °C, as a result of the fast reaction of ye'elimite and gypsum with water and the consequent formation of ettringite, which significantly contributes to early strength [25], [59], [63],

[65], [105]. In both cements, strength development is rather slow at 5 °C, which is in agreement with other studies [65], [81], [104], [105]. Results from X-ray diffraction and thermogravimetric analysis show that, in BCSA-B, gypsum is fully consumed within the initial 24 hours of hydration at 20 °C, 40 °C and 60 °C, while at 5 °C, a small amount remains unreacted. In BCSA-Y, a far higher amount of unreacted gypsum remains present at 5 °C, which results in lower strength after 1 day of hydration compared to in BCSA-B.

The results show that, in both cements, the compressive strength at late ages increases as the curing temperature increases. In BCSA-B, the highest compressive strength after 150 days (38.3 MPa) is attained at 60 °C, followed by those cured at 40 °C (30.7 MPa) and 20 °C (30.3 MPa), while at 5 °C the compressive strength is only 22.1 MPa. In BCSA-Y, the values of compressive strength were 51.3 MPa, 49.3 MPa, 45.7 MPa and 38.2 MPa at 60 °C, 40 °C, 20 °C and 5 °C, respectively. While studies on ordinary Portland cement and calcium sulfoaluminate cements have reported that compressive strength decreases at higher curing temperatures, previous studies on belite cements have shown that compressive strength actually increases at elevated temperatures [106], [115], [116], as a result of the increased degree of belite hydration. In the case of the present study, the increased hydration of belite at elevated temperatures, which takes place beyond 7 days of hydration, led to the formation of additional space-filling hydrates such as strätlingite, C—S—H and siliceous hydrogarnet, causing an increase in strength at elevated temperatures [83], while recent studied showed that the increase of strength might be even higher at 60 °C but is not due to the heterogenous microstructure and micro-cracks that occur on the mortar samples [83].

Comparing the two cements, it can be observed that BCSA-Y develops a higher compressive strength than BCSA-B, probably due to the higher ye'elimite content and the associated increase in the formation of ettringite. At 5 °C, however, the early compressive strength in BCSA-Y is lower than it is in BCSA-B, due to the slow hydration of ye'elimite during the first 24 hours at this temperature.

Figure 5.24a depicts the comparison between bound water as determined by with the compressive strength measured at the various temperatures investigated. As the bound water content increases, higher compressive strengths are found, as a greater volume of hydrates forms. It is worth noting that, even at 5 °C, when the compressive strength is lowest, a significant amount of water is still bound. As expected, the compressive strength increases as the porosity, derived from thermodynamic modelling, decreases, as shown in Figure 5.24b.

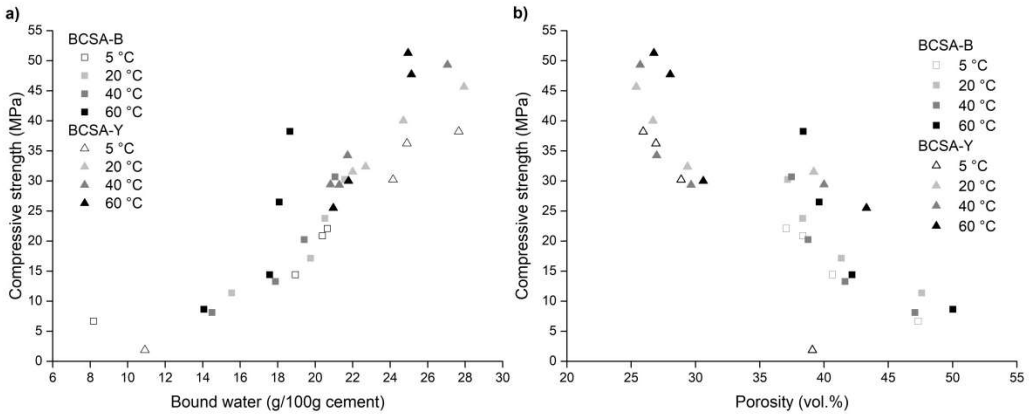

Figure 5.24: (a) Bound water, determined by TGA, versus compressive strength measured in BCSA-B and BCSA-Y. (b) Calculated total porosity derived from

thermodynamic modelling versus compressive strength measured in BCSA-B and BCSA-Y. The data for 20 °C was taken from [89].

5.3.7 Thermodynamic Modelling of the Effect of Temperature on the Hydrate Assemblage

The modelled phase composition of the BCSA-B cement paste at late ages according to temperature is plotted in Figure 5.25a. The stable hydrate phases predicted across the whole temperature range, from 0 to 85 °C, are siliceous hydrogarnet, C—S—H, monosulfate and hydrotalcite. Low amounts of ettringite are calculated to be present between 0 and 25 °C. Traces of katoite are predicted to occur between 55-70 °C, although in reality the additional aluminium may instead be bound in C—S—H, which was not taken into account in the modelling. Above 70 °C, small amounts of portlandite are calculated to be present, as well as more belite reacts at higher temperatures. C—S—H and monosulfate are the most abundant phases, followed by siliceous hydrogarnet, which is calculated to be present across the whole temperature range as a result of the hydration of ferrite and belite. The hydration state of monosulfate can, however, vary according to temperature [117]. At a low temperature, monosulfate with 14 waters ($\mathbf{C_4A\bar{S}H_{14}}$) is predicted, while above 20 °C, instead monosulfate with 16 waters ($\mathbf{C_4A\bar{S}H_{16}}$) is calculated. Aluminium hydroxide is predicted to be absent at the high reaction degrees considered.

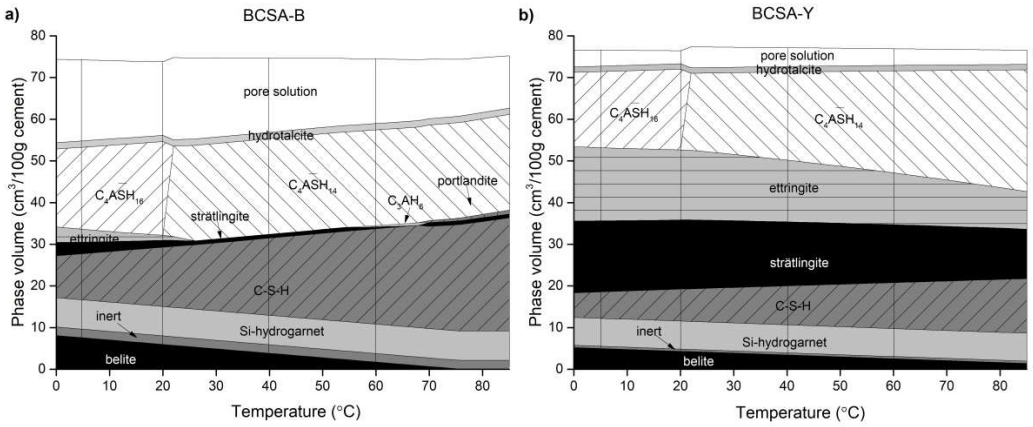

Figure 5.25: Phase assemblages, calculated in cm^3 per 100 g unhydrated cement, for the belite-rich BCSA-B (a) and the ye'elimite-rich BCSA-Y (b) cements, shown as a function of temperature. The lines indicate the samples studied experimentally at 5 °C, 20 °C, 40 °C and 60 °C. The reaction degrees of 100% in ye'elimite, ferrite, periclase and mayenite correspond to the reaction degree observed at approximately 150 days, as discussed in section 5.3.3. The reaction degree of belite was assumed to increase linearly with temperature based on X-ray diffraction data.

For BCSA-Y (Figure 5.25b), the phases calculated are siliceous hydrogarnet, C—S—H, strätlingite, ettringite, monosulfate and hydrotalcite. It is worth noting that, as the Al-uptake in C—S—H was neglected during modelling, due to a lack of experimental data, it is likely that the amount of strätlingite is overpredicted. The amounts of phases calculated are not significantly impacted by temperature. The amounts of strätlingite, C—S—H and siliceous hydrogarnet remain almost the same between 0 and 85 °C, while the quantity of ettringite decreases, and the amount of monosulfate increases at higher

temperatures. The amount of pore solution is lower than that in BCSA-B, due to the greater presence of water-rich ettringite, and slightly increases at higher temperatures. The higher content of ye'elimite in the BCSA-Y cement results in the formation of more ettringite and strätlingite than occurs in BCSA-B, while the lower belite content of BCSA-Y means less C—S—H is predicted.

These observations agree well with the long-term composition observed experimentally, with the exception of hydrogarnet, where we have observed experimentally more hydrogarnet at higher temperature. This difference is related to the slow formation kinetics of hydrogarnet at increased temperatures due to kinetic reasons [72], [112], while during thermodynamic modelling immediate precipitation was assumed at all temperatures.

5.4 Conclusions

Different curing temperatures change the type of hydrates and their amounts. Higher temperatures expedite the dissolution of anhydrous phases, an effect most noticeable in hydration of ye'elimite. At 5 °C, the degrees of hydration of ye'elimite, gypsum and belite are lower than at ambient and elevated temperatures. The reaction of belite is promoted in the first 24 hours, slowing down later, but after 150 days at 60 °C it still reaches a reaction degree of nearly 90 %. In contrast, the reaction degree of belite after 150 days at 5 °C is only around 50 %.

At 20 °C, 40 °C and 60 °C, more monosulfate but less ettringite precipitate in BCSA cements, due to an increase in the solubility of ettringite at higher temperatures; at 5 °C, on the other hand, a high amount of ettringite is present. The precipitation of aluminium hydroxide is associated with the hydration of ye'elimite, and its formation is only observed at early reaction times; aluminium, on the other hand, is taken up in C—S—H, siliceous hydrogarnet and AFm-phases at later ages, once belite and ferrite have already reacted to some extent. Despite the fact that the hydration of belite is slower at lower temperatures, the amount of strätlingite actually decreases at elevated temperatures, due to the formation of siliceous hydrogarnet, which takes up aluminum from strätlingite. The formation of siliceous hydrogarnet is favoured at higher temperatures and is not detected at 5 °C. According to EDXS analysis, more C—S—H precipitated at higher temperatures as more belite reacted. In the early ages, phase composition changes significantly from 5 °C to 20 °C and 40 °C to 60 °C, whereas between 20 °C and 40 °C they remain relatively consistent. On the other hand, at later ages, the compositions of 40 °C and 60 °C are more similar than those between 20 and 40 °C. When the cement clinker contains less belite, its composition changes continuously with increasing temperature.

At low temperatures (i.e. 5 °C), the microstructure is denser, and the distribution of hydration products is more homogenous, due to the slower hydration. When the temperature is increased from 20 to 60 °C, however, the microstructure becomes more and more heterogeneous, and the hydration products can be easily differentiated. Less anhydrous grains are visible at higher temperatures, indicating a higher degree of hydration. C—S—H is found in the interstitial free space between grains of ettringite and monosulfate.

Early compressive strength is significantly lower at 5 °C compared to at 20 °C, 40 °C and 60 °C. At late ages, the compressive strength is greater at higher curing temperatures, due to the increased hydration of belite at elevated temperatures, which leads to the formation of strätlingite, C—S—H and siliceous hydrogarnet, however the amount of ettringite decreases at later ages. Compressive strength shows a positive

correlation with bound water and a negative correlation to the calculated total porosity, as more volume filling hydrates form (increasing bound water) and fill the pores (decreasing porosity) leading to higher compressive strength.

Thermodynamic modelling confirmed that temperature primarily affects the reaction kinetics of belite-ye'elimite-ferrite cements and has a much lesser effect on the type of hydrates formed. Hydration kinetics are accelerated when the curing temperature is increased. At 5 °C the hydration is rather slow, while at elevated temperatures the clinker reactions occur significantly faster. The experimental results agree well with the thermodynamic modelling, which, in addition to ettringite, calculates aluminum hydroxide, monosulfate, strätlingite, C—S—H and siliceous hydrogarnet to be the main stable hydrate phases at all temperatures. Hydrotalcite, portlandite and brucite were calculated as minor phases. As the temperature increases, less ettringite and more monosulfate are predicted. Furthermore, higher amounts of C—S—H are calculated at elevated temperatures, due to the higher reaction degree of belite.

Finally, the results also show that the composition of the cement clinker affects both the type and amount of hydrates formed. At early ages, more heat is generated, and more bound water is observed in the ye'elimite-rich BCSA-Y compared to in BCSA-B, due to the formation of more ettringite in the BCSA-Y clinker. The compressive strength is also higher in BCSA-Y than it is in BCSA-B, due to the presence of more ettringite both early and late in the hydration process. More strätlingite precipitates in the BCSA-Y cement, which has a higher amount of ye'elimite, while in the belite-rich BCSA-B cement more siliceous hydrogarnet and C—S—H form, due to the higher availability of calcium. This trend is more pronounced at elevated temperatures, where a higher amount of strätlingite is detected in BCSA-Y compared to in BCSA-B.

Chapter 6

Influence of Different Secondary Raw Materials on the Physico-Mechanical Properties and Hydration Evolution of Belite-Ye'elimite-Ferrite Cement at Different Curing Temperatures

This chapter is based on previously unpublished results. The data presented are from part of a study investigating the influence of different secondary raw materials on the physico-mechanical properties and hydration evolution of belite-ye'elimite-ferrite cement at different curing temperatures.

This chapter addresses the thesis objectives 1, 2, 3 and 5.

6.1 Introduction

Currently, the general direction in the cement industry is to employ alternative raw materials in the manufacture of cement clinker. With this in mind, various materials, particularly waste and by-products generated from different industrial processes, have been suggested as potential substitutes for this objective [118]. In recent years, researchers have shown significant interest in construction and demolition waste (CDW) which is generated in large quantities worldwide [119], [120]. The construction industry alone is estimated to produce over 3 billion tons of CDW annually on a global scale [121]. The predominant use of concrete from construction and demolition waste is for the production of mortar and concrete as recycled aggregates. Recycled aggregates are, however, of lower quality compared to natural aggregates, due to the presence of residual hydrated cement [120]. Generally, the incorporation of recycled aggregates tends to have a detrimental impact on the properties of concrete, causing strength loss [122]. The fine fraction of concrete waste, which consists of a combination of residue from coarse and fine aggregates and hydrated cement paste, is also used, as a replacement of clinker in cement [123], furthermore, according to cement standard EN 197-6 the use of recycled concrete fines in cements is allowed. Another industrial residue is red mud, which is derived from the Bayer alumina production process using bauxite ore [124]–[126]. The global annual production of red mud is estimated to be around 70 million tons [127]. Due

to its highly alkaline nature, red mud is classified as hazardous waste and poses a risk for soil and groundwater contamination if disposed of in landfills. The proper disposal of red mud consequently presents a significant environmental concern, emphasizing the need for its re-utilization. In recent years, researchers worldwide have extensively explored the potential utilization of red mud, leading to a substantial body of research in this area [126], [128]–[133].

The use of alternative binders such as calcium sulfoaluminate cements offers an opportunity to reduce the environmental footprint since they allow the utilization of various industrial residues as alternative raw materials for their production [20], [28], [134], [135]. Nevertheless, it should be noted that the use of such raw materials may lead to an increase in the concentration of minor elements such as iron, alkalis, phosphorus, as well as heavy metals, in the resulting clinker [134]. When incorporating minor elements into cementitious binders, various minor components such as gehlenite, periclase, mayenite, perovskite, arcanite, thenardite and aphthitalite can form, which can significantly affects the hydration kinetics, composition, and microstructure pore solution chemistry, and early-age properties of the resulting material [134], [136], [137].

Mayenite, also known as $C_{12}A_7$, belongs to the calcium aluminate group of compounds. In recent years, it has gathered more attention in research owing to its ability to accelerate the hydration of cement. Experimental findings have shown that the formation of ettringite is accelerated, which explains the enhanced early hydration kinetics [138]. The dissimilarities observed are primarily attributed to the rapid dissolution of mayenite, and alters the Ca/Al ratio of the solution, leading to the accelerated formation of ettringite and a faster depletion of sulfate from the solution [138]. Mayenite dissolves fast, thereby increasing the concentration of aluminum and calcium ions. As a result, the initial hydration stage is accelerated, while the other hydration periods are shortened [138]. When mayenite is replaced in greater quantities, the consumption rates of gypsum and calcite, which are typically present in ordinary Portland cement, are accelerated [139]. As a result, the amount of ettringite is altered and the precipitation of carbonate phases (e.g. calcium monocarboaluminate and calcium hemicarboaluminate) occurs. Consequently, the microstructural properties of the hydrated products of ordinary Portland cement are affected, thus influencing the compressive strength [138]–[140]. The hydration of $C_{12}A_7$ can be influenced by various factors. Wang et al. [141] observed that increasing the initial alkalinity accelerates the hydration of $C_{12}A_7$. In another study by Damidot et al. [142], it was shown that the presence of gypsum significantly enhances the hydration of $C_{12}A_7$; the amount of aluminium hydroxide (AH_3) produced from the hydration of $C_{12}A_7$ with gypsum was approximately twice as high as that observed in the control group. A study by Koehler et al. [143] investigating the effect of mayenite on calcium aluminate cement (CAC) showed that the dissolution of mayenite significantly affects early hydration at different temperatures (10, 23, and 35 °C). Upon the addition of water, mayenite was observed to rapidly dissolve, suggesting that even small amounts of mayenite could accelerate and modify the early hydration process. This reaction is greatly accelerated at low temperatures, which are typically associated with slower reactions. The effect is not as pronounced at moderate temperatures, although the reaction is still accelerated. Surprisingly, during hydration at high ambient temperatures (35 °C), the reaction is not accelerated, and may even be slightly delayed. Numerous investigations by various authors have focused on the hydration of pure $C_{12}A_7$ [144], [145], and the results demonstrate that higher temperatures enhance phase reactivity and reduce their initial hydration period. At a low temperature (4 °C), the formation of calcium aluminate decahydrate (CAH_{10}) was observed as expected, but, additionally, the formation of C_2AH_8, a compound that is not typically formed at such low temperatures, was also

identified. Just below 20 °C, a mixture of CAH_{10} and C_2AH_8 was observed [144], [145]. At moderate temperatures (20 to 30 °C), only C_2AH_8 was found [144], [145].

Gehlenite (C_2AS), another phase in cement, belongs to the melilite mineral group [146]. Alongside belite, C_2AS is one of the clinker minerals found in low-energy cements. During the burning process of ordinary Portland cement, gehlenite forms as an intermediate clinker product [40]. Gehlenite can be present in significant amounts and is not entirely inert but feebly hydraulic [56], [147]. Similar to calcium aluminate cements, some gehlenite can react and transform into strätlingite in the long term [56], [148]. While gehlenite is generally considered to be almost inert, glass with a gehlenite composition [149] or gehlenite with a very fine particle size [146], exhibit higher reactivity. In calcium aluminate cements, it has been observed that gehlenite, especially at elevated temperatures, may partially react, as it contains more aluminum oxide than the stoichiometric amount [150]. Furthermore, it is suggested that impurities such as sodium or potassium have the potential to enhance the reactivity of gehlenite [151].

Periclase (MgO) is considered a minor phase within cement clinker. In clinker production, limestone is typically used as the primary calcareous raw material [152]. MgO is usually added to the raw meal in a controlled amount in order to enhance its reactivity, thus promoting clinker formation [21], [153], enhancing performance, and reducing the energy required for grinding [154]. It has been observed that magnesia present in cement clinker primarily exist as free MgO, commonly known as periclase. A small portion of magnesia may dissolve in the liquid phase and clinker minerals, however, leading to its amorphous form, which becomes incorporated into the lattice structure. During calcination of the clinker, the MgO content in the liquid phase can reach approximately 5 %, corresponding to 1 %–2 % of the overall clinker composition [40]. When the MgO content in the liquid phase exceeds 5 %, however, the excess amount from the liquid phase crystallizes as periclase [40]. Only about 2 % of MgO in the clinker is capable of dissolving into alite, belite, interstitials, and the glass phase, while any excess MgO crystallizes as periclase [155]. During the hydration of cement, MgO reacts with water to form magnesium hydroxide (MH). The presence of Mg^{2+} is a crucial factor in determining the stability and mechanical properties of the cement's hydration products. According to research conducted by de Weerdt et al. [156] on concretes exposed to seawater, Mg^{2+} ions can form magnesium silicate hydrates (M—S—H) and magnesium aluminate hydrates. In a separate study by Whittaker et al. [157] investigating slag cement pastes exposed to sulfate ions, it was observed that Mg tends to form an independent phase.

The presence of various alkali sulfates can be observed in cement clinker, including arcanite (K_2SO_4), thenardite (Na_2SO_4), aphthitalite ($K_3N\overline{S}_4$) and calcium langbeinite ($KC_2\overline{S}_3$) [158], [159]. When the mass ratio of $SO_3/(K_2O+Na_2O)$ is below 1 and the mass ratio of potassium oxide to sodium oxide exceeds 3, alkali sulfates are likely to occur in the form of arcanite, aphthitalite, and calcium langbeinite. If the mass ratio of potassium oxide to sodium oxide is below 3, the alkali sulfates tend to appear as aphthitalite and thenardite [158]. According to the findings by Kumar and Rao [160], the introduction of arcanite and thenardite leads to a delay in setting time. Samet and Sarkar [161] highlighted that the alkali ions present in alkali sulfates tend to accelerate the setting process, whereas the sulfate ions in alkali sulfates tend to slow it down. Numerous studies have consistently reported that alkali sulfates in Portland cement promote early strength development but result in a decrease in compressive strength after 28 days [162], [163]. A study conducted by Odler and Wonnemann [164], investigating the impact of alkalis as sulfates of sodium and potassium in Portland cement, setting time was reduced in both cases, but it was significantly shortened when potassium sulfates were used. This phenomenon was attributed to the formation of syngenite.

In contrast, the hydration of calcium sulfoaluminate cement has been shown to be slightly delayed, if they contain alkalis at low or moderate concentrations [165]. This slower reaction rate explains the lower mechanical strength at early stages and the subsequent increase in strength at later stages due to a higher degree of reaction of calcium sulfoaluminate cement reaction and the presence of crystalline hydrates.

The presence of arcanite, thenardite, and aphthitalite in Portland cement led to a notable decrease in 28-day compressive strength and an increase in drying shrinkage [159]. They increase the initial heat evolution of cement, particularly of the main peak. The presence of alkali sulfates promotes the formation and growth of C—S—H and portlandite during hydration [159]. When aphthitalite is introduced, early hydration is slowed, but the induction period is shortened. Moreover, the presence of aphthitalite enhances the acceleration period [166]. Furthermore, aphthitalite or calcium langbeinite amplifies both the initial heat release and the subsequent heat release peaks. Early strength is increased, but the 28-day strength is decreased. In the presence of aphthitalite, the formation of ettringite is inhibited during the early stages of cement hydration [167].

Significant research has been conducted to investigate the effect of various minor phases on cement hydration, particularly with respect to Portland cement. There are still, however, notable gaps in understanding how these minor phases influence hydration at different temperatures. In addition, despite the available studies, the knowledge regarding the effects of minor phases, present from introducing different secondary raw materials in cement clinker, on the hydration and strength development of belite-ye'elimite-ferrite cements remains quite limited.

In this study, the physico-mechanical properties and hydration evolution of belite-ye'elimite-ferrite cement containing different secondary raw materials (waste concrete and red mud) were investigated at 5 °C, 20 °C and 60 °C. The composition of the hydration products was studied using X-ray powder diffraction and thermogravimetric analysis. Compressive strength and porosity measured by mercury intrusion porosimetry were determined. The hydration kinetics was studied by isothermal calorimetry. Furthermore, for selected samples nuclear magnetic resonance spectra were obtained and the microstructure was assessed by transmission electron microscopy.

6.2 Materials and Methods

6.2.1 Materials

Three belite-ye'elimite-ferrite cement clinkers having the targeted phase composition of 65 wt. % belite (C_2S), 20 wt. % ye'elimite ($C_4A_3\overline{S}$) and 10 wt. % ferrite (C_4AF) were synthesized for the study. Clinker CNAT was prepared using the following natural raw materials: limestone, flysch, calcined bauxite, white titanogypsum and mill scale. In clinkers CCON and CRMD secondary raw materials were also included, waste concrete and red mud, respectively. The chemical composition of the raw materials, as determined by X-ray fluorescence is given in Table 6.1. The materials were proportioned using a modified Bogue method [23] (Table 6.2).

Table 6.1: Chemical compositions of the raw materials used (wt. %).

	Limestone	Flysch	Calcined bauxite	Titano-gypsum	Mill scale	Calcite	Waste concrete	Red mud
CaO	47.01	25.50	0.28	38.07	0.19	55.39	40.73	10.60

SiO_2	4.64	31.30	4.91	0.21	1.08	0.00	8.99	8.18
Al_2O_3	0.93	7.57	87.91	0.33	0.20	0.17	1.46	25.13
Fe_2O_3	1.78	3.43	1.20	0.15	95.75	0.02	0.61	29.44
MgO	0.90	1.59	0.41	0.13	0.29	0.80	7.14	0.82
K_2O	0.14	1.33	0.38	0.01	0.02	0.01	0.16	0.18
Na_2O	0.81	0.54	0.08	0.26	0.67	0.00	0.27	5.08
TiO_2	0.04	0.38	3.81	0.72	0.01	0.00	0.06	3.56
P_2O_5	0.04	0.08	0.13	0.00	0.06	0.01	0.03	0.18
Cr_2O_3	0.02	0.02	0.06	0.02	0.08	0.00	0.01	0.10
MnO	0.04	0.07	0.01	0.01	0.60	0.00	0.08	0.20
SO_3	0.08	0.14	0.00	36.64	0.01	0.01	0.27	1.60
L.O.I.[1]	41.38	25.50	0.28	21.39	0.00	43.79	38.81	12.96
Total	97.81	97.44	99.46	97.93	98.96	99.96	98.62	98.03

[1]Loss on ignition at 950 °C

Table 6.2: Amount of raw materials used in the raw meal (wt. %).

	Limestone	Flysch	Calcined bauxite	Titano-gypsum	Mill scale	Calcite	Waste concrete	Red mud
CNAT	48.35	42.05	5.30	3.80	0.45	-	-	-
CCON	25.20	35.60	5.50	3.55	0.60	1.00	28.50	-
CRMD	47.10	41.30	4.60	3.50	-	1.00	-	2.45

The detailed synthesis of cement clinkers is described in Chapter 2 (paper by Borštnar et al. [84]). X-ray fluorescence analyses of the clinkers were performed according to EN 196-2 (Table 6.3), while mineralogical compositions were derived from quantitative X-ray powder diffraction (Table 6.4). The final phase composition of the cement clinkers was close to the targeted one. The clinkers were initially ground to a particle size below 0.125 mm using a vibratory disc mill (SIEBTECHNIK Labor Scheibenschwingmühle TS. 250).

Table 6.3: Chemical analyses of the cement clinkers (wt. %).

	CNAT	CCON	CRMD
CaO	54.50	54.19	54.20
SiO_2	22.60	22.36	22.33
Al_2O_3	11.59	11.68	11.31
Fe_2O_3	3.34	3.53	3.80
MgO	1.65	3.95	1.54
K_2O	0.77	0.73	0.72
Na_2O	0.31	0.30	0.47
TiO_2	0.67	0.67	0.76
P_2O_5	0.07	0.07	0.07
Cr_2O_3	0.07	0.07	0.08

MnO	0.07	0.09	0.07
SO_3	2.54	2.42	2.14
L.O.I.[1]	0.20	0.50	2.30
Total	98.38	100.56	99.79

Table 6.4: Phase compositions of the cement clinkers determined by X-ray powder diffraction and Rietveld refinement (wt. %).

	CNAT	CCON	CRMD
β-Dicalcium silicate (belite)	65.7	63.5	64.4
γ-Dicalcium silicate	3.8	3.3	4.2
Ye'elimite orthorhombic	9.1	9.2	8.2
Ye'elimite cubic	7.0	7.7	6.2
∑ Ye'elimite	16.1	16.9	14.4
Ferrite	7.4	8.5	9.3
Mayenite	3.4	2.5	3.8
Gehlenite	0.5	0.5	0.7
Periclase	1.2	3.3	1.1
Arcanite	1.0	0.9	0.5
Aphthitalite	0.9	0.6	1.6

The cement mixtures NAT, CON and RMD were prepared by blending the ground clinkers with the appropriate amount of white titanogypsum in order to achieve a calcium sulfate to ye'elimite molar ratio of 1.5. The cements were then further processed with a ball mill (CAPCO Test Equipment Ball Mill Model 9VS) to achieve Blaine specific surface areas of 4800 ± 100 cm^2/g. The Blaine value for each of the three cement mixtures was 4880 ± 20 cm^2/g. The particle size distributions of the cements were determined using a laser particle analyzer (SYNC Microtrac MRB). The powders were dispersed in isopropanol by ultrasound. The results are given in Figure 6.1.

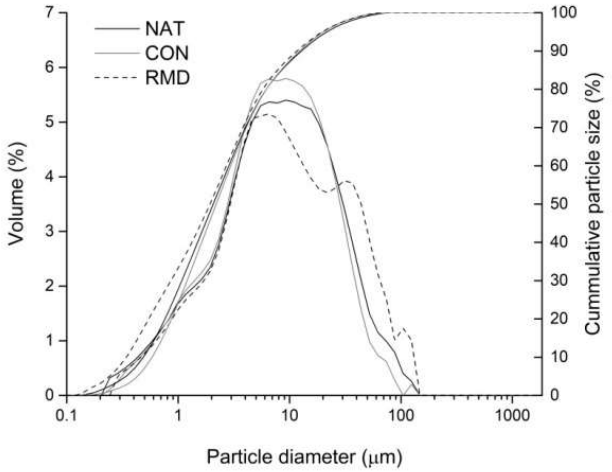

Figure 6.1: Particle size distributions of cements NAT, CON and RMD.

A water-to-cement ratio of 0.5 was used for the hydration experiments. The cement pastes were manually mixed for a duration of 3 minutes using a spatula, then cast into prismatic moulds measuring 10 × 10 × 25 mm. After 24 hours, the specimens were demoulded and cured in sealed plastic containers at temperatures of 5 °C, 20 °C, and 60 °C The hydration of the cement pastes was stopped by solvent exchange using isopropanol and diethyl ether at 1, 7, 28, 90 and 180 days. Following the protocol described by Snellings et al. [91], the crushed samples were immersed in isopropanol for a duration of 15 minutes. They were then filtered using a Büchner funnel and rinsed once with isopropanol and twice with diethyl ether. To remove any remaining solvent, the samples were dried for 8 minutes at a temperature of 40 °C.

6.2.2 Methods

Isothermal conduction calorimetry was conducted at 5 °C, 20 °C and 60 °C using a Thermometric TAM Air (TA instruments). The experimental procedure involved manually mixing 4 g of the prepared cement with 2 g of deionized water, resulting in a water-to-cement ratio of 0.5. Mixing was performed for 3 minutes using a spatula. The mixture was then transferred into a glass ampoule, capped, and placed directly into the calorimeter for testing. It is important to note that the initial heat of hydration within the first 30 minutes could not be determined due to the external mixing method employed.

X-ray powder diffraction analysis of the cement clinkers and cement pastes was performed using a PANalytical Empyrean X-ray diffractometer equipped with CuKα1 radiation. The detector used was an X'Celerator, and the instrument was operated at a voltage of 45 kV and a current of 40 mA. To minimize the effects of the preferred orientation, the samples were back loaded into a circular sample holder with a diameter of 27 mm. The measurements were carried out in a 2θ range of 5-75° with a step size of 0.017 °2θ. The data obtained were subjected to Rietveld refinement using PANalytical X'Pert High Score Plus diffraction software (version 4.9). The crystal structures proposed by Snellings [92] were used, and those provided by Cuesta et al. [46], [93] for the orthorhombic and cubic ye'elimite structures. For the quantification of amorphous content and poorly crystalline phases, the G-factor method [94]–[96] was employed, with corundum (Al_2O_3, NIST SRM 676a) serving as the external standard. The results were

normalized to 100 g of dry binder, incorporating the amount of bound water determined by thermogravimetric analysis.

Thermogravimetric analysis and differential thermal analysis of the cement pastes was conducted using a Netzsch STA 409 instrument. The measurements were conducted under a nitrogen atmosphere, using a heating rate of 10 K/min and covering a temperature range of 30 to 980 °C. Alumina crucibles were used, with approximately 15 mg of sample placed in each crucible. Chemically bound water was calculated from the weight loss up to 550 °C and normalized to 100 g of dry binder [97].

^{29}Si MAS NMR and ^{27}Al MAS NMR spectra were obtained for NAT samples at 90 days of hydration at different curing temperatures. Solid-state MAS (magic angle spinning) NMR spectra were recorded on a Bruker AVANCE NEO 400 MHz NMR spectrometer equipped with 4 mm CP-MAS probe. Larmor frequencies of ^{27}Al and ^{29}Si nuclei were 104.26 MHz and 79.48 Mhz. Sample MAS frequencies were 15 kHz for the measurements. ^{27}Al spectra were recorded using single pulse sequence of $\pi/2$ with a duration of 3.8μs, 4096 scans and a delay between scans of 1s. ^{29}Si spectra were recorded using single pulse sequence of $\pi/2$ with a duration of 3.84μs, 982 scans and a delay between scans of 60 s. The shift axis in all the spectra was referenced using an external reference of adamantane.

Freshly fractured surfaces of selected cement pastes (only NAT mixture) with hydration stopped at 90 days at different curing temperatures and carbon coated, were investigated by transmission electron microscopy to observe the morphology of the crystalline and amorphous phases and to determine their chemical composition at the nanoscale. The analyses were performed on FEG-TEM JEM 2010F (Jeol Ltd., Tokyo, Japan) with 200 KV electron source and equipped with energy dispersive X-ray spectrometer (EDXS; Oxford Instruments ISIS 300). Around 50 points were analyzed per each temperature.

The prepared cement pastes with a water-to-cement ratio of 0.5 were cast in 10 mm x 10 mm x 25 mm moulds and then cured at either 5 °C, 20°C or 60 °C at a relative humidity of 95 ± 2 %. The samples were demoulded after 24 hours. After 1, 7, 28, 90 and 180 days, the compressive strengths of the samples were determined using a ToniNORM, Toni Technic (by Zwick) testing machine. A loading rate of 0.05 kN/s was used, and measurements conducted on three prisms for each age.

The porosity of the cement samples NAT, CON, RMD, cured at different temperatures, were examined at 90 days of hydration using mercury intrusion porosimetry (MIP). Also, porosity depending on the hydration time was examined on NAT cement mixture at 20 °C. After hydration stoppage, small representative pieces of each sample (approximately 4 to 5 pieces, weighting 1g in total) were analysed within the range of 0–414 MPa using penetrometers for solid substrates using a Micromeritics® Autopore IV 9500 equipment (Micromeritics, Norcross, GA, USA). Two measurements were performed for each cement sample.

6.3 Results and Discussion

6.3.1 Isothermal Calorimetry

Figure 6.2 shows the comparison of the heat of hydration between the NAT, CON and RMD cement mixtures at different temperatures, which indicates that the use of different secondary raw materials influences the hydration kinetics. The presence of mayenite could play a significant role in kinetics, while it also strongly depends on the curing temperature. Namely, at a low temperature (5 °C), the hydration of RMD, which

contains the largest amount of mayenite in cement clinker (3.8 wt. %), is the fastest and the induction period is the shortest, while the main peak occurs at around 18 hours. However, on the other side the reaction of CON is the slowest and shows the main peak around 24 hours as it contains the lowest amount of mayenite (2.5 wt. %), suggesting mayenite accelerates hydration [138], [139], [144], [145], especially at low temperatures as shown by Koehler et al. [143]. At 20 °C and 60 °C, the influence of mayenite is not so well pronounced [143], but the reaction of CON is again shifted to a later hydration time (4.1 and 1.9 hours, respectively) compared to NAT and RMD (where the main peaks occurred around 3.8 hours and 1.4 hours at 20 °C and 60 °C, respectively). All three mixtures display a small shoulder before the first maximum peak at 20 °C, which is however the smallest in RMD mixture. This could be explained by the fact that XRD results showed the formation of the lowest amount of ettringite in this mixture at 1 day of hydration, as this peak is usually attributed to the hydration of ye'elimite and consequently the precipitation of ettringite. The maximum peak, which represents the precipitation of monosulfate (and/or ettringite) is greatest in the RMD mixture. At 60 °C, two maximum peaks are observed, where the second peak, which is related to the formation of monosulfate is higher as at higher temperatures more monosulfate forms than ettringite due to higher solubility of ettringite at high temperatures [63], [72], [74]. In addition, kinetics is also controlled by the presence of alkali sulfates as arcanite and aphthitalite are present in cement clinker. Previous studies have shown that alkali sulfates (arcanite, thenardite and aphthitalite) enhance the acceleration period during hydration [159], [166], [167], which is also evident at all the temperatures investigated.

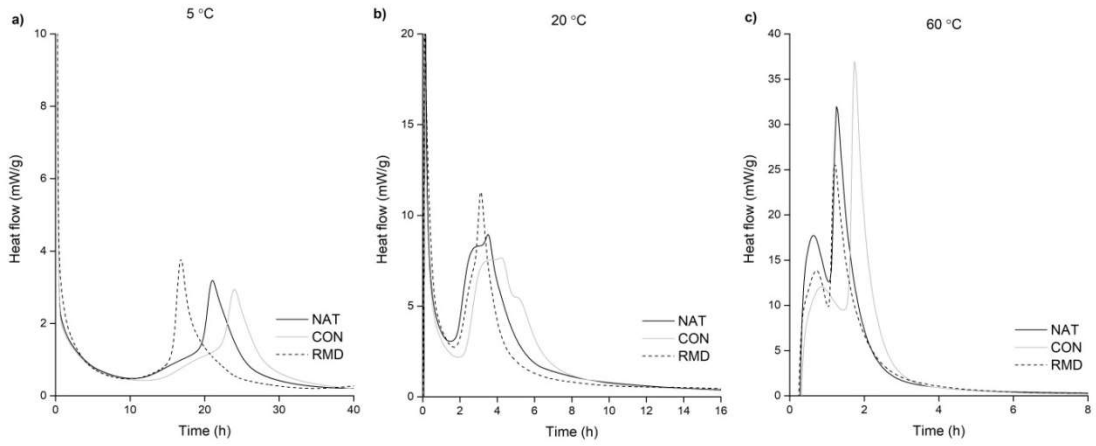

Figure 6.2: Hydration heat flow of the NAT, CON and RMD cements at (a) 5 °C, (b) 20 °C and (c) 60 °C, normalized to the weight of the cement.

The cumulative heat at 7 days of hydration was somewhat similar for all samples at all three temperatures (Table 6.5); it was, however, slightly lower in CON than in NAT and RMD at 5 °C and 60 °C, while at 20 °C it was lowest in RMD. Furthermore, the cumulative heat at 7 days of hydration increased in all mixtures when the temperature was increased from 5 to 20 °C. At 60 °C, however, it decreased, as was also observed in Chapter 5, which investigated cement mixtures with the same targeted phase composition but incorporating different secondary raw material (bottom ash). As reported elsewhere, after a long time the hydration decelerates more quickly at elevated temperatures [105] and lower degrees of hydration are often obtained [65].

Table 6.5: Cumulative heat after 7 days of hydration, normalized to the weight of the cement, in the NAT, CON and RMD cements at 5 °C, 20 °C and 60 °C.

Cumulative heat (J/g)	NAT	CON	RMD
5 °C	194	186	195
20 °C	222	221	212
60 °C	188	182	184

6.3.2 X-ray Powder Diffraction and Thermogravimetric analysis

The hydration process of NAT, CON and RMD cement mixture was investigated at 1, 7, 28, 90 days and 6 months by means of X-ray powder diffraction and thermogravimetry. Figures 6.3 to 6.5 display XRD patterns of the NAT, CON and RMD cements at 5, 20 and 60 °C, respectively. Phase quantifications of the cements at 5 °C, 20 °C and 60 °C at various hydration times are presented in Figures 6.6 to 6.9. Results of the thermogravimetric analysis are shown in Figures 6.10 to 6.12.

The use of different secondary raw materials significantly affects the phase assemblage of hydrated cement, as well as the formation kinetics and also the composition of hydrates that form. Secondary raw materials influence the hydration of belite and ferrite more at 5 °C and less at higher temperatures. This can also be observed in the variations of strätlingite and the amount of amorphous phase (C–S–H) that forms during the hydration of belite. Meanwhile, different secondary raw materials do not impact the hydration of ye'elimite as much as the hydration of belite at all temperatures, as changes in the quantities of ettringite and monosulfate are less pronounced.

The results showed that after 1 day of hydration at 5 °C only traces (< 0.5 wt. %) of ye'elimite and gypsum remained in all three mixtures, due to the formation of a high amount of ettringite and, after the depletion of gypsum, the formation of monosulfate. At 1 day of hydration a higher amount of monosulfate is observed in RMD, suggesting that the early reactions are faster in this mixture due to the higher mayenite content [138], [143]. Conversely, the lowest amount of monosulfate is observed in CON, where the least mayenite is present. At 7 days of hydration, the quantity of ettringite slightly decreases while small amounts of monosulfate precipitate. A lower amount of ettringite is observed in RMD and also lower amounts of monosulfate are present after 7 days of hydration in NAT and CON. During the hydration of ettringite and gypsum aluminium hydroxide is also formed as confirmed by TGA analysis with a weight loss around 250-280 °C [111]. Aluminium hydroxide is then consumed in the hydration reaction of belite to form strätlingite. At 5 °C, strätlingite appears at 7 days of hydration in NAT and CON and later (at 28 days), in lower amounts, in RMD. Verifying the presence of C—S—H (which is formed with the hydration of belite) through XRD is difficult, since it is amorphous, while TGA is also complicated as its primary water loss peak coincides with that of ettringite [110]. Furthermore, at 5 °C, a higher reaction degree of belite (Figure 6.6) and more amorphous content is confirmed in RMD at all hydration times compared to NAT and CON (Figure 6.7), suggesting, in line with previous findings that more C—S—H forms when a higher amount of alkali sulfate is present [159], as RMD contains higher amounts of arcanite and aphthitalite. This also suggests that a higher amount of belite transforms into C—S—H instead of strätlingite, as RMD contains the lowest amount of strätlingite and highest amount of amorphous content compared to NAT and CON. At 5 °C, ferrite starts slowly decreasing already after 1 day and it is almost fully consumed after 90 days of hydration. In RMD, the reaction of ferrite is at the beginning (at 7 days) lower than in NAT and CON. This might be due to the higher content of alkali sulfates

in the RMD, as a higher amount of sulfates delays the hydration of ferrite [55]. No siliceous hydrogarnet is observed at 5 °C, as its formation is promoted by elevated temperatures [72], [112].

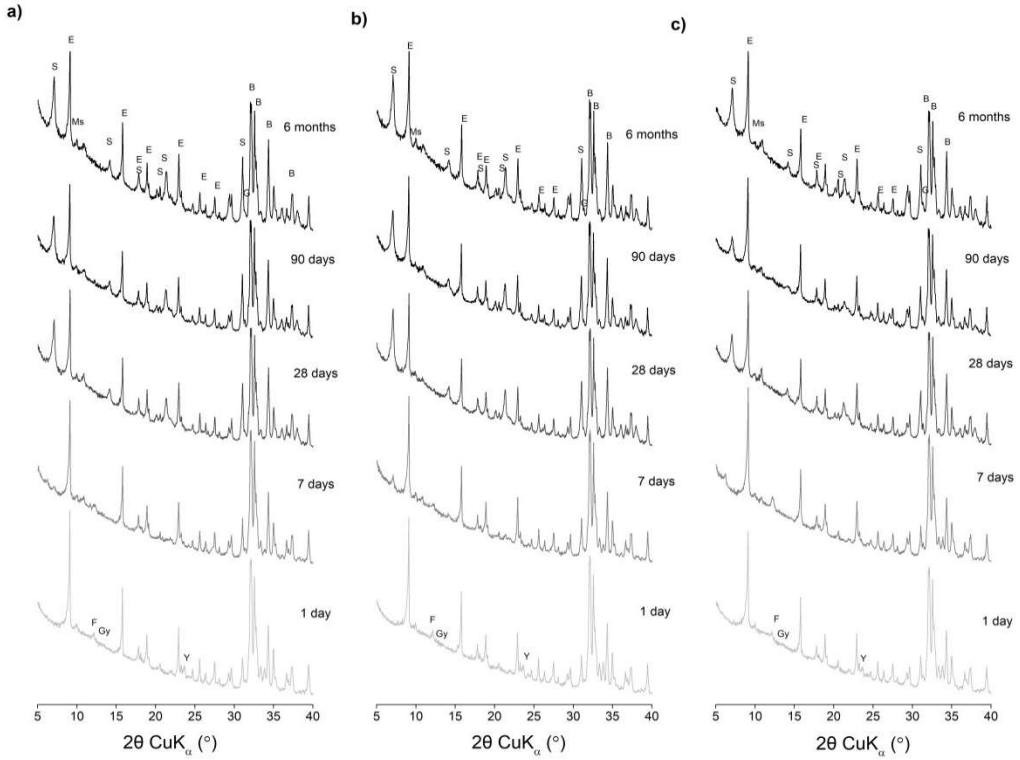

Figure 6.3: X−ray diffraction patterns of (a) NAT, (b) CON and (c) RMD at 5 °C at different curing times. B = belite, E = ettringite, F = ferrite, G = gehlenite, Gy = gypsum, Ms = monosulfate , S = strätlingite, Y = ye'elimite.

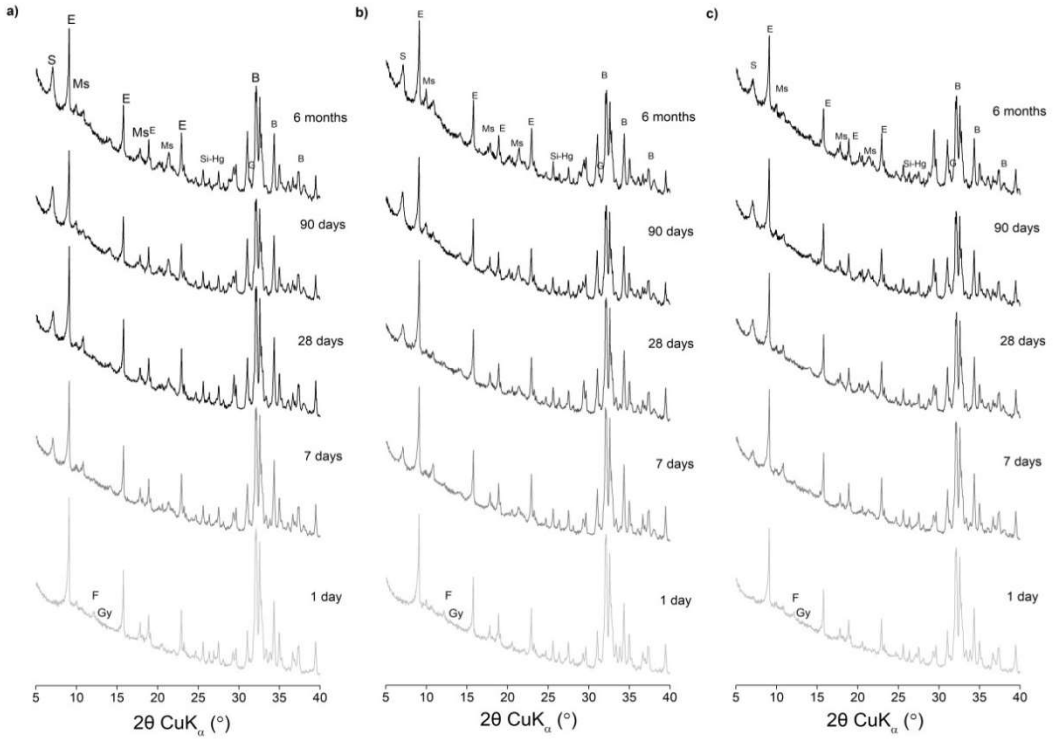

Figure 6.4: X−ray diffraction patterns of (a) NAT, (b) CON and (c) RMD at 20 °C at different curing times. B = belite, E = ettringite, F = ferrite, G = gehlenite, Gy = gypsum, Ms = monosulfate , S = strätlingite, Si-Hg = siliceous hydrogarnet.

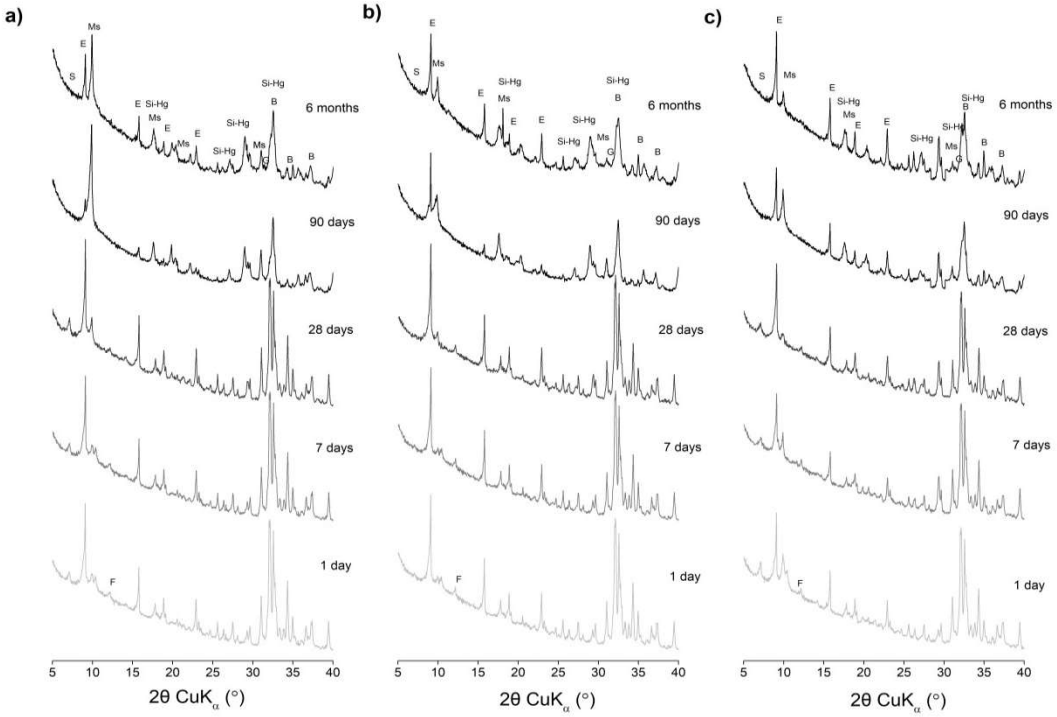

Figure 6.5: X−ray diffraction patterns of (a) NAT, (b) CON and (c) RMD at 60 °C at different curing times. B = belite, E = ettringite, F = ferrite, G = gehlenite, Gy = gypsum, Ms = monosulfate , S = strätlingite, Si-Hg = siliceous hydrogarnet.

At 1 day of hydration at 20 °C ye'elimite is already depleted, while only traces of gypsum are observed. From 7 days up until 90 days of hydration, the quantity of ettringite decreases while the amount of monosulfate continues to rise over time, which is also attributed to the continuous hydration of the ferrite phase. This process leads to the release of additional aluminum ions [162], [164], resulting in the changes observed in the content of ettringite and monosulfate. These findings align with the thermogravimetry (Figures 6.10 to 6.12), as the primary weight loss observed at 120 °C can be attributed to ettringite and that at 280 °C to monosulfate (AFm phases in general) [168], [169]. At an early age (i.e. 1 day) a lower amount of ettringite is observed in RMD, which could be due to the greater content of aphthitalite in this mixture, which, according to Sun et al. [167], inhibits the early formation of ettringite. Again, a higher amount of monosulfate is present in RMD at 1 day compared to in the other mixtures, probably due to accelerated hydration in the presence of more mayenite. Furthermore, after 7 days of hydration lower amounts of monosulfate are observed, in comparison to NAT and CON, with this trend being even more pronounced at 20 °C than it is at 5 °C. At higher temperatures, the amount of ettringite decreases, while the amount of monosulfate increases, due to the higher solubility of ettringite at high temperatures, as previously reported for BYF and Portland cements [63], [72], [74]. These results are also reflected in the hydration kinetics discussed in Chapter 6.3.1. Strätlingite appears at 1 day of hydration at 20 °C, and there are no significant differences in the amount of strätlingite at this temperature when different raw materials are incorporated into the mix. As observed at 5°C, there is a higher degree of reaction in belite and an increase in amorphous content in RMD at 20 °C, probably due to the greater presence of alkali sulfate in that cement mixture. At 20 °C, ferrite is completely consumed after 90 days. At this temperature, the reaction of ferrite is lower in RMD than it is in NAT and CON early on, as was already noted at 5 °C, as a consequence of the higher alkali sulfate content of RMD. Furthermore, the hydration of ferrite and belite leads to the formation of siliceous hydrogarnet. At 20 °C, it precipitated after 90 days in NAT and CON and after 28 days in RMD, where the degree of belite hydration is higher.

At 60 °C, both ye'elimite and gypsum are already depleted at 1 day of hydration. The trend relating to the occurrence of ettringite and monosulfate is similar to that at other temperatures, and, indeed, even more distinct - from 7 to 90 days of hydration, there is a decline in the quantity of ettringite, while the amount of monosulfate steadily increases over time. In RMD, a lower amount of ettringite and a higher amount of monosulfate is observed at 1 day, while lower amounts of monosulfate are observed after 7 days of hydration, in comparison to NAT and CON. As at 20 °C, strätlingite appears at 1 day at 60 °C. While there are no notable differences in the amount of strätlingite between the three cement mixtures, it can be observed that its amount decreases with increasing temperature, as also confirmed in Chapter 5. At 60 °C, the reaction degree of belite is the highest in RMD after 1, 7 and 28 days, leading to the highest amount of amorphous content. At 60 °C, ferrite is completely consumed after 90 days, as was also seen at 20 °C. The amount of ferrite hardly changes over 28 days, then the content suddenly drops to almost zero. Siliceous hydrogarnet is present after 7 days of hydration and at late ages (90d, 6m) is the highest in the CON mixture where a higher degree of belite hydration also occurs. More siliceous hydrogarnet precipitated at 60 °C compared to at 20 °C.

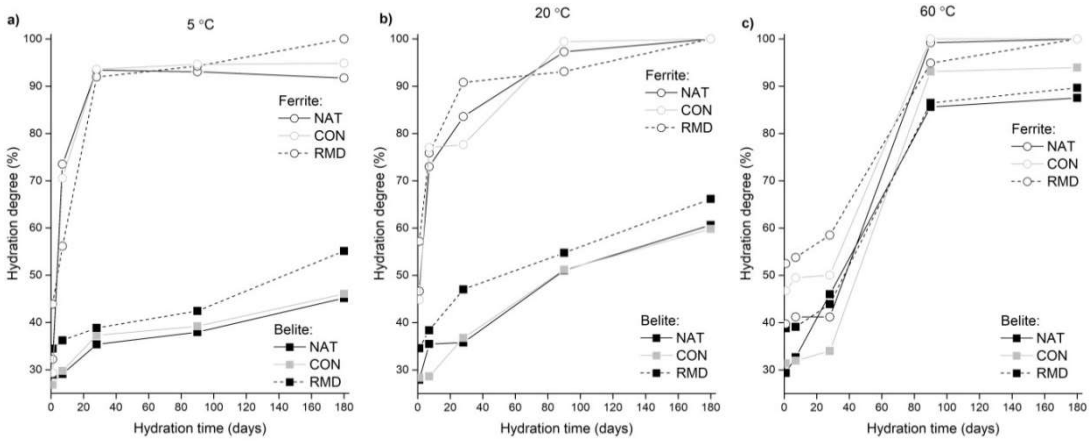

Figure 6.6: Phase contents of β-belite and ferrite in the NAT, CON and RMD mixtures at (a) 5 °C (b) 20 °C and (c) 60 °C, as determined by quantitative X-ray diffraction. Relative errors are estimated to be ±5 %.

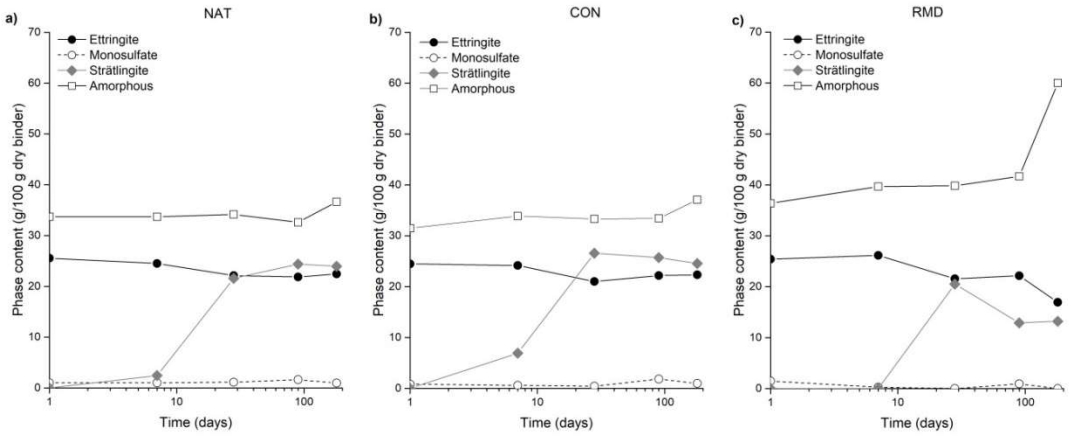

Figure 6.7: Comparison of the amount of hydration products formed in the NAT, CON and RMD cement mixtures at 5 °C, as determined by quantitative X-ray diffraction.

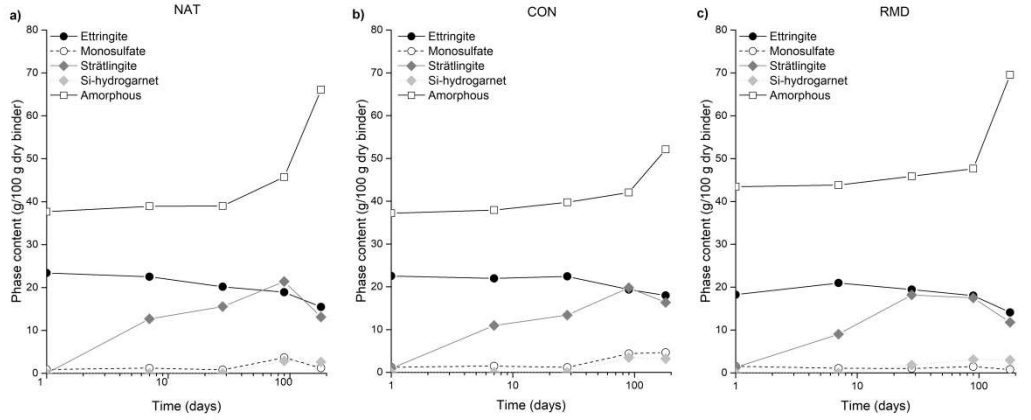

Figure 6.8: Comparison of the amount of hydration products formed in the NAT, CON and RMD cement mixtures at 20 °C, as determined by quantitative X-ray diffraction.

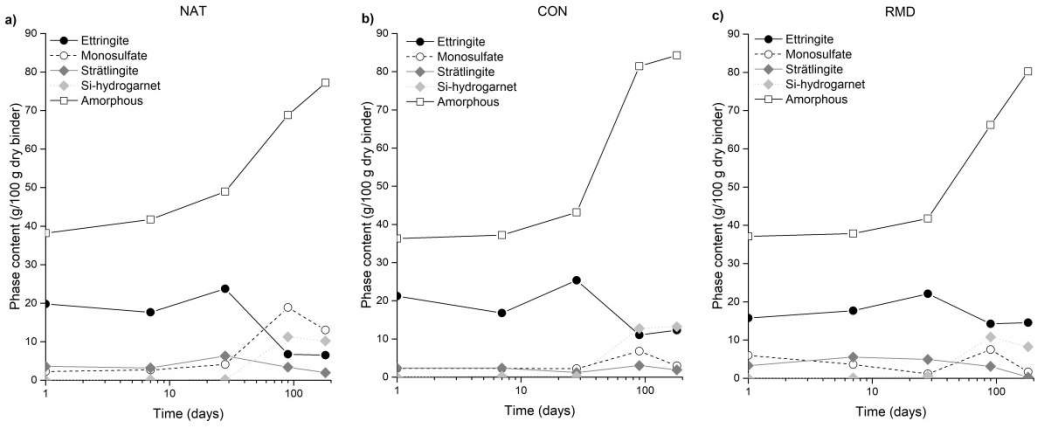

Figure 6.9: Comparison of the amount of hydration products formed in the NAT, CON and RMD cement mixtures at 60 °C, as determined by quantitative X-ray diffraction.

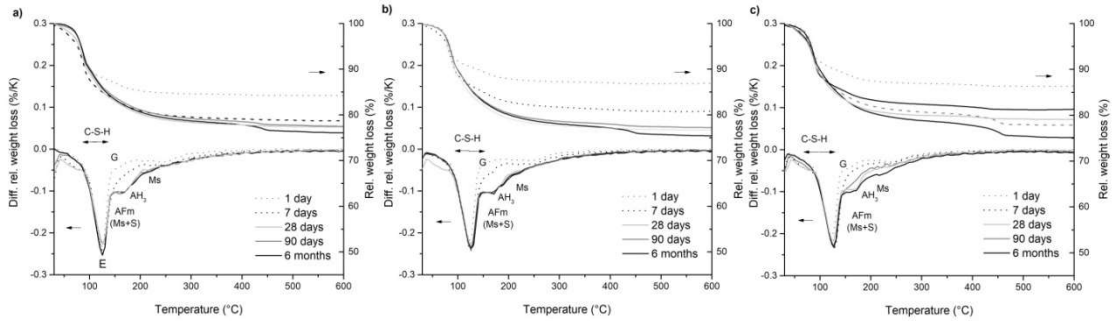

Figure 6.10: Thermogravimetric analyses of the (a) NAT, (b) CON and (c) RMD cement pastes cured at 5°C at different curing times. AH_3 = aluminium hydroxide, C—S—H = calcium silicate hydrate, E = ettringite, G = gypsum, Ms = monosulfate, S = strätlingite.

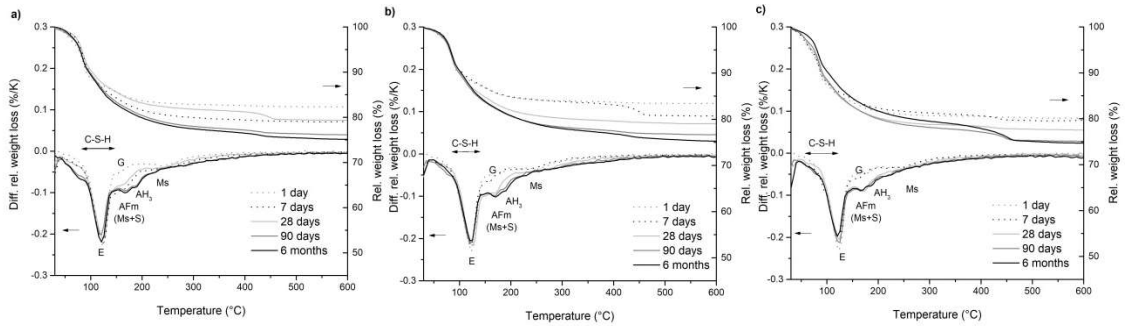

Figure 6.11: Thermogravimetric analyses of the (a) NAT, (b) CON and (c) RMD cement pastes cured at 20°C at different curing times. AH_3 = aluminium hydroxide, C—S—H = calcium silicate hydrate, E = ettringite, G = gypsum, Ms = monosulfate, S = strätlingite.

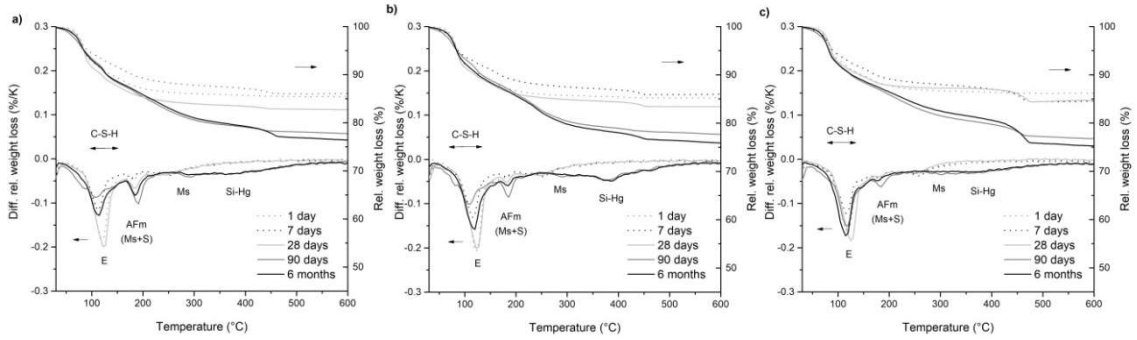

Figure 6.12: Thermogravimetric analyses of the (a) NAT, (b) CON and (c) RMD cement pastes cured at 60°C at different curing times. C—S—H = calcium silicate hydrate, E = ettringite, Ms = monosulfate, S = strätlingite, Si-Hg = siliceous hydrogarnet.

The influence of temperature on the hydration of cements is evident and the results confirm the findings shown in Chapter 5. Namely, the hydration of anhydrous phases is accelerated at elevated temperatures, which is also observed in NAT, CON and RMD. As the temperature increases, ettringite solubility is higher, leading to a lower amount of ettringite as also observed in Chapter 2, favoring monosulfate formation [65], [73]. Strätlingite amount decreases with increased temperatures after 28 of hydration for all samples regardless of secondary raw material. This decrease coincides with the appearance of siliceous hydrogarnet at 20 °C and is even more pronounced at 60 °C, which precipitates from the hydration of ferrite [20]. At higher temperatures, in NAT, CON and RMD, increased amounts of siliceous hydrogarnet form due to a significantly higher degree of hydration of belite, together with higher amounts of C—S—H. Also, high temperatures promote the formation of siliceous hydrogarnet owing to kinetic reasons [72], [112].

6.3.3 Nuclear Magnetic Resonance

To confirm the presence of the phases (e.g. C—S—H or C—(A) —S—H) which could not be absolutely determined by X-ray powder diffraction and thermogravimetric analysis, a NMR was employed for cement mixture NAT at 90 days of hydration. The results are shown in Figure 6.13.

^{27}Al NMR analysis confirmed the presence of ettringite and monosulfate, as chemical shifts were visible at 14.5 ppm and 11.5 ppm, respectively [170]–[172]. The amount of ettringite decreases with higher temperatures, while the amount of monosulfate increases with higher temperatures, which is in accordance with X-ray diffraction and thermogravimetric analysis. Furthermore, a narrow resonance attributed to strätlingite is visible at 62.5 ppm at all temperatures, decreasing with temperature [171].

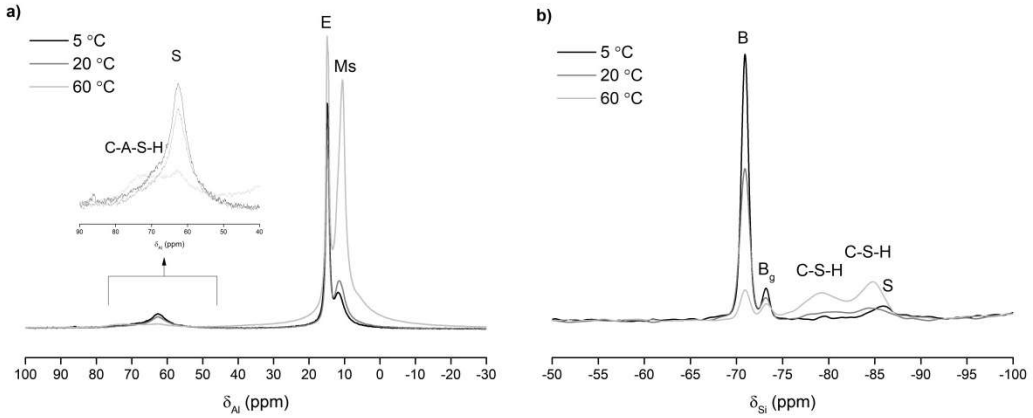

Figure 6.13: (a) ^{27}Al NMR and (b) ^{29}Si NMR analysis of NAT cement mixture after 90 days at different curing temperatures. B = belite, Bg = belite gamma, C—A—S—H = calcium aluminium silicate hydrate, C—S—H = calcium silicate hydrate, E = ettringite, Ms = monosulfate, S = strätlingite.

The presence of C—S—H was confirmed at all temperatures by ^{29}Si NMR analysis (Figure 6.13), where chemical shifts at around -79 ppm and -84 ppm correspond to C—S—H [168]–[170]. These resonances are decreased at a lower temperature, whereas the resonances of belite at around 71 ppm [170] are increased, due to a lower degree of hydration than at higher temperatures. A signal at around 73.5 ppm is associated with the non-reacted γ-C_2S [169]. No C—S—H with incorporated aluminium is observed at 5 °C using ^{27}Al NMR analysis. At 60 °C, the presence of a signal in ^{27}Al NMR at around 75 ppm, associated with C—A—S—H is detected, due to the partial substitution of silicon with aluminium in the bridging sites linking dimers of silicate tetrahedra [173]–[176]. At elevated temperatures, C—S—H exhibits a longer average chain length, a higher uptake of aluminium from the solution to bridging sites of the C—A—S—H phase and a higher Al/Si ratio [169], [174], [177], [178]. When the Al/Si ratio is 0.05 or less, most of the aluminum is incorporated into C—S—H, however, with a higher Al/Si ratio, the formation of stratlingite and/or katoite restricts the Al/Si ratio in C—S—H to approximately 0.15, irrespective of the Ca/Si ratio [179].

6.3.4 Transmission Electron Microscopy

The morphology and chemical composition of the hydration assemblage was investigated, only in the NAT cement mixture, by transmission electron microscopy (Figures 6.14-6.16, Table 6.6) after 90 days of hydration at 5 °C, 20 °C and 60 °C, in order to show differences in the microstructure that occur at various different temperatures.

At 5 °C, the matrix is more homogenous compared to at 20 °C and 60 °C, which is related to slower hydration [113], [177]. At 5 °C and 20 °C the remaining unhydrated belite grains are visible, only a few, however, are observed at 60 °C, as the degree of hydration is higher at elevated temperatures, as confirmed by X-ray powder diffraction. EDXS analysis identified ettringite, monosulfate, strätlingite and C—S—H in the matrix at all temperatures. Siliceous hydrogarnet is also observed, although only at 20 and 60 °C, which is in accordance with the results from the X-ray powder diffraction and thermogravimetric analysis.

Ettringite does not appear as needles or rods as in the previous literature assessed by TEM in OPC and blended OPC pastes [180]–[182] but more as large elongated plates

(Figure 6.14). The size of ettringite grains decreases with increasing temperature, which is in accordance with the results in Chapter 2, where smaller ettringite crystals due to accelerated hydration of ye'elimite are observed at elevated temperatures. The largest amount of ettringite is at 5 and 20 °C, on the other hand, the lowest amount is at 60 °C, which coincides with X-ray powder diffraction results. At 90 °C, metaettringite (dehydrated ettringite) could be formed if cement is cured also in dry conditions, which is X-ray amorphous [73], [183]. According to TEM/EDXS analysis, the composition of ettringite grains is fairly constant at different curing temperatures and it contains small amounts of Fe, Si and K. Ettringite can form a solid solution and substitute aluminium with iron (to form iron-rich ettringite), calcium, sulfate and silicon (also Cd and Cr), while sulfate can be replaced by Se or Cr [61], [184]. Formation of iron-rich ettringite is significantly slower than the formation of Al-ettringite, while according to literature higher temperatures reduce these differences [61]. Small amounts of iron were present in ettringite at all temperatures. In Chapter 3, ettringite shows the ability for higher ion uptake at elevated temperatures as higher d-values of the ettringite peaks were observed.

Monosulfate was observed by transmission electron microscopy only at 60 °C (Figure 6.15) when also according to X-ray powder diffraction a larger amount of monosulfate is formed. Monosulfate grains occur as large irregular plates (Figure 6.16), similar to ones in OPC and blended OPC paste in literature [180], [182], [185], also described as well-developed monosulfate plates [186]. Small amounts of Si and Fe are incorporated in monosulfate. In monosulfate, substitution of different anions such as OH^-, SO_4^{2-}, CO_3^{2-} an Cl^- has been reported, and replacement of aluminium by iron, resulting in formation of Fe-monosulfate [187].

Strätlingite, precipitated in higher amounts at 5 and 20 °C compared to 60 °C is found as grains with elongated morphology and laminar structure(Figure 6.15), while it is found to have plate-like morphology elsewhere [186]. More strätlingite is observed at 5 and 20 °C, compared to 60 °C, confirming the finding obtained from X-ray powder diffraction. It contains up to 3.4 wt. % of Fe, however, the chemical composition of strätlingite does not change significantly with temperature. Iron-rich strätlingite can be formed in cement as aluminium can be partially replaced by iron [188], [189].

Siliceous hydrogarnet occurs in rounded form, which was amorphized during TEM observation, with a uniform diameter of around 100 nm (Figure 6.16). Whereas the grains were not observed at 5 °C [112], the number of siliceous hydrogarnet grains increases with curing temperature with numerous grains of siliceous hydrogarnet at 60 °C. These results are in accordance with X-ray diffraction results in this Chapter and also with results in Chapter 5, where the amount of siliceous hydrogarnet increases with temperature while it is not observed at 5 °C. The phase contains up to 10 wt. % of Fe along with a small amount of Mg and S. The chemical composition of siliceous hydrogarnet varies with temperature. The amount of Fe is much higher at 20 °C (8.8 wt. %) compared to 60 °C (3.2 wt. %), while the amount of Al is slightly lower. In Portland cements, iron and aluminium intermixed siliceous hydrogarnet are usually observed [190]. Hydrogarnet structure can be changed by replacement of all or part of silicon atoms and solid solution between C_3AH_6, C_3FH_6, C_3AS, and C_3FS_3 exist [36], [112] Thermodynamic modelling shown in Chapter 5 indicate that Fe is incorporated in siliceous hydrogarnet, which is a result of partial replacement of aluminium ions by iron,[188] forming iron-rich siliceous hydrogarnet [188].

Various morphologies of C—S—H are observed (Figures 6.14-6.16). At 5 °C it shows a fine fibrillar structure, which is however less prominent at elevated temperatures, where more foil-like C—S—H is observed. At 60 °C it is strongly intermixed with siliceous hydrogarnet. In OPC in mature cement pastes it has coarse fibrillary morphology in larges spaces, while in small spaces it has fine fibrillary [180]. Also a granular appearance

of C—S—H within the shell and acicular and foil-like C—S—H is found in blended OPC cement [180], [185], [185]. In a recent investigation on iron incorporation in C–S–H it was found that at lower Fe amount C–S–H have foil-like morphology [191]. The composition of C–S–H changes with curing temperature, at higher curing temperature it contains more Ca and less Fe, while the fraction of Si remains fairly constant. In addition to the main elements, it also contains Al, S, K, and Ti. Despite the fact that NMR results revealed incorporation of Al in the C–S–H structure at 60 °C, the amount of Al is not higher according to TEM, probably due to intermixing with other phases. Previous studies on C–S–H in OPC at different temperatures also showed a slight increase in S and Al at elevated temperatures [67], [169].

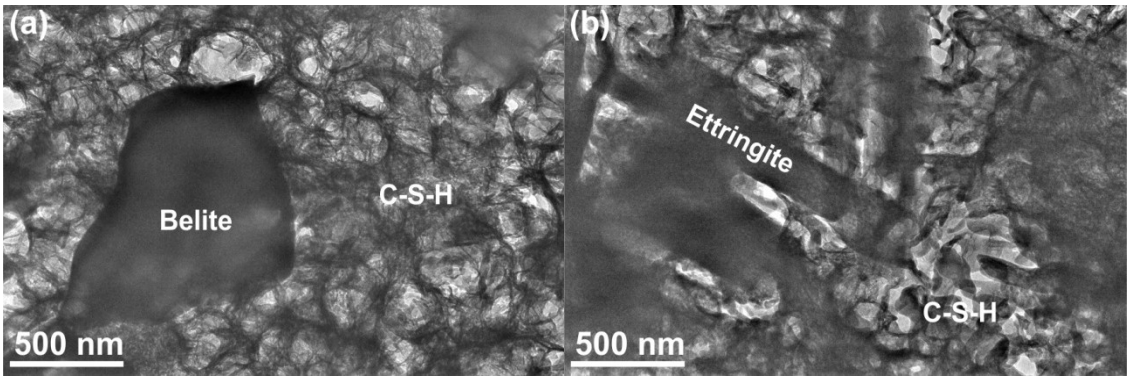

Figure 6.14: TEM micrograph of the NAT cement mixture at 90 days of hydration at 5 °C. (a) A large grain of belite, surrounded by C—S—H. (b) Ettringite showing elongated morphology and fibrilar C—S—H.

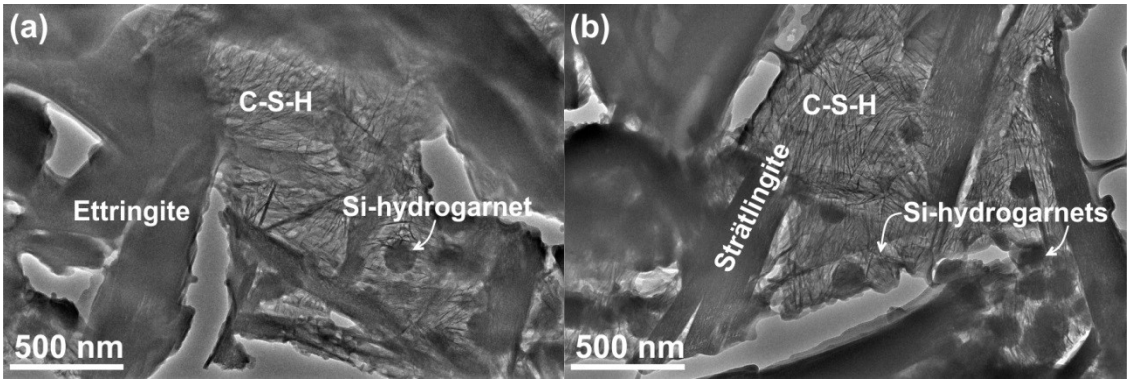

Figure 6.15: TEM micrograph of the NAT cement mixture at 90 days of hydration at 20 °C. Round grains of siliceous hydrogarnet, long rods of strätlingite and large plates of ettringite. C—S—H surround other hydration products.

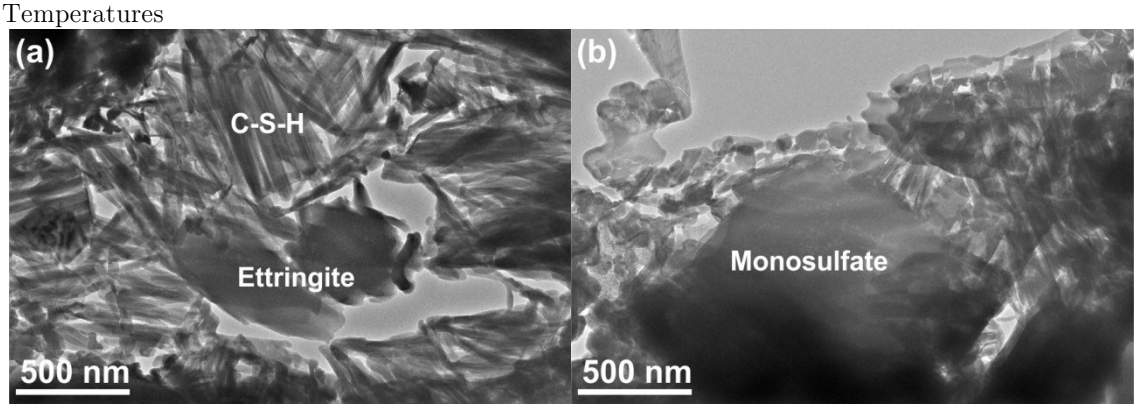

Figure 6.16: TEM micrograph of the NAT cement mixture at 90 days of hydration at 60 °C. Large grains of ettringite and monosulfate. The C—S—H and siliceous hydrogarnet are intermixed.

Table 6.6: Chemical composition of hydration phases as determined by TEM/EDXS. Compositions are calculated to all elements and only cations are considered in the calculations. Hydrogarnet is not observed at 5 °C.

Sample	Phase	Composition, at. %					
		Al K	Si K	S K	K K	Ca K	Fe K
90 days/5 °C Fig. 6.14a,b	Ettringite	16.1	3.7	26.1	1.5	50.5	0.9
	Strätlingite	34.1	17.5	1.1	1.9	41.3	3.6
	Hydrogarnet	n.d.	n.d	n.d	n.d	n.d	n.d
	C—S—H	6.3	30.2	4.6	2.6	50.7	5.4
90 days/20 °C Fig. 6.15a,b	Ettringite	17.8	1.5	26.5	1.4	52.3	0.4
	Strätlingite	32.7	17.7	2.2	1.5	42.3	3.4
	Hydrogarnet	11.3	23.1	2.0	0.9	52.8	8.8
	C—S—H	6.8	31.2	2.8	1.7	55.4	1.3
90 days/60 °C Fig. 6.16a,b	Ettringite	17.3	2.3	25.8	1.0	53.4	0.4
	Monosulfate	22.9	3.7	12.9	b.d	58.8	1.1
	Hydrogarnet	15.2	21.7	3.3	b.d.	54.8	3.2
	C—S—H	3.2	20.9	2.9	1.3	60.7	0.4

6.3.5 Compressive Strength

Figure 6.17 depicts the effect of different secondary raw materials on the development of compressive strength at 5 °C, 20 °C and 60 °C.

At early ages, strength development at all temperatures is similar in all mixtures, while differences after 28 days occur. The fast early strength development is displayed by NAT, CON and RMD cements at all curing temperatures. This is primarily attributed to the quick reaction of ye'elimite and gypsum with water, resulting in the formation of ettringite. The formation of ettringite plays a substantial role in contributing to the early strength of the cements [25], [59], [63], [177]. At 1 day of hydration, the lowest compressive strength is at 5 °C for all cement mixtures, which is due to the small amount of gypsum still present in the cement as shown by X-ray powder diffraction and thermogravimetry. The RMD cement mixture exhibits a slightly higher early strength (at 1 day) at 20 °C and 60 °C as it contains a higher amount of alkali sulfate in cement clinker.

At 20 °C and 60 °C, however, the compressive strength of RMD is lower (as also the amount of ettringite is lower) than in NAT and CON, in line with previous findings [159], [167]. Mayenite could also play a role here, as He and Li [139] found that mayenite cause a strength decrease after 14 and 28 days when increasing mayenite addition in ordinary Portland cement due to hydration of mayenite which produce additional AFm and lowering the AFt/AFm ratio. This effect is not observed at 5 °C, where the values of compressive strength are somewhat similar across all three mixtures.

At 180 days, the RMD mixture again shows slightly higher strength than the other two mixtures, while the CON mixture exhibits the lowest values at 20 and 60 °C. This strength reduction could be due to the higher periclase content in the CON mixture. Mo et al. [192] found that mortars that incorporate MgO exhibit reduced compressive strength due to the higher water consumption caused by the MgO reaction and formation of $Mg(OH)_2$, which lead to expansion, creation of cracks and increased porosity [193]–[195].

Results also show that compressive strength at late ages (i.e. 6 months) for all samples increases when the temperature rises, as the belite hydration is enhanced leading to the precipitation of strätlingite, C—S—H, and siliceous hydrogarnet, which fill more space, as shown in Chapter 5 and elsewhere [106], [115], [116].

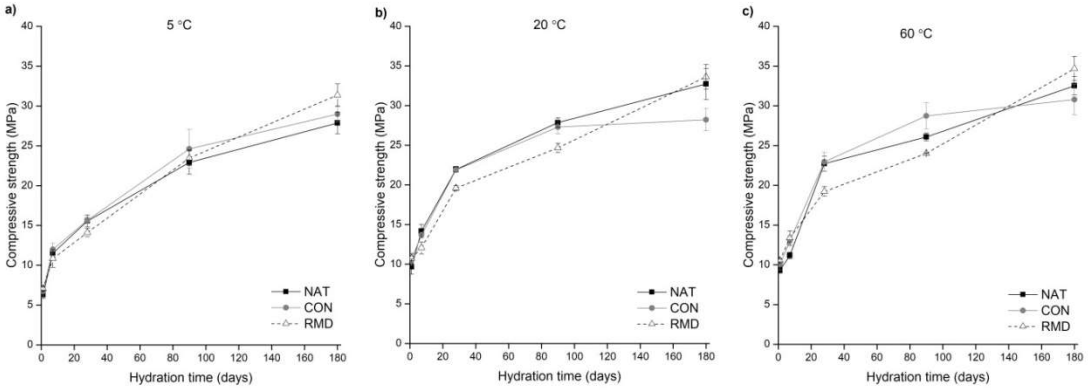

Figure 6.17: The development of compressive strength in the NAT, CON and RMD cements at (a) 5 °C (b) 20 °C and (c) 60 °C.

6.3.6 Hg-porosimetry

The influence of used secondary raw materials on the porosity of NAT, CON and RMD at 90 days of hydration measured by mercury intrusion porosimetry is shown in Figure 6.18. At 5 °C and 60 °C, the main peaks of the NAT, CON and RMD cement pastes are mainly within 0.07 μm, representing a unimodal distribution of the pore sizes, while at 20 °C an intrusion peak is shifted to lower values -around 0.02 μm. At 5 °C, another intrusion peak is observed in RMD at around 0.25 μm, leading to a bimodal distribution and suggesting that larger pores are also present at 90 days of hydration. This could be due to the formation of less monosulfate and strätlingite and more C—S—H that fill smaller pores in RMD compared to NAT and CON at that hydration time, as shown by X-ray powder diffraction. A higher degree of hydration leads to more hydration products which makes the microstructure more heterogeneous [72], [74], [81]. At 20 °C, this second intrusion peak is significantly smaller, while at 60 °C it is not observed at all, as according to X-ray powder diffraction differences in phase composition are smaller.

The median and average pore diameter are higher at 5 °C compared to at 20 °C and 60 °C due to differences in the quantity of hydration products that fill the empty spaces

– less hydrates formed at 5 °C as the degree of hydration is lower. There is no significant correlation observed between the incorporation of various secondary raw materials in cement, which mean different phase composition of cement clinker and consequently different hydrate phase assemblage, considering average and median pore diameters, but in RMD a smaller increase is observed in median pore diameter at both 5 and 20 °C.

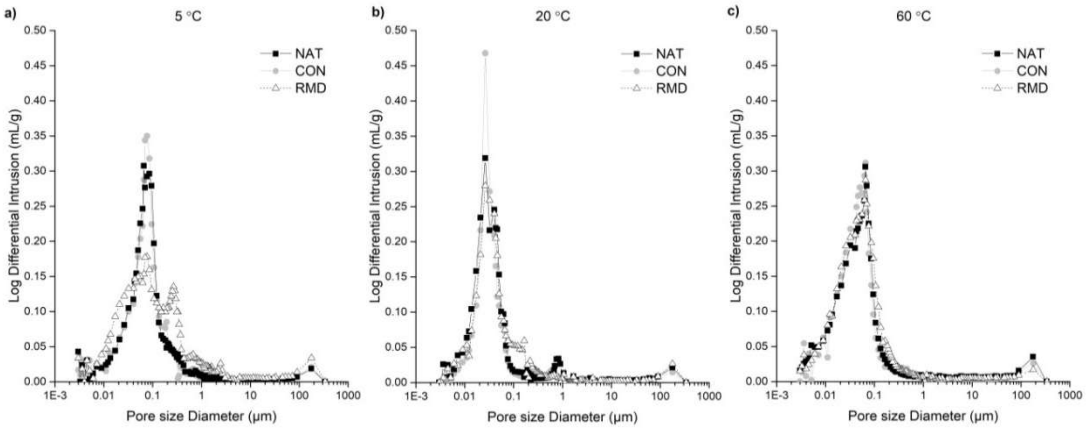

Figure 6.18: Log differential intrusion versus pore size diameter of the NAT, CON and RMD cement samples after 90 days of hydration at (a) 5 °C, (b) 20 °C and (c) 60 °C.

As can be seen from Table 6.7, the porosity at 90 days in RMD is higher than in NAT and CON at 5 and 60 °C. This is attributed to the slightly higher degree of reaction in RMD compared to NAT and CON at 90 days of hydration. It appears that porosity is also controlled by high temperatures, with an increase in porosity at 60 °C in comparison to 5 and 20 °C. The findings align closely with the literature [72], [74], [81], which suggest that a lower temperatures promotes a denser and more uniform matrix due to the slower progress of hydration. There is no significant difference between the porosity at 5 °C and 20 °C. Furthermore, there is no such correlation between different raw materials material incorporated in the cement and temperature in the case of bulk density (which ranges from 1.5 to 1.6 g/mL) and apparent density (which ranges from 2.2 to 2.4 g/mL).

The negative correlation between compressive strength and porosity is evident. Namely, the porosity at 90 days is the lowest at 20 °C, while the compressive strength is the highest at this temperature in NAT, CON and RMD.

Table 6.7: Porosity and pore size distribution at 90 days of hydration measured by mercury intrusion porosimetry.

	NAT	CON	RMD	NAT	CON	RMD	NAT	CON	RMD
Temperature	5 °C			20 °C			60 °C		
Porosity (%)	31.82	31.79	35.50	29.63	27.50	29.02	35.69	34.29	37.29
Median Pore Diameter (µm)	0.078	0.077	0.087	0.032	0.032	0.037	0.051	0.048	0.051
Average Pore Diameter (µm)	0.041	0.041	0.039	0.026	0.030	0.030	0.027	0.029	0.029
Bulk Density (g/mL)	1.57	1.56	1.51	1.58	1.63	1.59	1.50	1.50	1.50

Apparent Density (g/mL)	2.31	2.29	2.34	2.24	2.25	2.24	2.34	2.28	2.39

Figure 6.19 shows changes in the pore size diameter after different hydration times at 20 °C for the NAT cement mixture. It is observed that the (median and average) pore size diameters decrease with hydration time, with intrusion peaks at around 0.3 µm at 1 day of hydration and 0.02 µm at 6 months of hydration, as is also shown in Table 6.8. This is a result of the hydration of anhydrous phases and the precipitation of hydrates which fill the empty spaces [196]. The X-ray powder diffraction results and thermogravimetric analysis showed continuous hydration of ye'elimite and belite and the formation of hydration products. Total pore area, however, increased from 6.7 m^2/g at 1 day to 45.1 m^2/g at 6 months. The values of porosity decreased with curing time [197] and fell from 1 day to 6 months from 39.44 % to 31.51 %. This is inversely connected to the compressive strength measurement results, where the values are strength is increasing with the hydration time. Bulk density shows no apparent relationship with curing time, while apparent density decreases with the hydration time.

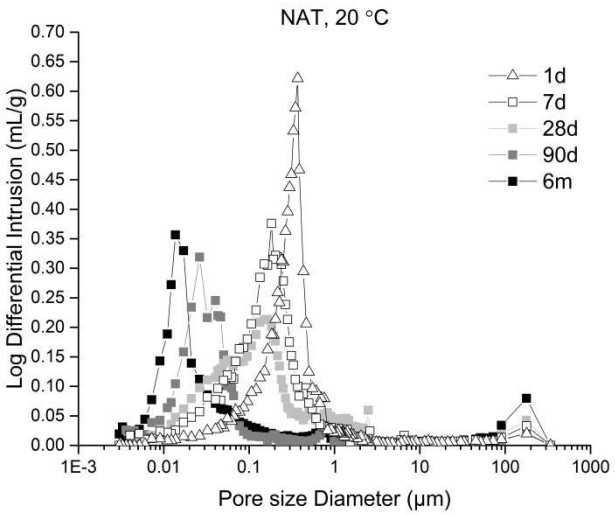

Figure 6.19: Log differential intrusion versus pore size diameter of the cement samples NAT at 20 °C at different hydration times.

Table 6.8: Porosity and pore size distribution at different hydration times for cement mixture NAT at 20 °C measured by mercury intrusion porosimetry.

	1 day	7 days	28 days	90 days	6 months
Porosity (%)	39.44	37.98	36.39	29.63	31.51
Median Pore Diameter (µm)	0.320	0.173	0.138	0.032	0.021
Average Pore Diameter (µm)	0.157	0.078	0.064	0.026	0.021
Bulk Density (g/mL)	1.46	1.41	1.47	1.58	1.49
Apparent Density (g/mL)	2.35	2.33	2.31	2.24	2.28

6.4 Conclusions

The introduction of different raw materials leads to changes in the amounts of minor phases and microstructure that form in the cement clinker, which influence the hydration kinetics and phase formation at low, ambient and elevated temperatures.

Different raw materials influence hydration kinetics, while its influence is heavily reliant on curing temperature. The hydration of cement with incorporated red mud (RMD) and containing the highest amount of mayenite and alkali sulfate, is the fastest in comparison to cement with natural materials (NAT) and waste concrete (CON). Conversely, the mixture with waste concrete has the lowest amount of mayenite and alkali sulfate and therefore exhibits the slowest hydration. This effect is the most pronounced at 5 °C, and is less distinct at 20 °C and 60 °C.

Using various secondary raw materials profoundly impacts the phase composition and phase development of hydrated cement. Secondary raw materials have a more pronounced effect on the hydration of belite and ferrite at 5 °C, mainly due to presence of alkali sulfates, diminishing at higher temperatures. This influence is evident in the fluctuations of strätlingite and the volume of the amorphous phase (C—S—H) forming during belite hydration. However, the secondary raw materials do not affect the hydration of ye'elimite as significantly as they affect belite hydration, evidenced by the subtler variations in ettringite and monosulfate amounts at different temperatures. At all temperatures, the precipitation of ettringite is slightly inhibited in cement with red mud (RMD) due to the presence of a higher amount of aphthitalite, as less ettringite precipitated at early ages compared to cement with natural materials (NAT) and waste concrete (CON), while on the other hand more monosulfate formed due to higher mayenite content which accelerates hydration of ye'elimite. Compared to NAT and CON, a higher belite reaction degree, less strätlingite and increased C—S—H content in RMD are observed especially at 5 and also at 20°C (but in a lesser extent) at all hydration times, suggesting that in the presence of higher alkali sulfate a predominant transformation of belite into C—S—H, rather than strätlingite occurs. At 60 °C, no significant differences in strätlingite amounts were observed among the three cement mixtures. In addition, in RMD at 5 and 20 °C, ferrite reaction is at early ages lower than in NAT and CON, as higher alkali sulfate content in RMD delays ferrite hydration. More siliceous hydrogarnet formed in RMD at 20 °C, as a higher degree of belite hydration occurred.

Ettringite is visible as large, elongated plates in TEM, while monosulfate is shown as large platelets. The size of ettringite grains decreases with increasing temperature. Strätlingite is identified by its distinct elongated shapes and lamellar structure, with Fe incorporated into it. Siliceous hydrogarnet exhibits a distinct rounded form. C—S—H is heavily intermixed with siliceous hydrogarnet at 60 °C. The temperature influences the morphology of C—S—H that changes from fine fibrillar-like to foil-like structure. Temperature influences the chemical composition of hydrates as less Fe is incorporated in hydrogarnet and C—S—H at increased temperatures. Solid state Si and Al NMR analysis revealed the presence of Al in C—A—S—H at increased temperatures, indicating a higher uptake of aluminium from solution to bridging sites of C—A—S—H.

Although high early strength is observed in all mixtures, RMD exhibits slightly higher strength at early ages probably due to the higher alkali sulfate content, which accelerates hydration. At later ages, it shows lower strength probably due to the presence of mayenite that causes a decrease in strength (reducing AFt/AFm ratio). CON mixture has the lowest late age strength due to the presence of periclase, suggesting a strength decrease due to water consumption of MgO, which causes expansion and increased

porosity that lower compressive strength. Porosity at 90 days is changed in RMD mixture compared to NAT and CON, significantly at 5 °C, while the differences are reduced with higher temperature. Another intrusion peak leading to bimodal distribution is observed, attributed to different phase assemblage that formed in RMD (less monosulfate and strätlingite and more C—S—H).

Chapter 7

Rheological Properties of Belite-Ye'elimite-Ferrite Cements at Different Temperatures

This chapter is based on previously unpublished results. The data presented are part of an ongoing study investigating the rheology of belite-ye'elimite-ferrite cements at different temperatures and with different phase compositions.

This chapter addresses the thesis objectives 4 and 6.

7.1 Introduction

The properties of fresh concrete are significantly affected by the rheological behavior of the cement paste they contain. Conventional fresh cementitious materials typically exhibit rheological properties defined by yield stress and viscosity. As highlighted by Roussel et al. [198], the yield stress represents the energy required to disrupt the inter-particle interactions in a cementitious system, due to colloidal and contact interactions between particles. Viscosity is a result of the interplay of hydrodynamic, colloidal, and contact forces acting on moving cement grains [198]. Yield stress is commonly viewed as the key metric for assessing workability and a material's capability to fill a mould without mechanical agitation. Viscosity also appears to be a crucial factor in characterizing the workability of cement or concrete [198], [199]. Depending on the strain rate, shear-thinning or shear-thickening behaviors may be observed in cement pastes [198]. Namely, viscosity increasing with an increasing shear rate is referred to as shear thickening, and viscosity decreasing with an increasing shear rate, is referred to as shear thinning [200]. Cement-based materials in a fresh state are defined as thixotropic materials and non-Newtonian fluids [201]. Thixotropy is typically characterized by an ongoing decrease in viscosity over time when a shear rate is applied, followed by a gradual recovery of viscosity once the shear rate is not applied anymore. A key feature of thixotropy is its reversibility. The reversible effect might be predominant during the initial hour, as the static yield stress of the paste exhibits a linear increase throughout this period [201], [202]. On the other hand, a term that describes structuration (strength/stiffness gain) of cement systems is structural build-up, which refers to the sum of both, reversible and irreversible effects [201], [203]. Recent research has increasingly more attention on this time-dependent rheological parameter, which occurs from the particle interactions and early age cement hydration [204], [205]. Upon mixing cementitious particles with water, the structural development of the material undergoes

three phases: colloidal network percolation, rigid percolation, and rigidification [206]. A fast build-up rate not only supports the weight of subsequent casting layers but also ensures a robust bond between them [207]. Moreover, a rapid structural build-up rate enhances the resistance to segregation and bleeding, improving the interface quality between the aggregate and the cement paste. This has a direct impact on permeability, steel bonding, and the mechanical properties[208].

The rheological properties of cement are heavily influenced by its chemical composition and physical characteristics. Mork et al. [209] observed an increase in yield stress and plastic viscosity in OPC paste with a higher SO_3 content. Dils et al. [210] highlighted that OPC pastes with a high amount of C_3A and low amount of SO_3 amount exhibited high yield value and plastic viscosity. Garcia Mate et al.[211] observed that within the studied range, the gypsum content doesn't significantly impact the viscosity of the pastes. They also studied the rheology of CSA pastes, where pastes without added superplasticizer showed shear thinning behavior and high viscosity, while the use of additives lowered the viscosity. Another study showed that the initial rheological properties of cement pastes in the ternary OPC-CSA-$C\overline{S}$ system are influenced by both the OPC/CSA ratio and the $C\overline{S}$ content[212]. A reduced OPC/CSA ratio increases both yield stress and plastic viscosity. Conversely, a higher percentage of $C\overline{S}$ in the system lowers the dynamic yield stress but elevates the plastic viscosity and shear-thinning intensity [212].

The rheological properties are also affected by different temperatures. A low temperature can delay setting, affecting the rate of hydration reactions and consequently impacting the rheological and fresh properties of mortars and concrete [213]. Temperature greatly affects the colloidal interactions and hydration kinetics, and consequently also the thixotropic development in cement-based materials. Increased temperatures typically, therefore, accelerate the structural development of fresh cementitious substances [206]. An increase in temperature elevates the yield stress and thixotropy of mixtures, while reducing their viscosity [205], [214], [215]. The initial fluidity of the cement paste remains relatively unaffected by variations in temperature, higher temperatures, however may slightly reduce the initial fluidity and cause a more pronounced loss in fluidity as time progresses [216], [217]. Champenois et al. [214] investigated rheological properties of calcium sulfate cement at an ambient temperature, pointing out that the first increase in storage modulus is related to the partial dissolution of gypsum, weak dissolution of ye'elimite and mayenite and the formation of a small amount of ettringite, leading to a slow stiffening of the paste. Before the stiffening, the coagulation of anhydrous cement grains probably occurs, resulting in a modulus increase shortly after mixing [214]. According to the literature, the dissolution of anhydrous phases is faster, producing more hydration products. The rise in ionic concentration and production of fine particles enhances particle attraction [202]. Additionally, higher temperatures increase Brownian motion (i.e. the random motion of particles), leading to a faster flocculation rate in cement suspensions. This growth in early hydration product bridges between cement particles enhances the structural build-up. Hence, elevated temperatures generally accelerate the structural build-up rate of fresh cementitious materials [202].

Although belite-ye'elimite-ferrite cements have been increasingly investigated over recent years, the understanding of their early-age mechanical properties, such as their rheological properties at low, ambient and elevated temperatures, remains somewhat limited. It is therefore crucial to understand the properties of fresh cement pastes and how early hydration and the formation of hydrates impact the rheological behavior of belite-ye'elimite-ferrite cement pastes. The aim of this chapter is to assess the rheological properties – storage modulus G' and viscosity – of belite-ye'elimite-ferrite cements at

different curing temperatures, rheometry geometries (vane probe and serrated plate-plate system), and different phase compositions.

7.2 Influence of Temperature on the Rheological Properties

7.2.1 Materials and Methods

7.2.1.1 Materials

A belite-ye'elimite-ferrite cement clinker NAT was synthesized having a nominal phase composition of 65 wt. % belite, 20 wt. % ye'elimite, and 10 wt. % ferrite. A comprehensive description of the clinker synthesis process can be found in Chapter 2 (paper by Borštnar et al. [82]), while Blaine specific surface, particle size distribution and phase composition measured is shown in Chapter 6. Blaine specific surface areas was 4880 ± 20 cm^2/g. The phase composition is shown in Table 7.1 below. Particle size distributions of the cement is given in Figure 7.1. Preparation of the cement with an M-ratio of 1.5 is described in Chapter 4 (paper by Mrak et al. [89]).

Table 7.1: Phase compositions of the cement clinker NAT, as determined by X-ray powder diffraction and Rietveld refinement (wt. %). Data reproduced from Chapter 6.

	CNAT
β-Dicalcium silicate (belite)	65.7
γ-Dicalcium silicate	3.8
Ye'elimite orthorhombic	9.1
Ye'elimite cubic	7.0
∑ Ye'elimite	16.1
Ferrite	7.4
Mayenite	3.4
Gehlenite	0.5
Periclase	1.2
Arcanite	1.0
Aphthitalite	0.9

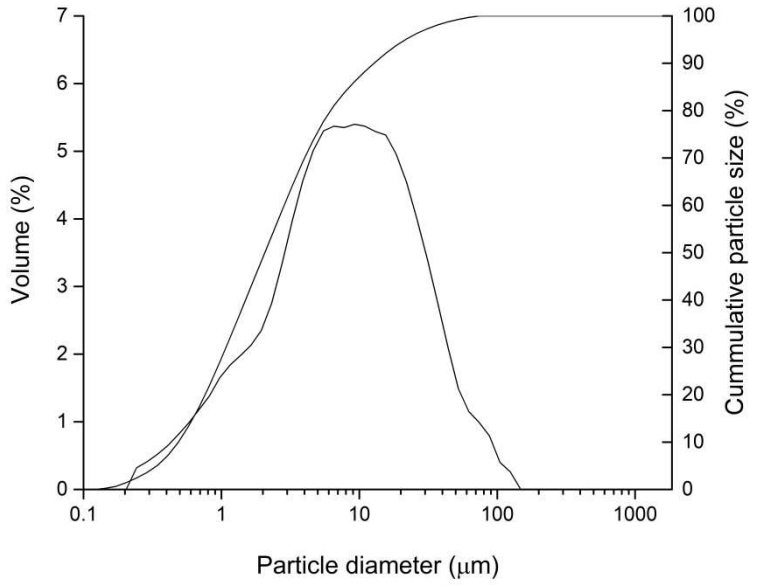

Figure 7.1: Particle size distributions of NAT cement. Data reproduced from Chapter 6.

7.2.1.2 Methods

Rheological characterization included small-amplitude oscillatory shear tests, carried out using an Anton Paar MCR 302 rheometer, equipped with a 4-blade Vane probe, and conducted at a temperature of 5 °C, 20 °C and 60 °C. Cement and water were preheated at defined temperatures, then 40 g of paste was mixed with 20 g of water to achieve water to cement ratio of 0.5 in the temperature controlled-bath at respective temperature. Only one measurement was performed at each temperature. After 3 minutes of mixing by hand, the cement paste was transferred into a cup. Samples were first pre-sheared by logarithmically increasing the shear rate from 0 to 50 s-1 for 30 seconds, then a 60-second recovery period was allowed prior to any measurements being taken. The storage modulus G' and loss modulus G'' were measured at a constant shear strain of 0.003 % and a constant frequency of 1 Hz until slightly before setting, accurately until the halfway point between ending of the induction period and setting time in the calorimetric curve, determined by in-situ isothermal calorimetry (while setting time is usually determined when the calorimetric curve reached half of the average maximum power of the primary hydration peak). Namely, for 15.5 hours, 2.1 hours and 0.5 hour at 5 °C, 20 °C and 60 °C, respectively.

In situ isothermal conduction calorimetry was conducted at 5, 20 and 60 °C using a Thermometric TAM Air instrument (TA instruments). 2 g of cement was placed in the admix glass ampoule and 1 g of deionized water in the admix syringe and placed into the calorimeter. In situ mixing was then performed for 1 minute and after heat flow was monitored for 3 days. 2 replicates were measured for each temperature being investigated.

7.2.2 Results and Discussion

Figure 7.2a depicts the evolution of the storage modulus G' with the time of the cement pastes KN at 5 °C, 20 °C and 60 °C obtained by a small amplitude oscillatory test, which allows us to characterize the structural build-up of cement pastes. Generally, the storage

modulus indicates the strength of the connections, such as C–S–H and/or ettringite, between cement particles [206].

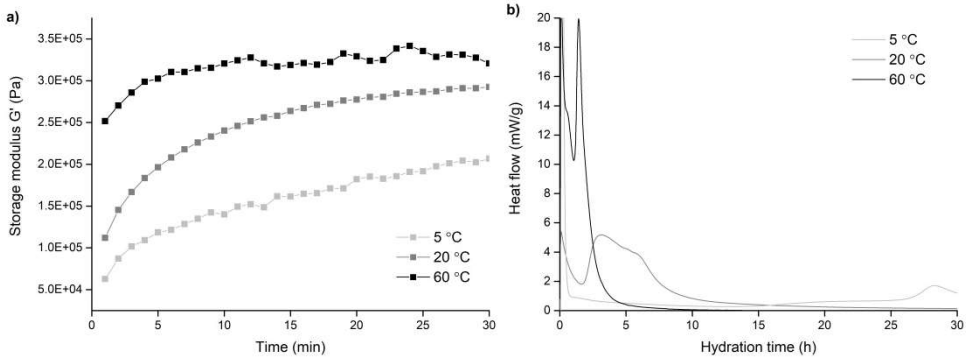

Figure 7.2: a) Storage modulus with time of KN at 5, 20 and 60 °C in the first 30 minutes.b) Hydration heat flow at 5, 20 and 60 °C.

The initial value of the storage modulus increases with temperature, which could be related to the faster kinetics of hydration at increased temperatures. The trend is correlated to in-situ isothermal calorimetry, as depicted in Figure 7.2b, which shows the hydration heat flow of the cement pastes investigated at different curing temperatures. It can be observed that elevated temperatures accelerate hydration, and that the induction period is shifted to earlier times. At all temperatures, the storage modulus sharply increases at the beginning, while during the induction period, i.e. the period, when only a few anhydrous phases are consumed and slow formation of hydrates occurs [48], [74], [102], [103], the storage modulus becomes more steady and just increases slowly (Figure 7.3). At elevated temperatures, however, the increase of the storage modulus G' to the point when it becomes more steady occurs earlier. This point is observed after around 100 minutes at 5 °C, 22 minutes at 20 °C and at 6 minutes at 60 °C, suggesting the structural build-up occurs earlier if the temperature is increased. Results from isothermal calorimetry showed that at 5 °C around 100 minutes, induction period occurs, however, results of rheometry showed increasing storage modulus, which indicate that the structure is still developing during the induction period. When increasing temperature to 20 °C, at 2 minutes the induction period has not started yet, but the first peak which is attributed to wetting of the system already occurred. While at 60 °C at 6 minutes coincide with the first hydration peak. This suggest that the structural build up is already formed before induction period at ambient and elevated temperature, while at lower temperatures it is still forming, which is therefore related to the dissolution of ye'elimite and gypsum which occur in belite-ye'elimite-ferrite cement in the early hours of hydration. In Chapter 6, where the hydration of belite-ye'elimite-ferrite cement pastes was investigated through X-ray powder diffraction it was shown that increased temperatures accelerate early hydration of NAT cement mixture, leading to early dissolution of ye'elimite and formation of ettringite. At 1 day of hydration less ettringite is found at higher temperatures, while the amounts of monosulfate are significantly higher at 60 °C indicating faster hydration of ye'elimite. In addition, the storage modulus increases more slowly at 5 °C, but rises up continuously in a linear fashion. At 60 °C a sharp increase is observed at the beginning, but later it does not change significantly. Huang et al. [218] also reported that the rate of structural build-up of cement pastes

increased more significantly when the temperature increased from 20 °C to 40 °C compared to the increase from 10 °C to 20 °C [218].

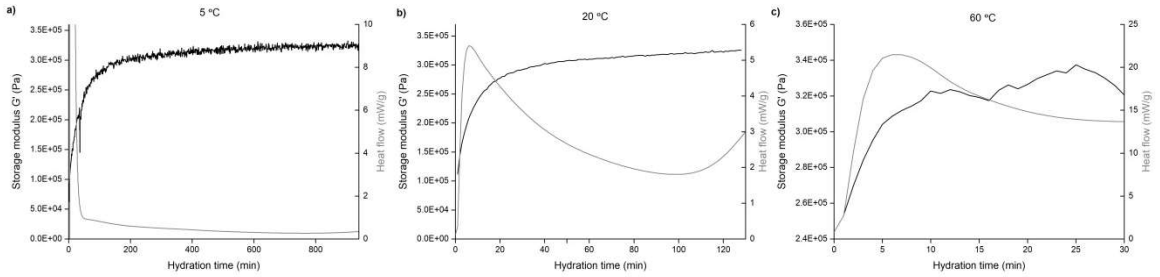

Figure 7.3: Evolution of hydration heat flow and storage modulus G‘ up a)15.5 hours at 5 °C, b) 2.1 hours at 20 °C and c) 0.5 hour at 60 °C.

7.3 Influence of Phase Composition on the Rheological Properties

7.3.1 Materials and Methods

7.3.1.1 Materials

Two belite-ye'elimite-ferrite cement clinkers, namely CBCSA-B and CBCSA-Y, were synthesized. CBCSA-B, was aimed to have a targeted nominal phase composition of 65 wt.% belite, 20 wt.% ye'elimite, and 10 wt.% ferrite. On the other hand, CBCSA-Y was formulated to have a composition of 50 wt.% belite, 35 wt.% ye'elimite, and 10 wt.% ferrite.

A comprehensive description of the clinker synthesis process can be found in Chapter 2 (paper by Borštnar et al. [84]), while their measured Blaine specific surfaces, particle size distribution and phase composition are shown in Chapter 4 [89]. Blaine specific surface areas were 4740 cm2/g for cement clinker CBCSA-B and 4250 cm2/g for CBCSA-Y [89]. Particle size distributions of the cements and gypsum is given in Figure 7.4. The phase compositions are shown in Table 7.2 below. The preparation of cement with M-ratio of 1.5 is described in Chapter 4 (paper by Mrak et al. [89]).

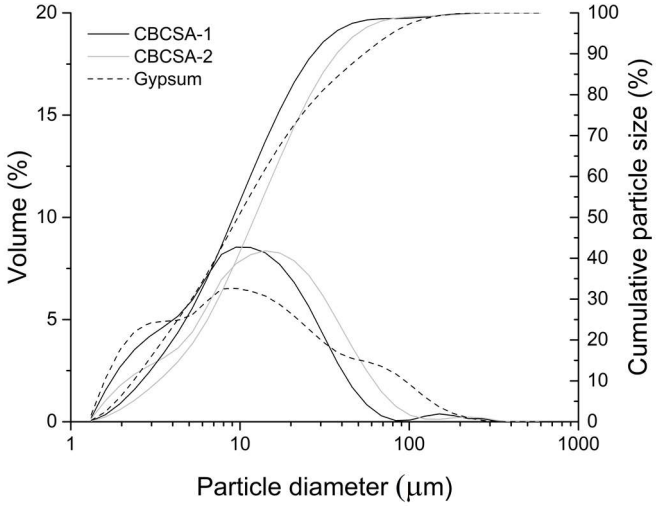

Figure 7.4: Particle size distributions of cement and gypsum NAT, CON and RMD. Data reproduced from [89].

Table 7.2: Phase compositions of cement clinkers determined by X-ray powder diffraction and Rietveld refinement in wt. %. Data reproduced from [89].

	CBCSA-B	CBCSA-Y
β -Dicalcium silicate (belite)	60.6	50.9
γ -Dicalcium silicate	6.9	0.8
Ye'elimite orthorhombic	6.9	17.4
Ye'elimite cubic	9.3	14.9
∑ Ye'elimite	16.2	32.3
Ferrite	11.9	10.4
Mayenite	2.3	3.2
Periclase	1.1	1.0
Gehlenite	0.4	-
Perovskite	-	1.0
Aphthitalite	0.3	0.2
Arcanite	0.3	0.2

7.3.1.2 Methods

For rheological measurements the mixing of cement pastes was conducted utilizing an Ultra Turrax tube dispenser for a duration of 1 minute, employing 10 grams of cement alongside the necessary amount of water in order to achieve a water-to-cement ratio of 0.5. Immediately after mixing, the cement pastes were transferred to the lower plate of the rheometer for further analysis.

The rheological assessments were carried out using an Anton Paar MCR 302 rheometer, equipped with serrated parallel plates, and conducted at a temperature of 20°C. Only one measurement per different phase composition was performed. To establish a well-defined initial dispersed state and ensure reproducibility for each sample, they were first presheared for 30 seconds at a rate of 100 s-1 [198], [202]. This was followed by a 60-second recovery prior to any measurements being taken. The flow curve

was plotted, starting by increasing the shear rate from 0.1 s^{-1} to 100 s^{-1} within 60 s. Before performing the small amplitude oscillatory shear (SAOS) tests, the linear viscoelastic range (LVR) for each paste was determined where the critical value of shear strain was identified. Shear strain from 0.0001 % to 1000 % was applied at a constant frequency of 1 Hz. With the LVR identified (by applying a constant shear strain), changes in the storage modulus G' and loss modulus G'' were measured over a duration of 4 hours at a constant frequency of 1 Hz. This allowed us to determine the time-dependent structural changes within the material. Furthermore, an examination of the viscosity evolution of the cement pastes was conducted, while measuring over 4 hours at a constant shear rate of 100 s^{-1}.

It should be noted that results from the isothermal calorimetry experiments on cement mixtures BCSA-B and BCSA-Y at 20 °C presented in the latter part of this work have been reported previously in [89].

7.3.2 Results and Discussion

Typical rheological flow curves depicting shear stress against shear rate and viscosity against shear rate are shown in Figure 7.5 for both BCSA-B and BCSA-Y. There is an increase in shear stress correlating with a higher shear rate observed, indicating a stiffening behavior of the pastes. A notable characteristic shared by both cement pastes is the shear thinning behavior, as demonstrated by the decline in viscosity with increasing shear rate [198], [212]. Among the two, BCSA-Y exhibits a slightly higher viscosity in comparison to BCSA-B. This difference in viscosity could be consequential to the different phase compositions of the two cement pastes, namely due to the faster kinetics of BCSA-Y mixture as it contains more fast reacting ye'elimite that forms a higher amount of ettringite in the early ages (see results shown in Chapter 5). Similar behavior was reported in the OPC-CSA-C$\overline{S}$ blend, where with increasing CSA content the shear thinning behavior became more intense, due to enhanced the nucleation and growth kinetics of hydrates (particularly ettringite) during the structural build-up, which intensifies particle interactions, making it harder for aggregates to disperse [212].

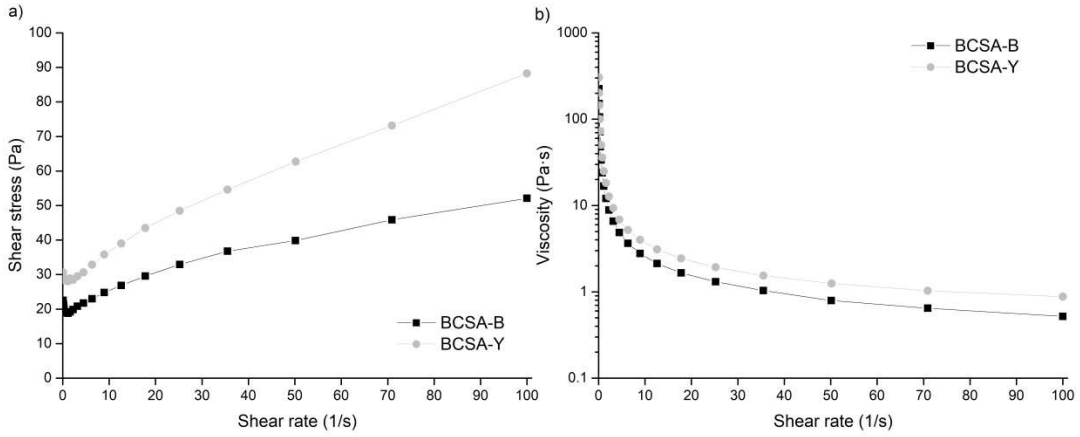

Figure 7.5: Typical rheological flow curves of cement pastes BCSA-B and BCSA-Y: a) shear stress vs. shear rate and b) viscosity vs. shear rate.

Figure 7.6a depicts the critical strain of the cement pastes as determined by the amplitude sweep test, with a value of 0.003% being observed for both BCSA-B and BCSA-Y. This critical strain value marks the limit of the linear viscoelastic regime

(LVR), beyond which the storage modulus begins to decrease. This point is attributed to the strain level at which the initial structure of the paste begins to alter, due to changes in the particle network interactions [198], [219]. Figure 7.6b shows the evolution of the storage modulus G' with time of cement pastes BCSA-B and BCSA-Y. The increase in storage modulus G' is indirectly associated with the structural build-up of the cement paste [201]. The literature outlines two principal mechanisms that contribute to the storage modulus [198], [201]. Firstly, at early ages, the storage modulus is primarily influenced by the colloidal interactions occurring among cement particles. Later, the formation of C—S—H bridges becomes the dominant factor affecting the storage modulus [198], [201]. From the data observed, the storage modulus remained relatively unchanged during the initial 15 minutes after mixing. A slight increase, however, is noted thereafter. A pronounced increase in the storage modulus is distinctly observed after 120 minutes for BCSA-B and after 130 minutes for BCSA-Y. Moreover, the timing of the observed sharp increase in the storage modulus aligns well with the findings from calorimetry depicted in Figures 7.7a and 7.7b, as previously reported in Chapter 5 (paper by Mrak et al. [89]). This time also corresponds with the end of the induction period that is associated with the slow dissolution of clinker phases alongside the slow formation of ettringite and the beginning of the acceleration period related to the hydration reaction of ye'elimite with gypsum and the formation of ettringite and aluminium hydroxide [39], [49]. According to X-ray powder diffraction analysis in Capter 5, more ettringite formed at 1 day of hydration in BCSA-Y compared to BCSA-B. Despite the higher viscosity in BCSA-Y, however, the storage modulus G' is surprisingly lower, indicating that it has a higher resistance to flowing meaning more power is needed to make the sample flow [220] but a weaker gel structure.

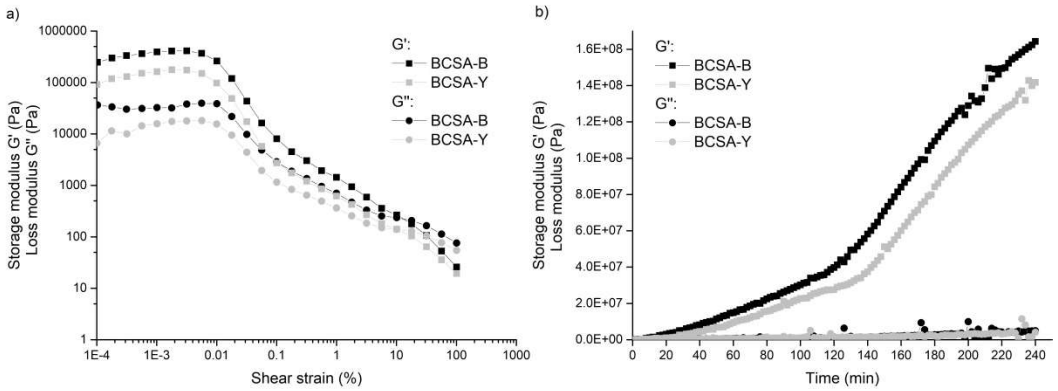

Figure 7.6: a) Critical strain of cement paste defined with SAOS. b) Development of storage G' and loss modulus G'' with time of cement paste BCSA-B and BCSA-Y.

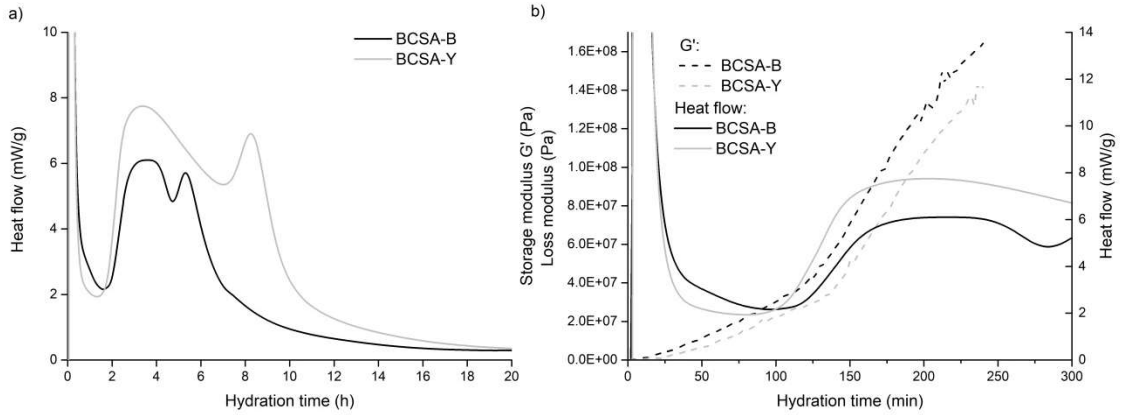

Figure 7.7: a) Hydration heat flow of BCSA-B and BCSA-Y. Data are taken from Chapter 3 (paper by Mrak et al. [89]). b) Comparison of hydration heat flow and storage modulus G‘ with time.

7.4 Conclusions

Curing cement at different temperatures showed variations in the rheological properties of the fresh belite-ye'elimite-ferrite cement pastes. Increasing the curing temperature results in a higher storage modulus due to faster kinetics, and its evolution is faster which could be related to the rapid structural build-up at elevated temperatures. The results agreed with the in-situ isothermal calorimetry, which shows accelerated hydration and shifting induction period to earlier times when the temperature is increased. The structure of the belite-ye'elimite-ferrite cement pastes was forming before the induction period at both ambient and higher temperatures. At lower temperatures, however, structure forms continuously during induction period. This can be attributed to the delayed early dissolution of ye'elimite and gypsum during the initial hydration phase of belite-ye'elimite-ferrite cement at low temperatures.

Differences in the clinker compositions showed variations in the rheological properties of the fresh cement pastes. Both BCSA-B and BCSA-Y cement pastes, exhibited shear thinning behavior. Higher amount ye'elimite slightly increases viscosity. A crucial strain was identified, and the analyzed storage modulus revealed changes in the rheological evolution of the cement pastes, as a result of hydration and formation of hydrates, which align well with the findings from isothermal calorimetry. The increase in storage modulus observed is related to the hydration of ye'elimite with gypsum and the precipitation of ettringite and aluminium hydroxide. Despite a higher viscosity, the system with a greater amount of ye'elimite exhibits a lower storage modulus, suggesting that although it resists flow more, its gel structure is weaker.

The results of rheological measurements showed that temperature and composition of cement clinker influence storage modulus, which was attributed to hydration of ye'elimite and gypsum producing ettringite and aluminium hydroxide. Rising temperature led to higher storage modulus related to accelerated hydration and more ettringite, while more belite in cement clinker also results in higher storage modulus, despite lower amount of formed ettringite, probably due to stronger gel structure that form.

Chapter 8

Conclusions

Elevated temperatures notably accelerate early hydration, especially when increasing temperature from 5 °C to 40 °C, rather than from 40 °C to 60 °C. Fast early hydration of ye'elimite and gypsum at elevated temperatures is observed, leading to a high ettringite amount resulting in enhanced compressive strength at an early age (1 day). The hydration of belite is slower than that of ye'elimite but reaches a high degree of hydration at late ages, which increases with temperature. At early ages, changes in the phase composition are pronounced between 5 °C and 20 °C and 40 and 60 °C, while the composition between 20 °C and 40 °C is more similar. At later ages, however, the composition is more alike between 40 °C and 60 °C, than between 20 °C and 40 °C.
With less belite in the cement clinker, the composition changes gradually as the temperature rises. After 7 days of hydration, less ettringite is present at elevated temperatures, due to its increasing solubility (despite a different M-ratio or phase composition), while more monosulfate is observed. Furthermore, at 20 °C, 40 °C and 60 °C siliceous hydrogarnet forms at the expense of strätlingite, which amount increases with elevated temperature and time. In addition, more C—S—H is found at higher temperature, as more belite reacts, resulting in a higher compressive strength. At 60 °C, C—A—S—H is identified, as at increased temperatures a higher uptake of aluminium from the solution to the C—A—S—H bridging sites prevails.

A dense and homogenous microstructure is observed at 5 °C, whereas at higher temperatures it is more heterogeneous, and phases are intermixed. Ettringite is observed as long prismatic crystals under FE/SEM, while under TEM more like large, elongated plates, and monosulfate as large platelets. Strätlingite has an elongated shape and siliceous hydrogarnet shows a rounded amorphized form. With increasing temperature, the shape of C—S—H turns from flake- to honeycomb-like observed with FE/SEM, while with TEM, finer fibrillary C—S—H is seen at 5 °C, while it is more foil-like at elevated temperatures. Temperature influences the size of ettringite grains, as they become smaller at increased temperatures. While there are no changes in chemical composition with temperature observed for ettringite and strätlingite, iron is found to be promoted with lower temperatures in siliceous hydrogarnet and C—S—H.

At low w/c ratios, however, the insufficient water addition for full hydration of the cement, slows down the late hydration and belite only reacts in lower amounts, as the high water consumption by ye'elimite leaves an insufficient amount for belite to hydrate. In this case, at later ages, cements cured at 60 °C had a lower amount of ettringite, a higher amount of residual gypsum, and lower compressive strength, indicating a decreased degree of hydration at elevated temperatures. This also led to a lower amount of precipitated C—S—H at elevated temperatures.

When more gypsum is added to the cement clinker, hydration is accelerated, and more heat is emitted. Calcium sulfate amount controls the quantity of the ettringite and monosulfate, as the ettringite amount is higher when higher molar ratio of calcium sulfate to ye'elimite is applied and the amount of monosulfate decreased, resulting in differences in early compressive strength as less ettringite yields lower strengths. Furthermore, the amount of pore solution is reduced as the more water-rich ettringite forms, also belite and ferrite dissolution is delayed. More strätlingite is formed at lower molar ratio of calcium sulfate to ye'elimite, because lower amount of ettringite is formed and thus leaving more aluminium for the formation of strätlingite.

The presence of more ye'elimite in the cement clinker resulted in an increased formation of ettringite and strätlingite and a higher compressive strength, while more belite yields more siliceous hydrogarnet and C—S—H and less strätlingite leading to a lower compressive strength (while also a lower degree of belite reaction compared to ye'elimite' contribute).

Different secondary raw materials lead to changes in cement hydration. Cement with red mud exhibited accelerated cement hydration, especially noticeable at low temperatures, as higher amounts of mayenite and alkali sulfates are present compared to cement with natural materials and waste concrete. The impact of secondary raw materials on the hydration processes of belite and ferrite is more noticeable at 5 °C, but much less so at increased temperatures. Such effects can be seen in the changes in strätlingite levels and the quantity of the amorphous phase (C—S—H) during hydration of belite, which are higher at lower temperatures. Its impact on the hydration of ye'elimite is even smaller compared to belite, as only minor changes in the amounts of ettringite and monosulfate across the various temperatures are observed. The early ettringite formation is slightly inhibited in cement with red mud due to more aphthitalite present and more monosulfate occurs due to higher mayenite amount, which accelerates the hydration of ye'elimite. Early hydration of ferrite at all temperatures is delayed in red mud cement, due to the greater presence of alkali sulfate. The presence of alkali sulfate leads to a higher reaction degree of belite, less strätlingite and an increased C—S—H content, indicating that, in the presence of higher alkali sulfate content a predominant transformation of belite into C—S—H, rather than strätlingite occurs. Alkali sulfate presence also leads to higher early compressive strength, while late strength is decreased as more periclase is present.

An increase in temperature results in a higher storage modulus due to faster hydration, with its progression occurring earlier, likely because of rapid structural build-up at elevated temperatures. Cement pastes display a shear-thinning behavior, as viscosity is decreasing. with increasing shear rate. The presence of ye'elimite increases viscosity, yet the storage modulus is reduced, possibly because of its weaker gel structure.

The results of this doctoral dissertation showed that temperature along with other factors such as the amount of calcium sulfate, the phase composition, and the use of secondary raw materials affect the hydration of belite-ye'elimite-ferrite cement. The properties of cement are closely related to the kinetics of hydration of the clinker phases, which is accelerated with increasing temperatures. Curing at temperatures above 5 °C will lead to less ettringite and strätlingite and more monosulfate, C—S—H and siliceous hydrogarnet, the latter only form at ambient and elevated temperatures, leading to higher compressive strength. The amount of calcium sulfate controls the phases that precipitate and affect the physical and mechanical properties of the cement. Namely, more ettringite and less monosulfate and strätlingite form at higher gypsum addition and higher compressive strength is developed. The phase composition of cement clinker has a pronounced impact on both the hydration process and the resulting hydration products. More ye'elimite leads to higher compressive strength, more ettringite and strätlingite, but

less siliceous hydrogarnet and C—S—H. Adding various secondary raw materials to the cement clinker can modify the hydration kinetics and phase assemblage formed, as differences in mayenite, periclase and alkali sulfate content change the kinetics and precipitation of hydrates.

Further research is needed to evaluate fresh properties coherently as the study of early hydration is crucial because this period influences not only the behavior of fresh concrete but also the ultimate mechanical properties and durability of hardened concrete. Comprehensive knowledge about the pore water in cement (such as chemical composition, pH and conductivity) and furthermore rheological and mechanical properties (such as setting time, compressive strength and porosity) of the cement in the first days of hydration is essential for a thorough understanding of the mechanisms and kinetics of cement hydration at an early age and development of the structure of belite-ye'elimite-ferrite cement.

References

[1] K. L. Scrivener, V. M. John, and E. M. Gartner, 'Eco-efficient cements: Potential economically viable solutions for a low-CO2 cement-based materials industry', *Cement and Concrete Research*, vol. 114, pp. 2–26, 2018.

[2] K. Ram, M. Serdar, D. Londono-Zuluaga, and K. Scrivener, 'Does carbon footprint reduction impair mechanical properties and service life of concrete?', *Materials and Structures*, vol. 56, no. 1, p. 6, 2023.

[3] S. A. Miller, V. M. John, S. A. Pacca, and A. Horvath, 'Carbon dioxide reduction potential in the global cement industry by 2050', *Cement and Concrete Research*, vol. 114, pp. 115–124, 2018.

[4] G. Habert *et al.*, 'Environmental impacts and decarbonization strategies in the cement and concrete industries', *Nature Reviews Earth & Environment*, vol. 1, no. 11, pp. 559–573, 2020.

[5] E. Gartner and H. Hirao, 'A review of alternative approaches to the reduction of CO2 emissions associated with the manufacture of the binder phase in concrete', *Cement and Concrete Research*, vol. 78, pp. 126–142, 2015.

[6] N. Muller and J. Harrisch, 'A blueprint for a climate friendly cement industry', 2008.

[7] E. Gartner, 'Industrially interesting approaches to "low-CO2" cements', *Cement and Concrete Research*, vol. 34, no. 9, pp. 1489–1498, 2004.

[8] J. S. Damtoft, J. Lukasik, D. Herfort, D. Sorrentino, and E. M. Gartner, 'Sustainable development and climate change initiatives', *Cement and Concrete Research*, vol. 38, no. 2, pp. 115–127, 2008.

[9] Y. Cancio Díaz *et al.*, 'Limestone calcined clay cement as a low-carbon solution to meet expanding cement demand in emerging economies', *Development Engineering*, vol. 2, pp. 82–91, 2017.

[10] S. Sánchez Berriel *et al.*, 'Assessing the environmental and economic potential of Limestone Calcined Clay Cement in Cuba', *Journal of Cleaner Production*, vol. 124, pp. 361–369, 2016.

[11] K. Scrivener, F. Martirena, S. Bishnoi, and S. Maity, 'Calcined clay limestone cements (LC3)', *Cement and Concrete Research*, vol. 114, pp. 49–56, 2018.

[12] E. Gartner and T. Sui, 'Alternative cement clinkers', *Cement and Concrete Research*, vol. 114, pp. 27–39, 2018.

[13] H. Justnes, 'Alternative Low-CO2 "Green" Clinkering Processes', *Reviews in Mineralogy and Geochemistry*, vol. 74, no. 1, pp. 83–99, 2012.

[14] L. Barcelo, J. Kline, G. Walenta, and E. Gartner, 'Cement and carbon emissions', *Materials and Structures*, vol. 47, no. 6, pp. 1055–1065, 2014.

[15] A. J. M. Cuberos *et al.*, 'Active Iron-Rich Belite Sulfoaluminate Cements: Clinkering and Hydration', *Environmental Science & Technology*, vol. 44, no. 17, pp. 6855–6862, 2010.

[16] K. Quillin, 'Performance of belite–sulfoaluminate cements', *Cement and Concrete Research*, vol. 31, no. 9, pp. 1341–1349, 2001.
[17] I. Odler, 'Special Inorganic Cements', London: CRC Press, 2000.
[18] M. C. Martín-Sedeño *et al.*, 'Aluminum-rich belite sulfoaluminate cements: Clinkering and early age hydration', *Cement and Concrete Research*, vol. 40, no. 3, pp. 359–369, 2010.
[19] Á. G. De la Torre, A. J. M. Cuberos, G. Álvarez-Pinazo, A. Cuesta, and M. A. G. Aranda, '*In situ* powder diffraction study of belite sulfoaluminate clinkering', *Journal of Synchrotron Radiation*, vol. 18, no. 3, pp. 506–514, 2011.
[20] G. Álvarez-Pinazo, I. Santacruz, M. A. G. Aranda, and Á. G. De la Torre, 'Hydration of belite–ye'elimite–ferrite cements with different calcium sulfate sources', *Advances in Cement Research*, vol. 28, no. 8, pp. 529–543, 2016.
[21] G. Q. Liu, Q. X. Yang, L. Jiang, P. Xue, X. L. Zhang, and F. L. Han, 'Sintering characteristics of BCSAF cement clinker with added wastes from production of manganese and magnesium metals', *Advances in Cement Research*, pp. 1–9, 2017.
[22] G. S. Li, G. Walenta, and E. Gartner, 'Formation and hydration of low CO2 cements based on belite, calcium sulfoaluminate and calcium aluminoferrite', in *Proceedings of the 12th ICCC*, Montreal, Canada, 2007.
[23] I. A. Chen and M. C. G. Juenger, 'Synthesis and hydration of calcium sulfoaluminate-belite cements with varied phase compositions', *Journal of Materials Science*, vol. 46, no. 8, pp. 2568–2577, 2011.
[24] P. Arjunan, M. R. Silsbee, and Della M. Roy, 'Sulfoaluminate-belite cement from low-calcium fly ash and sulfur-rich and other industrial by-products', *Cement and Concrete Research*, vol. 29, no. 8, pp. 1305–1311, 1999.
[25] B. Lothenbach, B. Albert, M. Vincent, and G. Ellis, 'Hydration of Belite-Ye'elimite-Ferrite cements: thermodynamic modeling', in *14th International Conference on the Chemistry of Cement*, Beijing, China, 2015, p. 12.
[26] S. Sahu and J. Majling, 'Preparation of sulphoaluminate belite cement from fly ash', *Cement and Concrete Research*, vol. 24, no. 6, pp. 1065–1072, 1994.
[27] G. Artioli and J. W. Bullard, 'Cement hydration: the role of adsorption and crystal growth: Cement hydration', *Crystal Research and Technology*, vol. 48, no. 10, pp. 903–918, 2013.
[28] E. Gartner, 'What are BYF cements, and how do they differ from CSA cements?', p. 9, 2017.
[29] F. Winnefeld and B. Lothenbach, 'Phase equilibria in the system Ca4Al6O12SO4 – Ca2SiO4 – CaSO4 – H2O referring to the hydration of calcium sulfoaluminate cements', *RILEM Technical Letters*, vol. 1, no. 1, pp. 10–16, 2016.
[30] M. García-Maté, A. G. De la Torre, L. León-Reina, E. R. Losilla, M. A. G. Aranda, and I. Santacruz, 'Effect of calcium sulfate source on the hydration of calcium sulfoaluminate eco-cement', *Cement and Concrete Composites*, vol. 55, pp. 53–61, 2015.
[31] F. Bullerjahn, D. Schmitt, and M. Ben Haha, 'Effect of raw mix design and of clinkering process on the formation and mineralogical composition of (ternesite) belite calcium sulphoaluminate ferrite clinker', *Cement and Concrete Research*, vol. 59, pp. 87–95, 2014.
[32] E. Bescher and J. Kim, 'Belitic Calcium Sulfoaluminate Cement: History, Chemistry, Performance, and Use in the United States', in *Proceedings of 1st International Conference on Innovation in Low-Carbon Cement and Concrete Technology*. Garden Grove, CA.

[33] M. C. G. Juenger, F. Winnefeld, J. L. Provis, and J. H. Ideker, 'Advances in alternative cementitious binders', *Cement and Concrete Research*, vol. 41, no. 12, pp. 1232–1243, 2011.
[34] L. Zhang, M. Su, and Y. Wang, 'Development of the use of sulfo- and ferroaluminate cements in China', *Advances in Cement Research*, vol. 11, no. 1, pp. 15–21, 1999.
[35] N. B. Winter, *Understanding Cement: An Introduction to Cement Production, Cement Hydration and Deleterious Processes in Concrete*. Microanalysis Consultants, 2012.
[36] H. F. Taylor, *Cement chemistry*. London: Academic Pr, 1990.
[37] F. P. Glasser and L. Zhang, 'High-performance cement matrices based on calcium sulfoaluminate–belite compositions', *Cement and Concrete Research*, vol. 31, no. 12, pp. 1881–1886, 2001.
[38] J. Majling, S. Sahu, M. Vlna, and D. M. Roy, 'Relationship between raw mixture and mineralogical composition of sulphoaluminate belite clinkers in the system CaO-SiO2-AI203-Fe203.SO3', *Cement and Concrete Research*, vol. 23, no. 6, pp. 1351–1356, 1993.
[39] L. Zhang and F. P. Glasser, 'Hydration of calcium sulfoaluminate cement at less than 24 h', *Advances in Cement Research*, vol. 14, no. 141–155, p. 15, 2002.
[40] P. C. Hewlett, *Lea's Chemistry of Cement and Concrete*. Butterworth-Heinemann, 2004.
[41] K. Morsli, 'Quantitative Phase Analysis of Laboratory-Active Belite Clinkers by Synchrotron Powder Diffraction - Morsli - 2007 - Journal of the American Ceramic Society - Wiley Online Library', Accessed: Sep. 12, 2023. [Online]. Available: https://ceramics.onlinelibrary.wiley.com/doi/10.1111/j.1551-2916.2007.01870.x
[42] G.-C. Lai, T. Nojiri, and K. Nakano, 'Studies of the stability of β-Ca2SiO4 doped by minor ions', *Cement and Concrete Research*, vol. 22, no. 5, pp. 743–754, 1992.
[43] J. Dachtar, 'Calcium sulfoaluminate cement as binder for structural concrete', Faculty of Engineering at the University of Sheffield, Sheffield, 2004.
[44] M. Ben Haha, F. Winnefeld, and A. Pisch, 'Advances in understanding ye'elimite-rich cements', *Cement and Concrete Research*, vol. 123, p. 105778, 2019.
[45] D. Jansen, A. Spies, J. Neubauer, D. Ectors, and F. Goetz-Neunhoeffer, 'Studies on the early hydration of two modifications of ye'elimite with gypsum', *Cem. Conc. Res.*, vol. 91, pp. 106–116, 2017.
[46] A. Cuesta, Á. G. De la Torre, E. R. Losilla, I. Santacruz, and M. A. G. Aranda, 'Pseudocubic Crystal Structure and Phase Transition in Doped Ye'elimite', *Crystal Growth & Design*, vol. 14, no. 10, pp. 5158–5163, 2014.
[47] H. F. McMurdie, 'Studies on a portion of the system: CaO-Al2O3-Fe2O3', *J. RES. NATL. BUR. STAN.*, vol. 18, no. 4, p. 475, 1937.
[48] F. Winnefeld and S. Barlag, 'Calorimetric and thermogravimetric study on the influence of calcium sulfate on the hydration of ye'elimite', *Journal of Thermal Analysis and Calorimetry*, vol. 101, no. 3, pp. 949–957, 2010.
[49] F. Winnefeld and B. Lothenbach, 'Hydration of calcium sulfoaluminate cements — Experimental findings and thermodynamic modelling', *Cement and Concrete Research*, vol. 40, no. 8, pp. 1239–1247, 2010.
[50] G. Jen, S. Skalamprinos, M. Whittaker, I. Galan, M. S. Imbabi, and F. P. Glasser, 'The impact of intrinsic anhydrite in an experimental calcium sulfoaluminate cement from a novel, carbon-minimized production process', *Mater Struct*, vol. 50, no. 2, p. 144, 2017,.

[51] S. Skalamprinos, G. Jen, I. Galan, M. Whittaker, A. Elhoweris, and F. Glasser, 'The synthesis and hydration of ternesite, Ca5(SiO4)2SO4', *Cement and Concrete Research*, vol. 113, pp. 27–40, 2018.

[52] S. Ma, R. Snellings, X. Li, X. Shen, and K. L. Scrivener, 'Alite-ye'elimite cement: Synthesis and mineralogical analysis', *Cement and Concrete Research*, vol. 45, pp. 15–20, 2013.

[53] S. Sahu, J. Havlica, V. Tomkova, and J. Majling, 'Hydration behaviour of sulphoaluminate belite cement in the presence of various calcium sulphates', *Thermochimica Acta*, vol. 175, no. 1, pp. 45–52, 1991.

[54] A. Telesca, M. Marroccoli, M. L. Pace, M. Tomasulo, G. L. Valenti, and P. J. M. Monteiro, 'A hydration study of various calcium sulfoaluminate cements', *Cement and Concrete Composites*, vol. 53, pp. 224–232, 2014.

[55] V. Morin, P. Termkhajornkit, B. Huet, and G. Pham, 'Impact of quantity of anhydrite, water to binder ratio, fineness on kinetics and phase assemblage of belite-ye'elimite-ferrite cement', *Cement and Concrete Research*, vol. 99, pp. 8–17, 2017.

[56] F. Winnefeld, L. H. J. Martin, C. J. Müller, and B. Lothenbach, 'Using gypsum to control hydration kinetics of CSA cements', *Construction and Building Materials*, vol. 155, pp. 154–163, 2017.

[57] D. Gastaldi *et al.*, 'Hydration products in sulfoaluminate cements: Evaluation of amorphous phases by XRD/solid-state NMR', *Cement and Concrete Research*, vol. 90, pp. 162–173, 2016.

[58] M. Zajac, J. Skocek, F. Bullerjahn, and M. Ben Haha, 'Effect of retarders on the early hydration of calcium-sulpho-aluminate (CSA) type cements', *Cement and Concrete Research*, vol. 84, pp. 62–75, 2016.

[59] Y. Jeong, C. W. Hargis, S.-C. Chun, and J. Moon, 'The effect of water and gypsum content on strätlingite formation in calcium sulfoaluminate-belite cement pastes', *Construction and Building Materials*, vol. 166, pp. 712–722, 2018.

[60] M. Zajac, J. Skocek, F. Bullerjahn, B. Lothenbach, K. Scrivener, and M. Ben Haha, 'Early hydration of ye'elimite: Insights from thermodynamic modelling', *Cement and Concrete Research*, vol. 120, pp. 152–163, 2019.

[61] G. Möschner, B. Lothenbach, F. Winnefeld, A. Ulrich, R. Figi, and R. Kretzschmar, 'Solid solution between Al-ettringite and Fe-ettringite (Ca6[Al1−xFex(OH)6]2(SO4)3 · 26H2O)', *Cement and Concrete Research*, vol. 39, no. 6, pp. 482–489, 2009.

[62] B. Dilnesa, E. Wieland, B. Lothenbach, R. Dähn, and K. Scrivener, 'Fe-Containing Phases in Hydrated Cements', *Cement and Concrete Research*, vol. 58, pp. 45–55, 2014.

[63] B. Lothenbach, T. Matschei, G. Möschner, and F. P. Glasser, 'Thermodynamic modelling of the effect of temperature on the hydration and porosity of Portland cement', *Cement and Concrete Research*, vol. 38, no. 1, pp. 1–18, 2008.

[64] X. Zhang, 'Quantitative microstructural characterisation of concrete cured under realistic temperature conditions', EPFL, Lausanne, 2007..

[65] B. Lothenbach, F. Winnefeld, C. Alder, E. Wieland, and P. Lunk, 'Effect of temperature on the pore solution, microstructure and hydration products of Portland cement pastes', *Cement and Concrete Research*, vol. 37, no. 4, pp. 483–491, 2007.

[66] J. I. Escalante-García and J. H. Sharp, 'Effect of temperature on the hydration of the main clinker phases in portland cements: part i, neat cements', *Cement and Concrete Research*, vol. 28, no. 9, pp. 1245–1257, 1998.

[67] E. Gallucci, X. Zhang, and K. L. Scrivener, 'Effect of temperature on the microstructure of calcium silicate hydrate (C-S-H)', *Cement and Concrete Research*, vol. 53, pp. 185–195, 2013.

[68] J. I. Escalante-Garcia and J. H. Sharp, 'The effect of temperature on the early hydration of Portland cement and blended cements', *Advances in Cement Research*, vol. 12, no. 3, pp. 121–130, 2000.

[69] F. Deschner, B. Lothenbach, F. Winnefeld, and J. Neubauer, 'Effect of temperature on the hydration of Portland cement blended with siliceous fly ash', *Cement and Concrete Research*, vol. 52, pp. 169–181, 2013.

[70] K. O. Kjellsen, R. J. Detwiler, and O. E. Gjørv, 'Development of microstructures in plain cement pastes hydrated at different temperatures', *Cement and Concrete Research*, vol. 21, no. 1, pp. 179–189, 1991.

[71] I. Elkhadiri and F. Puertas, 'The effect of curing temperature on sulphate-resistant cement hydration and strength', *Construction and Building Materials*, vol. 22, no. 7, pp. 1331–1341, 2008.

[72] P. Wang, N. Li, and L. Xu, 'Hydration evolution and compressive strength of calcium sulphoaluminate cement constantly cured over the temperature range of 0 to 80°C', *Cem. Conc. Res.*, vol. 100, pp. 203–213, 2017.

[73] J. Kaufmann, F. Winnefeld, and B. Lothenbach, 'Stability of ettringite in CSA cement at elevated temperatures', *Advances in Cement Research*, vol. 28, no. 4, pp. 251–261, 2016.

[74] L. Xu, S. Liu, N. Li, Y. Peng, K. Wu, and P. Wang, 'Retardation effect of elevated temperature on the setting of calcium sulfoaluminate cement clinker', *Construction and Building Materials*, vol. 178, pp. 112–119, 2018.

[75] I. Elkhadiri, M. Palacios, and F. Puertas, 'Effect of curing temperature on cement hydration', *Ceramics Silikaty*, vol. 53, no. 2, pp. 65–75, 2009.

[76] W. Ma, D. Sample, I. R. Martin, and P. W. Brown, 'Calorimetric Study of Cement Blends Containing Fly Ash, Silica Fume, and Slag at Elevated Temperatures', *Cement, Concrete, and Aggregates*, vol. 16, no. 2, p. 7, 1994.

[77] R. B. Perkins and C. D. Palmer, 'Solubility of ettringite (Ca6[Al(OH)6]2(SO4)3 · 26H2O) at 5–75°C', *Geochimica et Cosmochimica Acta*, vol. 63, no. 13, pp. 1969–1980, 1999.

[78] B. Lothenbach *et al.*, 'Cemdata18: A chemical thermodynamic database for hydrated Portland cements and alkali-activated materials', *Cement and Concrete Research*, vol. 115, pp. 472–506, 2019.

[79] F. Avet and K. Scrivener, 'Effect of temperature on the water content of C-A-S-H in plain Portland and blended cements', *Cement and Concrete Research*, vol. 136, p. 106124, 2020.

[80] A. Bentur, R. L. Berger, J. H. Kung, N. B. Milestone, and J. F. Young, 'Structural Properties of Calcium Silicate Pastes: II, Effect of Curing Temperature', *Journal of the American Ceramic Society*, vol. 62, no. 7–8, pp. 362–366, 1979.

[81] L. Li, R. Wang, and S. Zhang, 'Effect of curing temperature and relative humidity on the hydrates and porosity of calcium sulfoaluminate cement', *Construction and Building Materials*, vol. 213, pp. 627–636, 2019.

[82] Y. Jeong, C. W. Hargis, H. Kang, S.-C. Chun, and J. Moon, 'The Effect of Elevated Curing Temperatures on High Ye'elimite Calcium Sulfoaluminate Cement Mortars', *Materials*, vol. 12, no. 7, p. 1072, 2019.

[83] N. Chitvoranund, B. Lothenbach, D. Londono-Zuluaga, F. Winnefeld, and K. Scrivener, 'Influence of temperature on phase assemblages of belite-ye'elimite cement', *Cement and Concrete Research*, vol. 174, p. 107339, 2023.

[84] M. Borštnar, N. Daneu, and S. Dolenec, 'Phase development and hydration kinetics of belite-calcium sulfoaluminate cements at different curing temperatures', *Ceramics International*, vol. 46, no. 18, pp. 29421–29428, 2020.

[85] M. Borštnar, C. L. Lengauer, and S. Dolenec, 'Quantitative in Situ X-ray Diffraction Analysis of Early Hydration of Belite-Calcium Sulfoaluminate Cement at Various Defined Temperatures', *Minerals*, vol. 11, no. 3, p. 297, 2021.

[86] G. Álvarez-Pinazo *et al.*, 'In-situ early-age hydration study of sulfobelite cements by synchrotron powder diffraction', *Cement and Concrete Research*, vol. 56, pp. 12–19, 2014.

[87] M. Merlini, G. Artioli, C. Meneghini, T. Cerulli, A. Bravo, and F. Cella, 'The early hydration and the set of Portland cements: *In situ* X-ray powder diffraction studies', *Powder Diffraction*, vol. 22, no. 3, pp. 201–208, 2007.

[88] C. Hesse, F. Goetz-Neunhoeffer, and J. Neubauer, 'A new approach in quantitative in-situ XRD of cement pastes: Correlation of heat flow curves with early hydration reactions', *Cement and Concrete Research*, vol. 41, no. 1, pp. 123–128, 2011.

[89] M. Mrak, F. Winnefeld, B. Lothenbach, and S. Dolenec, 'The influence of calcium sulfate content on the hydration of belite-calcium sulfoaluminate cements with different clinker phase compositions', *Materials and Structures*, vol. 54, no. 6, p. 212, 2021.

[90] J. I. Escalante-García and J. H. Sharp, 'The microstructure and mechanical properties of blended cements hydrated at various temperatures', *Cement and Concrete Research*, vol. 31, no. 5, pp. 695–702, 2001.

[91] R. Snellings *et al.*, 'Report of TC 238-SCM: hydration stoppage methods for phase assemblage studies of blended cements—results of a round robin test', *Materials and Structures*, vol. 51, no. 4, p. 111, 2018.

[92] R. Snellings, 'X-ray powder diffraction applied to cement', in *A Practical Guide to Microstructural Analysis of Cementitious Materials*, First., CRC Press, 2016, pp. 126–195.

[93] A. Cuesta *et al.*, 'Structure, Atomistic Simulations, and Phase Transition of Stoichiometric Yeelimite', *Chemistry of Materials*, vol. 25, no. 9, pp. 1680–1687, 2013.

[94] D. Jansen, Ch. Stabler, F. Goetz-Neunhoeffer, S. Dittrich, and J. Neubauer, 'Does Ordinary Portland Cement contain amorphous phase? A quantitative study using an external standard method', *Powder Diffraction*, vol. 26, no. 1, pp. 31–38, 2011.

[95] D. Jansen, F. Goetz-Neunhoeffer, C. Stabler, and J. Neubauer, 'A remastered external standard method applied to the quantification of early OPC hydration', *Cement and Concrete Research*, vol. 41, no. 6, pp. 602–608, 2011.

[96] B. H. O'Connor and M. D. Raven, 'Application of the Rietveld Refinement Procedure in Assaying Powdered Mixtures', *Powder Diffraction*, vol. 3, no. 1, pp. 2–6, 1988.

[97] B. Lothenbach, P. Durdzinski, and K. De Weerdt, 'Thermogravimetric analysis', in *A Practical Guide to Microstructural Analysis of Cementitious Materials*, First., CRC Press, 2016.

[98] D. A. Kulik *et al.*, 'GEM-Selektor geochemical modeling package: Revised algorithm and GEMS3K numerical kernel for coupled simulation codes', *Computational Geosciences*, vol. 17, no. 1, pp. 1–24, 2013.

[99] D. A. Kulik, 'Improving the structural consistency of C-S-H solid solution thermodynamic models', *Cement and Concrete Research*, vol. 41, no. 5, pp. 477–495, 2011.

[100] D. A. Kulik, F. Winnefeld, A. Kulik, G. D. Miron, and B. Lothenbach, 'CemGEMS – an easy-to-use web application for thermodynamic modeling of cementitious materials', *RILEM Technical Letters*, vol. 6, pp. 36–52, 2021.

[101] N. Chitvoranund, F. Winnefeld, C. W. Hargis, S. Sinthupinyo, and B. Lothenbach, 'Synthesis and hydration of alite-calcium sulfoaluminate cement', *Advances in Cement Research*, vol. 29, no. 3, pp. 101–111, 2017..

[102] A. Rungchet, C. S. Poon, P. Chindaprasirt, and K. Pimraksa, 'Synthesis of low-temperature calcium sulfoaluminate-belite cements from industrial wastes and their hydration: Comparative studies between lignite fly ash and bottom ash', *Cement and Concrete Composites*, vol. 83, pp. 10–19, 2017.

[103] Y. Shen, X. Li, X. Chen, W. Zhang, and D. Yang, 'Synthesis and calorimetric study of hydration behavior of sulfate-rich belite sulfoaluminate cements with different phase compositions', *Journal of Thermal Analysis and Calorimetry*, vol. 133, no. 3, pp. 1281–1289, 2018.

[104] L. Pelletier-Chaignat, F. Winnefeld, B. Lothenbach, and C. J. Müller, 'Beneficial use of limestone filler with calcium sulphoaluminate cement', *Construction and Building Materials*, vol. 26, no. 1, pp. 619–627, 2012.

[105] N. Chitvoranund, 'Stability of hydrate assemblages and properties of cementitious systems with higher alumina content', EPFL, Laussane, 2021.

[106] S. Shirani, A. Cuesta, A. Morales-Cantero, A. G. De la Torre, M. P. Olbinado, and M. A. G. Aranda, 'Influence of curing temperature on belite cement hydration: A comparative study with Portland cement', *Cement and Concrete Research*, vol. 147, p. 106499, 2021.

[107] N. Li, L. Xu, R. Wang, L. Li, and P. Wang, 'Experimental study of calcium sulfoaluminate cement-based self-leveling compound exposed to various temperatures and moisture conditions: Hydration mechanism and mortar properties', *Cement and Concrete Research*, vol. 108, pp. 103–115, 2018.

[108] I. A. Chen and M. C. G. Juenger, 'Incorporation of coal combustion residuals into calcium sulfoaluminate-belite cement clinkers', *Cement and Concrete Composites*, vol. 34, no. 8, pp. 893–902, 2012.

[109] S. Berger, C. C. D. Coumes, P. Le Bescop, and D. Damidot, 'Influence of a thermal cycle at early age on the hydration of calcium sulphoaluminate cements with variable gypsum contents', *Cement and Concrete Research*, vol. 41, no. 2, pp. 149–160, 2011.

[110] M. Zajac, J. Skocek, C. Stabler, F. Bullerjahn, and M. Ben Haha, 'Hydration and performance evolution of belite-ye'elimite-ferrite cement', *Advances in Cement Research.*, vol. 31, no. 3, pp. 124–137, 2019.

[111] K. Scrivener, R. Snellings, and B. Lothenbach, *A Practical Guide to Microstructural Analysis of Cementitious Materials*, First. Boca Raton: CRC Press, 2016.

[112] B. Z. Dilnesa, B. Lothenbach, G. Renaudin, A. Wichser, and D. Kulik, 'Synthesis and characterization of hydrogarnet Ca3(AlxFe1−x)2(SiO4)y(OH)4(3−y)', *Cement and Concrete Research*, vol. 59, pp. 96–111, 2014.

[113] K. De Weerdt, M. Ben Haha, G. Le Saout, K. O. Kjellsen, H. Justnes, and B. Lothenbach, 'The effect of temperature on the hydration of composite cements containing limestone powder and fly ash', *Materials and Structures*, vol. 45, no. 7, pp. 1101–1114, 2012.

[114] K. L. Scrivener, 'Backscattered electron imaging of cementitious microstructures: understanding and quantification', *Cement and Concrete Composites*, vol. 26, no. 8, pp. 935–945, 2004.

[115] T. Sui, L. Fan, Z. Wen, and J. Wang, 'Properties of Belite-Rich Portland Cement and Concrete in China', *Journal of Civil Engineering and Architecture*, vol. 9, 2015.
[116] T. Sui, L. Fan, Z. Wen, J. Wang, and Z. Zhang, 'Study on the Properties of High Strength Concrete using High Belite Cement', *ACT*, vol. 2, no. 2, pp. 201–206, 2004.
[117] L. G. Baquerizo, T. Matschei, K. L. Scrivener, M. Saeidpour, and L. Wadsö, 'Hydration states of AFm cement phases', *Cement and Concrete Research*, vol. 73, pp. 143–157, 2015.
[118] C.-T. Galbenis and S. Tsimas, 'Use of construction and demolition wastes as raw materials in cement clinker production', *China Particuology*, vol. 4, no. 2, pp. 83–85, 2006.
[119] R. Vigil de la Villa Mencía, M. Frías, S. M. Ramírez, L. F. Carrasco, and R. G. Giménez, 'Concrete/Glass Construction and Demolition Waste (CDW) Synergies in Ternary Eco-Cement-Paste Mineralogy', *Materials*, vol. 15, no. 13, Art. no. 13, 2022.
[120] D. Gastaldi, F. Canonico, L. Capelli, L. Buzzi, E. Boccaleri, and S. Irico, 'An investigation on the recycling of hydrated cement from concrete demolition waste', *Cement and Concrete Composites*, vol. 61, pp. 29–35, 2015.
[121] A. Akhtar and A. K. Sarmah, 'Construction and demolition waste generation and properties of recycled aggregate concrete: A global perspective', *Journal of Cleaner Production*, vol. 186, pp. 262–281, 2018.
[122] S. Kou, C. Poon, and F. Agrela, 'Comparisons of natural and recycled aggregate concretes prepared with the addition of different mineral admixtures', *Cement and Concrete Composites*, vol. 33, no. 8, pp. 788–795, 2011,.
[123] T. C. F. Oliveira, B. G. S. Dezen, and E. Possan, 'Use of concrete fine fraction waste as a replacement of Portland cement', *Journal of Cleaner Production*, vol. 273, p. 123126, 2020.
[124] A. R. Hind, S. K. Bhargava, and S. C. Grocott, 'The surface chemistry of Bayer process solids: a review', *Colloids and Surfaces A: Physicochemical and Engineering Aspects*, vol. 146, no. 1, pp. 359–374, 1999.
[125] L. Kljajevic *et al.*, 'Radiological and physico-chemical characterization of red mud as an Al-containing precursor in inorganic binders for the building industry', *Nuclear Technology & Radiation Protection*, vol. 36, no. 2, pp. 182–191, 2021.
[126] N. Zhang, X. Liu, H. Sun, and L. Li, 'Evaluation of blends bauxite-calcination-method red mud with other industrial wastes as a cementitious material: Properties and hydration characteristics', *Journal of Hazardous Materials*, vol. 185, no. 1, pp. 329–335, 2011.
[127] I. Vangelatos, G. N. Angelopoulos, and D. Boufounos, 'Utilization of ferroalumina as raw material in the production of Ordinary Portland Cement', *Journal of Hazardous Materials*, vol. 168, no. 1, pp. 473–478, 2009.
[128] Y. Jun, J. H. Kim, and T. Kim, 'Hydration of Calcium Sulfoaluminate-Based Binder Incorporating Red Mud and Silica Fume', *Applied Sciences*, vol. 9, no. 11, Art. no. 11, 2019.
[129] N. Zhang, H. Sun, X. Liu, and J. Zhang, 'Early-age characteristics of red mud–coal gangue cementitious material', *Journal of Hazardous Materials*, vol. 167, no. 1, pp. 927–932, 2009.
[130] M. Singh, S. N. Upadhayay, and P. M. Prasad, 'Preparation of special cements from red mud', *Waste Management*, vol. 16, no. 8, pp. 665–670, 1996.

[131] Y. Yao, Y. Li, X. Liu, S. Jiang, C. Feng, and E. Rafanan, 'Characterization on a cementitious material composed of red mud and coal industry byproducts', *Construction and Building Materials*, vol. 47, pp. 496–501, 2013.
[132] E. P. Manfroi, M. Cheriaf, and J. C. Rocha, 'Microstructure, mineralogy and environmental evaluation of cementitious composites produced with red mud waste', *Construction and Building Materials*, vol. 67, pp. 29–36, 2014.
[133] J. N. Gordon, W. R. Pinnock, and M. M. Moore, 'A preliminary investigation of strength development in Jamaican red mud composites', *Cement and Concrete Composites*, vol. 18, no. 6, pp. 371–379, 1996.
[134] F. Bullerjahn, M. Zajac, and M. Ben Haha, 'CSA raw mix design: effect on clinker formation and reactivity', *Materials and Structures*, vol. 48, no. 12, pp. 3895–3911, 2015.
[135] A. Telesca, M. Marroccoli, and F. Winnefeld, 'Synthesis and characterisation of calcium sulfoaluminate cements produced by different chemical gypsums', *Advances in Cement Research*, vol. 31, no. 3, pp. 113–123, 2019.
[136] I. Jawed and J. Skalny, 'Alkalies in cement: A review: II. Effects of alkalies on hydration and performance of Portland cement', *Cement and Concrete Research*, vol. 8, no. 1, pp. 37–51, 1978.
[137] K. Baltakys, T. Dambrauskas, D. Rubinaite, R. Siauciunas, and A. Grineviciene, 'Formation and hydration of eco-friendly cement using industrial wastes as raw materials', *Scientific Reports*, vol. 11, no. 1, p. 14742, 2021.
[138] F. Bullerjahn, M. Zajac, M. Ben Haha, and K. L. Scrivener, 'Factors influencing the hydration kinetics of ye'elimite; effect of mayenite', *Cement and Concrete Research*, vol. 116, pp. 113–119, 2019.
[139] Z. He and Y. Li, 'The Influence of Mayenite Employed as a Functional Component on Hydration Properties of Ordinary Portland Cement', *Materials (Basel)*, vol. 11, no. 10, p. 1958, 2018,.
[140] F. Bullerjahn, E. Boehm-Courjault, M. Zajac, M. Ben Haha, and K. Scrivener, 'Hydration reactions and stages of clinker composed mainly of stoichiometric ye'elimite', *Cement and Concrete Research*, vol. 116, pp. 120–133, 2019.
[141] Q. Wang, J. Yang, and P. Yan, 'Influence of initial alkalinity on the hydration of steel slag', *Science China Technological Sciences,* vol. 55, no. 12, pp. 3378–3387, 2012.
[142] D. Damidot and A. Rettel, 'Effect of Gypsum on CA and C12A7 Hydration at Room Temperature', Proceedings of the 11th International Congress on the Chemistry of Cement (ICCC), Durban, South Africa, 2003.
[143] A. Koehler, J. Neubauer, and F. Goetz-Neunhoeffer, 'How C12A7 influences the early hydration of calcium aluminate cement at different temperatures', *Cement and Concrete Research*, vol. 162, p. 106972,. 2022.
[144] J. Koplík, L. Tomala, and R. Novotný, 'Hydration of calcium aluminate phases at different temperatures', *Advanced Materials Research*, vol. 1000, pp. 24–27, 2014.
[145] R. N. Edmonds and A. J. Majumdar, 'The hydration of 12CaO.7A12O3 at different temperatures', *Cement and Concrete Research*, vol. 18, no. 3, pp. 473–478, 1988.
[146] M. Dovál, M. Palou, and S. C. Mojumdar, 'Hydrationbehavior of C2S and C2AS nanomaterials,synthetized by sol–gel method', *Journal of Thermal Analysis and Calorimetry*, vol. 86, no. 3, pp. 595–599, 2006.
[147] S. Dolenec, K. Šter, M. Borštnar, K. Nagode, A. Ipavec, and L. Žibret, 'Effect of the Cooling Regime on the Mineralogy and Reactivity of Belite-Sulfoaluminate Clinkers', *Minerals*, vol. 10, no. 910, p. 16, 2020.

[148] H. El-Didamony, M. Heikal, and Kh. A. Khalil, 'Characteristics of cement pastes containing sulphoaluminate and belite prepared from nano-materials', *Construction and Building Materials*, vol. 38, pp. 14–21, 2013.
[149] R. Snellings, 'Solution-Controlled Dissolution of Supplementary Cementitious Material Glasses at pH 13: The Effect of Solution Composition on Glass Dissolution Rates', *Journal of the American Ceramic Society*, vol. 96, no. 8, pp. 2467–2475, 2013.
[150] K. L. Scrivener and A. Capmas, 'Calcium aluminate cements', in Editor(s): Peter C. Hewlett, Lea's Chemistry of Cement and Concrete,Butterworth-Heinemann, 1998.
[151] J. Qin, C. Yang, C. Cui, J. Huang, A. Hussain, and H. Ma, 'Ca2+ and OH− release of ceramsites containing anorthite and gehlenite prepared from waste lime mud', *Journal of Environmental Sciences*, vol. 47, pp. 91–99, 2016.
[152] S. S. Rehsi, 'Magnesium Oxide in Portland Cement', in *Advances in Cement Technology*, S. N. Ghosh, Ed., Pergamon, 1983, pp. 467–483.
[153] C. Wang, Z. Zhou, C. Liu, and X. Cheng, 'Formation kinetics of Portland cement clinker containing with magnesium oxide', *Kuei Suan Jen Hsueh Pao/Journal of the Chinese Ceramic Society*, vol. 39, no. 4, pp. 714–717, 2011.
[154] V. C. G. de Souza, J. C. Koppe, J. F. C. L. Costa, A. L. M. Vargas, E. Blando, and R. Hübler, 'The influence of mineralogical, chemical and physical properties on grindability of commercial clinkers with high MgO level', *Cement and Concrete Research*, vol. 38, no. 8, pp. 1119–1125, 2008.
[155] W. Kurdowski, *Cement and Concrete Chemistry*. Springer Netherlands, 2014.
[156] K. De Weerdt and H. Justnes, 'The effect of sea water on the phase assemblage of hydrated cement paste', *Cement and Concrete Composites*, vol. 55, pp. 215–222,. 2015.
[157] M. Whittaker, Z. Maciej, M. Ben Haha, and L. Black, 'The impact of alumina availability on sulfate resistance of slag composite cements', *Construction and Building Materials*, vol. 119, pp. 356–369, 2016.
[158] H. F. W. Taylor, 'Distribution of sulfate between phases in Portland cement clinkers', *Cement and Concrete Research*, vol. 29, no. 8, pp. 1173–1179, 1999.
[159] Y. Ma and J. Qian, 'Influence of alkali sulfates in clinker on the hydration and hardening of Portland cement', *Construction and Building Materials*, vol. 180, pp. 351–363, 2018.
[160] S. Kumar and C. V. S. Kameswara Rao, 'Effect of sulfates on the setting time of cement and strength of concrete', *Cement and Concrete Research*, vol. 24, no. 7, pp. 1237–1244, 1994.
[161] B. Samet and S. L. Sarkar, 'The influence of calcium sulfate form on the initial hydration of clinkers containing different alkali combinations', *Cement and Concrete Research*, vol. 27, no. 3, pp. 369–380, 1997.
[162] H. F. W. Taylor, *Cement chemistry*, 2nd ed. London: T. Telford, 1997.
[163] F. J. Tang and E. M. Gartner, 'Influence of sulphate source on Portland cement hydration', *Advances in Cement Research*, vol. 1, no. 2, pp. 67–74, 1988.
[164] I. Odler and R. Wonnemann, 'Effect of alkalies on portland cement hydration II. Alkalies present in form of sulphates', *Cement and Concrete Research*, vol. 13, no. 6, pp. 771–777, 1983.
[165] P. Padilla-Encinas, A. Palomo, M. T. Blanco-Varela, and A. Fernández-Jiménez, 'Calcium sulfoaluminate clinker hydration at different alkali concentrations', *Cement and Concrete Research*, vol. 138, p. 106251, 2020.

[166] L. Huang, W. Song, H. Li, H. Zhang, and Z. Yang, 'Effects of aphthitalite on the formation of clinker minerals and hydration properties', *Construction and Building Materials*, vol. 183, pp. 275–282, 2018.

[167] H. Sun *et al.*, 'Effects of alkali sulfates in clinker on hydration and hardening performance of Portland cement', *Advances in Cement Research*, vol. 30, no. 4, pp. 172–184, 2018.

[168] M. D. Andersen, H. J. Jakobsen, and J. Skibsted, 'Characterization of white Portland cement hydration and the C-S-H structure in the presence of sodium aluminate by 27Al and 29Si MAS NMR spectroscopy', *Cement and Concrete Research*, vol. 34, no. 5, pp. 857–868, 2004.

[169] I. F. Sáez del Bosque, S. Martínez-Ramírez, M. Martín-Pastor, and M. T. Blanco-Varela, 'Effect of temperature on C–S–H gel nanostructure in white cement', *Materials and Structures*, vol. 47, no. 11, pp. 1867–1878, 2014.

[170] G. Le Saoût, B. Lothenbach, A. Hori, T. Higuchi, and F. Winnefeld, 'Hydration of Portland cement with additions of calcium sulfoaluminates', *Cement and Concrete Research*, vol. 43, pp. 81–94, 2013.

[171] G. Paul, E. Boccaleri, L. Buzzi, F. Canonico, and D. Gastaldi, 'Friedel's salt formation in sulfoaluminate cements: A combined XRD and 27Al MAS NMR study', *Cement and Concrete Research*, vol. 67, pp. 93–102, 2015.

[172] F. Bertola, D. Gastaldi, S. Irico, G. Paul, and F. Canonico, 'Behavior of blends of CSA and Portland cements in high chloride environment', *Construction and Building Materials*, vol. 262, p. 120852, 2020.

[173] R. J. Myers, S. A. Bernal, J. D. Gehman, J. S. J. van Deventer, and J. L. Provis, 'The Role of Al in Cross-Linking of Alkali-Activated Slag Cements', *Journal of the American Ceramic Society*, vol. 98, no. 3, pp. 996–1004, 2015.

[174] J. J. Thomas, D. Rothstein, H. M. Jennings, and B. J. Christensen, 'Effect of hydration temperature on the solubility behavior of Ca-, S-, Al-, and Si-bearing solid phases in Portland cement pastes', *Cement and Concrete Research*, vol. 33, no. 12, pp. 2037–2047, 2003.

[175] M. D. Andersen, H. J. Jakobsen, and J. Skibsted, 'Incorporation of Aluminum in the Calcium Silicate Hydrate (C−S−H) of Hydrated Portland Cements: A High-Field 27Al and 29Si MAS NMR Investigation', *Inorganic Chemistry.*, vol. 42, no. 7, pp. 2280–2287, 2003.

[176] F. Avet, E. Boehm-Courjault, and K. Scrivener, 'Investigation of C-A-S-H composition, morphology and density in Limestone Calcined Clay Cement (LC3)', *Cement and Concrete Research*,, vol. 115, pp. 70–79, 2019.

[177] R. J. Myers, E. L'Hôpital, J. L. Provis, and B. Lothenbach, 'Effect of temperature and aluminium on calcium (alumino)silicate hydrate chemistry under equilibrium conditions', *Cement and Concrete Research*, vol. 68, pp. 83–93, 2015.

[178] T. T. H. Bach, C. C. D. Coumes, I. Pochard, C. Mercier, B. Revel, and A. Nonat, 'Influence of temperature on the hydration products of low pH cements', *Cement and Concrete Research*, vol. 42, no. 6, pp. 805–817, 2012.

[179] E. L'Hôpital, B. Lothenbach, D. A. Kulik, and K. Scrivener, 'Influence of calcium to silica ratio on aluminium uptake in calcium silicate hydrate', *Cement and Concrete Research*, vol. 85, pp. 111–121, 2016.

[180] Mathur, 'Study of cementitious materials using transmission electron microscopy', EPFL, Laussane, 2007.

[181] S. A. Rodger and G. W. Groves, 'Electron Microscopy Study of Ordinary Portland Cement and Ordinary Portland Cement-Pulverized Fuel Ash Blended Pastes', *Journal of American Ceramic Society*, vol. 72, no. 6, pp. 1037–1039, 1989.

[182] I. g. Richardson, J. Skibsted, L. Black, and R. j. Kirkpatrick, 'Characterisation of cement hydrate phases by TEM, NMR and Raman spectroscopy', *Advances in Cement Research*, vol. 22, no. 4, pp. 233–248, 2010.
[183] Q. Zhou, E. E. Lachowski, and F. P. Glasser, 'Metaettringite, a decomposition product of ettringite', *Cement and Concrete Research*, vol. 34, no. 4, pp. 703–710, 2004.
[184] W. Lukas, 'Substitution of Si in the lattice of ettringite', *Cement and Concrete Research*, vol. 6, no. 2, pp. 225–233, 1976.
[185] I. G. Richardson, 'The nature of the hydration products in hardened cement pastes', *Cement and Concrete Composites*, vol. 22, no. 2, pp. 97–113, 2000.
[186] J. Astoveza, 'Calcium aluminate blended cements incorporating engineered residues', Université de Lorraine; Katholieke universiteit te Leuven, 2022.
[187] B. Z. Dilnesa, B. Lothenbach, G. Renaudin, A. Wichser, and E. Wieland, 'Stability of Monosulfate in the Presence of Iron', *Journal of Americal Ceramics Society.*, vol. 95, no. 10, pp. 3305–3316, 2012.
[188] G. Álvarez-Pinazo, I. Santacruz, L. León-Reina, M. A. G. Aranda, and A. G. De la Torre, 'Hydration Reactions and Mechanical Strength Developments of Iron-Rich Sulfobelite Eco-cements', *Industrial & Engineering Chemistry Research*, vol. 52, no. 47, pp. 16606–16614, 2013.
[189] J. Wang, 'Hydration mechanism of cements based on low-CO2 clinkers containing belite, ye'elimite and calcium alumino-ferrite', Université des Sciences et Technologie de Lille, Lille, 2011.
[190] H. F. W. Taylor and D. E. Newbury, 'An electron microprobe study of a mature cement paste', *Cement and Concrete Research*, vol. 14, no. 4, pp. 565–573, 1984.
[191] J. Siramanont, B. J. Walder, L. Emsley, and P. Bowen, 'Iron incorporation in synthetic precipitated calcium silicate hydrates', *Cement and Concrete Research*, vol. 142, p. 106365, 2021.
[192] L. Mo, M. Liu, A. Al-Tabbaa, and M. Deng, 'Deformation and mechanical properties of the expansive cements produced by inter-grinding cement clinker and MgOs with various reactivities', *Construction and Building Materials*, vol. 80, pp. 1–8, 2015.
[193] L. Wang *et al.*, 'Influence of MgO on the Hydration and Shrinkage Behavior of Low Heat Portland Cement-Based Materials via Pore Structural and Fractal Analysis', *Fractal and Fractional*, vol. 6, no. 1, Art. no. 1, 2022.
[194] M. M. Ali and A. K. Mullick, 'Volume stabilisation of high MgO cement: effect of curing conditions and fly ash addition', *Cement and Concrete Research*, vol. 28, no. 11, pp. 1585–1594, 1998.
[195] L. Sequeira, B. Cantero, M. Bravo, J. de Brito, and C. Medina, 'The Influence of Recycled Cement, Fly Ash, and Magnesium Oxide on the Mechanical Performance of Sustainable Cementitious Materials', *Materials*, vol. 16, no. 7, Art. no. 7, 2023.
[196] E. Berodier and K. Scrivener, 'Evolution of pore structure in blended systems', *Cement and Concrete Research*, vol. 73, pp. 25–35, 2015.
[197] G. Bernardo, A. Telesca, and G. L. Valenti, 'A porosimetric study of calcium sulfoaluminate cement pastes cured at early ages', *Cement and Concrete Research*, vol. 36, no. 6, pp. 1042–1047, 2006.
[198] N. Roussel, Ed., *Understanding the Rheology of Concrete*. in Woodhead Publishing Series in Civil and Structural Engineering. Woodhead Publishing, 2012..
[199] J. Hot, H. Bessaies-Bey, C. Brumaud, M. Duc, C. Castella, and N. Roussel, 'Adsorbing polymers and viscosity of cement pastes', *Cement and Concrete Research*, vol. 63, pp. 12–19, 2014.

[200] G. Ke, J. Zhang, S. Xie, and T. Pei, 'Rheological behavior of calcium sulfoaluminate cement paste with supplementary cementitious materials', *Construction and Building Materials*, vol. 243, p. 118234, 2020.
[201] Q. Yuan, D. Zhou, K. H. Khayat, D. Feys, and C. Shi, 'On the measurement of evolution of structural build-up of cement paste with time by static yield stress test vs. small amplitude oscillatory shear test', *Cement and Concrete Research*, vol. 99, pp. 183–189, 2017.
[202] A. M. Mostafa and A. Yahia, 'New approach to assess build-up of cement-based suspensions', *Cement and Concrete Research*, vol. 85, pp. 174–182, 2016.
[203] P. F. G. Banfill, 'Rheology of fresh cement and concrete', in Proceedings of an International Conference, Liverpool, 1990.
[204] A. M. Mostafa and A. Yahia, 'Physico-chemical kinetics of structural build-up of neat cement-based suspensions', *Cement and Concrete Research*, vol. 97, pp. 11–27, Jul. 2017, doi: 10.1016/j.cemconres.2017.03.003.
[205] N. Roussel, G. Ovarlez, S. Garrault, and C. Brumaud, 'The origins of thixotropy of fresh cement pastes', *Cement and Concrete Research*, vol. 42, no. 1, pp. 148–157, 2012.
[206] D. Jiao, R. De Schryver, C. Shi, and G. De Schutter, 'Thixotropic structural build-up of cement-based materials: A state-of-the-art review', *Cement and Concrete Composites*, vol. 122, p. 104152, 2021.
[207] A. Perrot, D. Rangeard, and A. Pierre, 'Structural built-up of cement-based materials used for 3D-printing extrusion techniques', *Materials and Structures*, vol. 49, no. 4, pp. 1213–1220, 2016.
[208] J. J. Assaad and K. H. Khayat, 'Effect of viscosity-enhancing admixtures on formwork pressure and thixotropy of self-consolidating concrete', *ACI Materials Journal*, vol. 103, no. 4, pp. 280–287, 2006.
[209] J. H. Mork and O. E. Gjoerv, 'Effect of gypsum-hemihydrate ratio in cement on rheological properties of fresh concrete', *ACI Materials Journal*, vol. 94, no. 2, pp. 142–146, 1997.
[210] J. Dils, V. Boel, and G. De Schutter, 'Influence of cement type and mixing pressure on air content, rheology and mechanical properties of UHPC', *Construction and Building Materials*, vol. 41, pp. 455–463, 2013.
[211] M. García-Maté, I. Santacruz, Á. G. De la Torre, L. León-Reina, and M. A. G. Aranda, 'Rheological and hydration characterization of calcium sulfoaluminate cement pastes', *Cement and Concrete Composites*, vol. 34, no. 5, pp. 684–691, 2012.
[212] T. Huang, B. Li, Q. Yuan, Z. Shi, Y. Xie, and C. Shi, 'Rheological behavior of Portland clinker-calcium sulphoaluminate clinker-anhydrite ternary blend', *Cement and Concrete Composites*, vol. 104, p. 103403, 2019.
[213] H. Dada, A. S. E. Belaidi, H. Soualhi, E.-H. Kadri, and B. Benabed, 'Influence of temperature on the rheological behaviour of eco-mortar with binary and ternary cementitious blends of natural pozzolana and marble powder', *Powder Technology*, vol. 384, pp. 223–235, 2021.
[214] J.-Y. Petit, E. Wirquin, Y. Vanhove, and K. Khayat, 'Yield stress and viscosity equations for mortars and self-consolidating concrete', *Cement and Concrete Research*, vol. 37, no. 5, pp. 655–670, 2007.
[215] M. Nehdi and S. Al Martini, 'Effect of Temperature on Oscillatory Shear Behavior of Portland Cement Paste Incorporating Chemical Admixtures', *Journal of Materials in Civil Engineering*, vol. 19, no. 12, pp. 1090–1100, 2007.

[216] X. Kong, Y. Zhang, and S. Hou, 'Study on the rheological properties of Portland cement pastes with polycarboxylate superplasticizers', *Rheologica Acta*, vol. 52, no. 7, pp. 707–718, 2013.

[217] Y. Zhang, X. Kong, L. Gao, and J. Wang, 'Rheological behaviors of fresh cement pastes with polycarboxylate superplasticizer', *J. Wuhan Univ. Technol.-Mat. Sci. Edit.*, vol. 31, no. 2, pp. 286–299, 2016.

[218] H. Huang, T. Huang, Q. Yuan, D. Zhou, D. Deng, and L. Zhang, 'Temperature dependence of structural build-up and its relation with hydration kinetics of cement paste', *Construction and Building Materials*, vol. 201, pp. 553–562, 2019.

[219] M. Palacios *et al.*, 'Early reactivity of sodium silicate-activated slag pastes and its impact on rheological properties', *Cement and Concrete Research*, vol. 140, p. 106302, 2021.

[220] A. Colombo, M. R. Geiker, H. Justnes, R. A. Lauten, and K. De Weerdt, 'On the effect of calcium lignosulfonate on the rheology and setting time of cement paste', *Cement and Concrete Research*, vol. 100, pp. 435–444, 2017.

Bibliography

Publications Related to the Thesis

Journal Articles

M. Borštnar, N. Daneu, and S. Dolenec, 'Phase development and hydration kinetics of belite-calcium sulfoaluminate cements at different curing temperatures', Ceramics International, vol. 46, no. 18, pp. 29421–29428, 2020.

M. Borštnar, C. L. Lengauer, and S. Dolenec, 'Quantitative in Situ X-ray Diffraction Analysis of Early Hydration of Belite-Calcium Sulfoaluminate Cement at Various Defined Temperatures', Minerals, vol. 11, no. 3, p. 297, 2021.

M. Mrak, F. Winnefeld, B. Lothenbach, and S. Dolenec, 'The influence of calcium sulfate content on the hydration of belite-calcium sulfoaluminate cements with different clinker phase compositions', *Materials and Structures*, vol. 54, no. 6, p. 212, 2021.

Conference Paper

M. Mrak, F. Winnefeld, B. Lothenbach, S. Dolenec. 'Uporaba termodinamskega modeliranja za napoved ravnotežne fazne sestave cementov'. In: B. Rožič, (ed.). *Razprave, poročila = Treatises, reports : 25. posvetovanje slovenskih geologov = 25th Meeting of Slovenian Geologists,* Ljubljana, october, 2021, Ljubljana: Univerza v Ljubljani, Naravoslovnotehniška fakulteta, Oddelek za geologijo, 2021.

M. Borštnar, S. Dolenec, N. Daneu. 'Potek hidratacije in nastanek hidratacijskih produktov belitno-kalcijevo sulfoaluminatnega cementa pri različnih temperaturah'. In: B. Rožič, (ed.). *Razprave, poročila = Treatises, reports. 24. posvetovanje slovenskih geologov = 24th Meeting of Slovenian Geologists*, Ljubljana, november 2019. Ljubljana: Univerza v Ljubljani, Naravoslovnotehniška fakulteta, Oddelek za geologijo, 2019.

Published scientific conference contribution abstract

M. Mrak, C. L. Lengauer, S. Dolenec. 'Early hydration of belite sulfoaluminate cement investigated by in-situ X-ray diffraction analysis'. In: *3rd International Conference on the Chemistry of Construction Materials*, March 15 - 17, 2021 : online : book of abstracts. Karlsruhe: Gesellschaft Deutscher Chemiker, 2021.

M. Mrak, F. Winnefeld, B. Lothenbach, S. Dolenec. 'Effect of temperature on phase assemblage of belite calcium-sulfoaluminate cement'. In: *Book of abstracts : 14th Students' Congress of SCTM* : 30th September - 2nd October 2021, Faculty of Technology and Metallurgy, Skopje, N. Macedonia. Skopje: Society of Chemists and Technologists of Macedonia, 2021.

M. Mrak, N. Daneu, F. Winnefeld, B. Lothenbach, S. Dolenec. 'Characterisation of hydrate phases composition of belite-calcium sulfoaluminate cements by

SEM/EDS'. In: *MC 2021 goes digital : proceedings*. Microscopy Conference, Joint Meeting of Dreiländertagung & Multinational Congress on Microscopy, 22-26 August 2021.

M. Borštnar, F. Winnefeld, B. Lothenbach, S. Dolenec. 'Hydration of belite sulfoaluminate cements at defined curing temperatures: experimental study and thermodynamic modelling : experimental study and thermodynamic modelling'. In: *Book of abstracts of the 74th RILEM Annual Week & the 40th Cement and Concrete Science Conference* : hosted (online) by The University of Sheffield, Sheffield, United Kingdom, 31 August - 4 September 2020. Sheffield: University of Sheffield, 2020.

M. Borštnar, N. Daneu, and S. Dolenec. 'Hydration of belite-calcium sulfoaluminate cements at different curing temperatures studied by isothermal calorimetry and thermal analysis'. In: A. Rotaru (ed.), S. Vecchio Ciprioti (ed.). *CEEC-TAC5 & Medicta2019 : book of abstracts*. 5th Central and Eastern European Conference on Thermal Analysis and Calorimetry & 14th Mediterranean Conference on Calorimetry and Thermal Analysis, 27-30 August 2019 Roma, Italy.

Biography

The author of this thesis Maruša Mrak was born in Ljubljana, Slovenia, on February 2, 1993. She completed both her BSc and MSc at the University of Ljubljana, Slovenia (Faculty of Natural Sciences and Engineering, Department of Geology) in 2016 and 2018, respectively. She studied abroad at Charles University in Prague as a part of an Erasmus+ exchange. She received a Prešeren award for her bachelor's thesis 'Influence of bacteria on cave pearls growth'. Since 2018, she worked as a young researcher in the Laboratory for cement, mortars and ceramics at the Slovenian Building and Civil Engineering Institute and pursuing her doctoral studies in Nanosciences and nanotechnologies at the Jožef Stefan International Postgraduate School. For her doctoral thesis she studied the influence of temperature on hydration processes of belite calcium sulfoaluminate (BCSA) cement. She received a second best poster award at the 2nd International Workshop on Calcium Sulfoaluminate Cements. She has been involved in the following international and national projects: (1) ARRS programme P2-0273: Building materials and structures (2015-present), (2) BI-AT/18-19-014: Effect of clinkering process on the mineralogy of belite-sulfoaluminate cement clinker (2018-2019), (3) NanoCEM partner project: Influence of temperature on the hydration of belite-calcium sulfoaluminate cements (2018-2021), (4) EU project KIC RM: ALiCE Al-rich industrial residues for mineral binders in ESEE region (2019-2021). She is a member of the RILEM TC EBD: Test methods to evaluate durability of blended cement pastes against deleterious ions (2020-present) and a previous TC TRM: Tests for reactivity of supplementary cementitious materials (2015-2020). Her research work has mostly focused on mineral binders (primarly cement clinkers, cement and mortars) – investigating both their synthesis and mineralogical, microstructural, mechanical and chemical characterization (using scanning electron microscopy, X-ray powder diffraction, the Rietveld method for quantitative analysis and isothermal calorimetry) in addition to thermodynamic modeling.